Inter-seasonal solar energy storage for buildings by absorption

Hui Liu

UNIVERSITÉ DE GRENOBLE

Pour obtenir le grade de

DOCTEUR DE L'UNIVERSITÉ DE GRENOBLE
Spécialité **Génie des Procédés**

Arrêté ministériel : 7 août 2006

Présentée et soutenue publiquement par

LIU Hui

Le **17 décembre 2010**

STOCKAGE INTER-SAISONNIER D'ENERGIE SOLAIRE POUR L'HABITAT PAR ABSORPTION

Thèse dirigée par **LUO Lingai** et codirigée par **LE PIERRES Nolwenn**

JURY

M. Breton Claude	Responsable de département, Solvay Carbonate	Examinateur
Mme Le Pierrès Nolwenn	Maître de Conférences, Université de Savoie	Codirectrice de thèse
Mme Luo Lingai	Professeur, université de Savoie	Directrice de thèse
M. Marty Philippe	Professeur, université Joseph Fourier	Président
Mme Mazet Nathalie	Directeur de recherche, PROMES CNRS	Rapporteur
M. Yuan Xigang	Professeur, Tianjin University	Rapporteur

Thèse préparée au sein du **Laboratoire LOCIE** dans **l'Ecole Doctorale SISEO**

To my parents, my wife and my son

Remerciements

Je tiens tout d’abord à adresser mes sincères remerciements à Mme LUO Lingai, professeur à l’Université de Savoie, qui m’a beaucoup soutenue depuis mon arrivée en France, et pour son encadrement de cette thèse.

Je remercie particulièrement mon co-directeur de thèse, Mme LE PIERRES Nolwenn, non seulement pour la qualité de son encadrement mais aussi pour sa patience énorme et sa disponibilité tout au long de ma thèse.

Je suis également très reconnaissant envers Monsieur Claude BRETON et Monsieur Olivier PATAT du Groupe Solvay pour leurs avis sur ma thèse.

Je tiens également à remercier l’assemblée des pays de Savoie (APS) et le Groupe Solvay qui ont cofinancés ma bourse de thèse.

Mes remerciements s’adressent également à notre techniciens Monsieur Thierry GOLDIN et Monsieur Romain GUYOMARC’H pour avoir passé un bon moment sur le montage du prototype à l’INES. Ma très sincère gratitude va également à Monsieur Thierry GOLDIN pour son aide dans l’apprentissage de la langue française.

Je voudrais exprimer ma gratitude aux membres du jury de thèse pour leurs soutiens et leurs conseils.

Merci aussi à tous mes collègues du LOCIE : Mademoiselle Yu BAI, Yinlin Fan, Adrien BRUN, Pierre TITTELEIN, Louis STEPHAN, Mademoiselle Layal CHAHWANE, Kokouvi Edem N'TSOUKPOE, Qiang MA, Tong ZHANG, Qi ZHANG, Hua ZHANG, Bin CAO, Limin WANG,…pour le temps consacré à toutes mes sollicitations. Il serait trop long de vouloir les citer tous, mais qu’ils trouvent ici le témoignage de ma profonde gratitude.

Finalement, j’adresse un grand merci à toute ma famille qui a toujours été présente lorsque j’en ai eu besoin, en particulier à mon père, à ma mère et à ma femme.

Abstract

An innovative concept of seasonal storage of solar energy for house heating by absorption is developed in this thesis. The process is introduced and described.

The study of the storage capacity, the efficiency, the operating pressure, the temperature need for solar energy, the possible temperature for house heating, the material security and the material economy of seven absorption couples: $CaCl_2/H_2O$, Glycerin/H_2O, KOH/H_2O, LiBr/H_2O, LiCl/H_2O, NaOH/H_2O and H_2O/NH_3 is performed by a static simulation.

A prototype of demonstration of the feasibility of the concept with the absorption couple $CaCl_2/H_2O$ is designed, dimensioned and built. It has been optimized, in order to minimize the number of components of the system. Experimentations are carried out at different operating conditions. The thermodynamic performances and the problems of the prototype are analyzed.

As the experimental results are influenced by several factors such as the presence of the air in the system (especially for the absorption phase), the precision of the sensors and some human factors during the operation, for a better understanding of the process, a dynamic simulation is developed to represent the prototype. The optimal functioning of the prototype is thus studied through the dynamic simulation.

A global annual dynamic simulation is performed in order to obtain the annual performance of the seasonal storage system in a building. Models of the storage system, of a solar collector, a building and weather conditions are used. The characteristics such as the pressure, the temperature, the mass, the mass fraction, the power, the efficiency, the storage capacity etc. of the storage system are presented and analyzed.

Keywords: Seasonal storage, absorption, static simulation, dynamic simulation, annual simulation, efficiency, storage capacity

Résumé

Un nouveau concept de stockage inter-saisonnier par absorption de l'énergie solaire pour l'habitat est développé dans cette thèse. Le processus est présenté et décrit.

L'étude de la capacité de stockage, du rendement, de la pression de fonctionnement, du besoin de température pour l'énergie solaire, de la température possible pour le chauffage du bâtiment, des critères de sécurité et du coût des matériaux de sept couples d'absorption: $CaCl_2/H_2O$, Glycérine/H_2O, KOH/H_2O, LiBr/H_2O, LiCl/H_2O, NaOH/H_2O et H_2O/NH_3 est effectuée à l'aide d'une simulation statique.

Un prototype de démonstration de la faisabilité de ce concept innovant avec le couple $CaCl_2/H_2O$ a été conçu, dimensionné et construit. Il est issu d'une optimisation minimisant le nombre de composants du système. Des expérimentations ont été effectuées à différentes conditions de fonctionnement. Les performances thermodynamiques et les différents problèmes du prototype sont analysés.

Comme les résultats expérimentaux sont influencés par plusieurs facteurs tels que la présence d'air dans le système (en particulier pour la phase d'absorption), la précision des capteurs et des facteurs humains lors de l'opération, pour une meilleure compréhension du processus, une simulation dynamique est développée. Le fonctionnement optimal du prototype est alors étudié.

Une simulation globale annuelle est effectuée afin d'étudier le fonctionnement annuel du système de stockage inter-saisonnier en lien avec un système solaire et un bâtiment. Les modèles du système de stockage, d'un capteur solaire, d'un bâtiment et des conditions météorologiques sont couplés. Les caractéristiques : pressions, températures, masses, fractions massiques, puissances échangées, rendements, capacités de stockage, etc. du système de stockage sont présentés et analysés.

Mots-clef : stockage saisonnier, chaleur, absorption, simulation statique, simulation dynamique, prototype, expérimentations

Table of contents

List of the figures

List of the tables

Nomenclature

Note: the symbols which are not included in this nomenclature are explained in the text.

Latin Symbols

Cp	Specific heat capacity [kJ/(kg·°C)]
d	Diameter [m]
E	Thickness of the walls [m]
h	Enthalpy [kJ/kg]
H	Height [m]
K	Heat transfer coefficient [kJ/(m.K)]
l	Length [m]
m	Relative mass [kg/kg absorbent]
M	Mass [kg]
$\dot{m}$	Mass flow rate [kg/h]
P	Pressure [Pa]
Pr	Prandtl number
Q	Heat [kJ]
$\dot{Q}$	Power of heat [kW]
R	Ratio of crystallization
Re	Reynolds number
s	Surface area of the tanks and heat exchangers [m^2]
T	Temperature [°C]
t	Time [s]
V	Volume [m^3]
$\dot{W}$	Power of the pump [kW]
x	Mass fraction of absorbent [kg absorbent/kg solution]

Greek symbols

α	Heat convection coefficient [kJ/(m^2·K)]
λ	Heat conductivity [kJ/(m·K)]
ρ	Density [kg/m^3]

Subscripts

a	Absorption/absorber
atm	Ambiant
c	Condensation/condenser
cr	Critical
cry	Crystal
d	Desorption
e	Evaporation/evaporator

ex	Heat exchanger
g	Generator
i	Inlet/inside
loss	Heat loss
o	Outlet/outside
s	Solution
sol	Solubility
t	Total
vap	Vapor
w	Water
1-6, 1’-6’	States in the figures of the static simulation

Synthèse de thèse (en Français)

R.1 Etat de l'art des Systèmes de stockage inter-saisonnier d'énergie solaire

Aujourd'hui, la plupart des bâtiments répondent à des charges thermiques en utilisant des systèmes qui produisent ou évacuent la chaleur lorsque les charges sont présentes. Des systèmes de stockage d'énergie thermique (TES) dans les bâtiments permettraient de répondre aux besoins de chauffage et de refroidissement en utilisant de l'énergie produite à un tout autre moment.

Les TES peuvent être conçus pour la charge et la décharge de l'énergie sur trois types de durées: diurne, hebdomadaire et saisonnière. Le stockage d'énergie thermique inter-saisonnier (STES) permet à un bâtiment l'utilisation de la chaleur recueillie durant l'été pour chauffer le bâtiment pendant l'hiver, ou l'utilisation du froid recueilli au cours de l'hiver pour refroidir le bâtiment en été. Par rapport aux systèmes de stockage diurne, les STES dans le bâtiment nécessitent un plus grand volume parce que la quantité d'énergie à stocker est augmentée. Les systèmes STES sont constitués de plusieurs éléments: la source chaude (ou froide), les systèmes d'échange de chaleur, le système de distribution de la chaleur, le matériau de stockage thermique, le tout lié aux charges thermiques du bâtiment. Une question clé dans la conception d'un système de stockage d'énergie thermique est sa capacité thermique - la quantité d'énergie qu'il peut stocker et fournir. Cependant, le choix du système approprié dépend d'un compromis coût-efficacité [Gil al A. et al. 2010].

Le coût d'un système TES dépend principalement des points suivants: le matériau de stockage lui-même, les échangeurs de chaleur pour charger et décharger le système, le coût de l'espace occupé. Tous ces points doivent être considérés au moment de décider du type et de la conception du stockage thermique. Beaucoup de méthodes et de systèmes ont été développés pour les systèmes STES. Les procédés de stockage d'énergie thermique peuvent être classés selon leur mécanisme de stockage : le stockage par chaleur sensible, le stockage par chaleur latente, le stockage par réaction et le stockage par sorption.

R.1.1 Stockage par chaleur sensible

Pour le stockage thermique par chaleur sensible, l'énergie thermique est stockée par le changement de la température du matériau de stockage. Ainsi, la capacité de stockage dépend de la différence de température, de la chaleur spécifique et de la quantité de matériau de stockage.

Les systèmes de stockage de chaleur sensible peuvent être classés sur la base du matériau de stockage : stockage par un liquide (l'eau, les liquides à base d'huile, de sels fondus, etc.) ou par un solide (comme les roches, les métaux et autres).

Stockage par un liquide

L'eau est l'un des meilleurs matériaux de stockage à basse température. Elle présente une plus grande chaleur spécifique que d'autres matériaux, est peu coûteuse et largement disponible.

Toutefois, en raison de sa pression de vapeur élevée, les systèmes utilisant de l'eau doivent résister à une haute pression de confinement pour les applications à haute température. L'eau peut être utilisée sur la large gamme de température de 25 à 90°C. Pour une variation de température de 60°C, l'eau peut stocker 250 kJ / kg soit 2,5 x 10^5 kJ/m^3 [Amaya V. Novo et al. 2010]. En raison de son abondance, une grande quantité de données sont publiées et disponibles sur les critères de conception des systèmes utilisant l'eau [Ucar A. 2005].

Un étang solaire est un moyen de stockage d'énergie thermique basé sur un phénomène de stratification d'eau contenant une quantité variable de sel. Le fond sombre de l'étang absorbe l'énergie solaire et chauffe l'eau fortement chargée en sel. Celle-ci, plus lourde que l'eau moins chargée, reste au fond; il n'y a pas de mouvement de convection, elle reste isolée de la surface (où elle aurait tendance à s'évaporer) par l'eau de surface, moins chargée en sel. L'eau du fond peut dépasser 80°C alors que l'eau de surface reste à 30°C [Velmurugan V. et al. 2008]. Ainsi, l'énergie solaire peut être stockée pendant longtemps avec une perte de chaleur beaucoup plus basse qu'un réservoir de stockage d'eau. Pendant la phase d'hiver, l'eau au fond de l'étang solaire peut être utilisée pour chauffer les bâtiments.

Les substituts les plus fréquemment proposés pour l'eau sont des huiles à base de pétrole et de sels fondus. Les capacités calorifiques massiques sont de 25 à 40% de celle de l'eau. Cependant, ces substituts ont de plus basses pressions de vapeur que l'eau et sont capables de fonctionner à des températures élevées (supérieures à 300°C). Les huiles sont limitées à moins de 350 °C pour des raisons de stabilité et de sécurité et peuvent être très coûteuses. Quelques mélanges de sels minéraux en fusion ont été considérés pour les hautes températures (300°C et plus). Les caractéristiques de ces matériaux peuvent être trouvées dans la Table 1-1 [Pilkington Solar GmbH International, 2000].

Stockage par des solides

L'énergie peut être stockée dans des roches ou des galets contenus dans des récipients isolés. Ce type de stockage est très souvent utilisé pour des températures jusqu'à 100°C en lien avec des capteurs solaires. Il est de conception simple et relativement peu coûteux. Typiquement, la taille caractéristique des morceaux de roche utilisés varie de 1 à 5 cm. Une règle approximative pour le dimensionnement est d'utiliser de 300 à 500 kg de roche par mètre carré de surface de capteurs solaires pour le chauffage des locaux. Des roches peuvent également être utilisées sur une grande gamme de températures supérieures à 1000°C [Hasnain S. M. 1998]. L'oxyde de magnésium (magnésie), l'oxyde d'aluminium (alumine) et d'oxyde de silicone sont des matériaux réfractaires, et ils sont également appropriés pour le stockage de chaleur sensible à haute température. Les propriétés des matériaux solides de stockage sont présentées Table 1-2.

R.1.2 Stockage par chaleur latente

Dans le stockage par chaleur latente, le principe est que lorsque de la chaleur est fournie à la matière, elle change de phase de l'état solide à l'état liquide pour le stockage de la chaleur sous forme de chaleur latente de fusion ou de liquide à vapeur sous forme de chaleur latente de vaporisation. Lorsque la chaleur emmagasinée est extraite par une charge, le matériel subit

à nouveau un changement de sa phase de liquide à solide ou de la vapeur à liquide. La chaleur latente de transformation d'une phase solide à liquide est faible. Les transitions solide-vapeur et liquide-vapeur impliquent de grandes quantités de chaleur de transformation, mais le grand changement de volume correspondant rend le système complexe et peu pratique. Les transformations solide-liquide par contre impliquent des changements de volume relativement faibles. Ces matériaux sont disponibles dans une large gamme de températures de transition.

Les matériaux à utiliser pour le stockage d'énergie thermique doivent avoir une grande chaleur latente et une grande conductivité thermique. Ils doivent avoir une température de fusion adaptée à leur utilisation pratique et être chimiquement stables, peu coûteux, non toxiques et non corrosifs. La Figure 1-3 montre la relation entre la température de fusion et la chaleur de fusion de ces matériaux [Hauer A.[2] et al. 2002]. Des listes détaillées de la plupart des matériaux qui peuvent être utilisés pour le stockage de chaleur latente sont indiquées dans la Table 1-3 [Agyenim et al. 2010].

Beaucoup des matériaux de stockage par chaleur latente ont une faible conductivité thermique, et donc besoin d'une grande surface d'échange de chaleur. D'autres sont corrosifs et nécessitent des matériaux de réservoirs spéciaux. Les matériaux de stockage par chaleur latente sont plus chers que les matériaux de stockage par chaleur sensible généralement utilisés, comme l'eau et les roches. En raison de son coût élevé, le stockage de chaleur latente est donc plus susceptible de trouver une application lorsque:

1. Une haute densité énergétique ou une haute capacité énergétique volumique est souhaitée, par exemple, dans un habitat où l'espace est très coûteux, ou dans les transports où le volume et le poids doivent être réduits au minimum,

2. La charge est telle que l'énergie est nécessaire à une température constante ou dans une petite plage de températures,

3. La taille du stockage est faible. Un stockage qui a un petit volume a une surface spécifique élevée, donc le coût des parois est relativement élevé. La compacité est donc très importante afin de limiter les coûts d'investissement.

R.1.3 Stockage par réaction chimique

Le principe du stockage de chaleur par réaction chimique est A+B ⇔ AB + chaleur.

Au cours de la phase d'été, le composé AB est séparé en composants A et B par l'action de l'énergie solaire. A et B peuvent être stockés séparément pendant la phase de stockage. Pendant la phase d'hiver, A et B sont mis en contact pour la réaction et AB est formé. La chaleur de réaction est libérée pour le chauffage des logements ou d'autres usages. La capacité de stockage dépend de la chaleur de la réaction.

Pour ce type de stockage, il est nécessaire que les réactions chimiques en jeu soient totalement renversables. La chaleur produite par le capteur solaire est utilisée pour exciter une réaction chimique endothermique. Si cette réaction est totalement renversable, de la chaleur peut être récupérée complètement par la réaction inverse. Souvent, des catalyseurs sont nécessaires

pour libérer la chaleur. Cela est d'autant plus avantageux que la réaction peut alors être contrôlée par le catalyseur [Pilkington Solar International GmbH, 2000].

Les avantages fréquemment cités du stockage d'énergie thermique par réaction sont leurs fortes densités de stockage de l'énergie et une durée indéfiniment longue de stockage à température ambiante. Leurs inconvénients peuvent comprendre : la complexité, des incertitudes sur les propriétés thermodynamiques des composants de la réaction et de la cinétique de réactions dans le cadre d'un large éventail de conditions d'exploitation, un coût élevé, la toxicité et l'inflammabilité.

Bien que le stockage d'énergie thermique par des réactions ait plusieurs avantages d'un point de vue thermodynamique, leur développement est à un stade très amont. À ce jour, aucun prototype viable n'a été construit. Le Table 1-4 présente plusieurs réactions qui ont été étudiées pour être utilisées comme matériaux de stockage chimiques [Van Berkel J. 2005].

R.1.4 Stockage par sorption

La sorption peut être définie comme un phénomène de fixation ou de capture d'un gaz ou d'une vapeur (sorbat) par une substance à l'état condensé (solide ou liquide) (sorbant) [Hauer A.[3] 2007]. La sorption peut impliquer à la fois l'absorption et l'adsorption [Aveyard R. & Haydon D.A. 1973]. L'absorption est définie comme un phénomène dans lequel un liquide ou un gaz entre en liaison avec un solide ou un liquide. Toutefois, dans le cas des applications de stockage, ce terme est généralement relatif à l'absorption d'un gaz par un liquide (absorbant). De la même manière, l'adsorption est généralement utilisée pour désigner un phénomène de liaison d'un gaz sur une surface d'un matériau solide poreux ou, dans une acception plus large du terme, se réfère à un phénomène de surface: une liaison d'un gaz ou d'un liquide d'un composant à la surface d'une autre substance [Srivastava N.C. et al. 1998].

Le principe de stockage par sorption est également AB + chaleur ⇔ A + B.

A / B est appelé une paire de travail ou un couple sorption. Sous l'influence d'un apport de chaleur, un composé AB est dissocié en composants A et B qui peuvent être stockés séparément (phénomène endothermique). Lorsque A et B sont mis en contact, le composant AB est formé avec un dégagement de chaleur (phénomène exothermique). L'énergie peut donc être stockée avec des pertes thermiques négligeables puisque la chaleur n'est pas maintenue dans une forme sensible ou latente, mais comme un potentiel [Kato Y. 2007].

Les matériaux choisis jouent un rôle clé dans le stockage par sorption. Un matériau approprié peut stocker l'énergie sans perte de chaleur et est capable de libérer cette énergie immédiatement lorsque cela est nécessaire. Il y a un grand nombre de matériaux qui pourraient être utilisés pour la sorption en considérant uniquement le principe thermodynamique de réactions réversibles [Hauer A.[3] 2007]. Certains critères techniques, économiques ou écologiques conduisent à une plus grande restriction. En effet, les critères de sélection habituels des matériaux utilisés dans les machines à sorption sont [Visscher K. 2004]:

- une grande affinité du sorbat pour le sorbant: cela a un effet sur le taux d'ab/adsorption, ce qui est important pour une densité importante de puissance utilisable:
- Une plus grande volatilité du sorbat (que de l'absorbant);
- Une grande densité de stockage;
- Une conductivité thermique élevée (en particulier pour l'adsorption);
- Une température basse pour la régénération (chargement);
- La neutralité vis-à-vis de l'environnement, la non-toxicité, un faible potentiel d'effet de serre et d'appauvrissement de la couche d'ozone;
- la non-corrosivité;
- le coût.

Les couples qui ont été étudiés pour les systèmes de stockage d'énergie thermique sont:

- Solide-gaz (adsorption)

Zéolites/H_2O: Hauer a rapporté dans ses résultats expérimentaux que la capacité de stockage par la zéolite synthétique 13X est de 124 kWh/m^3 avec un COP (coefficient de performance) de 0,9 pour le chauffage et est de 100 kWh/m^3 avec un COP de 0,86 pour le refroidissement [Hauer A.[1] 2002]. Des zéolithes naturelles pourraient être utilisées comme matériau de stockage au lieu de la zéolite 13X synthétique lorsque la température de chauffage est inférieure à 100°C.

Silicagel/H_2O: La densité de stockage du silicagel est jusqu'à environ 4 fois celle de l'eau (25/85°C) [Faninger G. 2004]. Le silicagel a été utilisé pour des systèmes de stockage d'énergie thermique par AEE-INTEC (Institut des technologies durables, Autriche) [Jaehnig D. et al. 2006] dans une série d'études. Ils ont obtenu expérimentalement environ 50 kWh/m^3 de capacité de stockage, alors qu'ils devaient théoriquement atteindre une densité de stockage de 200-300 kWh/m^3.

Liquide-gaz (absorption)

NaOH/H_2O: Un calcul effectué pour une maison unifamiliale selon la norme maison passive résulte dans un volume de stockage total de 7 m^3 [Weber RDV. 2008]. La température d'absorption maximale atteignable est de 95°C et la température de condensation minimale est de 13°C. Cependant, des précautions particulières doivent être prises lorsque l'on travaille avec de la soude caustique en raison de son caractère très corrosif.

LiCl/H_2O: Sur la base des résultats présentés par ClimateWell (en Suède) [Bales C.[2] 2008], cette paire n'est pas appropriée pour un stockage saisonnier, non pas à cause de sa densité de stockage (253 kWh/m^3 LiCl), qui est 2,7 fois plus élevée que celle de l'eau (25/85 °C), mais à cause du coût élevé de ce sel (environ 3600 EURO/m^3).

R.1.5 Conclusion

Ce chapitre a présenté les informations disponibles dans la littérature concernant le stockage d'énergie thermique solaire, en mettant l'accent sur la classification des concepts de stockage et la description des matériaux utilisés. Les conclusions suivantes peuvent être tirées:

1. Le développement d'un système de stockage thermique efficace et rentable est essentiel pour le développement futur de l'énergie solaire.

2. Selon les matériaux de stockage, les systèmes de stockage sont classés en tant que stockage par chaleur sensible, par chaleur latente, par réaction ou par chaleur de sorption. Seuls les systèmes par chaleur sensible ont été effectivement utilisés dans des stockages d'énergie solaire, bien que d'autres méthodes soient possibles et offrent des avantages.

3. Le stockage de chaleur sensible par des solides a été étudié et testé. Le faible coût de la matière solide utilisée doit contrebalancer l'augmentation du coût de la conception du stockage de chaleur par rapport aux systèmes avec du liquide, en particulier concernant l'échangeur de chaleur nécessaire.

4. Le stockage de la chaleur latente est une technologie prometteuse, car elle une apporte une plus grande densité de stockage et une température de fonctionnement presque constante. Plusieurs matériaux ont été analysés et identifiés.

5. La technologie de stockage chimique et de sorption est également prometteuse, mais elle est encore moins développée que la technologie par chaleur latente. Des recherches plus approfondies sont encore nécessaires pour son développement.

R.2 Stockage inter-saisonnier d'énergie solaire par différents couples d'absorption

D'après l'étude bibliographique précédente, le stockage par absorption est avantagé par sa faible perte de chaleur et sa capacité de stockage élevée. Même si la capacité de stockage concernée est inférieure à celle du stockage par réaction chimique, compte tenu de la faible température nécessaire pour l'énergie solaire, le stockage par absorption semble être une méthode appropriée. Dans ce chapitre, un procédé de stockage inter-saisonnier d'énergie solaire par absorption sera introduit et sept couples absorbat/absorbant seront étudiés pour ce système.

R.2.1 Description du procédé et modèle statique

R.2.1.1 Description du procédé

Les différents composants du système de stockage inter-saisonnier d'énergie solaire peuvent être trouvées dans la Figure 2-1.

Pendant la phase d'été (désorption), la solution pauvre (avec une faible fraction massique d'absorbant) dans le réservoir de solution est transportée vers le générateur où elle est chauffée par l'énergie solaire (Q_d). L'absorbat de la solution est vaporisé et transféré vers le condenseur, où sa chaleur latente (Q_c) est libérée dans l'environnement ou utilisée pour préchauffer l'eau chaude sanitaire. L'absorbat condensé est stocké dans le réservoir d'absorbat. La solution riche (avec une fraction massique d'absorbant élevée) qui est produite dans le générateur est transférée au réservoir de solution.

Au cours de la période inerte de stockage, la solution est stockée dans le réservoir de solution et l'absorbat liquide dans le réservoir d'absorbat. Les températures de la solution et de l'absorbat varient en fonction de la température ambiante.

Pendant la phase d'hiver (absorption), l'absorbat est transféré du réservoir d'absorbat à l'évaporateur, où il est vaporisé par la chaleur géothermie à basse température (Q_e). Suivant l'équilibre thermodynamique de la solution, la vapeur d'absorbat est absorbée par la solution riche dans l'absorbeur. L'énergie thermique (Q_a) est libérée dans l'absorbeur pour répondre aux besoins de chauffage du bâtiment. La solution pauvre dans l'absorbeur après l'absorption est transférée au réservoir de solution.

Le procédé fonctionne sous vide à l'exception des couples qui présentent une pression d'équilibre plus élevée que la pression atmosphérique (comme H_2O/NH_3).

L'innovation dans ce procédé est que la solution peut atteindre le point de cristallisation, ce qui est généralement évité dans les machines frigorifiques à absorption en raison du possible blocage de circulation des fluides. La capacité de stockage peut ainsi être augmentée en raison de l'augmentation de la fraction massique de l'absorbant dans la solution riche à la fin de la phase d'été, mais la complexité de la conception du réservoir de solution et de l'absorbeur est augmentée en raison de la présence de cristaux.

R.2.1.2 Modèle statique

Un modèle statique a été développé pour évaluer la faisabilité et la performance du système. Une représentation du cycle du procédé peut être trouvée avec l'exemple du couple d'absorption $CaCl_2/H_2O$ sur le diagramme pression-température-fraction massique dans la Figure 2-2 (sans cristal) et la Figure 2-3 (avec cristallisation).

L'état E est l'eau pure à l'évaporateur. La température de l'état E (T_e) est choisie à 10°C, qui représente la température de l'énergie géothermique au cours de la phase d'hiver. L'état C est l'eau pure dans le condenseur. La température de État C (T_c) est choisie à 30°C, qui représente la température ambiante pendant la phase d'été.

L'état 1 est la solution pauvre dans le réservoir de solution pendant la phase de désorption (phase d'été). La température de l'état 1 (T_1) est la température de stockage qui est également choisie à 10°C. La solution est chauffée de l'état 1 à l'état 2 par l'énergie solaire, qui vient du capteur solaire. De l'état 2 à l'état 3, l'énergie solaire est constamment utilisée pour chauffer la solution. L'absorbat est désorbé de la solution et condensé dans le condenseur à 30°C (État C). L'état 3 est la solution riche après la désorption. La fraction massique de l'absorbant à l'état 3 est choisie de manière qu'il n'y a pas de cristaux formés lors de la phase de stockage de l'état 3 à l'état 5. L'état 5 est la solution dans le stockage à la température (T_5) de 10°C, qui est représente la température du stock à la fin de la phase d'hiver. La température de l'état 3 nécessaire est T_3 = 72°C, ce qui peut facilement être atteint par des capteurs solaires. Au cours de la phase intermédiaire de l'été à l'hiver, la température de la solution à l'état 3 diminue avec la température ambiante jusqu'à l'état 5. Pendant la phase d'hiver, l'eau est évaporée par l'énergie géothermique à basse température (10°C par exemple) dans l'évaporateur (état E). La solution à l'état 5 absorbe de la vapeur venant de l'évaporateur. La chaleur d'absorption est libérée pour chauffer l'eau qui est utilisée dans un système de chauffage au sol à la température minimale T_1 = 20°C. La fraction massique de la solution diminue et la pression augmente jusqu'à l'état 6. L'état 6 est la solution pauvre après la désorption. À la fin de la phase d'absorption, la solution à l'état 6 retourne dans le stockage à l'état 1 à la même concentration.

Dans le cycle avec apparition de cristal (Figure 2-3), la fraction massique de l'absorbant à l'état 3' est supérieure à celle à l'état 3. Pendant la transition de l'été à l'hiver, la ligne isostère franchit la ligne de cristallisation à l'état 4, et le cristal apparaît dans le réservoir de stockage. De l'état 4 à l'état 5, le cristal est continuellement formé en raison de la diminution de la température de stockage.

Le besoin en énergie solaire pendant la phase d'été Q_d est $Q_{1\to3}$ ou $Q_{1\to3'}$. L'énergie qui est libérée à l'échangeur de chaleur pour chauffer le bâtiment au cours de la phase d'absorption Q_a est $Q_{5\to6}$.

Sept couples d'absorption, $CaCl_2/H_2O$, Glycérine/H_2O, KOH/H_2O, $LiBr/H_2O$, $LiCl/H_2O$, $NaOH/H_2O$ et H_2O/NH_3 ont été analysés pour ce système.

R.2.2 Principes pour le choix des couples d'absorption

Une liste de critères de sélection des matériaux appropriés est [IEA task 32, 2008]:

(A) La capacité et le rendement du stockage.

La capacité de stockage est définie comme l'énergie qui est libérée au cours de la phase d'absorption par kilogramme d'absorbant. Le rendement du stockage est défini comme la production d'énergie de l'absorption, divisée par la consommation d'énergie thermique de la désorption. Le résultat du calcul de la capacité de stockage et du rendement de sept couples à différentes conditions de fonctionnement sera présenté dans la section R.2.3.

(B) Les contraintes en température pour les capteurs solaires (désorption).

Les contraintes en température pour les capteurs solaires dépendent des caractéristiques du couple. C'est une caractéristique très importante car l'efficacité des capteurs solaires diminue rapidement avec l'augmentation de la différence de température entre l'eau dans le capteur solaire et l'atmosphère en raison des pertes de chaleur.

Un exemple de la pression de sept couples et de l'eau pure en fonction de la température est présenté dans la Figure 2-4. La fraction massique de la solution de $CaCl_2/H_2O$, KOH/H_2O, $LiBr/H_2O$, $LiCl/H_2O$, $NaOH/H_2O$ est choisie comme leur solubilité à 10°C. La fraction massique de Glycérine/H_2O et H_2O/NH_3 est choisie à 90% car il est très difficile d'augmenter la fraction massique jusqu'à 100%.

Sauf pour le couple H_2O/NH_3, à une pression de condensation donnée (la pression d'équilibre liquide-vapeur de l'eau), la température nécessaire pour la chaleur fournie par le capteur solaire des six autres couples peut être trouvée dans la Figure 2-4: la température pour le couple $CaCl_2/H_2O$ est inférieure à celle du couple $NaOH/H_2O$, inférieure au couple Glycérine/H_2O, inférieure au couple KOH/H_2O, inférieure au couple $LiCl/H_2O$ elle-même inférieure au couple $LiBr/H_2O$.

Pour le couple H_2O/NH_3, NH_3 est l'absorbat du processus. La contrainte de température pour le capteur solaire est la température de la solution (à 0,1 kg NH_3/kg de solution) à la pression d'équilibre liquide-vapeur de NH_3 à la température de condensation. Le besoin thermique du capteur solaire atteint 120°C même lorsque la température de condensation est de 0°C.

(C) L'absorption à une température suffisamment élevée pour le plancher chauffant

La température maximale d'absorption des couples peut également être trouvée dans la Figure 2-4 dans les mêmes conditions de fraction massique que pour le critère (B). A une température d'évaporation donnée, l'ordre des températures maximales d'absorption est: couple $CaCl_2/H_2O$ inférieur au $NaOH/H_2O$ inférieur au Glycérine/H_2O inférieur au KOH/H_2O inférieur au $LiCl/H_2O$, inférieur au $LiBr/H_2O$. C'est le même ordre que la contrainte de température pour le capteur solaire présentée en (B).

Selon les critères (B) et (C), il est difficile de dire quel est le couple le plus approprié pour le système de stockage inter-saisonnier, car plus la température de l'absorption pour le chauffage

du bâtiment est élevée, plus le besoin de température du capteur solaire au cours de l'été l'est aussi. Cependant, certains couples peuvent être sélectionnés pour des situations spécifiques. Par exemple, si le besoin de température de l'absorption est à 30°C lorsque la température d'évaporation est de 10°C (indiqué par la ligne rouge pointillée Figure 2-4), le $CaCl_2/H_2O$, $NaOH/H_2O$ et Glycérine/H_2O sont inutilisables parce que leur température maximale d'absorption est inférieure à 30°C. KOH/H_2O pourrait être choisi parce qu'il a le besoin minimal de température pour le capteur solaire parmi les couples qui peuvent satisfaire au besoin de température pour l'absorption.

(D) Un couple facile à manipuler - de préférence non toxique

Les critères de sécurité des couples donnés dans la Table 2-1 proviennent de la NFPA 704 [NFPA704, 2007] qui est un standard mis à jour par la société américaine National Fire Protection Association. Chacun de ces critères : santé, inflammabilité et réactivité est évalué sur une échelle de 0 (aucun risque; substance normale) à 4 (risque important).

Le risque de corrosion est un critère important de la conception du système. La corrosion de l'acier inoxydable 304 de sept couples est connue quand il n'y a pas d'agitation et pas d'aération [Craig et Anderson, 1995]. Le risque de corrosion augmente avec la fraction massique et la température. Pour le couple $CaCl_2/H_2O$, l'acier inoxydable 304 est résistant à la corrosion lorsque la fraction massique est d'environ 10%. Mais lorsque la fraction massique est d'environ 28%, la corrosion est d'environ 0,003 mm/an à 79°C. Pour la Glycérine/H_2O, l'acier inoxydable 304 est résistant à la corrosion à toute fraction massique jusqu'à la température d'ébullition. Pour le couple KOH/H_2O, la corrosion est d'environ 0,003 mm/an à la température de 93°C et une fraction massique de 20% à 50%. Pour le couple $LiBr/H_2O$, la corrosion est d'environ 0,008 mm/an à la température de 50°C et la fraction massique de 50%. Pour le couple $LiCl/H_2O$, la corrosion est d'environ 0,003 mm/an à la température de 116°C et la fraction massique de 30%. Pour le $NaOH/H_2O$, la corrosion est d'environ 0,003 mm/an à la température de 65°C et la fraction massique de 50%. Mais la corrosion augmente à 0,68 mm/an à des températures de 90°C à 143°C et la fraction massique de 70%. Pour le couple H_2O/NH_3, l'acier inoxydable 304 est résistant à la corrosion à toute fraction massique jusqu'à la température d'ébullition.

(E) Un faible coût d'investissement pour le couple d'absorption

Par rapport aux systèmes de stockage à court terme, la masse de solution dans le stockage est évidemment moins importante que pour un système de stockage inter-saisonnier à cause de la quantité d'énergie qui doit être stockée. Les coûts d'investissement pour les couples doivent donc être pris en compte. Les prix de sept couples sur le marché chinois [Alibaba, 2008] d'une même pureté supérieure à 99% sont indiqués dans la Table 2-2.

R.2.3 Simulation statique de la performance des couples d'absorption

L'analyse de la capacité de stockage et du rendement de sept couples est effectuée aux conditions de fonctionnement suivantes (Table 2-3).

La température de stockage avant l'absorption (état 5) est choisie à 5°C et 10°C. La température d'évaporation (état E) est choisie à 5°C et 10°C. La température de l'absorption (état 6) est variée de 20 à 45°C pour répondre aux besoins de température pour le chauffage du bâtiment. Le ratio de la cristallisation (R) est défini comme la masse de cristal à l'état 5 divisé par la masse de solution liquide au même état. R = 0 veut dire qu'il n'y a pas de cristaux à l'état 5 et la solution à cet état est saturée. R = 4 signifie que, au début de l'absorption, la quantité de solution liquide est 20% de la masse totale du stockage. Une proportion de 20% de liquide est suffisante pour le démarrage de la phase d'absorption.

Capacité de stockage

La capacité de stockage de sept couples en fonction de la température d'absorption est présentée Figure 2-5. Toutes les conditions proposées dans la Table 2-3 sont présentées dans la figure, sauf les conditions qui sont impossibles pour un couple spécifique.

Pour le couple $CaCl_2/H_2O$, le processus de stockage est possible lorsque la température d'évaporation est de 10°C, mais impossible lorsque la température d'évaporation est de 5°C. La plage de température possible d'absorption est de 20 à 24°C. Pour le couple Glycérine/H_2O, le processus de stockage est disponible à toutes les conditions étudiées, mais la capacité de stockage est faible. Pour les couples KOH/H_2O, $LiBr/H_2O$ et $LiCl/H_2O$, le processus de stockage est disponible à toutes les conditions étudiées. La plage de température possible d'absorption est de 25 à 35°C. Pour le couple $NaOH/H_2O$, le processus de stockage est possible seulement pour les six points qui sont présentés dans la Figure 2-5. Pour le couple H_2O/NH_3, le processus de stockage est disponible à toutes les conditions étudiées. La plage de température possible d'absorption est de 20 à 40°C.

La capacité de stockage est augmentée avec l'apparition de cristaux (R = 4 dans la Figure 2-5) par rapport à l'absence de cristal (R = 0) aux mêmes conditions de fonctionnement. La capacité de stockage diminue avec la température de l'absorbeur (Figure 2-6) et augmente avec la température de l'évaporateur (Figure 2-7) et la température du réservoir de stockage avant la phase d'absorption (état 5).

Rendement

Le rendement de sept couples en fonction de la température d'absorption est présenté Figure 2-8. À une condition de fonctionnement donnée, le couple $LiCl/H_2O$ a le meilleur rendement par rapport aux autres couples.

Le rendement est diminué à des températures d'absorption faibles (état 6) et augmenté à des températures d'absorption élevées avec apparition de cristaux. Le rendement diminue avec la température d'absorption et augmente avec la température d'évaporation et la température du stockage avant l'absorption.

R.2.4 Points d'évaluation principaux

Afin de comparer les caractères et les performances des sept couples, les points d'évaluation principaux sont résumés dans la Table 2-4 aux mêmes conditions de fonctionnement:

- Température du condenseur, T_c = 30°C;
- Température de l'absorbeur, T_1 = 20°C;
- Température du stockage avant l'absorption, T_5 = 10°C;
- Température de l'évaporateur, T_e = 10°C.

Selon les résultats de la Table 2-4, le KOH/H_2O, LiCl/H_2O, LiBr/H_2O et NaOH/H_2O ont d'excellentes performances de capacité de stockage. Le KOH/H_2O et NaOH/H_2O sont avantagés par leur bas prix, mais sont désavantagés par les questions de sécurité. La capacité de stockage et le prix du H_2O/NH_3 est acceptable. Mais il est désavantagé par l'exigence en température de l'énergie solaire (> 150°C) et les questions de sécurité. Le couple $CaCl_2$/H_2O est le moins cher, mais sa capacité de stockage est faible, de sorte que le coût d'investissement pour les réservoirs peut être plus élevé que pour les autres couples. Comparé avec d'autres couples, la capacité de stockage du couple Glycérine/H_2O est trop faible pour qu'il soit utilisé dans un système de stockage à absorption.

R.2.5 Conclusion

Cette partie vise à développer un système de stockage inter-saisonnier de l'énergie solaire pour le bâtiment. Les performances et les caractéristiques thermodynamiques de sept couples d'absorption, $CaCl_2$/H_2O, Glycérine/H_2O, KOH/H_2O, LiBr/H_2O, LiCl/H_2O, NaOH/H_2O et H_2O/NH_3, ont été étudiées.

La capacité de stockage augmente avec la température de l'évaporateur et la température de stockage avant la phase d'absorption, et diminue avec la température absorbeur. L'apparition de cristaux augmente la capacité de stockage. Inévitablement, la complexité du système sera également augmentée. Après la comparaison des performances de sept couples, le couple KOH/H_2O pourrait être le matériau le plus économique en raison de son faible prix et sa grande capacité de stockage, mais présente des difficultés de sécurité. Pour le couple $CaCl_2$/H_2O, le coût d'investissement pour les réservoirs peut être plus élevé que pour les autres couples en raison de sa faible capacité de stockage. Toutefois, compte tenu de son prix et du besoin faible en température pour les capteurs solaires, il est un candidat possible. Le couple LiCl/H_2O a d'excellentes performances en capacité de stockage et rendement, son seul inconvénient est son prix très élevé.

R.3 Expérimentation de stockage inter-saisonnier par le couple $CaCl_2/H_2O$

Suite à l'analyse du chapitre 2, le système de stockage inter-saisonnier par absorption semble théoriquement possible. Afin de vérifier la faisabilité du processus, un prototype est construit. Les caractéristiques thermodynamiques et les problèmes du prototype sont analysés dans cette partie.

R.3.1 Conception du prototype

Le schéma du prototype est représenté dans la figure 3-1. Il comprend le réservoir de solution, le réservoir d'eau, le réacteur, un réservoir d'entrée de la solution, les thermostats, la pompe à vide, les circulateurs (C), les pompes de dosage (DP) et les vannes (V). La température (T), la pression (P), le niveau de liquide (m) et le débit (D) sont mesurés dans le prototype.

Les quatre réacteurs: le générateur, le condenseur, l'absorbeur et l'évaporateur sont combinés en un seul réacteur pour simplifier le procédé. Le condenseur et l'évaporateur sont combinés en un seul échangeur qui joue le rôle de condenseur au cours de la phase de désorption et de l'évaporateur au cours de la phase d'absorption. Le générateur et l'absorbeur sont combinés en un seul échangeur qui joue le rôle de générateur pendant la phase de désorption et l'absorbeur au cours de l'absorption. Afin de diminuer la perte de chaleur et la perte de charge au cours du transfert de vapeur d'eau entre l'évaporateur/condenseur et le générateur/absorbeur, ces deux composants sont inclus dans un seul réacteur.

Au cours de la phase de désorption:

La solution pauvre dans le réservoir de solution est transférée par la pompe DP1 au générateur où elle est chauffée par l'échangeur. L'énergie thermique pour la désorption est fournie par le thermostat 2. L'absorbat qui est désorbé de la solution est transféré dans le condenseur où il est condensé grâce à l'échangeur de chaleur. L'énergie de condensation est fournie au thermostat 1. Les vannes V2 et V8 sont fermées. L'absorbat liquide condensé est ensuite transféré dans le réservoir d'eau par la pompe DP3. La solution riche est extraite du générateur vers le réservoir de solution par la pompe DP2.

Au cours de la phase de stockage (transition):

Après la phase de désorption, la température de la solution riche dans le réservoir de solution (T1) est élevée. La solution est circulée entre le réservoir de solution et le générateur et refroidie par l'échangeur de chaleur du générateur. Après la phase transitoire, la température de la solution est inférieure à T12.

Au cours de la phase d'absorption:

La vanne V3 est fermée. L'absorbat dans le réservoir d'eau est transféré par la pompe DP3 à l'évaporateur où il s'évapore grâce à la chaleur du thermostat 1 à basse température. La vapeur d'absorbat est transférée à l'absorbeur. La solution riche dans le réservoir de solution est transférée par la pompe DP1 à l'absorbeur où elle absorbe la vapeur d'absorbat. La chaleur d'absorption est transférée au thermostat 2 par l'échangeur. La solution pauvre est ensuite extraite de l'absorbeur par la pompe DP2.

La masse, le débit, la température, la pression sont mesurés pour une analyse ultérieure. Les données de l'expérimentation sont recueillies par des modules Napac et Agilent et stockées.

R.3.2 Conception des composants du prototype

Le couple choisi pour l'expérimentation est $CaCl_2/H_2O$. Le $CaCl_2$ anhydre est fourni par le Groupe Solvay, qui est le financeur de ce projet. La pureté du $CaCl_2$ est d'environ 95%. Sa composition se trouve dans la Table 3-1.

Les caractéristiques de corrosion du couple d'absorption est une donnée importante pour la conception du prototype. Les données de corrosion de la solution $CaCl_2/H_2O$ pour différents matériaux peuvent être trouvées dans la Table 3-2. Le matériau choisi pour le système est l'acier inoxydable 316 L (SS-316), qui présente un bon compromis résistance à la corrosion / coût.

Les paramètres des réservoirs se trouvent dans la Table 3-3. Le réservoir de solution est d'environ 150 L. Le réservoir d'eau est d'environ 50 L. Il est beaucoup plus petit que le réservoir de solution parce que seulement une petite partie de l'eau sera désorbée de la solution. Le volume du réacteur est d'environ 130 L. Il est conçu pour être suffisamment grand pour contenir les distributeurs et les échangeurs intérieurs. Le récupérateur d'eau dans le réacteur est utilisé pour stocker temporairement l'eau qui est distribuée dans l'évaporateur ou l'eau condensée dans le condenseur. Le volume du récupérateur d'eau est d'environ 5 L. Tous les composants sont en acier inoxydable 316L, sauf le réservoir d'eau. Comme il n’est pas en contact avec la solution, l'acier inoxydable 304L est suffisant pour ce composant. L'épaisseur des réservoirs est calculée par un bureau d'études extérieur.

Les échangeurs de chaleur qui sont utilisés dans le réacteur ont 16 tubes avec ailette hélicoïdale à l'extérieur. Ils sont représentés Figure 3-2. L'eau provenant du thermostat s’écoule à l'intérieur des tubes. Elle est distribuée par le distributeur qui est relié à l'entrée de l'échangeur et collectée par le distributeur qui est connecté à la sortie de l'échangeur. Comme les distances entre l'entrée et la sortie pour tous les tubes sont uniformes, la différence de débit des 16 tubes sera faible. La solution ou l'absorbat qui doit être chauffé ou refroidi par l'échangeur s'écoule sur les ailettes hélicoïdales extérieures des tubes. L'eau ou la solution est distribuée par un distributeur sur chaque ailette. La surface d’échange pour le transfert de chaleur et de masse est augmentée par ces ailettes hélicoïdales. Le temps de séjour de l'eau ou la solution sur l'échangeur de chaleur est aussi augmenté. Les caractéristiques de l'échangeur peuvent être trouvées dans la Table 3-4.

Le distributeur qui est utilisé pour la répartition de la solution ou de l'eau sur l’ailette hélicoïdale de l'échangeur est représenté sur la Figure 3-3. Chaque point de sortie du distributeur correspond à une ailette hélicoïdale de l'échangeur de chaleur.

Le plan d'ensemble du prototype est présenté sur la Figure 3-4.

R.3.3 Planning de l’expérimentation

Les conditions de fonctionnement du prototype sont présentées dans Table 3-6:

Au début de l'expérience, 207 kg de solution pauvre avec une fraction massique de 0,369 kg de sel/kg de solution est stocké dans le réservoir de solution. Dans le réservoir d'eau, il n'y a rien. Au cours des expérimentations, la température de l'eau à l'entrée de l'échangeur de chaleur du générateur est réduite de 80°C à 70°C et la température de l'eau à l'entrée de l'échangeur de l'évaporateur diminue de 15°C à 10°C (Cas n°1 → Cas n°2) pour quantifier leur influence sur la performance de ce système.

R.3.4 Résultats d'expérimentation

Avant l'expérimentation, la fraction massique de la solution est calculée en fonction de sa densité (Table 3-7). La relation entre la densité, la température et la fraction massique peut être trouvée dans l'Annexe 7. La fraction massique moyenne de la solution est 0,345 kg $CaCl_2$/kg solution.

R.3.4.1 La phase de désorption

Au cours de la phase de désorption, la puissance $\dot{Q}_d$ et l'énergie Q_d de désorption sont calculés par le bilan énergétique sur l'eau dans l'échangeur du générateur (Eq.R-1 et Eq.R-2):

$$\dot{Q}_d = \dot{m}_{exg} \cdot \left[h_{iexg}(T_{iexg}) - h_{oexg}(T_{oexg}) \right] \quad \text{Eq.R-1}$$

$$Q_d = \int \dot{Q}_d \, dt \quad \text{Eq.R-2}$$

$\dot{m}_{exg}$ est le débit d'eau de l'échangeur dans le générateur, h_{iexg} est l'enthalpie de l'eau à l'entrée de l'échangeur à sa température T_{iexg}, h_{oexg} est l'enthalpie de l'eau à la sortie de l'échangeur à sa température T_{oexg}.

La puissance $\dot{Q}_c$ et l'énergie Q_c de condensation sont calculées par le bilan énergétique sur l'eau dans l'échangeur du condenseur avec des équations similaires à Eq.R-1 et Eq.R-2.

Les résultats de l'expérimentation de la phase de désorption peuvent être trouvés dans la Table 3-8. Les cas 1-1 et 1-2 sont des phases de désorption selon les conditions de fonctionnement du cas 1 dans la Table 3-6. Les cas 2-1 et 2-2 sont les phases de désorption selon les conditions de fonctionnement du cas 2 dans la Table 3-6.

Au cours du cas 1-1, 19,5 kg d'eau est désorbé de la solution. La masse de la solution passe de 207.5 kg à 188 kg. La fraction massique est augmentée en conséquence de 0,345 kg $CaCl_2$/kg solution à 0,381 kg $CaCl_2$/kg solution. La masse et la fraction massique sont calculées grâce au niveau d'eau dans le réservoir d'eau qui est présenté sur la Figure 3-6. Le niveau d'eau augmente pendant la phase de désorption parce que l'eau qui se condense dans le condenseur est transférée au réservoir d'eau. L'augmentation est discontinue parce que la pompe fonctionne de façon discontinue en fonction du niveau de l'eau dans le condenseur.

L'évolution de la température du réservoir de solution (T_{sd}) et la température du réservoir d'eau (T_{wd}) sont présentées sur la Figure 3-7.

Au cours de la phase de désorption, T_{sd} augmente (de 41,7 à 66,4°C) parce que la solution est chauffée par l'échangeur dans le générateur. T_{wd} augmente de 21,2 à 30°C au cours de la phase de désorption parce que l'eau qui se condense dans le condenseur est transférée au réservoir d'eau. Mais cette augmentation est discontinue car la pompe qui transfère l'eau du condenseur au réservoir d'eau fonctionne de façon discontinue. La température de l'eau dans le réservoir d'eau augmente rapidement lorsque l'eau dans le condenseur est transférée au

réservoir d'eau et diminue lentement aux autres moments à cause de la perte de chaleur du réservoir vers l'environnement.

Les évolutions de la pression du réservoir d'eau, du réservoir de solution et du réacteur sont présentées Figure 3-8. L'évolution de la température de l'eau à l'entrée (T_{iexg}) et la sortie (T_{oexg}) de l'échangeur du générateur et la température de l'eau à l'entrée (T_{iexc}) et la sortie (T_{oexc}) de l'échangeur du condenseur du cas 1-1 peut être trouvée Figure 3-9. Ces températures sont utilisées pour le calcul de la puissance et l'énergie qui est utilisée pour la désorption et la condensation (Figure 3-10).

En général, la puissance de l'échangeur dans le générateur diminue au cours de la désorption. C'est principalement parce que la température de la solution dans le réservoir de solution augmente au cours de la désorption, la différence de température dans l'échangeur du générateur est donc diminuée. A 3,6 h (Figure 3-8), l'air dans le réservoir d'eau est transféré vers le réacteur en raison de la différence de pression. La puissance des échangeurs dans le générateur et le condenseur diminue rapidement. $\dot{Q}_d$ diminue de 3,35 kW à 3,05 kW (environ 9%) et $\dot{Q}_c$ diminue de 1,65 kW à 1,1 kW (environ 33%). À 7,2 h, comme la pression dans le réservoir d'eau est diminuée par l'utilisation de la pompe à vide, l'air dans le réacteur est transféré au réservoir d'eau en raison de la différence de pression. $\dot{Q}_d$ augmente de 2,5 kW à 3,1 kW (environ 24%) et $\dot{Q}_c$ augmente de 1,05 kW à 3 kW (environ 185%). L'effet de l'air sur l'efficacité de la désorption est remarquable.

L'énergie fournie par l'échangeur dans le générateur pour la désorption Q_d est de 23,5 kWh. L'énergie rejetée par l'échangeur de chaleur dans le condenseur Q_c est de 9,9 kWh.

Pour le cas 1-2, 16 kg d'eau est désorbé de la solution. La masse de la solution passe de 188 kg à 172 kg. La fraction massique est augmentée en conséquence de 0,381 kg $CaCl_2$/kg solution à 0,417 kg $CaCl_2$/kg solution. L'énergie fournie par l'échangeur dans le générateur Q_d est de 26,4 kWh. L'énergie rejetée par l'échangeur de chaleur dans le condenseur Q_c est de 12 kWh.

Par rapport au cas 1-1 et 1-2, la température à l'entrée de l'échangeur de chaleur du générateur (T_{iexg}) est diminuée de 80 à 70°C dans les cas 2-1 et 2-2. La puissance de l'échangeur de chaleur est diminuée par rapport au cas 1 en raison de la diminution de T_{iexg}. Un exemple de la comparaison des cas 1-1 et 2-2 peut être trouvé Figure 3-10.

Au cours du cas 2-1, 1,3 kg d'eau est désorbé de la solution. La fraction massique de la solution est augmentée en conséquence de 0,397 kg $CaCl_2$/kg solution à 0,4 kg $CaCl_2$/kg solution. L'énergie fournie par l'échangeur dans le générateur Q_d est de 10,3 kWh. L'énergie rejetée par l'échangeur dans le condenseur Q_c est de 1,2 kWh. Au cours du cas 2-2, 12,1 kg d'eau sont désorbés de la solution. La fraction massique est augmentée en conséquence passant de 0,4 kg $CaCl_2$/kg solution à 0.428 kg $CaCl_2$/kg solution. L'énergie fournie par l'échangeur dans le générateur Q_d est de 18,2 kWh. L'énergie rejetée par l'échangeur dans le condenseur Q_c est de 6,7 kWh.

R.3.4.2 La phase d'absorption

Au cours de la phase d'absorption, la puissance $\dot{Q}_a$ et l'énergie Q_a d'absorption sont calculées par un bilan énergétique sur l'échangeur de chaleur dans l'absorbeur, similaire à Eq.R-1 et Eq.R-2. La puissance et l'énergie de l'évaporation sont également calculées.

Les résultats d'expérimentation de la phase d'absorption peuvent être trouvés Table 3-9. Les cas 1-3 et 1-4 sont des phases d'absorption suivant les conditions de fonctionnement du cas 1 dans la Table 3-6. Le cas 2-3 est la phase d'absorption suivant les conditions de fonctionnement du cas 2 dans la Table 3-6. Le Case S-1 est un cas particulier. Ses conditions de fonctionnement et résultats seront discutés à la fin.

Au cours du cas 1-3, 3,4 kg d'eau est absorbée par la solution. La masse de la solution passe de 171,8 kg à 175,2 kg. La fraction massique est diminuée en conséquence de 0,417 kg $CaCl_2$/kg solution à 0,41 kg $CaCl_2$/kg solution. La masse et la fraction massique sont calculés par le niveau d'eau dans le réservoir d'eau qui est présenté Figure 3-11. Le niveau d'eau diminue au cours de la phase d'absorption, car l'eau est transférée à l'évaporateur où elle est évaporée dans l'échangeur. La diminution est discontinue parce que la pompe fonctionne de façon discontinue en fonction du niveau de l'eau dans le récepteur de l'évaporateur. À la fin de la phase d'absorption, l'eau qui n'est pas évaporée est retransférée vers le réservoir d'eau.

L'évolution de la température du réservoir de solution (T_{sa}) et la température du réservoir d'eau (T_{wa}) sont présentés Figure 3-12. Les évolutions de la pression dans le réservoir d'eau, le réservoir de solution et le réacteur sont présentées Figure 3-13. L'évolution de la température de l'eau à l'entrée (T_{iexa}) et la sortie (T_{oexa}) de l'échangeur de chaleur de l'absorbeur et la température de l'eau à l'entrée (T_{iexe}) et la sortie (T_{oexe}) de l'échangeur de l'évaporateur du cas 1-3 peut être trouvée Figure 3-14. Ces températures sont utilisées pour calculer la puissance et l'énergie qui est utilisée pour l'absorption et l'évaporation (Figure 3-15).

La puissance est environ 30 W pour l'absorption et environ 40 W pour l'évaporation. Cette puissance est faible. Les raisons de la faible puissance peuvent être trouvées comme suit: l'air dans le réacteur, le dimensionnement de l'échangeur de chaleur et les caractéristiques thermodynamiques du couple $CaCl_2/H_2O$.

L'énergie libérée dans l'échangeur de l'absorbeur Q_a est de 0,31 kWh. L'énergie fournie à l'échangeur dans l'évaporateur Q_c est 0,2 kWh.

Au cours du cas 1-4, 5,2 kg d'eau est absorbée par la solution. La fraction massique est diminuée en conséquence de 0,409 kg $CaCl_2$/kg solution à 0,397 kg $CaCl_2$/kg solution. L'énergie libérée à l'échangeur dans l'absorbeur Q_a est 0,17 kWh. L'énergie fournie par l'échangeur dans l'évaporateur Q_e est 0,14 kWh.

Par rapport au cas 1-3 et 1-4, la température de l'eau à l'entrée de l'échangeur de chaleur dans l'évaporateur (T_{iexe}) passe de 15°C à 10°C dans le cas 2-3 pour vérifier son influence sur la puissance de l'absorption et l'évaporation. Théoriquement, la puissance doit diminuer car la diminution de T_{iexe} diminue la pression d'équilibre de l'eau dans l'évaporateur. La différence entre la pression d'équilibre de l'eau dans l'évaporateur et la pression d'équilibre de la solution dans le générateur est la force d'absorption.

L'évolution de la puissance d'absorption et d'évaporation peut être trouvée Figure 3-17.Selon les résultats obtenus, contrairement à ce qui pouvait être attendu, la puissance ne diminue pas mais augmente par rapport au cas 1-3. La raison est que la pression partielle de l'air dans le réacteur du cas 2-3 est inférieure à celle du cas 1-3. La comparaison de la pression dans le réacteur des cas 1-3 et 2-3 peut être trouvée Figure 3-18. La différence de pression du réacteur est environ 12 mbar. Mais la différence de pression d'équilibre théorique pour l'eau entre 15°C (17,7 mbar) et 10°C (12,2 mbar) est environ 5,5 mbar. Cela signifie que la pression partielle de l'air dans le cas 1-3 est environ 6,5 mbar plus élevée que dans le cas 2-3. L'influence de l'air dans cette expérience est supérieure à l'influence de la température d'évaporation. L'air dans le système est le problème le plus important pour le système présenté de stockage saisonnier par absorption.

Comme le problème de fuites du prototype ne peut pas être résolu dans le temps imparti pour la thèse, afin de diminuer l'influence de l'air dans le réacteur, le cas S-1 est réalisé. Dans cas S-1, T_{iexe} est porté à environ 40°C. Le débit de l'eau dans l'échangeur de chaleur de l'évaporateur est également augmenté, passant de 200 kg/h à 1000 kg/h pour s'assurer que la puissance d'évaporation est suffisante. T_{iexa} est fixé à 30°C. L'équilibre de pression de l'eau à 40°C est de 73,6 mbar. La gamme de pression dans le réacteur dans le cas S-1 est de 40,5 à 87,5 mbar (Figure 3-19). La pression du réacteur est inférieure à la pression d'équilibre de l'eau à 40°C. C'est principalement parce que l'eau dans l'évaporateur ne peut pas être chauffée à la même température que l'eau dans l'échangeur. Mais il est certain que la pression partielle de l'air est diminuée pour cette expérimentation par rapport aux cas présentés plus haut. La puissance de l'échangeur de chaleur dans l'absorbeur ($\dot{Q}_a$) et dans l'évaporateur ($\dot{Q}_e$) est présentée sur la Figure 3-20. La puissance varie de 80 à 560 W pour l'absorption et de 0 à 1080 W pour l'évaporation. La puissance est beaucoup plus élevée que dans les cas 1-3, 1-4 et 2-3.

R.3.5 Conclusion des expérimentations

Un prototype a été construit pour vérifier la faisabilité du système de stockage inter-saisonnier par absorption avec le couple $CaCl_2$-H_2O. Selon les résultats de l'expérimentation et leur analyse, plusieurs conclusions peuvent être trouvées ici:

- La phase de désorption est possible. Au cours de la phase de désorption, l'eau est désorbée de la solution et stockée dans le réservoir d'eau. La puissance de désorption (environ 0,6 à 4 kW) et de condensation (environ 0-3 kW) est acceptable par rapport au dimensionnement du prototype utilisé.

- Il a été vérifié que la présence d'air dans le système peut diminuer la vitesse de transfert de chaleur et de masse dans le système et que son influence sur les performances du système est importante.

- Lorsque la température de l'eau à l'entrée de l'échangeur de chaleur dans l'évaporateur est de 10 ou 15°C, les performances de la phase d'absorption sont faibles. Bien que de l'eau soit absorbée par la solution, la puissance de l'absorption et l'augmentation de la température de l'eau dans l'échangeur de l'absorbeur sont faibles.

- L'air dans le réacteur est la principale cause de la faible puissance d'absorption. L'influence est plus importante que dans la phase de désorption, car la pression d'équilibre de l'eau dans le réacteur en absorption est beaucoup plus faible que dans la phase de désorption. Afin de résoudre le problème de l'air, il est fondamental de s'assurer que le système est parfaitement hermétique.

R.4 Simulation dynamique du prototype avec le couple $CaCl_2/H_2O$

La faisabilité du système de stockage inter-saisonnier par absorption a été vérifiée par l'expérimentation présentée dans le chapitre 3. Mais les résultats expérimentaux sont influencés par plusieurs facteurs: la présence d'air dans le système, la pureté du $CaCl_2$ utilisé, la précision des capteurs, des facteurs humains lors des opérations sur le prototype... Pour une meilleure compréhension du processus, une modélisation dynamique qui permet d'éviter les problèmes posés lors de l'expérience est développée. Le modèle et les résultats de simulation sont présentés dans ce chapitre.

R.4.1 Modèle

Le modèle dynamique est développé selon les paramètres de fonctionnement et de contrôle du prototype et basé sur le couple $CaCl_2/H_2O$.

Les principales hypothèses de la modélisation sont les suivantes:

- L'eau et la solution dans le réservoir d'eau, le réacteur et le réservoir de solution sont toujours à l'état d'équilibre thermodynamique

- Les imitations de transfert de masse ne sont pas pris en compte dans la simulation;

- L'eau dans le réservoir d'eau et la solution dans le réservoir de solution sont homogènes à n'importe quelle position. Il n'y a pas de gradient de température, de pression et de fraction massique dans un réservoir;

- L'eau peut être évaporée ou condensée seulement sur un échangeur de chaleur;

- La masse de solution dans le générateur / absorbeur est supposée constante à 0.

R.4.1.1 Modèle pour la phase de désorption

Le schéma au cours de la phase de désorption est présenté Figure 4-1.

- Dans le générateur, la solution qui vient du réservoir de solution ($\dot{m}_{522}(t)$) est chauffée par l'énergie qui vient du thermostat 2. La vapeur d'eau ($\dot{m}_{23}(t)$) qui est désorbée de la solution est transférée vers le condenseur. La solution après désorption reflue vers le réservoir de solution. La masse de la solution dans le générateur est :

$$\frac{dm_2(t)}{dt} = \dot{m}_{522}(t) - \dot{m}_{252}(t) - \dot{m}_{23}(t) = 0 \qquad \text{Eq.R-3}$$

Le bilan sur le sel $CaCl_2$ dans le générateur est Eq.R-4.

$$\frac{dm_2(t)x_2(t)}{dt} = \dot{m}_{522}(t)x_{522}(t) - \dot{m}_{252}(t)x_{252}(t) \qquad \text{Eq.R-4}$$

Le bilan énergétique dans le générateur est le suivant:

$$\frac{dm_2(t)h_2(t)}{dt} = \dot{Q}_{12}(t) + \dot{m}_{522}(t)h_{522}(t) - \dot{m}_{23}(t)h_{23}(t) - \dot{m}_{252}(t)h_{252}(t) - \frac{dQ_{loss2}(t)}{dt} = 0 \qquad \text{Eq.R-5}$$

La puissance de désorption qui est fournie par l'échangeur dans le générateur $\dot{Q}_{12}(t)$ peut être calculée par le bilan énergétique de l'eau dans l'échangeur:

$$\dot{Q}_{12}(t) = \dot{m}_{12}\left(h_{12}(t) - h_{21}(t)\right) \qquad \text{Eq.R-6}$$

$\dot{Q}_{12}(t)$ peut également être calculée par les performances de transfert de chaleur de l'échangeur:

$$\dot{Q}_{12}(t) = K_{he2}S_{he2}\left(\left(\mathrm{T_{21}}\text{-}\mathrm{T_{522}}\right)\text{-}\left(\mathrm{T_{12}}\text{-}\mathrm{T_{252}}\right)\right)/\mathrm{Ln}\left(\left(\mathrm{T_{21}}\text{-}\mathrm{T_{522}}\right)/\left(\mathrm{T_{12}}\text{-}\mathrm{T_{252}}\right)\right) \qquad \text{Eq.R-7}$$

La perte de chaleur du générateur Q_{loss2} peut être calculée comme suit:

$$\frac{dQ_{loss2}(t)}{dt} = K_2 \cdot s_2 \cdot (T_{252}(t) - T_{atm}(t)) \qquad \text{Eq.R-8}$$

L'équilibre dans le générateur peut être calculé comme suit (voir Annexe 2) :

$$P_{23}(t) = f\left(T_{23}(t)\right) = P_2(t) = f\left(T_{252}(t), x_{252}(t)\right) \qquad \text{Eq.R-9}$$

- Dans le condenseur, la vapeur d'eau qui vient du générateur ($\dot{m}_{23}(t)$) est condensée dans le condenseur, l'eau liquide $\dot{m}_{363}(t)$ est transférée dans le réservoir d'eau. La masse de l'eau dans le générateur est $m_3(t)$. Le bilan de masse dans le condenseur est Eq.R-10.

$$\frac{dm_3(t)}{dt} = \dot{m}_{23}(t) - \dot{m}_{363}(t) \qquad \text{Eq.R-10}$$

Le bilan énergétique dans le condenseur est:

$$\frac{dm_3(t)h_3(t)}{dt} = \dot{Q}_{34}(t) + \dot{m}_{23}(t)h_{23}(t) - \dot{m}_{363}(t)h_{363} - \frac{dQ_{loss3}(t)}{dt} = 0 \qquad \text{Eq.R-11}$$

La puissance de condensation qui est fournie par l'échangeur dans le condenseur peut être calculée par le bilan énergétique de l'eau dans l'échangeur:

$$\dot{Q}_{34}(t) = \dot{m}_{43}\left(h_{34}(t) - h_{43}(t)\right) \qquad \text{Eq.R-12}$$

$\dot{Q}_{34}(t)$ peut également être calculée par les performances de transfert de chaleur de l'échangeur:

$$\dot{Q}_{34}(t) = K_{he3}s_{he3}\left(\left(\mathrm{T_{23}}\text{-}\mathrm{T_{43}}\right)\text{-}\left(\mathrm{T_{363}}\text{-}\mathrm{T_{34}}\right)\right)/\mathrm{Ln}\left(\left(\mathrm{T_{23}}\text{-}\mathrm{T_{43}}\right)/\left(\mathrm{T_{363}}\text{-}\mathrm{T_{34}}\right)\right) \qquad \text{Eq.R-13}$$

La perte de chaleur du condenseur Q_{loss3} peut être calculée de façon similaire à Eq.R-8.

L'équilibre liquide-vapeur dans le condenseur peut être calculé comme suit (voir annexe 3):

$$P_{23}(t) = f\left(T_{23}(t)\right) = P_3(t) = f\left(T_3(t)\right) = P_2(t) = f\left(T_2(t), x_2(t)\right) \quad \text{Eq.R-14}$$

- Dans le réservoir de solution, la solution $\dot{m}_{525}(t)$ est transférée au générateur et la solution du générateur $\dot{m}_{255}(t)$ reflue dans le réservoir de solution. Le bilan de masse est en Eq.R-15:

$$\frac{dm_{5sol}(t)}{dt} + \frac{dm_{5cry}(t)}{dt} = \dot{m}_{255}(t) - \dot{m}_{525}(t) \quad \text{Eq.R-15}$$

Le bilan sur le $CaCl_2$ dans le réservoir de solution est Eq.R-16.

$$\frac{dm_{5sol}(t)x_{5sol}(t)}{dt} + \frac{dm_{5cry}(t)x_{5cry}(t)}{dt} = \dot{m}_{255}(t)x_{255}(t) - \dot{m}_{525}(t)x_{525}(t) \quad \text{Eq.R-16}$$

Le bilan énergétique dans le réservoir de solution peut être calculé comme suit:

$$\frac{dm_{5sol}(t)h_{5sol}(t)}{dt} + \frac{dm_{5cry}(t)h_{5cry}(t)}{dt} = \dot{m}_{255}(t)h_{255}(t) - \dot{m}_{525}(t)h_{525} - \frac{dQ_{loss5}(t)}{dt} \quad \text{Eq.R-17}$$

La perte de chaleur du réservoir de solution Q_{loss5} peut être calculée de façon similaire à Eq.R-8.

- Dans le réservoir d'eau, le changement de la masse d'eau ($dm_6(t)/dt$) est décidé par le débit de l'eau qui vient du condenseur ($\dot{m}_{366}(t)$).

$$\frac{dm_6(t)}{dt} = \dot{m}_{366}(t) \quad \text{Eq.R-18}$$

Le bilan énergétique dans le réservoir d'eau est:

$$\frac{dm_6(t)h_6(t)}{dt} = \dot{m}_{366}(t)h_{366}(t) - \frac{dQ_{loss6}(t)}{dt} \quad \text{Eq.R-19}$$

La perte de chaleur du réservoir d'eau Q_{loss6} peut être calculée de façon similaire à Eq.R-8.

R.4.1.2 Modèle pour la phase d'absorption

Le modèle de la phase d'absorption est présenté Figure 4-2. Les bilans de masse et d'énergie sont similaires au modèle de désorption, mais adaptés.

R.4.2 Résultat de la simulation et comparaison avec l'expérimentation

La simulation dynamique est réalisée selon les conditions de fonctionnement du cas 1 et 2 dans la Table 3-6 (chapitre 3). Les conditions initiales de masse, fraction massique et de température de solution et d'eau correspondent aux conditions expérimentales présentées dans la Table 3-8 du chapitre 3.

R.4.2.1 Cas de la désorption

Les simulations pour les cas 1-1, 1-2, 2-1 et 2-2 de désorption sont réalisées et comparées avec les résultats expérimentaux.

Pour le cas 1-1, les résultats de simulation sont comme suit:

L'évolution de la température est représentée sur la Figure 4-3. Selon la simulation, la température de la solution dans le réservoir de solution (Si-T_5) augmente continuellement avec la désorption parce que la solution, qui est circulée entre le réservoir de solution et le générateur, est chauffée par l'échangeur dans le générateur. La température de l'eau dans le réservoir d'eau (Si-T_6) augmente lorsque l'eau est transférée du condenseur vers le réservoir d'eau. En dehors de ces instants, Si-T_6 diminue en raison de la perte de chaleur du réservoir d'eau vers son environnement. L'évolution de la température du réservoir de solution et du réservoir d'eau est similaire entre l'expérience et la simulation. Par rapport à l'expérience, la température de l'eau simulée à la sortie de l'échangeur dans le condenseur (Si-T_{34}) est plus élevée d'environ 8°C et la température de l'eau simulée à la sortie de l'échangeur dans le générateur (Si-T_{21}) est plus faible d'environ 2°C. Ces différences sont principalement dues au fait que les transferts de chaleur et de masse dans la simulation sont plus efficaces que dans l'expérience (en raison de la présence d'air lors de l'expérience, qui a été mise en évidence dans le chapitre 3).

En raison de l'augmentation de la Si-T_5, la différence de température de l'échangeur dans le générateur diminue. La puissance de l'échangeur de chaleur dans le générateur diminue donc (Si-$\dot{Q}_{12}$ Figure 4-4). Donc la température de l'eau à la sortie de l'échangeur de chaleur dans le générateur (Si-T_{21}) augmente continuellement. Comme la puissance de l'échangeur de chaleur dans le générateur diminue, la quantité de vapeur d'eau qui est désorbée de la solution diminue. La puissance de l'échangeur de chaleur dans le condenseur diminue (Si-$\dot{Q}_{12}$ Figure 4-4). Donc la température de l'eau à la sortie de l'échangeur de chaleur dans le condenseur (Si-T_{34}) diminue avec le temps.

Par rapport à la puissance des échangeurs dans l'expérimentation, la puissance des échangeurs dans la simulation est plus élevée. C'est principalement parce que la performance de l'échangeur est diminuée par la présence d'air dans le réacteur pendant les expériences. La vapeur d'eau qui se condense à la surface de la paroi extérieure du réacteur par échange de chaleur avec l'air ambiant au cours des expériences n'est pas prise en compte dans la simulation. Toute la vapeur d'eau est supposée être condensée dans le condenseur dans la simulation. En conséquence, la différence entre les puissances $\dot{Q}_{12}$ et $\dot{Q}_{43}$ est plus faible dans la simulation que dans l'expérimentation.

Les évolutions de pression du réservoir de solution, du réacteur et du réservoir d'eau sont présentées dans la Figure 4-5. Comparée avec les résultats expérimentaux, la pression dans la simulation est la pression d'équilibre, sans l'influence de l'air. Au cours de la désorption, la température du réservoir de solution augmente, ce qui tend à augmenter la pression du réservoir de solution. Mais par contre la fraction massique de la solution augmente lors de la désorption, ce qui tend à diminuer la pression du réservoir de solution. Selon les résultats de la Figure 4-5, la pression augmente au cours de la phase de désorption, ce qui signifie que la température est le facteur principal d'influence sur la pression du réservoir de solution au cours de cette phase. La pression du réservoir d'eau de la simulation (Si-Réservoir d'eau) change avec la température de l'eau dans le réservoir d'eau (Si-T6 sur la Figure 4-3). La

pression du réacteur (Si-Réacteur) dépend de la température de l'eau dans le condenseur. Comme la quantité de vapeur d'eau qui est désorbée dans le générateur diminue avec le temps, la température de l'eau diminue dans le condenseur. Ainsi, la pression dans le réacteur dans la simulation diminue avec le temps.

La comparaison des performances entre l'expérimentation et la simulation du cas 1-1 est montré dans la Table 4-2.

Au cours de la simulation du cas 1-1, 19,5 kg de l'eau est désorbé de la solution. La masse de solution passe de 207.5 kg à 188 kg. La fraction massique est augmentée en conséquence de 0,345 kg $CaCl_2$/kg solution à 0,381 kg $CaCl_2$/kg solution. L'énergie fournie par l'échangeur dans le générateur pour la désorption Q_{12} est 16,5 kWh. La différence de la consommation d'énergie pour la désorption entre l'expérience et la simulation est due à la vapeur d'eau qui se condense sur la paroi extérieure du réacteur. L'énergie rejetée par l'échangeur de chaleur dans le condenseur Q_{43} est de 13,2 kWh, ce qui est plus élevé que dans l'expérience. C'est principalement parce que la perte de chaleur du condenseur vers l'environnement permet de contribuer à la condensation. Donc, l'énergie qui est rejetée par l'échangeur est diminuée. La puissance des échangeurs de chaleur ($\dot{Q}_{12}$ et $\dot{Q}_{43}$) dans la simulation est plus grande que ce qu'ils sont dans l'expérience. La plus faible puissance dans l'expérience est principalement due à la présence d'air dans le réacteur, qui est négligée dans la simulation. Grâce à la différence de puissance, le temps pour la désorption de la simulation est diminué par rapport à l'expérience (de 7,6 h à 3,8 h). Le vide dans le réacteur est un paramètre extrêmement important.

La comparaison des performances entre l'expérimentation et la simulation des cas 1-2, 2-1 et 2-2 est montrée dans la Table 4-3.

Selon les résultats de la simulation et la comparaison avec les résultats expérimentaux, plusieurs conclusions peuvent être trouvées:

- La puissance de l'échangeur de chaleur dans le générateur et le condenseur dans la simulation est plus grande que dans l'expérience. La raison principale est la présence d'air dans le réacteur pendant l'expérience qui diminue la vitesse de transfert de masse et la chaleur.

- Comme la puissance des échangeurs dans la simulation est plus élevée que dans l'expérience, le temps nécessaire pour la phase de désorption diminue au moins de 50%.

- Comme le temps nécessaire pour la phase de désorption est diminué, la chaleur nécessaire pour chauffer la solution lors de la recirculation de la solution entre le réservoir de solution et le générateur est diminuée. La température de la solution dans le réservoir de solution à la fin de la désorption dans la simulation est inférieure à l'expérience.

- Le besoin de chaleur pour la désorption dans la simulation est inférieur à ce qu'il est dans l'expérimentation, car la chaleur apportée à la solution est diminuée et la vapeur d'eau qui se condense sur la paroi externe du réacteur dans le générateur est négligée dans la simulation.

R.4.2.2 Cas de l'absorption

La simulation pour les cas 1-3, 1-4 et 2-3 d'absorption est effectuée selon les conditions de fonctionnement de l'expérience et comparée avec les résultats expérimentaux.

Pour le cas 1-1, les résultats de simulation sont les suivants:

L'évolution de la température est représentée sur la Figure 4-6. Selon la simulation, la température de la solution dans le réservoir de solution (Si-T_5) augmente de façon continue avec l'absorption parce que la solution, qui est recirculée entre le réservoir de solution et l'absorbeur est chauffée par la chaleur d'absorption. La température de l'eau dans le réservoir d'eau (Si-T_6) est uniquement fonction du transfert de chaleur entre l'environnement et le réservoir d'eau. Comme la température de l'environnement est supposée constante à 20°C et la température initiale de l'eau dans le réservoir d'eau est d'environ 19,8°C, la température de Si-T_6 est presque constante.

En raison de l'augmentation de la Si-T5 et de la fraction massique de la solution, la capacité d'absorption de la solution est diminuée. La puissance de l'échangeur de chaleur dans l'évaporateur diminue (Si-$\dot{Q}_{109}$ dans Figure 4-7). Donc la température de l'eau à la sortie de l'échangeur dans l'évaporateur (Si-T_{910}) augmente continuellement. Avec l'augmentation de la Si-T_5, la différence de température dans l'échangeur de l'absorbeur est augmentée. Donc la puissance de l'échangeur de chaleur dans l'absorbeur l'est également (Si-$\dot{Q}_{78}$ sur la Figure 4-7). La température de l'eau à la sortie de l'échangeur de chaleur dans l'absorbeur (Si-T_{78}) augmente avec le temps.

Par rapport à la puissance des échangeurs dans l'expérimentation, la puissance des échangeurs dans la simulation est beaucoup plus élevée. C'est principalement parce que la performance de l'échangeur est diminuée par la présence d'air dans le réacteur pendant les expériences. Dans l'expérience, en raison de la température de la pièce dans laquelle est placé le prototype, quand l'eau est transférée du réservoir d'eau à l'évaporateur, la puissance fournie par le caloporteur dans l'échangeur de l'évaporateur est devient négative parce que la température de l'eau (absorbat) injectée est supérieure à la température de l'eau du fluide caloporteur à l'entrée de l'échangeur de chaleur de l'évaporateur. Mais dans la simulation, sans l'influence de l'air, la puissance d'évaporation et d'absorption sont plus élevées. Par rapport à l'énergie totale fournie par l'échangeur de chaleur dans l'absorbeur, la chaleur sensible fournie par l'eau qui vient du réservoir d'eau est très faible. Donc l'influence de cette eau provenant du réservoir d'eau sur la capacité d'absorption et d'évaporation n'est pas décelable dans les résultats de simulation.

Les évolutions de la pression du réservoir de solution, du réservoir d'eau et du réacteur sont présentées Figure 4-8.

Comparées avec les résultats expérimentaux, les pressions dans la simulation sont les pressions d'équilibre, sans l'influence de l'air. Pendant la simulation, la pression du réservoir de solution (Si- réservoir de solution) augmente avec la température de la solution (Si-T_5 à Figure 4-6) et augmente avec la diminution de la fraction massique de la solution dans le réservoir de solution. Donc, la pression du réservoir de solution dans la simulation augmente avec le temps. La pression du réservoir d'eau de la simulation (Si- réservoir d'eau) change avec la température de l'eau dans le réservoir d'eau (Si-T_6 à la Figure 4-6). La pression du réacteur (Si-Réacteur) dépend de la température de l'eau dans l'évaporateur. Comme la puissance de l'échangeur dans l'évaporateur diminue avec le temps, la température de l'eau

dans l'évaporateur diminue. Ainsi, la pression du réacteur dans la simulation diminue avec le temps.

La comparaison des performances globales de l'expérimentation et par simulation du cas 1-3 est présentée dans la Table 4-4. La comparaison des performances globales de l'expérimentation et par simulation des cas 1-4 et 2-3 est présentée dans la Table 4-5.

Selon la simulation et les résultats expérimentaux, plusieurs conclusions peuvent être trouvées comme suit:

- La puissance des échangeurs dans l'absorbeur et l'évaporateur dans la simulation est plus grande que dans l'expérience. La raison principale est la présence d'air dans le réacteur pendant l'expérience qui diminue la vitesse de transfert de masse et de chaleur.

- Le besoin de chaleur pour l'évaporation et la production de la chaleur par absorption dans la simulation sont plus élevés que dans l'expérimentation. En prenant le cas 1-4 expérimental comme exemple, 5,2 kg d'eau sont absorbés par la solution, mais l'énergie utilisée pour l'évaporation est seulement de 0,14 kWh et la production d'énergie d'absorption est seulement de 0,17 kWh. Or, il est impossible d'évaporer 5,2 kg d'eau avec cette énergie (l'enthalpie de changement de phase est environ 2500 kJ/kg). L'explication possible est que lorsque l'eau est distribuée sur l'échangeur de chaleur dans l'évaporateur, l'eau liquide déborde de l'absorbeur et se mélange avec la solution directement. La conception du réacteur doit encore être améliorée. La précision des capteurs de température est aussi une raison fortement suspectée parce que la différence de température entre l'entrée et la sortie des échangeurs de chaleur est très faible.

R.4.3 Conclusion

Un modèle de simulation dynamique sur le prototype a été construit. La simulation est réalisée dans les mêmes conditions que dans les expériences. Après l'analyse des résultats et la comparaison avec les résultats expérimentaux, plusieurs conclusions peuvent être trouvées:

- La puissance des échangeurs dans le générateur, le condenseur, l'absorbeur et l'évaporateur de la simulation est plus grande que dans l'expérience. La raison principale est la présence d'air dans le réacteur pendant l'expérience qui diminue la vitesse de transfert de chaleur et de masse.

- Le temps simulé nécessaire pour la phase de désorption est diminué de plus de 50% puisque la puissance des échangeurs de chaleur dans la simulation est plus élevée que dans l'expérience. Comme le temps nécessaire pour la phase de désorption est diminué, la chaleur apportée à la solution dans le réservoir de solution est également diminuée.

- Le besoin de chaleur pour la désorption dans la simulation est inférieur à l'expérimentation, car la chaleur apportée à la solution est diminuée (en effet, on suppose que la solution quittant le réacteur est toujours à l'équilibre thermodynamique, ce qui n'est pas forcément le cas en raison de la cinétique de sorption) et la vapeur d'eau qui se condense sur la paroi externe du réacteur est négligée dans la simulation.

- Le besoin de chaleur pour l'évaporation et la production de la chaleur par absorption dans la simulation sont plus élevés que dans l'expérimentation. Mais l'énergie nécessaire pour l'évaporation mesurée dans l'expérience est trop faible pour évaporer l'eau qui est absorbée par la solution. La conception du réacteur doit encore être améliorée. La précision des capteurs de mesure est également mise en cause.

R.5 Simulation dynamique d'un logement équipé avec le système de stockage inter-saisonnier d'énergie solaire par absorption

Afin de déterminer la performance annuelle du système de stockage inter-saisonnier dans un bâtiment, le modèle qui a été utilisé pour la simulation dynamique du prototype est adapté et enrichi. Un modèle de capteur solaire, de besoins thermiques de bâtiment et les conditions météorologiques du site de Chambéry sont ajoutés au modèle dynamique.

R.5.1 modèle annuel de simulation dynamique

Le modèle en phase de désorption est présenté Figure 5-1, et la phase d'absorption Figure 5-2. Le modèle pour la simulation annuelle est le même que le modèle pour le prototype avec l'ajout d'un modèle de capteur solaire et de besoins thermiques d'un bâtiment. Les conditions météorologiques horaires sont utilisées comme paramètre d'entrée de la simulation dynamique.

Au cours de la phase de désorption, l'énergie pour la désorption est assurée par un capteur solaire, le modèle pour le capteur solaire est suivant [ISO 1994, Oscar M. et al, 2005]:

$$\dot{Q}_s = (0,8G_s/3600\times1000 - 3,5((T_{12}+T_{21})/2 - T_{atm}) - 0,015((T_{12}+T_{21})/2 - T_{atm})^2) \times S_{cs}/1000 - \dot{Q}_n \quad \text{Eq.5-1}$$

$\dot{Q}_s$ est la puissance qui peut être fournie par l'échangeur dans le générateur en supposant qu'il n'y a pas de ballon d'eau chaude tampon dans le système, G_s est le rayonnement solaire horizontal global, $\dot{Q}_n$ est la puissance nécessaire au bâtiment. $\dot{Q}_s$ est calculé par l'énergie qui est fournie par le capteur solaire à laquelle est soustrait le besoin d'énergie pour le bâtiment. Cela signifie que l'énergie qui vient du capteur solaire sera en priorité utilisée directement pour chauffer le bâtiment. Si l'énergie qui vient du capteur solaire est plus élevée que le besoin énergétique du bâtiment, l'énergie en excès sera utilisée pour la désorption.

Le rayonnement solaire horizontal global G_s provient des données météorologiques de Chambéry (France) et peut être trouvé sur la Figure 5-3. La température ambiante T_{atm} est également issue des conditions météorologiques à Chambéry (Figure 5-4). L'eau dans le condenseur est refroidie par l'air extérieur. La température à l'entrée de l'échangeur de chaleur T_{43} (Figure 5-1) est supposée la même que la température ambiante T_{atm}.

Au cours de la phase d'absorption, l'énergie d'évaporation est fournie par des sondes géothermiques. La température de l'eau à l'entrée de l'échangeur de chaleur T_{109} (Figure 5-2) est supposée constante à 15°C, qui est la même température que dans la simulation dynamique sur le prototype seul.

La chaleur d'absorption est utilisée pour chauffer le bâtiment par l'intermédiaire de l'échangeur de l'absorbeur. Un modèle simple de bâtiment a été développé dans le logiciel Trnsys suivant le type 56a en utilisant le logiciel TRNBuild (Annexe 8). La surface du bâtiment est de 120 m^2 (15 m x 8 m). La hauteur du bâtiment est de 2,5 m.

Pour maintenir la température du bâtiment à 20°C pendant la journée (de 6h à 22h) et 18°C pendant la nuit (de 0h à 6h et de 22h à 24h), le besoin de chaleur du bâtiment est représenté Figure 5-5. Le besoin de chaleur du bâtiment est de 4950 kWh/an. La puissance maximale correspondante est de 2,8 kW.

La solution et l'eau sont stockées dans des réservoirs souterrains. La profondeur des réservoirs est de 4 m.

La température à cette profondeur T_{ug4} est calculée comme suit [TRILLAT-BERDAL V. 2006]:

$$T_{ug4} = 283.15 + 8 \cdot \sin\left(2\pi \cdot \left(t - 142.75 \cdot 86400\right) / 86400 / 365\right) \qquad \text{Eq.5-2}$$

t est le temps en seconde. L'évolution T_{ug4} pendant un an peut être trouvée Figure 5-6.

R.5.2 Dimensionnement du système et conditions de fonctionnement de la simulation

En raison des grands besoins de chaleur et des puissances nécessaires, les composants du système de stockage dans la simulation annuelle sont plus grands qu'ils ne le sont dans la simulation du prototype. Le volume du réservoir de solution est ici de 21,9 m^3, le volume du réservoir d'eau est de 9,4 m^3, la surface du capteur solaire est de 12 m^2, la surface des deux échangeurs dans le réacteur est 2 m^2. Ces valeurs ont été obtenues à partir de simulations pour correspondre au besoin de chaleur du bâtiment considéré.

Le système a trois phases opérationnelles: la désorption, l'absorption et le stockage. Le choix de la phase de fonctionnement du système dépend de la production de chaleur du capteur solaire comparé au besoin de chaleur du bâtiment:

- La phase de désorption: si la production de chaleur du capteur solaire est plus élevée que le besoin de chaleur du bâtiment, la chaleur en excès sera utilisée pour la désorption. Comme indiqué au chapitre 3, pour éviter la prise en masse de la solution dans le réservoir de solution par cristallisation, la fraction massique maximale d'absorbant après désorption est limitée en fonction de la forme du cristal (hydratation du cristal). Le cristal de $CaCl_2$ à l'état 5 (10°C) est sous forme de $CaCl_2.6H_2O$ avec un pourcentage d'absorbat à 50,7%. La fraction massique maximale dans le réservoir de solution pour la simulation est donc décidée à 0,495. Lorsque la fraction massique dans le réservoir de solution est supérieure à 0,495, même si la production de chaleur du capteur solaire est plus élevée que le besoin de chaleur du bâtiment, le système ne fonctionne pas en phase de désorption.

- La phase d'absorption: si la production de chaleur du capteur solaire est plus faible que le besoin de chaleur du bâtiment et qu'il y a de l'eau dans le réservoir d'eau, la chaleur de compensation nécessaire sera fournie par l'absorption.

- La phase de stockage (transition): si la production de chaleur du capteur solaire est inférieure au besoin de chaleur du bâtiment et qu'il n'y a pas d'eau dans le réservoir d'eau, ou si la production de chaleur du capteur solaire est plus élevée que le besoin de chaleur du bâtiment et la fraction massique dans le réservoir de solution est supérieure à 0,495, ou si la production

de chaleur du capteur solaire est la même que le besoin de chaleur du bâtiment, le système est dans une phase de stockage.

Pendant la phase de désorption, les conditions de fonctionnement sont: le débit d'eau caloporteur dans les échangeurs du condenseur et du générateur est de 2100 kg/h, qui est le débit minimum pour atteindre le régime turbulent. Le débit de la solution circulant du réservoir de solution au générateur est de 200 kg/h. Le débit de l'eau du condenseur au réservoir d'eau est de 20 kg/h lorsque le niveau d'eau dans le condenseur est au-dessus du niveau maximum (100 mm) et nul quand le niveau est inférieur au niveau minimum (50 mm). Ce débit est suffisant pour éviter le débordement de l'eau dans le récepteur du condenseur.

Pendant la phase d'absorption, les conditions de fonctionnement sont: le débit d'eau de l'échangeur de l'évaporateur est de 5000 kg/h pour s'assurer que la puissance de l'évaporation est suffisante pour tous les besoins de chaleur du bâtiment. Le débit d'eau de l'échangeur dans l'absorbeur est de 1000 kg/h. Le débit de la solution du réservoir de solution au générateur n'est pas constant. Il est calculé en fonction des besoins de chaleur du bâtiment à chaque pas de temps. Le débit de l'eau qui circule dans l'évaporateur est de 10 kg/h. Lorsque le niveau d'eau dans l'évaporateur est inférieur au niveau minimum (50 mm), l'eau dans le réservoir d'eau est transférée à l'évaporateur au même débit.

Pendant la phase de stockage, les conditions de fonctionnement sont: l'eau est stockée dans le réservoir de l'eau et la solution est stockée dans le réservoir de la solution. La température de l'eau et de la solution sont changeantes en fonction du transfert de chaleur entre les réservoirs et leur environnement.

R.5.3 Résultats de simulation

Tous les paramètres comme la masse, fraction massique, température, pression, puissance etc. sont calculés par la simulation dynamique.

Les évolutions de la masse d'eau dans le réservoir d'eau, de la solution dans le réservoir de solution, le cristal dans le réservoir de solution, le mélange (solution+cristaux) dans le réservoir de solution avec le temps sont présentées Figure 5-7. Sur cette figure, le temps 0 représente 0h, le 1er janvier 2005; 1 représente 0h, le 2 janvier 2005, et enfin 365 représente 0h, le 1er janvier 2006. La masse du mélange est la somme de la masse de la solution et du cristal. La masse du mélange dans le réservoir de solution diminue au cours de la phase de désorption et augmente pendant la phase d'absorption. Lorsque la solubilité est inférieure à la fraction massique du mélange (jours 0 à 60 et 180 à 365), il y a du cristal dans le réservoir de solution. La masse maximale du cristal est 13 700 kg. La masse de solution correspondante (qui correspond à la masse minimale de la solution) est de 1 900 kg. Cette quantité de solution minimale est choisie afin d'éviter tout problème de circulation de solution dans le système, même en présence de cristal solide. Le cristal disparaît lorsque la solubilité est plus grande que la fraction massique du mélange dans le réservoir de solution (jours 60 à 180). La masse d'eau augmente dans le réservoir d'eau lors de la désorption et diminue lors de l'absorption. La masse maximale de l'eau est 5 300 kg. La somme de la quantité de mélange (dans le réservoir de solution) et de l'eau (dans le réservoir d'eau) est constante dans le système (système fermé).

Au jour 90, il existe un gradient important sur la Figure 5-7. Cela est dû au fait que la simulation est en fait réalisée à partir du jour 90 (le 1 avril 2005). À ce stade, la masse d'eau est de 0. Mais un an plus tard, la masse de la solution et d'eau est différente. Il y a encore environ 277 kg d'eau dans le réservoir d'eau. Il est vraiment difficile de faire en sorte que toute l'eau désorbée soit absorbée exactement en un an. Cette différence entre les conditions initiales et finales dans le réservoir d'eau est acceptable par rapport à la quantité d'eau cyclée (5 300 kg).

L'évolution de la fraction massique dans le réservoir de solution est présentée Figure 5-8. La fraction massique du mélange diminue lors de la désorption et augmente lors de l'absorption. Quand il y a du cristal (jours 0 à 60 et 180 à 365), la solubilité est inférieure à la fraction massique du mélange, la fraction massique de la solution est égale à la solubilité. Quand il n'y a pas de cristal (jours 60 à 180), la solubilité est supérieure à la fraction massique du mélange. La fraction massique de la solution est la même que celle du mélange. Cette figure présente également un saut important au jour 90, pour la même raison que dans l'évolution de la masse dans les réservoirs.

L'évolution de la fraction massique de la solution à la sortie du générateur/absorbeur est présentée Figure 5-9. Au cours de la phase de stockage, comme il n'y a pas de solution circulée dans le réacteur, la fraction massique à la sortie du générateur ou absorbeur est fixée à 0. Dans la phase d'absorption (0h à 12h, le 1 Janvier 2005, Figure 5-10), la fraction massique de la solution à la sortie de l'absorbeur est inférieure à la fraction massique dans le réservoir de solution tant que la vapeur d'eau est absorbée par la solution. Dans la phase de désorption (8h à 18h le 20 Juillet 2005, Figure 5-11), la fraction massique de la solution à la sortie du générateur est supérieure à la fraction massique du réservoir de solution tant que la vapeur d'eau est désorbée de la solution. La phase de stockage se produit principalement lors de la nuit en été (0h à 6h sur le 20 Juillet, 2005, Figure 5-11 par exemple) car il n'y a ni besoin de chauffage, ni énergie solaire reçue.

La Figure 5-12 montre l'évolution de la température du générateur/absorbeur, du condenseur/évaporateur, du réservoir de solution, du réservoir d'eau et de l'atmosphère. La Figure 5-13 montre le détail de ces évolutions sur 2 jours. Les températures du générateur et du condenseur varient avec la puissance produite par le capteur solaire. La température du réservoir de solution est supérieure à la température du réservoir d'eau car la température de la solution qui vient du générateur est toujours supérieure à la température de l'eau qui vient du condenseur. La température du réservoir d'eau est proche de la température de l'atmosphère. En absorption (Figure 5-14), la température de l'absorbeur est supérieure à 20°C pour chauffer le bâtiment. La température de l'évaporateur est d'environ 15°C. Pendant le stockage, comme il n'y a ni absorption ni désorption, la température du générateur et du condenseur sont les mêmes que la température ambiante.

La Figure 5-15 présente l'évolution de la pression du générateur/absorbeur, du réservoir de solution et du réservoir d'eau. Pendant les phases de désorption et d'absorption, la pression du générateur/absorbeur change avec la température et la fraction massique (pression d'équilibre thermodynamique). Au cours de la phase de stockage, la pression du générateur/absorbeur est

supposée à la même pression que la pression du réservoir d'eau parce que le générateur/absorbeur n'est plus en fonctionnement. La pression du réservoir de solution est à l'équilibre thermodynamique. La pression du réservoir d'eau change avec la température (pression de vapeur saturée de l'eau). La pression du système varie de 200 Pa à 5000 Pa.

La Figure 5-16 montre l'évolution de la puissance des échangeurs dans le capteur solaire, le générateur, l'absorbeur, le condenseur, l'évaporateur et le besoin de chaleur du bâtiment. Au cours de la phase de stockage, les puissances du générateur, de l'absorbeur, du condenseur et de l'évaporateur sont nulles parce que le processus est inerte. Le débit de la solution du réservoir de solution à l'absorbeur est calculé pour atteindre la puissance suffisante. La Figure 5-17 montre deux jours en été. De 8h à 18h, le 20 Juillet 2005 le système est en phase de désorption. De 0h à 8h, le système est en phase de stockage. La Figure 5-18 présente deux jours en hiver. La puissance d'absorption est approximativement la même que le besoin de chaleur quand il n'y a pas d'énergie solaire (de 0h à 9h, le 1er Janvier 2005). Quand il y a l'énergie solaire, la puissance d'absorption est inférieure au besoin de chaleur (de 9h à 12h) parce que l'énergie solaire est aussi utilisée pour chauffer le bâtiment directement. Lorsque la puissance solaire est insuffisante, de l'énergie est produite par absorption. Durant certaines périodes (de 12h à 15h), l'énergie solaire est suffisante pour les besoins de chaleur du bâtiment, l'absorption n'est pas nécessaire. L'énergie solaire en excès est alors utilisée pour la désorption.

Au cours de l'absorption, le débit de la solution du réservoir de solution à l'absorbeur est déterminé pour répondre au besoin de puissance du bâtiment (Figure 5-19). La puissance augmente avec ce débit. Mais la corrélation puissance-débit n'est pas linéaire car le débit d'eau dans l'échangeur de l'évaporateur est, par contre, constant. Il y a donc une puissance maximale d'évaporation. Bien que le débit de la solution soit augmenté, la vapeur d'eau qui provient de l'évaporateur n'est alors pas suffisante. L'augmentation de la puissance d'absorption avec le débit est faible lorsque le débit est supérieur à 100 kg/h.

Un calcul est utilisé pour éviter la cristallisation dans le générateur. Le résultat est donné dans la Figure 5-20. Pour chaque température du condenseur, il y a une fraction massique maximale de solution possible dans le générateur et donc une température maximale du générateur pour éviter la cristallisation. La Figure 5-21 est plus facile à utiliser pour l'expérimentateur. Au cours de l'utilisation du système, la température dans le générateur et le condenseur sont mesurées et placées dans la Figure 5-21. Si le point est dans la région 'Cristallisation', soit la température de condensation doit être augmentée en diminuant le débit de l'eau dans l'échangeur du condenseur soit la température de désorption doit être réduite en diminuant le débit de l'eau dans l'échangeur du générateur.

Selon la simulation réalisée, toutes les conditions de fonctionnement présentes dans ces tubes sont dans la région sans cristallisation (Figure 5-22). C'est-à-dire que lorsque le système est dans une phase active, il n'y a pas de cristallisation. Mais un problème peut exister lorsque le système est dans la phase de stockage. La solution peut rester dans les tubes de connexion entre les réservoirs et le réacteur et leur température diminuer jusqu'à la température ambiante.

Sur la figure, il y a beaucoup de points proches de la ligne de solubilité. Le problème correspondant de cristallisation et donc de blocage des tubes ne peut donc pas être négligé.

Suite à la simulation annuelle, les principaux résultats sont présentés dans la Table 5-1: l'énergie solaire qui est reçue par le capteur solaire est de 14 619 kWh avec 12 m^2 de capteurs solaires. L'énergie qui est utilisée dans le générateur est de 5 492 kWh. Elle est principalement utilisée pour la désorption de l'eau de la solution. Cette partie est environ la même que l'énergie libérée par la condensation (4 467 kWh). L'autre partie est transférée vers le réservoir de solution parce que la solution à la sortie du générateur est plus chaude qu'à l'entrée. L'énergie produite lors de l'absorption est 3 645 kWh. L'énergie solaire utilisée directement pour le bâtiment en hiver est de 1 374 kWh. L'énergie nécessaire à l'évaporation est de 3 534 kWh. La capacité de stockage du système est de 116 kWh/m^3 (en prenant en compte le volume des réservoirs de solution et d'eau). Le rendement du système de stockage, qui est défini comme l'énergie produite lors de l'absorption divisée par l'énergie utilisée par la désorption est de 66,4%. Le rendement solaire du système de stockage est défini comme l'énergie produite lors de l'absorption divisée par l'énergie solaire reçue par les capteurs solaires. Il est d'environ 24,9%. La température de l'eau pour le chauffage du bâtiment est de 21°C en moyenne.

R.5.4 Conclusion

La simulation annuelle d'un bâtiment avec le système de stockage inter-saisonnier d'énergie solaire a été réalisée dans ce chapitre. Les évolutions de la masse, fraction massique, température, pression, puissance etc. en fonction du temps sont analysés. Le modèle pour la simulation annuelle considère presque tous les composants qui sont utilisés dans le bâtiment avec le système de stockage saisonnier. Il peut être utilisé pour des simulations avec des besoins de chaleur et des conditions météorologiques différents, de même que pour d'autres couples d'absorption en changeant les caractéristiques thermodynamiques correspondantes.

Selon les résultats de la simulation, les besoins de chaleur d'un bâtiment peuvent être entièrement couverts par le système de stockage inter-saisonnier et de l'énergie solaire utilisée directement pour le bâtiment. La capacité de stockage et le rendement du système sont les facteurs clé du système de stockage inter-saisonnier par absorption. La capacité de stockage est de 116 kWh/m^3 dans l'exemple étudié et le rendement du système de stockage est d'environ 66,4%. Cependant, pour un bâtiment de 120 m^2, il est difficile d'avoir au total 30 m^3 de réservoirs de stockage (dimensionnement obtenu). La température de la production de chaleur (environ 21°C) n'est pas satisfaite non plus. La prochaine étape de la recherche devrait se concentrer dans l'amélioration de la capacité de stockage, le rendement du stockage et la température de la production de chaleur.

Références de la synthèse de thèse

Agyenim F., Hewitt N., Eames P., Smyth M.. 2010. A review of materials, heat transfer and phase change problem formulation for latent heat thermal energy storage systems (LHTESS). Renewable and Sustainable Energy Reviews. 14(2), pp. 615-628

Amaya V. Novo, Joseba R. Bayon, Daniel Castro-Fresno, Jorge Rodriguez-Hernandez. 2010. Review of seasonal heat storage in large basins: Water tanks and gravel–water pits. Applied Energy. 87(2), pp. 390-397

Alibaba. http://www.alibaba.com.

Aveyard R., Haydon D.A.. 1973. An introduction to the principles of surface chemistry, CUP Archive.

Bales C.[1]. 2008. Laboratory tests of chemical reactions and prototype sorption storage units. www.iea-shc.org

Bales C.[2]. 2008. Final report of Subtask B ‘‘Chemical and Sorption Storage’’ the overview. pp. 23. www.iea-shc.org

Boer R.D., Haije W., Veldhuis J., Smeding S.. 2004. Solid sorption cooling with integrated storage: the SWEAT prototype. In: 3rd international heat powered cycles conference—HPC 2004

Craig BD., Anderson DS.. 1995. Handbook of corrosion data. ASM International, Materials Park, OH

Faninger G. 2004.Thermal energy storage; etn.wsr.ac.at.

Gil Antoni, Medrano Marc, Martorell Ingrid, Lázaro Ana, Dolado Pablo, Zalba Belén, Cabeza Luisa F. . 2010. State of the art on high temperature thermal energy storage for power generation. Part 1—Concepts, materials and modellization Review Article. Renewable and Sustainable Energy Reviews. 14(1), pp. 31-55

Hasnain S. M.. 1998. Review on sustainable thermal energy storage technologies, Part I: heat storage materials and techniques. Energy Conversion and Management. 39(11), pp.1127-1138

Hauer A.[1]. 2002. Thermal energy storage with zeolite for heating and cooling applications. In: Proceedings of 3rd workshop of annex 17 ECES IA/IEA

Hauer A.[2], Mehlin H., Schossig P., Yamaha M., Cabeza L., Martin V., Setterwall F.. 2002. Annex 17, Advanced Thermal Energy Storage Techniques – Feasibility Studies and Demonstration Projects, final report. www.iea-eces.org

Hauer A.[3]. 2007. Sorption theory for thermal energy storage, Thermal energy storage for sustainable energy consumption, Springer, Netherlands, pp. 393–408

Hongois S., Stevens P., Coince A-S., Kuznik F., Roux J-J.. 2008. Thermochemical storage using composite materials. In: Proceedings of the Eurosun 2008, 1st international conference on solar heating, cooling and buildings

IEA task 32. 2008. Advanced Storage Concepts for Solar and Low Energy Buildings. http://www.iea-shc.org/task32/index.html

ISO (1994). 1994. ISO 9806-1, Thermal performance of glazed liquid heating collectors.

Jaehnig D., Hausner R.,Wagner W., Isaksson C.. 2006. Thermo-chemical storage for solar space heating in single-family house. In: ECOSTOCK conference

Kato Y.. 2007. Chemical energy conversion technologies for efficient energy use, Thermal energy storage for sustainable energy consumption, Springer, pp. 377–91

NFPA704. 2007. Standard System for the Identification of the Hazards of Materials for Emergency Response. http://www.nfpa.org

Pilkington Solar International GmbH. 2000. Survey of thermal storage for parabolic trough power plants. National Renewable Energy Laboratory. [SR-550-27925]

Srivastava N.C. and Eames I.W.. 1998. A review of adsorbents and adsorbates in solid-vapour adsorption heat pump systems. Applied Thermal Engineering 18 (9–10), pp. 707–714

TRILLAT-BERDAL Valentin. 2006. Thèse : Intégration énergétique dans les bâtiments par l'utilisation combinée de l'énergie solaire et de la géothermie basse température. Université de Savoie – Chambéry

Ucar A., Inalli M.. 2005. Thermal and economical analysis of a central solar heating system with underground seasonal storage in Turkey. Renewable Energy. 30(7), pp. 1005-1019

Van Berkel J.. 2005. Storage of solar energy in chemical reactions. In: Jean-Christophe Hadorn, editor. Thermal energy storage for solar and low energy buildings. Spain, Lleida

Velmurugan V., Srithar K.. 2008. Prospects and scopes of solar pond: A detailed review. Renewable and Sustainable Energy Reviews. 12(8), pp. 2253-2263

Visscher K.. 2004. Energy research Center of the Netherlands (ECN). Simulation of thermo chemical seasonal storage of solar heat—material selection and optimum performance simulation. In: Proceedings of workshop 2004 2nd workshop Matlab/Simulink for building simulation, CSTB, Paris, France. http://ddd.cstb.fr/simbad/workshop2

Weber RVD.. 2008. Long-term heat storage with NaOH. Vacuum. 82(7), pp. 708–16

General introduction

In France, the present house heating boilers mostly use fossil fuels and release large quantities of pollutants and greenhouse gases that can be particularly harmful in densely populated areas. The heating systems in urban areas in France represent 10% of the SO_2 emissions, 5% of the NO_2 emissions and 30% of the CO emissions [ADEME 2008].

Thermal storage systems for heat and cold are essential components of energy efficient processes, especially when considering renewable energy sources which often are discontinuous or unsynchronized with the heat and/or cold needs. Thermal storage systems are crucial components for solar energy applications due to the intermittent nature of this energy source [Dincer I. 2002]. Several research projects on thermal storage systems have been driven during the previous years at the European as well as the international levels [PCRD 2006, IEA annex 10 2000]. Low storage efficiencies, the consequential energy losses and the building and maintenance of storage devices usually increase significantly the total cost of solar systems.

The aim of the present project is to develop a long-term thermal solar energy storage equipment for house heating using the absorption technology. The developed process would have three environmental advantages: the use of solar energy of summer in winter, the saving of fossil fuels, and the reduction of CO_2 emissions and atmospheric pollution.

Solar energy is considered to be stored in a chemical way. Unlike the latent or thermal heat storage solutions, the sorption storage technology has a potentially infinite duration time thanks to its particular concept which is already well known from the existing solar powered refrigeration machines. The originality of this project comes from the possibility to store energy during periods where a high solar heat flux is available and to release this energy when heat is needed. Figure I-1 represents the heat produced by 10 m^2 solar collectors and the space heating and domestic hot water needs for a modern 120 m^2 house situated in Chambéry, in the Alpine region of France. This modern house follows the current French law on buildings isolation and thermal performances RT2005.

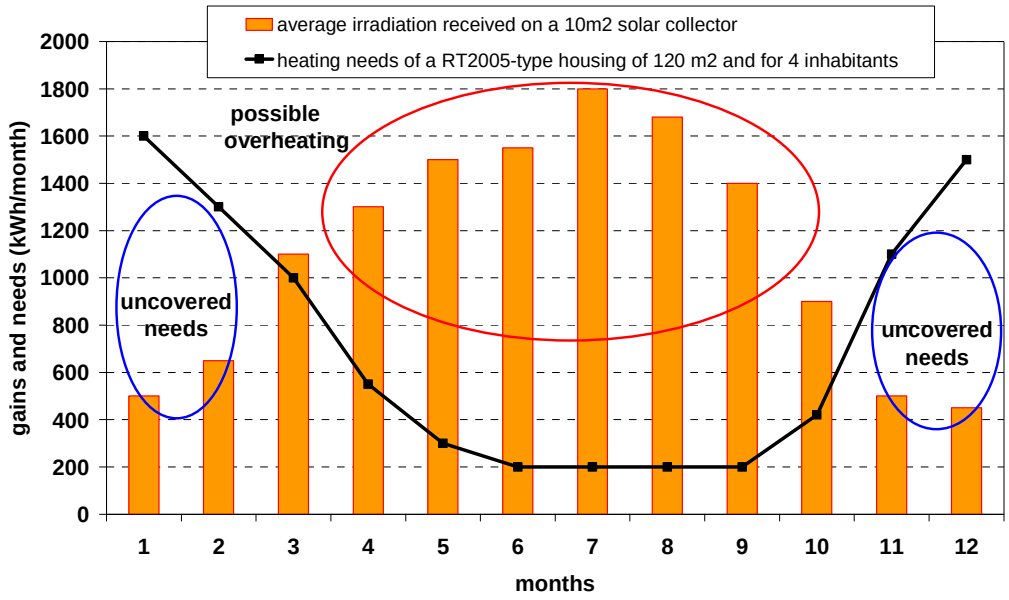

Figure I-1 Results of the simulation by Trnsys of a building in Chambéry (France)

The availability of the solar heat is strongly shifted compared to the needs. Indeed, the solar collectors dimensioned not only for domestic hot water production but also for space heating are over-dimensioned for the summer periods during which no space heating is required (from June to September in Figure I-1) whereas all the heating needs are not covered during the coldest periods. The warm periods can also be harmful to the solar system and heat has to be rejected to the environment to avoid overheating of the components. Thus, the idea of this project is to use this waste heat, introduce it into an absorption storage process to be able to use it during the coldest periods when the heating needs are higher than the solar gains.

The structure of the thesis is as follows:

Chapter 1 presents a brief summary of some relevant work and the general problems in the field of thermal energy storage.

The process of seasonal storage of solar energy for house heating by absorption is introduced and described in Chapter 2. The study of the performance of this system with the seven absorption couples: $CaCl_2/H_2O$, Glycerin/H_2O, KOH/H_2O, LiBr/H_2O, LiCl/H_2O, NaOH/H_2O and H_2O/NH_3 is performed by a static simulation.

A prototype is designed and described and experimentations are carried out at different operating conditions with the absorption couple $CaCl_2/H_2O$. The thermodynamic performances and the problems of the prototype are analyzed in Chapter 3.

Chapter 4 presents a dynamic simulation on the prototype. The optimal performances of the prototype are obtained by the dynamic simulation and compared with the experimental results from Chapter 3.

In Chapter 5, an annual dynamic simulation is performed in order to obtain the performance of the seasonal storage system connected to a building. The characteristics such as the pressure, the temperature, the mass, the mass fraction, the power, the energy, the efficiency and the storage capacity etc. of the storage system are presented and analyzed.

References

ADEME. 2008. Guide pratique, information des citoyens, *Qualité de l'air*, France. http://www.ademe.fr/particuliers/fiches/3688/default.htm

Dincer, I.. 2002. Thermal energy storage systems as a key technology in energy conservation. International Journal of Energy Research. 26, pp. 567-588

IEA annex 10. http://www.fskab.com/annex10/index.html

PCRD. 2006. Décision No 1982/2006/CE du parlement européen et du conseil du 18 décembre 2006 relative au septième programme-cadre de la Communauté européenne pour des actions de recherche, de développement technologique et de démonstration. http://www.eurosfaire.prd.fr/7pc/doc/1168931351_7pc_l_41220061230fr00010041.pdf

Chapter 1 – State of the art of seasonal storage systems of solar energy for house heating

Nowadays, most buildings meet thermal loads using equipments and systems that generate or remove heat when building loads exist. Thermal energy storage (TES) systems enable buildings to meet heating and cooling loads using energy produced at another time.

TES can be designed for storing and providing energy on three basic timescales: diurnal, weekly, and seasonal. The seasonal thermal energy storage (STES) systems enable a building to use heat collected during the summer to heat the building during the winter, or to use cold collected during the winter to cool the building in the summer. Relatively to diurnal storage systems, STES require a much larger total size, while the time scale of charge and discharge is enlarged.

STES systems consist of several components, including the heat (or cold) source, the heat exchange system, the thermal distribution system, the thermal storage medium and the thermal loads. A well known disadvantage of sensible or latent TES is the fact that they have to be at a higher (or lower) temperature than the ambience. Due to this temperature difference they are able to operate as heat (or cold) storage. A thermal insulation is thus necessary to avoid losses over the storage period.

A key issue in the design of a thermal energy storage system is its thermal capacity - the amount of energy that it can store and provide. However, selection of the appropriate system depends on many cost-benefit considerations **[Gil A. et al. 2010]**.

The cost of a TES system mainly depends on the following items:

- The storage material itself
- The heat exchangers for charging and discharging the system
- The cost for the space and/or enclosure for the TES

From the technical point of view, the crucial requirements are:

- High energy density (per-unit mass or per-unit volume) in the storage material
- Good heat transfer between the heat transfer fluid (HTF) and the storage medium
- Mechanical and chemical stability of the storage material
- Compatibility between the HTF, heat exchanger and/or storage medium
- Complete reversibility for a large number of charging/discharging cycles

• Low thermal losses
• Ease of control

The most important design criteria are:

• Nominal temperatures
• Maximum load
• Operational strategy

All these facts have to be considered when deciding on the type and the design of thermal storage. Lots of methods and systems have been developed for STES systems. The purpose of this chapter is to identify and selectively review previous work done on the evaluation and use of TES. Appropriate storage concepts and technical options are discussed, followed by a review of previous work. TES systems can be classified by the storage mechanism as sensible storage, latent storage, sorption storage and chemical reaction storage.

1.1 Sensible thermal storage

For the sensible thermal storage, the thermal energy is stored by the change of the temperature of the storage medium. Thus, the storage capacity depends on the temperature change, the specific heat and the quantity of storage medium.

The storage capacity of a sensible thermal storage system with a solid or liquid storage medium is given by:

$$Q = MCp\Delta T = V\rho Cp\Delta T \qquad \text{Eq.1-1}$$

where M is the mass; V is the volume; Cp is the specific heat; ρ is the density and $\Delta T = T_{max} - T_{min}$ is the temperature difference between the maximum and minimum temperatures of the medium. This temperature range depends on the application and is limited by the temperature of the heat source and of the delivery temperature from the storage. This expression can be used to calculate the mass and volume of storage material required to store a given quantity of energy.

Sensible heat storage may be classified on the basis of the heat storage media as liquid media storage (like water, oil based fluids, molten salts etc.) and solid media storage (like rocks, metals and others).

1.1.1 Sensible storage by liquid form

Storage by water

At moderate temperature, water is one of the best storage media. It has higher specific heat than other materials, and it is cheap and widely available. However, due to its high vapor pressure, it requires costly insulation and pressure withstanding containment for high temperature applications. Water can be used over the wide range of temperature of 25-90°C. For a 60°C temperature change, water can store 250 kJ/kg or 2.5 x 10^5 kJ/m^3 [**Amaya V. Novo et al. 2010**]. Because of its simplicity, a large amount of published data is available on the design criteria for water storage media [Ucar A. 2005, Bauer D. 2010, Kübler R. et al 1997, Tanaka H. et al 2000]. The schematic diagram of a solar heating system with seasonal storage system by water can be found in Figure 1-1. The thermal energy which comes from the solar collector is stored in the water store by the increase of its temperature during the summer phase and is used for house heating during the winter phase. A heat pump has to be used to promote the thermal energy quality for higher temperature using.

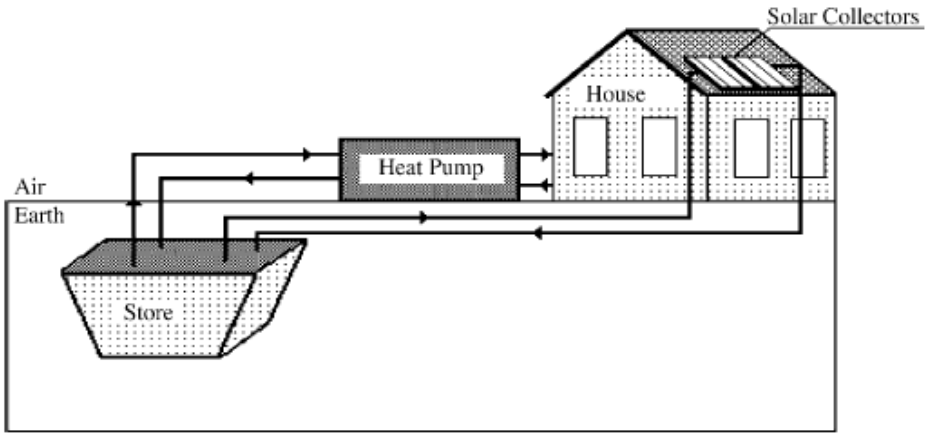

Figure 1-1 A solar heating system with seasonal storage by water [Ucar A. 2005]

Water storage tanks are made from a wide variety of materials, like steel, aluminum, reinforced concrete and fiber glass. The tanks are insulated with glass wool, mineral wool or polyurethane. The size of the tanks used varies from a few hundred liters to a few thousand cubic meters.

Storage by solar pond

A solar pond is a pool of saltwater which collects and stores solar thermal energy. The saltwater naturally forms a vertical salinity gradient also known as a "halocline", in which low-salinity water floats on top of high-salinity water. The layers of salt solutions increase in concentration (and therefore density) with depth. Below a certain depth, the solution has a uniformly high salt concentration as shown in Figure 1-2 [V. Velmurugan et al. 2008, Solar Gradient Solar Ponds, 2009].

There are 3 distinct layers of water in the pond: the top layer, which has a low salt content; an intermediate insulating layer with a salt gradient, which establishes a density gradient that prevents heat exchange by natural convection and the bottom layer, which has a high salt content. If the water is relatively translucent, and the pond's bottom has high optical absorption, then nearly all of the incident solar radiation (sunlight) will go into heating the bottom layer. When solar energy is absorbed in the water, thermal expansion and reduced density occur due to the increase of the temperature. If the water were fresh, the low-density warm water would float to the surface, causing convection current. The temperature gradient alone causes a density gradient that decreases with depth. However the salinity gradient forms a density gradient that increases with depth, and this counteracts the temperature gradient, thus preventing heat in the lower layers from moving upwards by convection and leaving the

pond. This means that the temperature at the bottom of the pond will rise to over 90°C while the temperature at the top of the pond is usually around 30°C. Thus the solar energy can be stored during long time with a much lower heat loss than with a water tank storage. During the winter phase, the water at the bottom of the solar pond can be used for house heating.

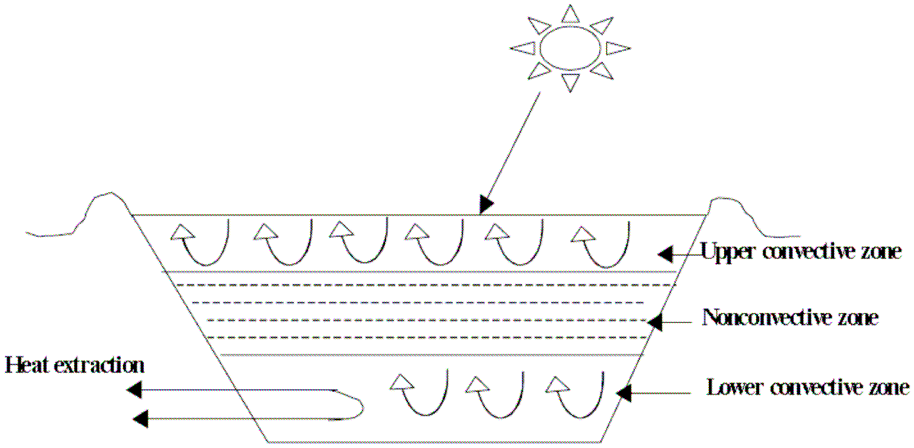

Figure 1-2 The solar pond

The advantages of a solar pond can be found as follows. The approach is particularly attractive for rural areas in developing countries. Very large area collectors can be set up for just the cost of the clay or plastic pond liner. There is no need of a separate collector for this thermal storage system. However, the evaporated surface water needs to be constantly replenished. The accumulating salt crystals have to be removed and can be both a valuable by-product and a maintenance expense.

Storage by other liquids

The most commonly proposed substitutes for water are petroleum based oils and molten salts [Pilkington Solar International GmbH, 2000]. The heat capacities are 25-40% of that of water on a weight basis. However, these substitutes have lower vapor pressure than water and are capable of operating at high temperatures exceeding 300°C. The oils are limited to less than 350°C due to stability and safety reasons and can be quite expensive. Some of the oil candidates that have been considered are Therminol and Caloria-HT. A few molten mixtures of inorganic salts have been considered for high temperatures (300°C and above). One is sodium hydroxide which has a melting point of 320°C and could be used for temperatures up to 800°C. However, it is highly corrosive, and there is a difficulty in containing it at high temperatures. Liquid metals are also mentioned as possible sensible heat storage media. While

most or their properties are similar to those of water, they, along with the petroleum based oils, have low specific heats and higher potential for reactivity with the container. They do, however, enjoy higher thermal conductivity. The stainless steel type 304 is the most common material used for containment of oils and liquid metals, with special attention usually given to the maintenance of an oxygen and oxide free environment in order to prevent corrosion [Hasnain S. M. 1998]. The characteristics of those materials can be found in Table 1-1 [Pilkington Solar International GmbH, 2000].

Table 1-1 Characteristics of the liquid media [Pilkington Solar International GmbH, 2000]

Medium of storage	Temperature		Average density	Average heat conductivity	Average specific heat	Storage capacity	Price of medium	Cost of medium per kWh
	cold (°C)	hot (°C)	(kg/m³)	(W/mK)	(kJ/kgK)	(kWh/m³)	($/kg)	($/kWh)
Mineral oil	200	300	770	0.12	2.6	55	0.30	4.2
Synthetic oil	250	350	900	0.11	2.3	57	3.00	43.0
Silicone oil	300	400	900	0.10	2.1	52	5.00	80.0
Nitrite salts	250	450	1,825	0.57	1.5	152	1.00	12.0
Nitrate salts	265	565	1,870	0.52	1.6	250	0.70	5.2
Carbonate salts	450	850	2,100	2.0	1.8	430	2.40	11.0
Liquid sodium	270	530	850	71.0	1.3	80	2.00	21.0

Summary of sensible storage in liquid form

Presently, most thermal storage devices use sensible heat storage and a good technology is developed for the design of such systems. However, above 100°C, the storage tank must be able to contain water at its vapor pressure and the storage tank cost rises sharply for temperatures above this point. Organic oils molten salts and liquid metals do not exhibit the same pressure problems but their use is limited because of their handling, containment, storage capacities and cost. Between liquid materials, water appears to be the most convenient because it is inexpensive and has a high specific heat.

1.1.2 Sensible storage by solid form

Energy can be stored in rocks or pebbles packed in insulated vessels. This type of storage is used very often for temperatures up to 100°C in conjunction with solar air heaters. It is simple in design and relatively inexpensive. Typically, the characteristic size of the pieces of rock

used varies from 1 to 5 cm. An approximate rule of thumb for sizing is to use 300 to 500 kg of rock per square meter of collector area for space heating applications. Rock or pebble-bed storages can also be used for much higher temperatures up to 1000°C [Hasnain S. M. 1998].

The difficulties and limitations relative to the liquid storage can be avoided by using solid materials for storing thermal energy as sensible heat. But larger amounts of solids are needed than using water, due to the fact that solids, in general, exhibit a lower storing capacity than water [Lundh M. 2008, Pfeil M. et al. 2000, Doerte Laing 2006, Reuss M. et al. 1997]. The cost of the storage media per unit energy stored is, however, still acceptable for rocks.

Direct contact between the solid storage media and a heat transfer fluid is necessary to minimize the cost of heat exchange in a solid storage medium. The use of rocks for thermal storage provides the following advantages:

• Rocks are not toxic and non-flammable
• Rocks are inexpensive
• Rocks act both as heat transfer surface and storage medium
• The heat transfer between air and a rock bed is good, due to the very large heat transfer area, and the effective heat conductance of the rock pile is low, due to the small area of contact between the rocks. Then the heat losses from the pile are low.

Magnesium oxide (magnesia), aluminum oxide (alumina) and silicone oxide are refractory materials, and they are also suitable for high-temperature sensible heat storage. Bricks made of magnesia have been used in many countries for many years for storing heat. They are available in the form of devices with electric heater elements embedded in the bricks. The heat is stored at night (when electricity rates are low) by switching on the electric heaters and is supplied during the day for space-heating purposes by allowing air to pass through the devices. Below, the properties of solid media storage are listed in Table 1-2.

Table 1-2 Solid media properties for sensible heat storage [Ataer O. Ercan]

Medium	Density (kg/m3)	Specific Heat (J/kgK)	Heat Capacity $\rho c \times 10^{-6}$ ($J/m^3 \cdot K$)	Thermal Conductivity (W/mK)	Thermal Diffusivity $\alpha = k/\rho c\ 10^6$ (m^2/s)
Aluminum	2707	896	2.4255	204 at 20°C	84.100
Aluminum oxide	3900	840	3.2760	-	-
Aluminum sulfate	2710	750	2.0325	-	-
Brick	1698	840	1.4263	0.69 at 29°C	0.484
Brick magnesia	3000	1130	3.3900	5.07	1.496
Concrete	2240	1130	2.5310	0.9 – 1.3	0.356-0514
Cast iron	7900	837	6.6123	29.3	4.431
Pure iron	7897	452	3.5694	73.0 at 20°C	20.450
Calcium chloride	2510	670	1.6817	-	-
Copper	8954	383	3.4294	385 at 20°C	112.300
Earth (wet)	1700	2093	3.5581	2.51	0.705
Earth (dry)	1260	795	1.0017	0.25	0.250
Potassium chloride	1980	670	1.3266	-	-
Potassium sulfate	2660	920	2.4472	-	-
Sodium carbonate	2510	1090	2.7359	-	-
Stone, granite	2640	820	2.1648	1.73 to 3.98	0.799-1.840
Stone, limestone	2500	900	2.2500	1.26 to1.33	0.560-0.591
Stone, marble	2600	800	2.0800	2.07 to 2.94	0.995-1.413
Stone, sandstone	2200	710	1.5620	1.83	1.172

1.2 Latent thermal storage

In latent heat storage the principle is that when heat is applied to the material it changes its phase from solid to liquid by storing the heat as latent heat of fusion or from liquid to vapor as latent heat of vaporization. When the stored heat is extracted by the load, the material will again change its phase from liquid to solid or from vapor to liquid. The latent heat of transformation from a solid into a liquid phase is small. Solid-vapor and liquid-vapor transitions have large amounts of heat of transformation, but large changes in volume make the system complex and impractical. The solid-liquid transformations involve relatively small changes in volume. Such materials are available in a range of transition temperatures.

Materials to be used for phase change thermal energy storage must have a large latent heat and high thermal conductivity. They should have a melting temperature lying in the practical range of operation, melt congruently with minimum subcooling and be chemically stable, low in cost, nontoxic and non-corrosive. Materials that have been studied during the last 40 years are hydrated salts, paraffin waxes, fatty acids and eutectics of organic and non-organic compounds.

Depending on the applications, the phase change materials (PCMs) should first be selected based on their melting temperature. Figure 1-3 shows the relation between melting temperature and heat of fusion for these materials [Hauer A.[2] et al. 2002]. Materials that melt below 15°C are used for storing coolness in air conditioning applications, while materials that melt above 90°C are used for absorption refrigeration. All other materials that melt between these two temperatures can be applied in solar heating and for heat load leveling applications.

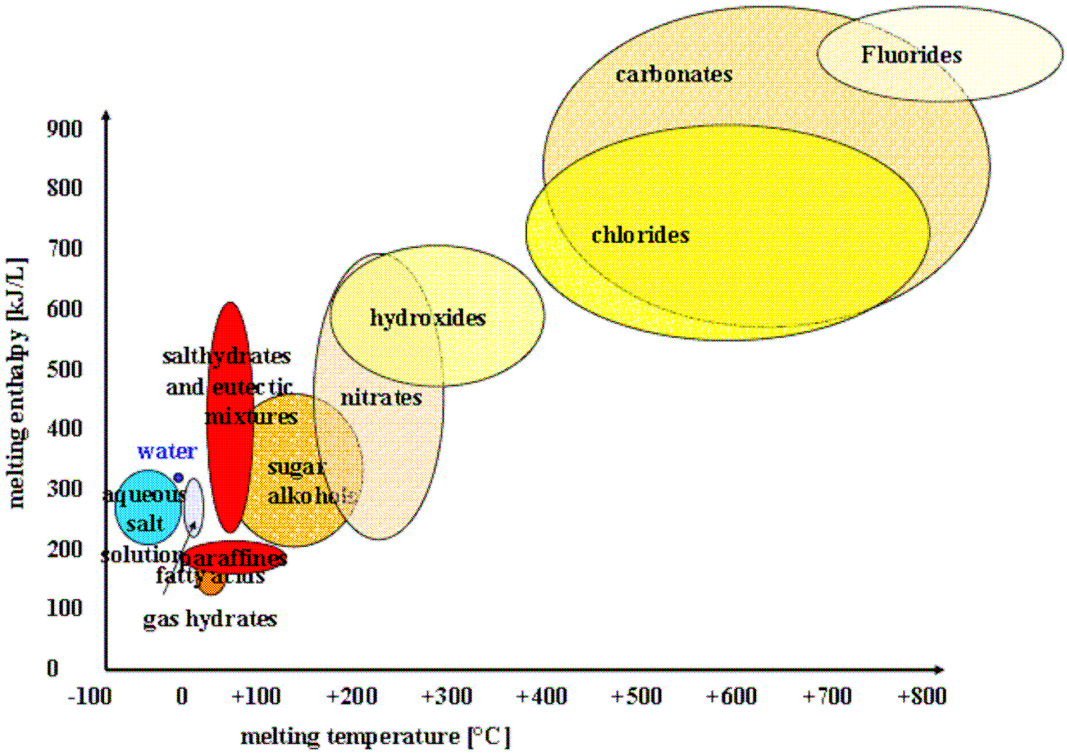

Figure 1-3 Relation between melting temperature and heat of fusion for PCMs [Hauer A.[2] et al. 2002]

The energy density of sensible storage can be increased by introducing a substance having its phase change temperature within the temperature range of the storage.

Within a temperature interval $\Delta T = T_2 - T_1$ the stored heat is then:

$$Q = \int_{T_1}^{T_{ls}} Cp_{ph1}\, dt + \int_{T_{ls}}^{T_2} Cp_{ph2}\, dt + \Delta H_{ls} \qquad \text{Eq.1-2}$$

where Q is the sensible and latent heat stored, Cp_{ph1} and Cp_{ph2} are the heat capacities of the PCM on its different phases, and ΔH_{ls} is the heat of phase change at the phase change temperature T_{ls} with $T_1 \le T_{ls} \le T_2$.

The reachable temperature difference ΔT is determined by the charging temperature, which is given by the heat source.

A list of possible materials that may be used for latent heat storage is shown in Table 1-3 [Agyenim et al. 2010, Lorsch H. G. et al. 1976]. Lane G. A. and Humphries W. R. have

reported a large number of possible candidates for latent heat storage covering a wide range of temperatures [Lane G. A. et al 1977, Humphries W. R. et al. 1975, Abhat A. 1983].

Many PCMs have poor thermal conductivity and therefore require large heat exchange area. Others are corrosive and require special containers. Latent heat storage materials are more expensive than the sensible heat storage media generally employed, like water and rocks. These increase the system cost.

Due to its high cost, latent heat storage is more likely to find application when:

1. High energy density or high volumetric energy capacity is desired, e.g., in habitat where space is at a premium, or in transportation where both volume or weight must be kept to a minimum,

2. The load is such that energy is required at a constant temperature or within a small range of temperatures,

3. The storage size is small. Smaller storage has higher surface area to volume ratio and therefore cost of packing is high. Compactness is then very important in order to limit the containment costs. Similarly, heat losses are also more or less proportional to the surface area.

Table 1-3 Thermo-physical properties of PCMs investigated for different applications. [Agyenim et al. 2010, Lorsch H. G. et al. 1976]

PCMs	Melting temperature T_m (°C)	Heat of fusion, ΔH_{ls} (kJ kg^{-1})	Specific heat capacity, C_p (kJ kg^{-1} K^{-1})	Heat conductivity, λ (W m^{-1} K^{-1})	Density, ρ (kg m^{-3})
Water-ice	0	335	4,2	2,4 (liquid) 0,6	1000
GR25	23,2–24,1	45,3	1,2 (solid) 1,2 (liquid)	–	–
RT25–RT30	26,6	232,0	1,80 (liquid) 1,41 (solid)	0,18 (liquid) 0,19 (solid)	749 (liquid) 785 (solid)
n-Octadecane	27,7	243,5	2,66 (liquid) 2,14	0,148 (liquid) 0,190 (solid)	785 (liquid) 865 (solid)
$CaCl_2 \cdot 6H_2O$	29,9	187	2,2 (liquid) 1,4 (solid)	0,53 (liquid) 1,09 (solid)	1530 (liquid) 1710 (solid)
$Na_2SO_4 \cdot 10H_2O$	32, 39	180	2,0 (liquid) 2,0 (solid)	0,15 (liquid) 0,3(solid)	1460 (solid)
Paraffin wax	32–32,1	251	1,92(solid) 3,26(liquid)	0,514 (solid) 0,224 (liquid)	830
Capric acid	32	152,7	–	0,153 (liquid)	878 (liquid) 1004 (solid)
Polyethelene glycol 900 (PEG900)	34	150,5	2,26 (liquid) 2,26 (solid)	0,188 (liquid) 0,188 (solid)	1100 (liquid) 1200 (solid)
Lauric–palmitic acid (69:31) eutectic	35,2	166,3	2,41 (liquid) 1,77 (solid)		
Lauric acid	41–43	211,6	2,27(liquid) 1,76(solid)	1,6	1,76(solid) 0,862 (liquid)
Stearic acid	41–43 (67–69)*	211,6	2,27 (liquid) 1,76 (solid)	1,60 (solid)	862 (liquid) 1007 (solid)
Medicinal paraffin	40–44	146	2,3 (liquid) 2,2 (solid)	2,1 (liquid) 0,5 (solid)	830 (solid)
Paraffin wax	40–53				
P116-Wax	46,7–50	209	2,89 (liquid) 2,89 (solid)	0,277 (liquid) 0,140 (solid)	786 (solid)
Merck P56-58	48,86–58,06	250	2,37 (liquid) 1,84 (solid)	–	–
Commercial paraffin wax	52,1	243,5	–	0,15	809,5 (solid) 771 (liquid)
Myristic acid	52,2	182,6	–	–	–
Paraffin RT60/RT58	55 to 60	214,4–232	0,9	0,2	775 (liquid) 850 (solid)
Palmitic acid	57,8–61,8	185,4		0,162 (liquid)	850 (liquid) 989 (solid)
$Mg(NO_3)_2 \cdot 6H_2O$	89	162,8	–	0,490 (liquid) 0,611 (solid)	1550 (liquid) 1636 (solid)
RT100	99	168	2,4 (liquid) 1,8 (solid)	0,2 (liquid) 0,2 (solid)	770 (liquid) 940 (solid)
$MgCl_2 \cdot 6H_2O$	116,7	168,6	2,61 (liquid) 2,25 (solid)	0,570 (liquid) 0,704 (solid)	1450 (liquid) 1570 (solid)
Erythritol	117,7	339,8	2,61(liquid) 2,25(solid)	0,326 (liquid) 0,733 (solid)	1300 (liquid) 1480 (solid)
$Na/K/NO_3$ (0,5/0,5)	220	100,7	1,35	0,56	1920
$ZnCl_2$/KCl (0,319/0,681)	235	198	–	0,8	2480
$NaNO_3$	310	172	1,82	0,5	2260
KNO_3	330	266	1,22	0,5	2110
NaOH	318	165	2,08	0,92	2100
KOH	380	149,7	1,47	0,5	2044
$ZnCl_2$	280	75	0,74	0,5	2907
LiF–CaF_2 (80,5:19,5) mixture	767	816	1770 (liquid) 1,770 (liquid)	1,70 (liquid) 3,8 (solid)	2390 (liquid) 2390 (solid)

1.3 Storage by chemical reaction

The basic principle of the storage by chemical reaction is AB + heat ⇔ A+B. During the summer phase, the compound AB is broken into components A and B by solar heat. The A and B compounds can be stored separately during the storage phase. During the winter phase, A and B are mixed for reaction and AB is formed. The heat of reaction is released for house heating or other thermal use. The storage capacity depends on the heat of reaction.

For this type of storage it is necessary that the chemical reactions involved are completely reversible. The heat produced by the solar receiver is used in the endothermic chemical reaction. If this reaction is completely reversible, the heat can be recovered completely by the reversed reaction. Often, catalysts are necessary to release the heat. This is even advantageous as the reaction can then be controlled by the catalyst [Pilkington Solar International GmbH 2000].

Commonly cited advantages of thermal energy storage by reactions are high storage energy densities, indefinitely long storage duration at near ambient temperature, and heat-pumping capability. Drawbacks may include complexity, uncertainties in the thermodynamic properties of the reaction components and of the reactions kinetics under the wide range of operating conditions, high cost, toxicity, and flammability.

Although the thermal energy storage by reactions has several advantages concerning their thermodynamic characteristics, development is at a very early stage. To date, no viable prototype has been built.

Table 1-4 presents several reactions that have been investigated to be used as chemical storage materials.

Table 1-4. Chemical reaction storage materials [Van Berkel J. 2005]

Medium	Reaction	Energy density	Reaction temperature
Ammonia	$NH_3 + \Delta H \leftrightarrow 1/2N_2 + 3/2H_2$	67 kJ/mol	400–500°C
Hydroxides, e.g.	$Ca(OH_2) \leftrightarrow CaO + H_2O$	3 GJ/m^3	500°C
Calcium carbonate	$CaCO_3 \leftrightarrow CaO + CO_2$	4.4 GJ/m^3	800–900°C
Iron carbonate	$FeCO_3 \leftrightarrow FeO + CO_2$	2.6 GJ/m^3	180°C
Metal hydrides	Metal $xH_2 \leftrightarrow$ metal $yH_2 + (x - y)H_2$	4 GJ/m^3	200–300°C
Magnesium oxide	$MgO + H_2O \leftrightarrow Mg(OH)_2$	3.3 GJ/m^3	250–400°C

Metal oxide/metal (SnOx/Sn) reactions are also possible and technically feasible, for example [Forster M. 2004, Choi W.K. 1997]:

$$SnO_2 + 2CH_4 + heat \Leftrightarrow Sn + 2CO + 4H_2 \quad \text{Eq.1-3}$$

$$Sn + 2H_2O \Leftrightarrow SnO_2 + 2H_2 + heat \quad \text{Eq.1-4}$$

During the summer phase, the concentrated solar energy will increase the temperature in the reactor (Figure 1-4). Reaction (Eq.1-3) takes place at 980 K and the liquid Sn is stored in a tank. When the thermal energy is needed during the winter phase, cold Sn is sent to a tank where H_2O vapor is added, creating reaction (Eq.1-4). In this way, SnO_2 can be recuperated to restart the process. The critical point of this device is the kinetic behavior of reactions. Although the reaction is feasible with solar energy, technically, it is still not developed, and it is necessary to increase the investigation.

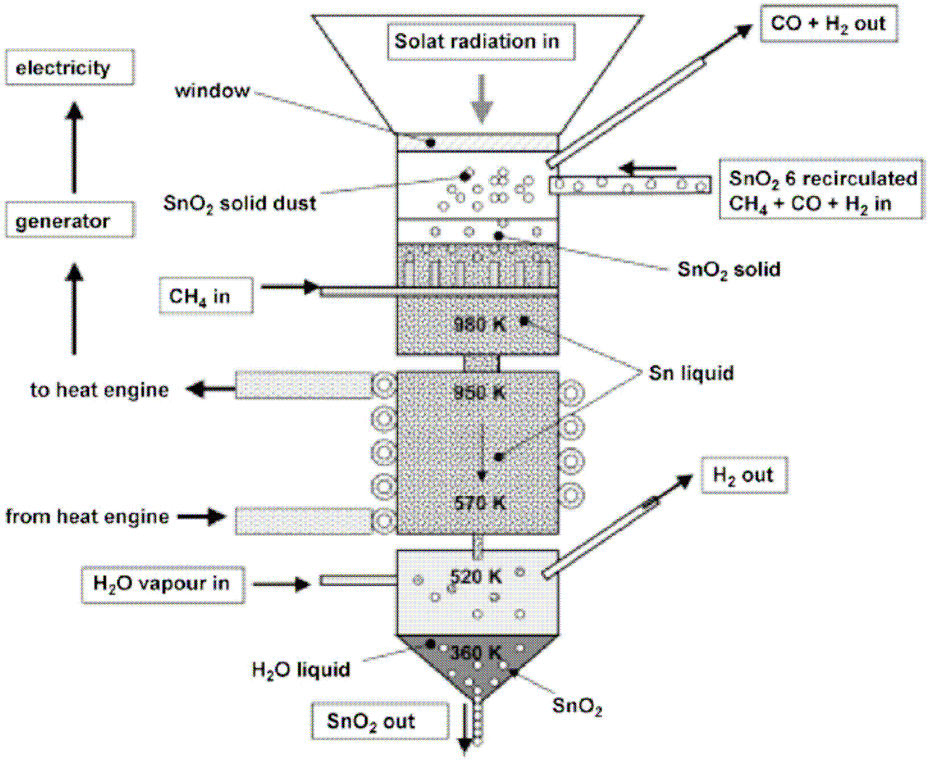

Figure 1-4 Proposed schematic solar reactor for reaction, in the upper part, heat recovery in the middle part, and hydrogen generation, in the lower part.

Some hydration reactions are also used for the storage system, the performance can be found as follows:

Na_2S/H_2O: Sodium sulphide presents a high sorption capacity and a high heat of sorption so it provides a high thermal power density combined with a high energy storage density. The storage capacity of Na_2S in form of $Na_2S{\cdot}9H_2O$ is almost 1.1 kWh/kg (1980 kWh/m^3) for heat and 0.7 kWh/kg (1300 kWh/m^3) for cooling with COP of 0.84 and 0.57. Considering the $Na_2S{\cdot}5H_2O$, the storage capacity is almost 780 kWh/m^3 for heating and 510 kWh/m^3 for cooling. However, sodium sulphide is very corrosive and operates under vacuum [Boer et al. 2004]

$MgSO_4{\cdot}7H_2O$: The magnesium sulphate heptahydrate is considered as a very good potential in terms of solar energy storage with high density of almost 780 kWh/m^3 at temperature level of 122°C [Bales C[1]. 2008]. $MgSO_4{\cdot}7H_2O$ is advantaged by its non-toxic and non-corrosive characteristics but it is expensive. However, some experiments performed by EDF R&D show that the practical use of pure magnesium sulphate is quite difficult because of its low power density [Hongois S. et al. 2008]

1.4 Storage by sorption

Sorption can be defined as a phenomenon of fixation or capture of a gas or a vapor (sorbate) by a substance in condensed state (solid or liquid) called sorbent [Hauer A.[3] 2007]. Sorption phenomena can involve both absorption and adsorption. [Aveyard R. & D.A. Haydon 1973]. Absorption is defined as a phenomenon in which a liquid or a gas enters a solid or a liquid. However, considering storage applications, this term is usually relative to the absorption of a gas by a liquid (absorbent). In the same way, adsorption is usually used to designate a phenomenon of binding of a gas on a surface of a solid or porous material when a more general acceptation of the word refers to a surface phenomenon: an attachment of gas or liquid phase of a component to the surface of another substance [Srivastava N.C. et al. 1998, Mandelis A. et al. 1993].

The principle of sorption storage can be described as follows:

$$AB + \text{heat} \Leftrightarrow A + B \qquad \text{Eq.1-5}$$

A/B is called a working pair or sorption couple. Under the influence of a heat supply, a compound AB is dissociated into components A and B which can be stored separately (endothermic phenomenon). When A and B are put in touch, component AB is formed with a heat release (exothermic phenomenon). Energy can therefore be stored with negligible thermal loss since heat is not kept in sensible or latent form but as a chemical potential [Kato Y. 2007].

In thermal energy storage systems by absorption, researchers are mainly submitted to the following challenges [Hadorn J-C. 2006]:

- The choice of the best system;
- The storage density optimization linked to the choice of materials (this point will be detailed in the following);
- The vessels/tanks design;
- The heat exchangers design and the reactors configuration;
- Pressure drop;
- The low-temperature heat source in winter;
- Efficiency;
- Cost.

Materials appear to play a key role in these challenges. A suitable material can store the energy without heat loss and is able to release this energy immediately when it is needed. There are a great number of materials that could be used for sorption when focusing only on the thermodynamic principle of reversible reactions [A. Hauer[3] 2007]. Some technical, economic or ecological criteria lead to a closer set. Indeed, usual selection criteria of materials used in sorption machines are [Visscher K. 2004]:

- High affinity for the sorbent by the sorbate: this has an effect on the rate of the ab/adsorption reaction, which is important for a usable power density;
- Higher volatility of the sorbate (than the sorbent) in absorption;
- High storage density;
- High thermal conductivity (in particular for adsorption) and high heat transfer from sorbate to heat exchangers;
- Regeneration (charging) temperature as low as possible: this results in higher solar collector efficiency in the case of solar heat storage;
- Heat source needed for the evaporation during discharging period at relatively low temperature;
- Environment safety, non-toxicity, low Global Warming Potential and Ozone Depletion Potential;
- Non-corrosiveness of materials;
- Good thermal and chemical stability under operating conditions (temperature, pressure);
- Moderate operating pressure range: no excessive pressure conditions and especially no high vacuum;
- Low material cost.

Different working pairs or materials, according to their ability to fulfill aforementioned requirements, have been considered in thermal energy storage systems. Studies aimed to describe physicochemical and thermodynamic properties of materials suitable for long-term storage of thermal energy, since knowledge on materials is a prerequisite to the design of different components of storage units and exchangers [Bales C.[3] 2005]. The couples which have been studied for the thermal energy storage systems can be found as follows:

Solid-gas (adsorption)

Zeolites/H_2O: Zeolites are alumina silicates with high micro-porosity and are considered to be compatible with the most stringent environmental regulations. Apart from natural zeolites

(minerals), different types of synthetic zeolites have been developed for special purposes. Alefeld et al. ruled out the use of zeolites in seasonal storage for economical reasons and suggested that zeolites could be used in the load leveling within a district heating network [Alefeld et al. 1981]. Hauer has reported in experimental results that the storage capacity is 124 kWh/m^3 with COP of 0.9 for heating and is 100 kWh/m^3 with COP of 0.86 for cooling using the synthetic Zeolite 13X [Hauer A.[1] 2002]. The natural zeolites could be used as storing material instead of the 13X synthetic zeolite when the heating temperature is below 100°C.

Silicagel/H_2O: The storage density of silicagel is up to about 4-times that of water (25/85°C). [Faninger G. 2004]. Silicagel has been used for thermal energy storage systems by AEE-INTEC (Institute for Sustainable Technologies, Austria) [Jaehnig D. et al. 2006, Van Essen M. et al 2008] in a series of studies. They achieved experimentally about 50 kWh/m^3 of storage capacity whereas they had theoretically estimated to reach a storage density of 200–300 kWh/m^3.

Liquid-gas (absorption)

NaOH/H_2O: A calculation made for a single family home according to the passive house standard (120 m^2, heat demand at 35°C = 15 kWh/m^2, Domestic Hot Water about 50 l/day at 60°C, evaporator temperature = 5°C) results in a total storage volume of 7 m^3, including tanks and heat exchangers, in a two stages process [Weber RVD. 2008]. The experimental measures performed on the prototype during charging have met the expectations of EMPA. The maximum attainable absorber temperature was 95°C and the lowest condenser temperature reached was 13°C, corresponding to a lye concentration of 62 wt%. This concentration value is approximately 7 wt% higher than expected. However, special care must be taken when working with caustic soda because it is highly corrosive.

LiCl/H_2O: Based on the results presented by ClimateWell (in Sweden) [Bales C.[2] 2008], this pair is not suitable for seasonal storage, not because of its storage density (253 kWh/m^3 LiCl salt), which is 2.7 times higher than that of water (25/85°C), but because of the high cost of the salt (about 6000 Euros/t).

A review paper on the storage systems by sorption has been published in Renewable and Sustainable Energy Reviews [N'Tsoukpoe et al. 2009].

1.5 Conclusion of the state of art of solar heat storage

This chapter has reviewed some of the information available in the literature regarding thermal energy storage, with the focus on the classification of storage system concepts and the description of the materials used in these different concepts. The following conclusions can be drawn:

1. The requirements for a thermal storage system are: high energy density in the storage material (storage capacity); good heat transfer between heat transfer fluid and the storage medium; mechanical and chemical stability of storage material; heat exchanger and/or storage medium (safety); complete reversibility of a number of charging/discharging cycles (lifetime); low thermal losses; ease of control; adequate operation strategy; adapted maximum load; and integration into the building.

2. According to the storage media, storage systems are classified as sensible heat storage, latent heat storage, reaction heat storage and sorption heat storage. Only the sensible heat and latent heat have been actually used in real solar power storage, although other storages offer some advantages and are the target storage technologies.

3. Solid sensible heat storage have been investigated and tested recently. The low cost of the solid material has to be balanced with the high cost of the heat storage design, especially the required heat exchanger.

4. Latent heat storage is a promising technology, as it brings higher storage density and nearly constant temperature. Several materials have been analyzed and used, but latent heat storage also suffers from high heat losses for long-term periods.

5. The chemical and sorption storage technology is also promising, but is even less developed than the latent heat. Much more investigation is still needed for the realization of those systems.

References of Chapter 1

Abhat A.. 1983. Low temperature latent heat thermal energy storage. Heat storage materials. Solar Energy. 30, pp. 313–332

Agyenim F., Hewitt N., Eames P., Smyth M.. 2010. A review of materials, heat transfer and phase change problem formulation for latent heat thermal energy storage systems (LHTESS). Renewable and Sustainable Energy Reviews. 14(2), pp. 615-628

Alefeld G, Maier-Laxhuber P, Rothmeyer M.. 1981. Thermochemical heat storage and heat transformation with zeolites as adsorbents. In: Proceedings of IEA conference on new energy conversion technologies and their commercialization, Berlin. pp. 796–819

Amaya V. Novo, Joseba R. Bayon, Daniel Castro-Fresno, Jorge Rodriguez-Hernandez. 2010. Review of seasonal heat storage in large basins: Water tanks and gravel–water pits. Applied Energy. 87(2), pp. 390-397

Ataer O. Ercan, Energy storage systems - Storage of solar energy. http://www.eolss.net/ebooks/Sample%20Chapters/C08/E3-14-02-00.pdf

Aveyard R., Haydon D.A.. 1973. An introduction to the principles of surface chemistry, CUP Archive.

Bales C.[1]. 2008. Laboratory tests of chemical reactions and prototype sorption storage units. www.iea-shc.org

Bales C.[2]. 2008. Final report of Subtask B ‘‘Chemical and Sorption Storage’’ the overview. pp. 23. www.iea-shc.org

Bales C.[3]. 2005. Thermal properties of materials for thermo-chemical storage of solar heat. pp. 18. www.iea-shc.org

Boer R.D., Haije W., Veldhuis J., Smeding S.. 2004. Solid sorption cooling with integrated storage: the SWEAT prototype. In: 3rd international heat powered cycles conference—HPC 2004

Bauer D., Marx R., Nußbicker-Lux J., Ochs F., Heidemann W., Müller-Steinhagen H.. 2010. German central solar heating plants with seasonal heat storage. Solar Energy. 84(4), pp. 612-623

Choi W.K., Song S.K, Cho J.S., Yoon Y.S., Choi D., Jung H.-J., Koh S.K.. 1997. H2 gas-sensing characteristics of SnOx sensors fabricated by a reactive ion-assisted deposition with/without an activator layer. Sensors and Actuators B: Chemical. 40(1), pp. 21-27

Doerte Laing, Wolf-Dieter Steinmann, Rainer Tamme, Christoph Richter. 2006. Solid media thermal storage for parabolic trough power plants. Solar Energy. 80(10), pp. 1283-1289

Faninger G. 2004.Thermal energy storage; etn.wsr.ac.at.

Forster Martin. 2004. Theoretical investigation of the system SnOx/Sn for the thermochemical storage of solar energy. Energy, 29(5-6), pp. 789-799

Gil Antoni, Medrano Marc, Martorell Ingrid, Lázaro Ana, Dolado Pablo, Zalba Belén, Cabeza Luisa F. . 2010. State of the art on high temperature thermal energy storage for power generation. Part 1—Concepts, materials and modellization Review Article. Renewable and Sustainable Energy Reviews. 14(1), pp. 31-55

Hadorn J-C. 2006. IEA solar heating and cooling programme—Task 32: advanced storage concepts for solar and low energy buildings. In: Proceedings of ECOSTOCK, Richard Stockton College, New Jersey. http://www.iea-shc.org

Hasnain S. M.. 1998. Review on sustainable thermal energy storage technologies, Part I: heat storage materials and techniques. Energy Conversion and Management. 39(11), pp.1127-1138

Hauer A.[1]. 2002. Thermal energy storage with zeolite for heating and cooling applications. In: Proceedings of 3rd workshop of annex 17 ECES IA/IEA

Hauer A.[2], Mehlin H., Schossig P., Yamaha M., Cabeza L., Martin V., Setterwall F.. 2002. Annex 17, Advanced Thermal Energy Storage Techniques – Feasibility Studies and Demonstration Projects, final report. www.iea-eces.org

Hauer A.[3]. 2007. Sorption theory for thermal energy storage, Thermal energy storage for sustainable energy consumption, Springer, Netherlands, pp. 393–408

Hongois S., Stevens P., Coince A-S., Kuznik F., Roux J-J.. 2008. Thermochemical storage using composite materials. In: Proceedings of the Eurosun 2008, 1st international conference on solar heating, cooling and buildings

Humphries W.R., Griggs E.I.. 1977. A designing handbook for phase change thermal control and energy storage devices. NASA Technical Paper. pp. 1074

Jaehnig D., Hausner R.,Wagner W., Isaksson C.. 2006. Thermo-chemical storage for solar space heating in single-family house. In: ECOSTOCK conference

Kato Y.. 2007. Chemical energy conversion technologies for efficient energy use, Thermal energy storage for sustainable energy consumption, Springer, pp. 377–91

Kübler R., Fisch N., Hahne E.. 1997. High temperature water pit storage projects for the seasonal storage of solar energy. Solar Energy. 61(2), pp. 97-105

Lane G. A., Glew D. N., Clark E. C., Rossow H. E.. 1975. Quigley SW, Drake SS, et al. Heat of fusion system for solar energy storage subsystems for the heating and cooling of building. Chalottesville, Virginia, USA

Lorsch H. G., Kauffman K. W., Denton J. C.. 1976. Thermal energy storage for heating and air conditioning, Future energy production system. Heat Mass Transfer Processes. 1, pp.69–85

Lundh M., Dalenbäck J.-O. 2008. Swedish solar heated residential area with seasonal storage in rock: Initial evaluation. Renewable Energy. 33(4), pp. 703-711

Mandelis A., Christofides C.. 1993. Physics and chemistry and technology of solid state gas sensor devices (illustrated ed.). Wiley-Interscience, New York

N'Tsoukpoe K. E.,Liu H., Le Pierrès N., Luo L.. 2009. A review on long-term sorption solar energy storage. Renewable and Sustainable Energy Reviews. 13(9), pp. 2385-2396

Pfeil Markus, Koch Holger. 2000. High performance–low cost seasonal gravel/water storage pit. Solar Energy. 69(6), pp. 461-467

Pilkington Solar International GmbH. 2000. Survey of thermal storage for parabolic trough power plants. National Renewable Energy Laboratory. [SR-550-27925]

Reuss M., Beck M., Müller J. P.. 1997. Design of a seasonal thermal energy storage in the ground. Solar Energy. 59(4-6), pp. 247-257

Solar Gradient Solar Ponds. 2009. http://www.teriin.org/tech_solarponds.php

Srivastava N.C. and Eames I.W.. 1998. A review of adsorbents and adsorbates in solid-vapour adsorption heat pump systems. Applied Thermal Engineering 18 (9–10), pp. 707–714

Tanaka Hideki, Tomita Takashi, Okumiya Masaya. 2000. Feasibility study of a district energy system with seasonal water thermal storage. Solar Energy. 69(6), pp. 535-547

Ucar A., Inalli M.. 2005. Thermal and economical analysis of a central solar heating system with underground seasonal storage in Turkey. Renewable Energy. 30(7), pp. 1005-1019

Van Berkel J.. 2005. Storage of solar energy in chemical reactions. In: Jean-Christophe Hadorn, editor. Thermal energy storage for solar and low energy buildings. Spain, Lleida

Van Essen M., Zondag AH., Schuitema R., van Helden WGJ., Rindt CCM.. 2008. Materials for thermochemical storage: characterization of magnesium sulfate. In: Proceedings of the Eurosun 2008, 1st international conference on solar heating, cooling and buildings

Velmurugan V., Srithar K.. 2008. Prospects and scopes of solar pond: A detailed review. Renewable and Sustainable Energy Reviews. 12(8), pp. 2253-2263

Visscher K.. 2004. Energy research Center of the Netherlands (ECN). Simulation of thermo chemical seasonal storage of solar heat—material selection and optimum performance simulation. In: Proceedings of workshop 2004 2nd workshop Matlab/Simulink for building simulation, CSTB, Paris, France. http://ddd.cstb.fr/simbad/workshop2

Weber RVD.. 2008. Long-term heat storage with NaOH. Vacuum. 82(7), pp. 708–16

Chapter 2 – Seasonal storage of solar energy for house heating by absorption technology

From the previous literature review, the absorption storage is advantaged by its low heat loss and high storage capacity. Even if the storage capacity is lower than the reaction storage technology, considering the low temperature needed for the solar energy, the absorption storage seems to be adapted for building needs. In this chapter, we propose to study a long-term energy storage system for house heating by absorption. The process will be introduced and described and seven absorbate/absorbent couples will be studied for the system. The studies of the storage capacity, the efficiency, the operating pressure, the temperature need for solar energy, the possible temperature for house heating, the material security and the material economy of the seven absorption couples: $CaCl_2/H_2O$, Glycerin/H_2O, KOH/H_2O, $LiBr/H_2O$, $LiCl/H_2O$, $NaOH/H_2O$ and H_2O/NH_3 are performed.

2.1 Process description and static model

2.1.1 Process description

The aim of this work is to develop a long-term energy storage system for house heating by absorption. The solar energy is stored in summer through desorption and the heat is released in winter through absorption. The different components of the seasonal storage system can be found in Figure 2-1.

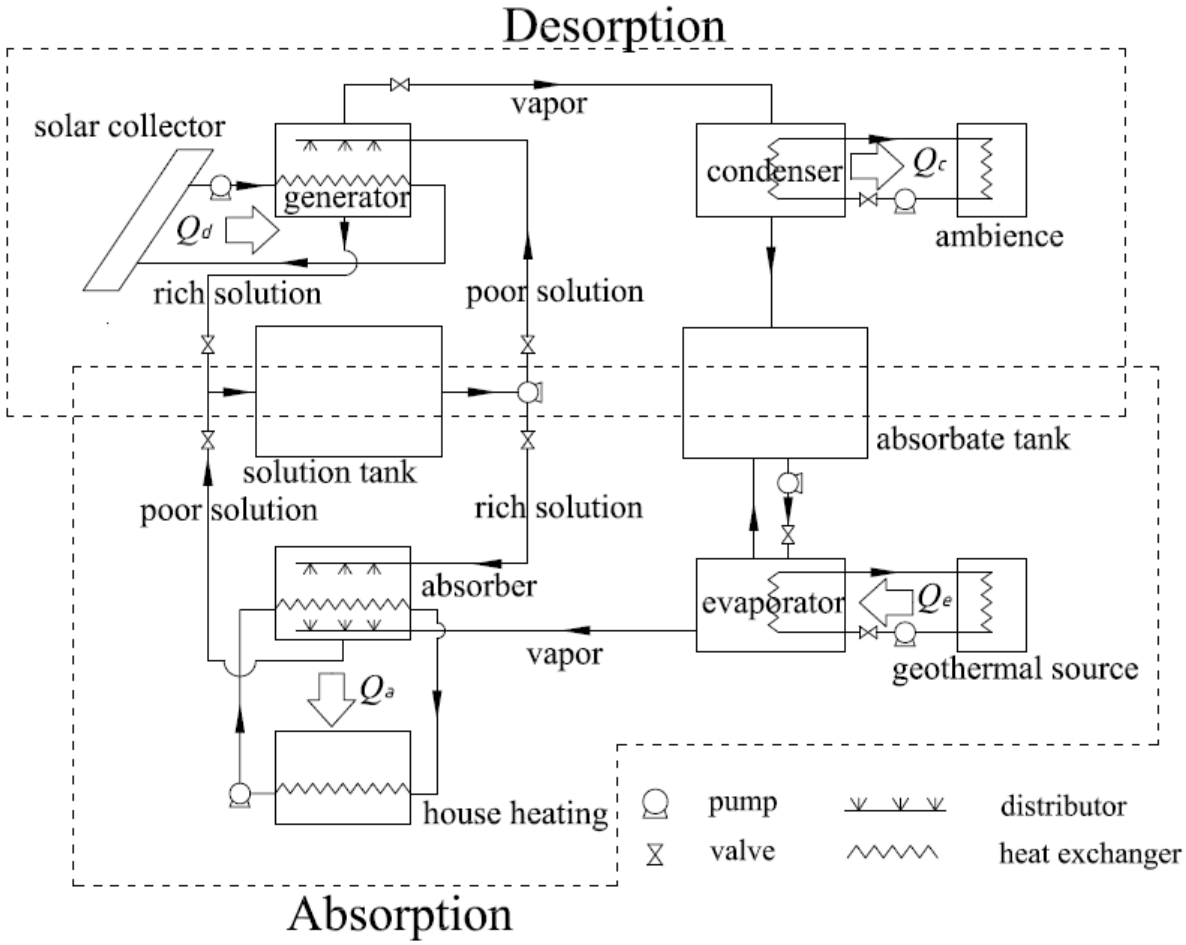

Figure 2-1 Solar energy seasonal storage system

During the summer phase (desorption), the poor solution (with low mass fraction of absorbent) in the solution tank is transported to the generator by a pump, where it is heated by the solar energy (Q_d) coming from a solar collector. Following the solution thermodynamic equilibrium, the absorbate in the solution can be vaporized and transferred to the condenser where its latent heat (Q_c) is released to the surrounding or used to preheat domestic hot water. The condensed absorbate flows to the absorbate tank where it is stored. The rich solution (with high mass fraction of absorbent) which is produced in the generator flows back to the solution tank.

During the inert storage period, the solution is kept in the solution tank and the liquid absorbate in the absorbate tank. The temperatures of the solution and absorbate change depending on the surrounding temperature. The different connection valves are closed, so no mass transfer happens during this period.

During the winter phase (absorption), the pressure in the system is lower than during the summer. The absorbate is circulated from the absorbate storage to the evaporator, where it is vaporized by low temperature geothermal heat (Q_e) coming from the ground following the liquid-vapor equilibrium. Because some characteristics of the heat exchanger in the evaporator such as the flow rate, the heat transfer area, the temperature difference etc. may not be optimized, the absorbate which is transferred to the evaporator could be not completely evaporated. Thus, the absorbate which is not vaporized flows back to the absorbate storage and can be recirculated. Following the solution thermodynamic equilibrium, the vapor of absorbate is absorbed by the rich solution which is circulated in the absorber. Thermal energy (Q_a) is released in the absorber along with the absorption process to meet the energy requirement for house heating. The energy need of this winter phase thus comes from geothermal energy which is upgraded by this system. The poor solution in the absorber after absorption flows back to the solution tank.

The process is run under vacuum conditions (meaning: absolute pressure in the system lower than the ambient pressure, and air-free environment) except for those couples which have higher equilibrium pressures at low temperatures than atmospheric pressure (such as H_2O/NH_3). The reasons for the vacuum condition are as follows:

1. The heat and mass transfer of desorption and absorption could be decreased by the presence of non-condensable gas (air).

2. Under vacuum conditions, heat losses to the surroundings by convection of the air in the reactor and tanks are minimized.

The innovation in this storage process is that the solution can reach the crystallization point, which is usually avoided in the absorption refrigeration machines because of the possible blockage of the fluid flows. The crystallization in the generator/absorber in this storage system is also forbidden for the same reason, but crystallization can be allowed in the solution tank, where there is little circulation of fluid. The storage capacity can be enhanced because of the increase of mass fraction of absorbent in the rich solution at the end of the summer phase, but the complexity of the solution tank/absorber conception is increased due to the appearance of crystal.

2.1.2 Static model

A static model has been developed for evaluating the feasibility and performance of the seasonal storage system. A representation of the process cycle can be found with the example of the $CaCl_2/H_2O$ absorption couple on the pressure-temperature-mass fraction diagram in Figure 2-2 (without crystal) and Figure 2-3 (with crystal).

2.1.2.1 Storage cycle without crystal

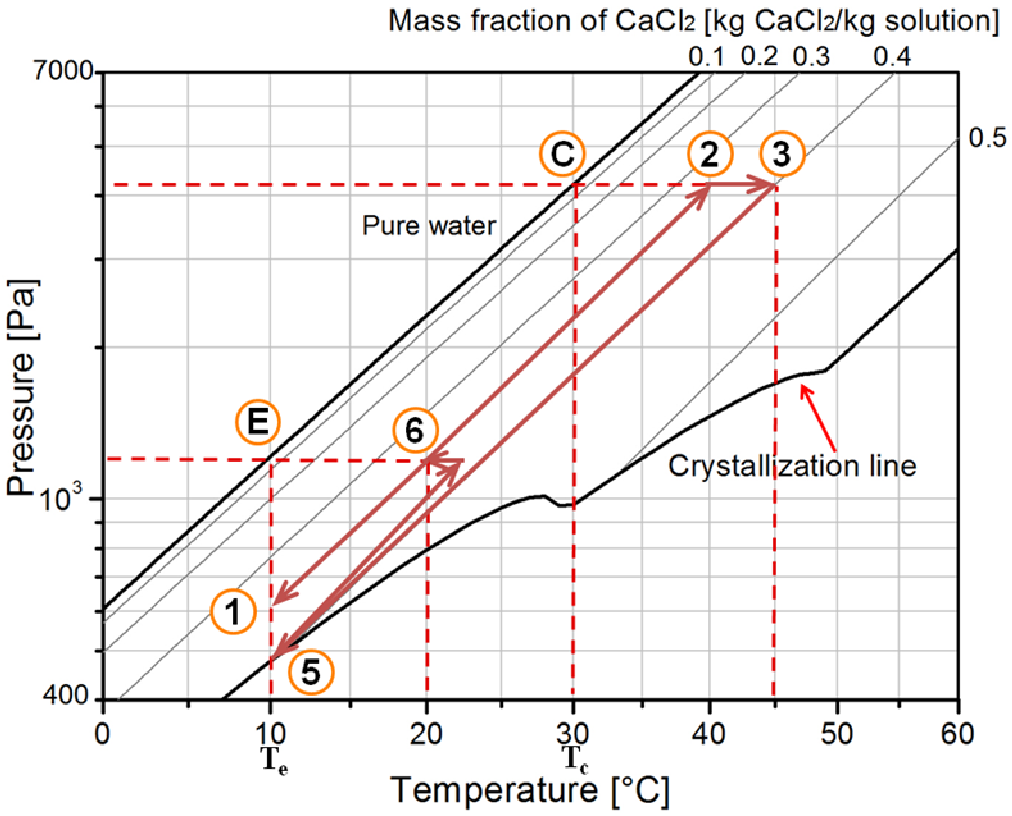

Figure 2-2 Seasonal solar energy storage cycle with $CaCl_2/H_2O$ (without crystal)

There are two states in the figure for pure water (state E and C). State E is the pure water at the evaporator. The temperature of state E (T_e) is chosen at 10°C, which is supposed to be the temperature of the ground during the winter phase. State C is the pure water in the condenser. The temperature of state C (T_c) is chosen at 30°C for condensation, which is supposed to be higher than the environment temperature during the summer phase.

There are five states for the solution in Figure 2-2 (state 1, 2, 3, 5 and 6). State 1 is the poor solution in the solution tank before the desorption phase (summer phase). The temperature of state 1 (T_1) is the temperature of the storage which is also chosen at 10°C.

During the charge phase, the solution at state 1 is heated by solar energy, which comes from the solar collector, to state 2. During this process, the valve which connects the condenser and generator is closed, the pressure of the solution increases with the temperature increase of the solution. The mass fraction of the solution is constant (Eq.2-1):

$$x_1 = x_2 \qquad \text{Eq.2-1}$$

The pressure balance of state 2 and state C is shown in Eq.2-2:

$$P_2 = f(x_2, T_2) = P_c = f'(T_c) \qquad \text{Eq.2-2}$$

In which, P_2 is the pressure of the solution at state 2 in the generator, which is linked to the solution temperature (T_2) and mass fraction (x_2), P_c is the pressure of state C, which is linked

to the water temperature (T_c), and $f(x, T)$ and $f'(T)$ are thermodynamic equilibria relations for the solution and pure water.

From state 2 to state 3, the solar energy is continually used to heat up the solution. The valve which connects the generator and condenser is open. Following the thermodynamic equilibria, the absorbate is desorbed from the solution and condensed in the condenser at 30°C (state C). State 3 is the rich solution after desorption. The pressure of state 2 and state 3 is the same as the pressure of state C.

The pressure balance of state 3 and state C is shown in Eq.2-3:

$$P_3 = f(x_3, T_3) = P_c = f'(T_c) \qquad \text{Eq.2-3}$$

In which, P_3 is the pressure of solution at state 3 in the generator, which is linked to the solution temperature (T_3) and mass fraction (x_3).

The mass fraction of absorbent at state 3 is chosen so that there is no crystal formed during the storage phase from state 3 to state 5. The state 5 is the solution in the solution tank at the temperature (T_5) of 10°C which is chosen as the ground temperature during the storage phase. This temperature is the same temperature as state 1 ($T_5 = T_1$). Because the solubility of $CaCl_2$ in water at T_5 is 0.398 kg $CaCl_2$/kg solution, the mass fraction of state 3 is chosen as such. Consequently, the temperature of state 3 is fixed at T_3 = 45°C, which can easily be attained by flat plate solar collectors.

During the storage phase from summer to winter, the solution temperature at state 3 decreases with the surrounding temperature till state 5. The rich solution and the absorbate are stored from the summer to the time when the heat production is needed. The solution has a constant mass fraction of absorbent.

$$x_3 = x_5 \qquad \text{Eq.2-4}$$

During the discharge phase, the water is evaporated by the geothermal energy at low temperature (10°C for example) in the evaporator (state E). The solution at state 5 absorbs vapor from the evaporator. The heat of absorption is released to heat up the water which is used in the floor heating system at the minimum temperature T_1 = 20°C (this low temperature can also meet the temperature requirements of optimized new heating floor technologies [Multibéton, 2009]). The mass fraction of the solution decreases and the pressure increases during the process to state 6. The state 6 is the poor solution after desorption. The mass fraction of state 6 is decided by the pressure balance of the absorber and evaporator (state E) in Eq.2-5:

$$P_6 = f(x_6, T_6) = P_e = f'(T_e) \qquad \text{Eq.2-5}$$

In which, P_6 is the pressure of solution at state 6 in the absorber, which is linked to the solution temperature (T_6) and mass fraction (x_6), P_e is the pressure of state E, which is linked to the water temperature (T_e).

At the end of the absorption phase, the solution at state 6 goes back to the solution tank at state 1 at the same mass fraction. The cycle is closed.

$$x_1 = x_6 \qquad \text{Eq.2-6}$$

The relative mass of solution for 1 kg absorbant at the different states can be calculated following Eq.2-7.

$$m_i = 1/x_i \qquad \text{Eq.2-7}$$

All the masses used in this static model are the relative masses for 1 kg absorbent, with the unit of kg/kg absorbent.

The corresponding vapor quantity which is released from the solution from state i to state j can be calculated following Eq.2-8.

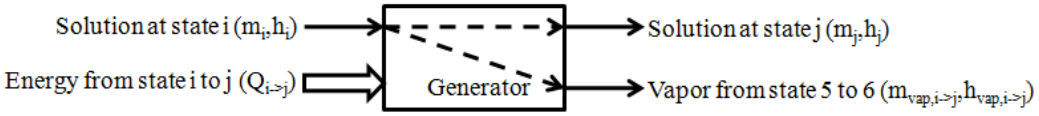

$$m_{vap,i\to j} = m_i - m_j \qquad \text{Eq.2-8}$$

The energy transfer from state i to state j $Q_{i\to j}$ can be calculated following Eq.2-9.

$$Q_{i\to j} = m_j \cdot h_j + m_{vap,i\to j} \cdot h_{vap,i\to j} - m_i \cdot h_i \qquad \text{Eq.2-9}$$

in which, $h_{vap,i\to j}$ is the enthalpy of vapor of absorbate which is absorbed/desorbed from the solution. This enthalpy is changed with the temperature of vapor during the phase of desorption/absorption. In this simplified model, the sensible heat of the components walls is neglected. The energy provided by the pumps to the liquids is also neglected.

Thus, the solar energy need during the summer phase Q_d is $Q_{1\to 3}$. The energy which is released to the heat exchanger for house heating during this phase Q_a is $Q_{5\to 6}$.

2.1.2.2 Storage cycle with crystal

Figure 2-3 shows the seasonal storage process with crystal.

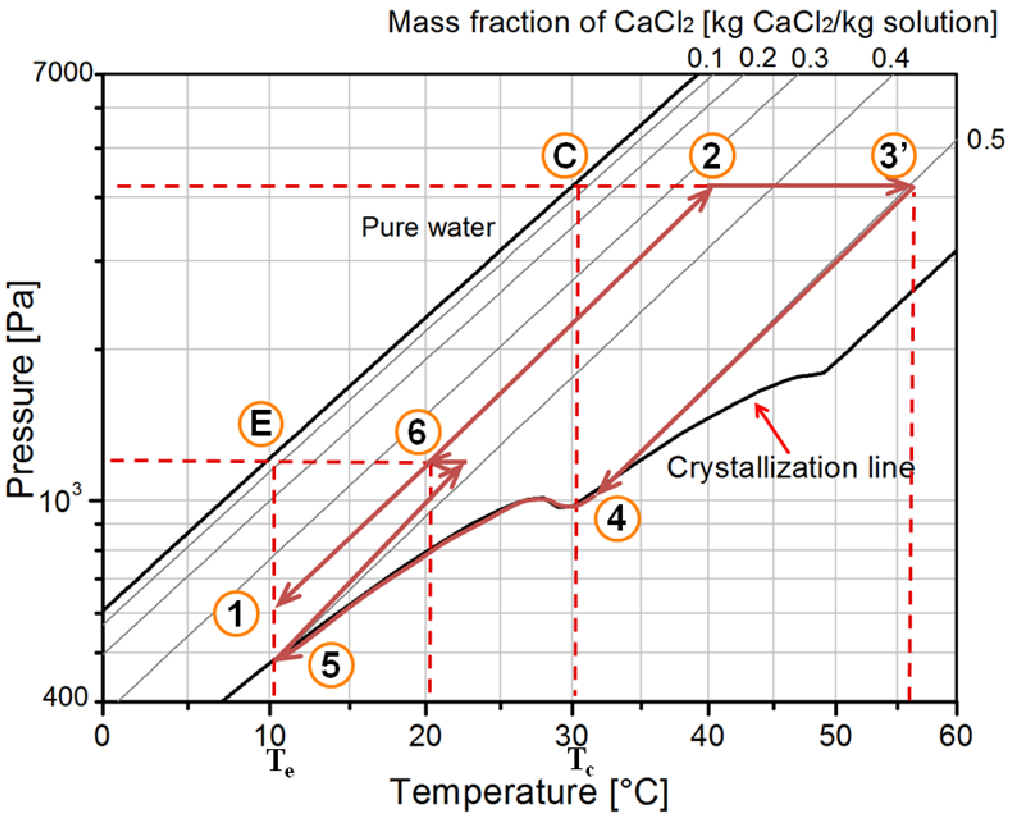

Figure 2-3 Seasonal solar energy storage cycle with $CaCl_2/H_2O$ (with crystal)

In the cycle with crystal, state 1, 2 and 6 are the same as in the cycle without crystal.

The mass fraction of absorbent at state 3' is higher than at state 3 (Figure 2-2). But to avoid entire crystal formation in the storage tank, the maximum mass fraction of absorbent after desorption is limited depending on the crystal form (hydratation of the solid). That is to say, the maximum mass fraction of the solution after desorption must be lower than the percentage of the absorbate in the crystal. The crystal of $CaCl_2$ at state 5 (10°C) is in form of $CaCl_2 \cdot 6H_2O$ with the percentage of absorbate at 50.7%. Thus the mass fraction of state 3' is chosen at 0.5 kg $CaCl_2$/kg solution for example. The pressure balance of state 3' and state C is shown in Eq.2-10:

$$P_{3'} = f(x_{3'}, T_{3'}) = P_c = f'(T_c) \qquad \text{Eq.2-10}$$

In which, $P_{3'}$ is the pressure of solution at state 3' in the generator, which is linked to the solution temperature ($T_{3'}$) and mass fraction ($x_{3'}$).

The solar energy needed during the summer phase Q_d can be calculated following Eq.2-9 as previously.

During the storage from summer to winter, the isosteric line crosses the crystallization line at state 4, so crystals appear in the storage tank. From state 4 to state 5, crystals are continually formed due to the decrease of the storage temperature.

The relative mass of the crystal appeared at state 5 m_{cry5} can be calculated following Eq.2-11.

$$m_{cry5} = m_{3'} - m_5 \qquad \text{Eq.2-11}$$

The corresponding relative mass of the solution at state 5 m_5 can be calculated following Eq.2-12.

$$m_5 x_5 + m_{cry5} x_{cry5} = m_{3'} x_{3'} \qquad \text{Eq.2-12}$$

in which x_5 can be calculated by the solubility of solution at the temperature of state 5. x_{cry5} is the percentage of the absorbate in the crystal at state 5.

At state 5, while solution from state 6 is recirculated to the solution tank, the crystal is progressively diluted but the mass fraction of the solution at state 5 is constant until all the crystal has disappeared, as the temperature of the solution tank is supposed to be constant.

The energy production during the winter phase Q_a can be calculated following Eq.2-13, in this simplified model.

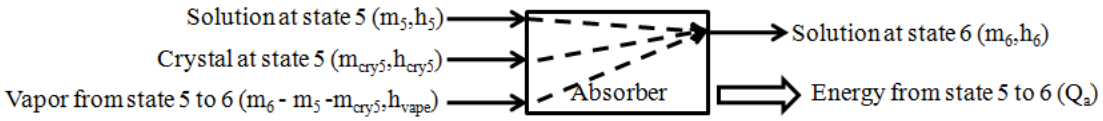

$$Q_a = m_5 \cdot h_5 + m_{cry5} \cdot h_{cry5} + (m_1 - m_5) \cdot h_{vape} - m_1 h_1 \qquad \text{Eq.2-13}$$

In which, h_{vape} is the enthalpy of vapor coming from the evaporator at state E.

But the enthalpy of crystal of absorption couples is seldom presented in the existing literature. In order to simplify Eq.2-13, considering that the heat released to the solution tank while cooling the solution form state 6 to state 1 could be used for the dissolution of crystal remaining in the tank, the energy need for the dissolution of crystal is not considered during the absorption process. The Eq.2-13 is simplified to Eq.2-14.

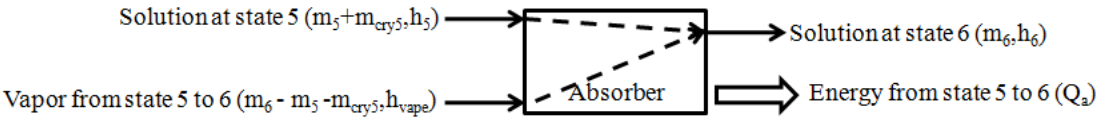

$$Q_a = \left(m_5 + m_{cry5}\right) \cdot h_5 + (m_6 - m_5 - m_{cry5}) \cdot h_{vape} - m_6 h_6 \qquad \text{Eq.2-14}$$

In fact, this is the energy balance of the absorber. At the inlet of the absorber, the solution comes from the solution tank at the same characteristics as the solution at state 5. The total mass of solution at the inlet of the absorber is the sum of the mass of solution and crystal at state 5. At the outlet of the absorber, it is the solution after absorption at state 6. The vapor absorbed by the solution comes from the evaporator at state E.

The heat loss to the surroundings during the desorption and absorption phases and the work of the pumps are not considered in the calculation for this simplified model.

Seven absorption couples, $CaCl_2/H_2O$, Glycerin/H_2O, KOH/H_2O, $LiBr/H_2O$, $LiCl/H_2O$, $NaOH/H_2O$ and H_2O/NH_3 will be presented and analyzed for the seasonal storage system. For KOH/H_2O, $LiBr/H_2O$, $LiCl/H_2O$ and $NaOH/H_2O$ couples, the process phases are the same as for $CaCl_2/H_2O$. But for Glycerin/H_2O and H_2O/NH_3 couples, there is no crystal appearance at any mass fraction. For the H_2O/NH_3 couple, NH_3 is the absorbate of the process.

The literature enthalpy, solubility, liquid-vapor equilibrium and other thermodynamic parameters for $CaCl_2/H_2O$ [Conde, 2004], Glycerin/H_2O [Tyner, 2004], KOH/H_2O [Zaytsev & Aseyev,1992; Oxychem[1], 2000; Ripoche & Rolin,1980], $LiBr/H_2O$ [Castaing-Lavignottes, 2001; Feuerecker et al., 1993], $LiCl/H_2O$ [Conde, 2004; Monnin and Dubois, 2003], $NaOH/H_2O$ [Oxychem[2], 2000] and H_2O/NH_3 [Ziegler & Trepp, 1984] are used in the calculation.

2.2 Principles for choosing the absorption couples

As a first step of the study of the appropriate heat storage system with solar collectors as heat source, the absorbate/absorbent couple has to be selected. A list of selection criteria for the appropriate materials has to be kept in mind [IEA task 32, 2008]. The most important parameters are:

(A) The capacity and efficiency of the storage.

The storage capacity Q_a is defined as the energy which is released during the absorption phase per kilogram absorbent. The storage efficiency of the system η is defined as the energy production during absorption divided by the thermal energy consumption during desorption $\eta = Q_a / Q_d$. The efficiency of the solar collector is not included in this storage efficiency of the system. The result of the calculation of storage capacity and efficiency of the seven couples at different operating conditions can be found in section 2.3.

(B) The temperature requirement for solar collectors.

The temperature requirement for desorption depends on the characteristics of the couple. It is a very important character for choosing the couples because the efficiency of solar collectors decreases rapidly with the temperature difference between the fluid in the solar collector and the ambience, due to heat losses.

The temperature requirement for desorption can be calculated by the balance of pressure according to Eq.2-3. An example of the equilibrium pressure of the seven couples, pure water and pure ammonia in function of the temperature is presented in Figure 2-4. In order to compare the characteristics of the couples at the same condition that there is no crystal during the storage process, the mass fraction of the solution of $CaCl_2/H_2O$, KOH/H_2O, $LiBr/H_2O$, $LiCl/H_2O$, $NaOH/H_2O$ is chosen as their solubility at 10°C in this figure. The mass fraction of $Glycerin/H_2O$ and H_2O/NH_3 is decided at 90% because it is very difficult to increase the mass fraction up to 100%. For H_2O/NH_3, 90% is the mass fraction of the water in the H_2O/NH_3 solution. In order to be uniform with other solutions, the mass fraction of the H_2O/NH_3 solution is given as the mass fraction of NH_3 which is 10% in the figure.

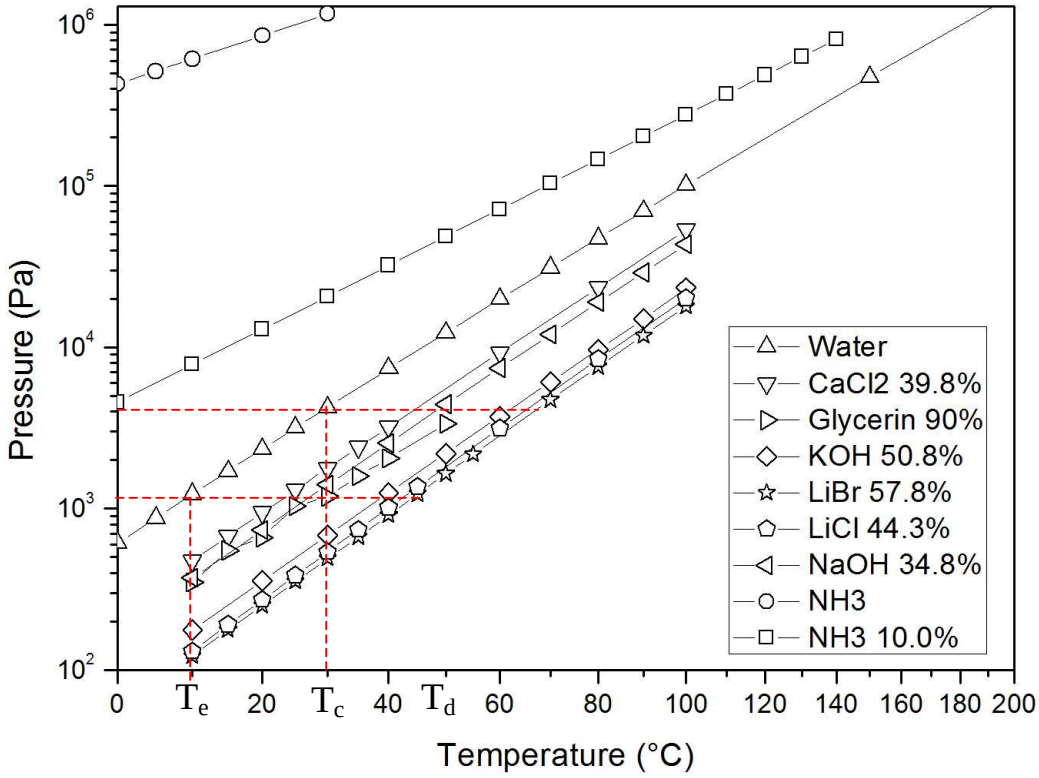

Figure 2-4 Thermodynamic equilibrium conditions of the seven couples, pure water and pure ammonia

At a given condensation temperature (thus a given liquid/vapor equilibrium pressure of water or ammonia), the order of the temperature need for the solar collector of the six couples which can be found in Figure 2-4 is:

$CaCl_2/H_2O < NaOH/H_2O < Glycerin/H_2O < KOH/H_2O < LiCl/H_2O < LiBr/H_2O < H_2O/NH_3$

For the H_2O/NH_3 couple, NH_3 is the absorbate of the process. The temperature requirement for the solar collector is the temperature of the solution (10% NH_3 in the solution) at the liquid/vapor equilibrium pressure of NH_3 which is a lot higher than the equilibrium pressure of water for a given temperature.

Classically, the temperature requirement for the solar collector increases with the temperature of condensation.

(C) The absorption at a high enough temperature for the heat floor

The maximum temperature of absorption can be calculated by the balance of pressure according to Eq.2-5. It can also be found in Figure 2-4 at the same mass fraction conditions as in criteria B. At a given temperature of evaporation (T_e), the maximum temperature of absorption (T_a) order is:

$CaCl_2/H_2O < NaOH/H_2O < Glycerin/H_2O < KOH/H_2O < LiCl/H_2O < LiBr/H_2O < H_2O/NH_3$

It is the same order as the temperature requirement for the solar collector. The maximum temperature of absorption (T_a) is increased with the temperature of evaporation (T_e).

According to the result of criteria (B) and criteria (C), it is difficult to say which couple is the most suitable for the seasonal storage system because the higher the temperature of absorption, the higher the temperature requirement for the solar collector. However some couples can be selected for specific situations. For example, if the temperature need of absorption is at 30°C when the evaporation temperature is 10°C (indicated by the red broken line in Figure 2-4), the $CaCl_2/H_2O$, $NaOH/H_2O$ and $Glycerin/H_2O$ couples are unusable because their maximum temperature for absorption is lower than 30°C. KOH/H_2O could be chosen because it has the minimum temperature requirement for the solar collector among the couples which can achieve the temperature requirement for absorption (30°C).

(D) An easy to handle couple – possibly non poisonous

The security characters of the couples (Table 2-1) come from the NFPA 704 [NFPA704, 2007] which is a standard maintained by the U.S.-based National Fire Protection Association. Each of health, flammability and reactivity is rated on a scale from 0 (no hazard; normal substance) to 4 (severe risk).

Table 2-1 Security characters of seven couples

Couple		$CaCl_2/H_2O$	$Glycerin/H_2O$	KOH/H_2O	$LiBr/H_2O$	$LiCl/H_2O$	$NaOH/H_2O$	H_2O/NH_3
NFPA 704	Health hazard	2	1	3	2	2	3	3
	Flammability	0	1	0	0	0	0	1
	Chemical reactivity	0	0	1	0	0	1	0

*scale from 0 (no hazard; normal substance) to 4 (severe risk)

The KOH/H_2O and $NaOH/H_2O$ will cause chemical burns, permanent injury or scarring if they contact unprotected human or animal tissue. They will cause blindness if they contact the eye. Protective equipment such as rubber gloves, safety clothing and eye protection should always be used when handling the material or its solutions. The $CaCl_2/H_2O$, $LiCl/H_2O$ and $LiBr/H_2O$ couples are irritating for skin and eyes. In the interest of safety and to avoid the requirement for specialized handling practices, hot water should never be used for dissolving those anhydrous chemicals. To illustrate the importance of using water at ambient temperatures, consider the make-up of a 34% solution of anhydrous calcium chloride. When such a solution is prepared, the temperature rise due to dissolution of the anhydrous calcium chloride is 78°C. If warm water, for example, water at 49°C, is used, the temperature of the resulting solution will be 127°C. The $Glycerin/H_2O$ couple is generally regarded as a safe material for which no special handling precautions are required. However, it is flammable. It also feels oily, so may cause a slipping hazard if spilled on the floor. The H_2O/NH_3 couple is irritating to the eyes and mucous membranes (respiratory and digestive tracts), and to a lesser extent the skin. Thus it is dangerous for household use, especially concerning the possibility of leak of NH_3 vapor at high operating pressure (3 to 10 bar from Figure 2-4).

In fact, all the couples except H_2O/NH_3 can be considered as safe in an energy storage system because as the system is operating at low pressure (under vacuum), the leak of the solution is generally impossible.

The corrosion is also an important character for the design of the system. The corrosion for stainless steel 304 of the seven couples is known when there is no agitation and no aeration [Craig & Anderson, 1995]. The corrosion is increased with the mass fraction and the temperature. For the $CaCl_2/H_2O$ couple, the stainless steel 304 is resistant to corrosion when the mass fraction is at about 10%. But when the mass fraction is about 28%, the corrosion is about 0.003 mm/year at 79°C. For the Glycerin/H_2O couple, the stainless steel 304 is resistant to corrosion at any mass fraction till the temperature of boiling. For the KOH/H_2O couple, the corrosion is about 0.003 mm/year at the temperature of 93°C and a mass fraction between 20% and 50%. For the LiBr/H_2O couple, the corrosion is about 0.008 mm/year at the temperature of 50°C and the mass fraction of 50%. For the LiCl/H_2O couple, the corrosion is about 0.003 mm/year at the temperature of 116°C and the mass fraction of 30%. For the NaOH/H_2O couple, the corrosion is about 0.003 mm/year at the temperature of 65°C and the mass fraction of 50%. But the corrosion increases to 0.68 mm/year at a temperature between 90°C and 143°C at the mass fraction of 70%. For the H_2O/NH_3 couple, the stainless steel 304 is resistant to corrosion at any mass fraction till the temperature of boiling.

(E) A low investment cost for the absorbate/absorbent couple.

Compared with short term storage systems, the quantity of material for storage is larger for seasonal storage systems because of the amount of energy which is stored is evidently increased. The investment costs for the couples must therefore be taken into account. The prices of the seven couples on the Chinese market [Alibaba, 2008] at the same purity (higher than 99%) are shown in Table 2-2. The given price is just a reference to compare relatively the cost of those couples, because this price is changing with time and regions. Compared with other couples, the $CaCl_2/H_2O$, Glycerin/H_2O and H_2O/NH_3 couples are attractive. The LiBr/H_2O and LiCl/H_2O couples which are often used in the absorption refrigeration systems are the most expensive couples (more than 14 times compared with $CaCl_2/H_2O$).

Table 2-2 Prices of different couples

Couple	$CaCl_2$ /H_2O	Glycerin /H_2O	KOH /H_2O	LiBr /H_2O	LiCl /H_2O	NaOH /H_2O	H_2O /NH_3
Price [€/ ton material] (purity≥99%)	350	500	1200	5000	6000	3000	400

2.3 Static simulation of the performances of seven absorption couples

The analysis of the storage capacity and efficiency of the seven couples are carried out at eight different operating conditions which are shown in Table 2-3.

The temperature of storage before absorption (state 5 in Figure 2-2 and 2-3) is varied at 5°C and 10°C, because the solution and water tanks are supposed to be located underground or in a basement which has a temperature between 5°C and 10°C during the winter period.

The temperature of evaporation (state E) is chosen at 5°C and 10°C, which are also typical temperatures of geothermal energy during the winter phase.

The temperature of absorption (state 6) is changed from 20 to 45°C to meet the temperature need for house heating.

The ratio of crystallization (R) is defined as the relative mass of crystal at state 5 divided by the relative mass of liquid solution at the same state. R = 0 means that there is no crystal at state 5 and the solution at that state is saturated. R = 4 means that at the beginning of absorption, the quantity of liquid solution is 20% of the total mass in solution tank. 20% of liquid is enough for starting the absorption process.

For the couple Glycerin-H_2O and H_2O-NH_3, there is no crystal during the process. The maximum mass fraction after desorption is decided at 0.9 kg absorbent/kg solution.

Labels of different operating conditions used in Table 2-3 and future figures represent their operating conditions. An example can be found in the following figure. R4-s10-e10 means that the case is carried out at the conditions that the quantity of liquid solution is 20% maximum of the total mass in solution tank, the other 80% is crystal (R4); the temperature of the storage tank before absorption is at 10°C (s10); the temperature of evaporation is at 10°C (e10).

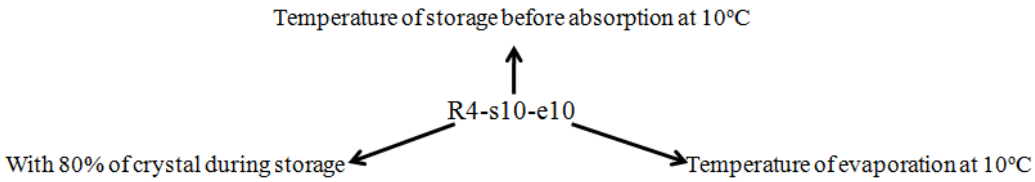

Table 2-3 Operating conditions of the static simulation

Case	Ratio of crystallization	Temperature of storage before absorption [°C]	Temperature of evaporation [°C]	Temperature of absorption [°C]
R0-s5-e5	0	5	5	20 to 45
R4-s5-e5	4	5	5	20 to 45
R0-s10-e5	0	10	5	20 to 45
R4-s10-e5	4	10	5	20 to 45
R0-s5-e10	0	5	10	20 to 45
R4-s5-e10	4	5	10	20 to 45
R0-s10-e10	0	10	10	20 to 45
R4-s10-e10	4	10	10	20 to 45

Storage capacity

The storage capacity of the seven couples depending on the temperature of absorption is shown in Figure 2-5. All the operating conditions shown in Table 2-3 are presented in the figure except the conditions that are impossible for the specific couple.

For the $CaCl_2/H_2O$ couple, the storage process is possible when the temperature of evaporation is 10°C but impossible when the temperature of evaporation is 5°C. The possible temperature range for absorption is 20 to 24°C. For the Glycerin/H_2O couple, the storage process is possible at all conditions in Figure 2-5. But compared to other couples, the storage capacity is low. For the KOH/H_2O, LiBr/H_2O and LiCl/H_2O couples, the storage process is possible at all conditions in Figure 2-5. The possible temperature range for absorption is 25 to 35°C. For the NaOH/H_2O couple, the storage process is possible just at six points which are shown in Figure 2-5. For the H_2O/NH_3 couple, the storage process is possible at all conditions in Figure 2-5. The temperature range for absorption is 20 to 40°C.

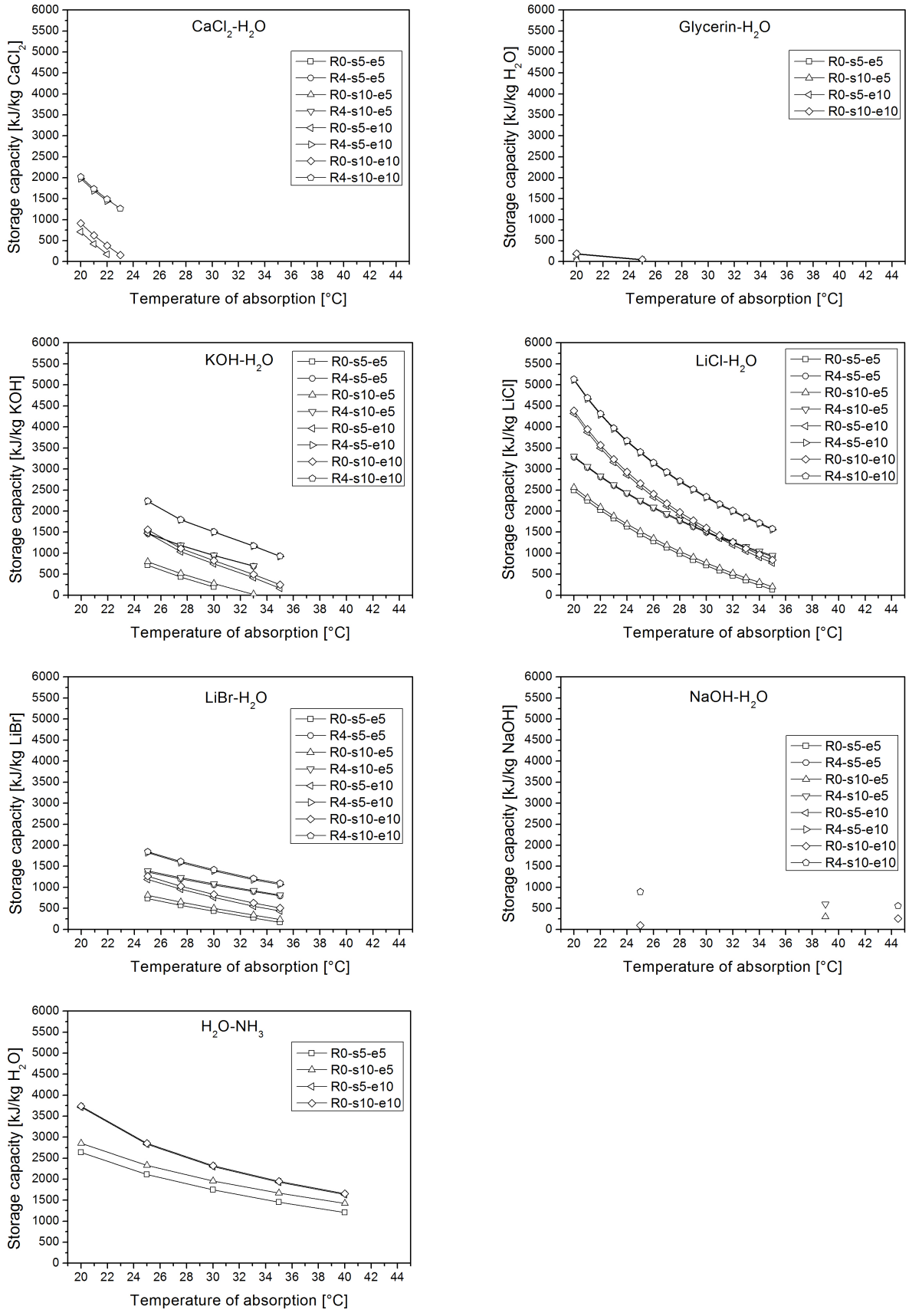

Figure 2-5 Variation of storage capacity with operating conditions

The storage capacity is increased with the appearance of crystal (R=4 in Figure 2-5) compared with no crystal (R=0) at the same operating conditions. That is mainly due to the enlarged difference of mass fraction of absorbent between the rich and the poor solution.

Figure 2-6 presents the effect of the absorber temperature change on the process cycle. In cycle 1-2-3-5-6-1, which is the same cycle as in Figure 2-2, the minimum temperature of the absorber is 20°C. If this temperature increases to 22°C, the position of state 6 is changed to state 6'. The other states are changed following the principle explained for Figure 2-2. The corresponding cycle is 1'-2'-3-5-6'-1'. The difference of mass fraction of absorbent between the rich and poor solution (states 2' and 3) is decreased compared to the base case (states 2 and 3). As a result, less absorbate can be absorbed during the heating phase, so the storage capacity decreases when the temperature of the absorber increases.

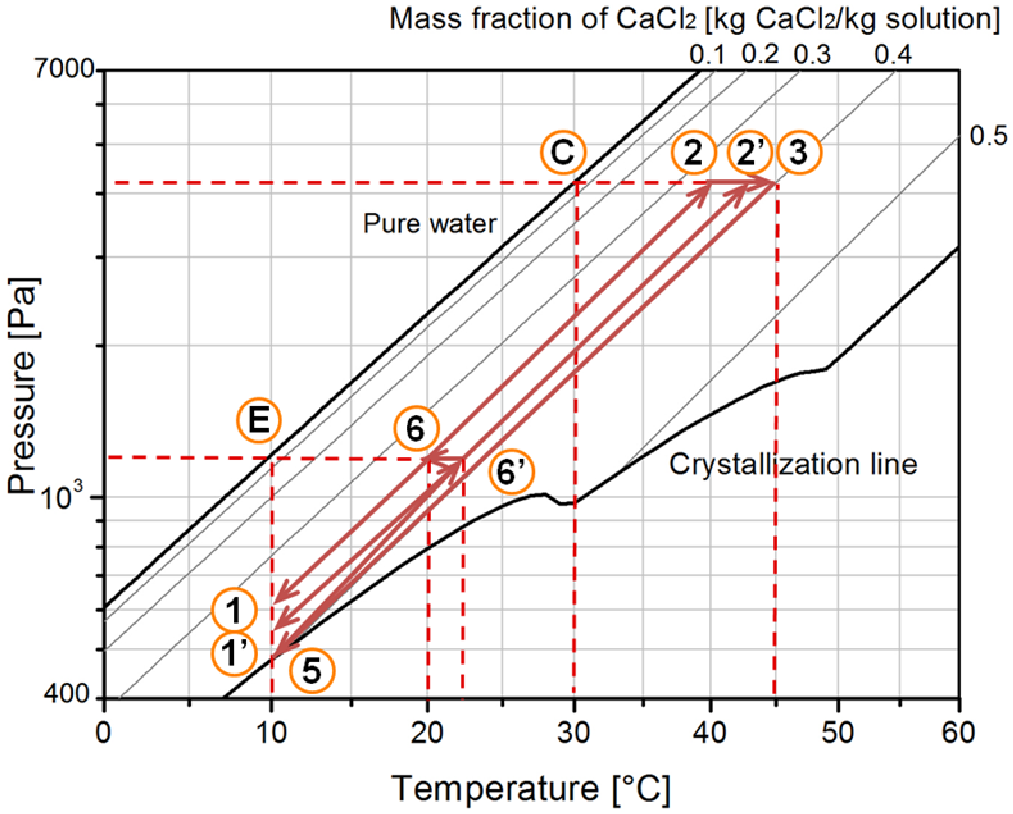

Figure 2-6 Cycle change depending on the absorber temperature

Figure 2-7 presents the effect of the evaporator temperature on the cycle. In the cycle 1-2-3-5-6-1, which is again the same as in Figure 2-2, the temperature of the evaporator is 10°C. If the temperature of the evaporator increases to 15°C (Point E'), the new cycle is 1'-2'-3-5-6'-1'. The difference of mass fraction of absorbent between the rich and the poor solution is increased compared to the base case. Consequently, the storage capacity increases with the temperature of the evaporator.

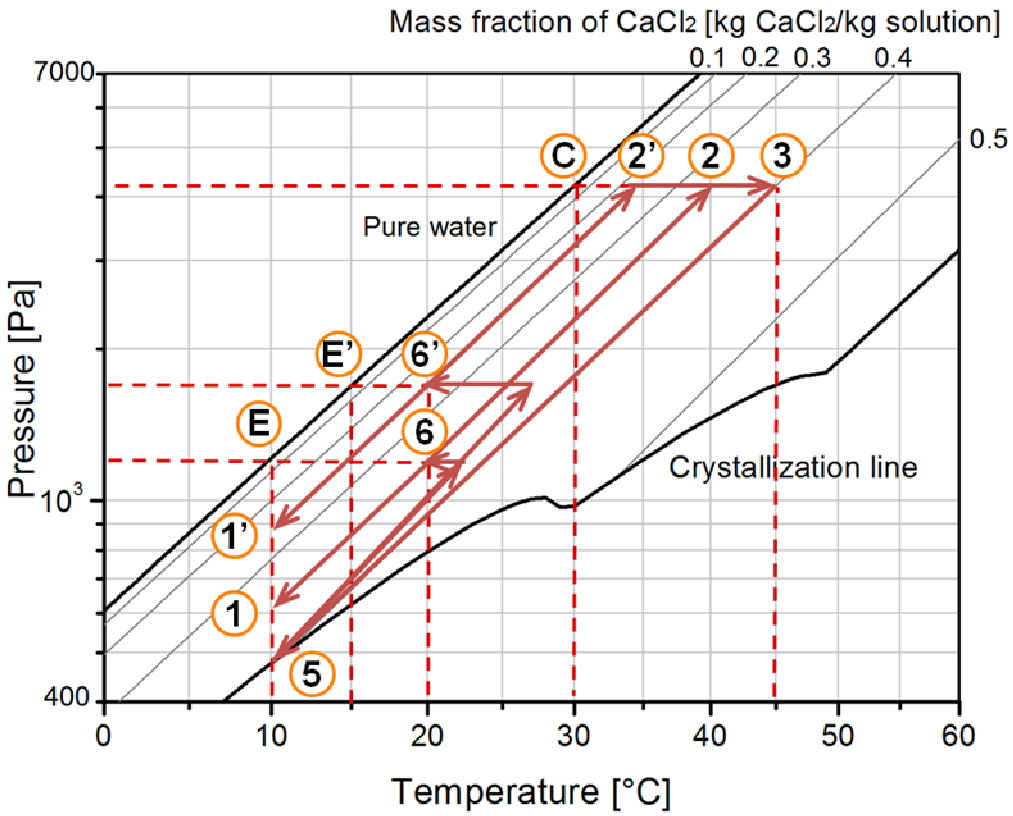

Figure 2-7 Cycle change depending on the evaporator temperature

The storage capacity is increased with the temperature of the storage tank before the absorption phase (state 5). Following the principle which has been explained for Figure 2-2, the maximum mass fraction of absorbent after desorption (state 3) is decided by the solubility of the solution before absorption (state 5). The difference of mass fraction of absorbent between the rich solution and the poor solution is increased with the temperature at state 5 due to its rise of solubility, and correspondingly, the storage capacity is increased. But generally, the variation of solubility depending on the temperature is feeble. Take the LiBr/H_2O couple for example: the solubility is 57.5 g/100g H_2O at 5°C and 57.8 g/100g H_2O at 10°C. For the H_2O/NH_3 couple, there is no crystal appearance during the process. The curves at different temperatures of storage before absorption (R0-s5-5 and R0-s10-5; R0-s5-10 and R0-s10-10) in Figure 2-5 are almost coincident. As a result, the influence of the temperature of storage before absorption on the storage capacity is low (Figure 2-5).

Efficiency

The efficiency of the seven couples depending on the temperature of absorption is shown in Figure 2-8. At the same operating conditions, the LiCl/H_2O couple has the best efficiency compared to other couples.

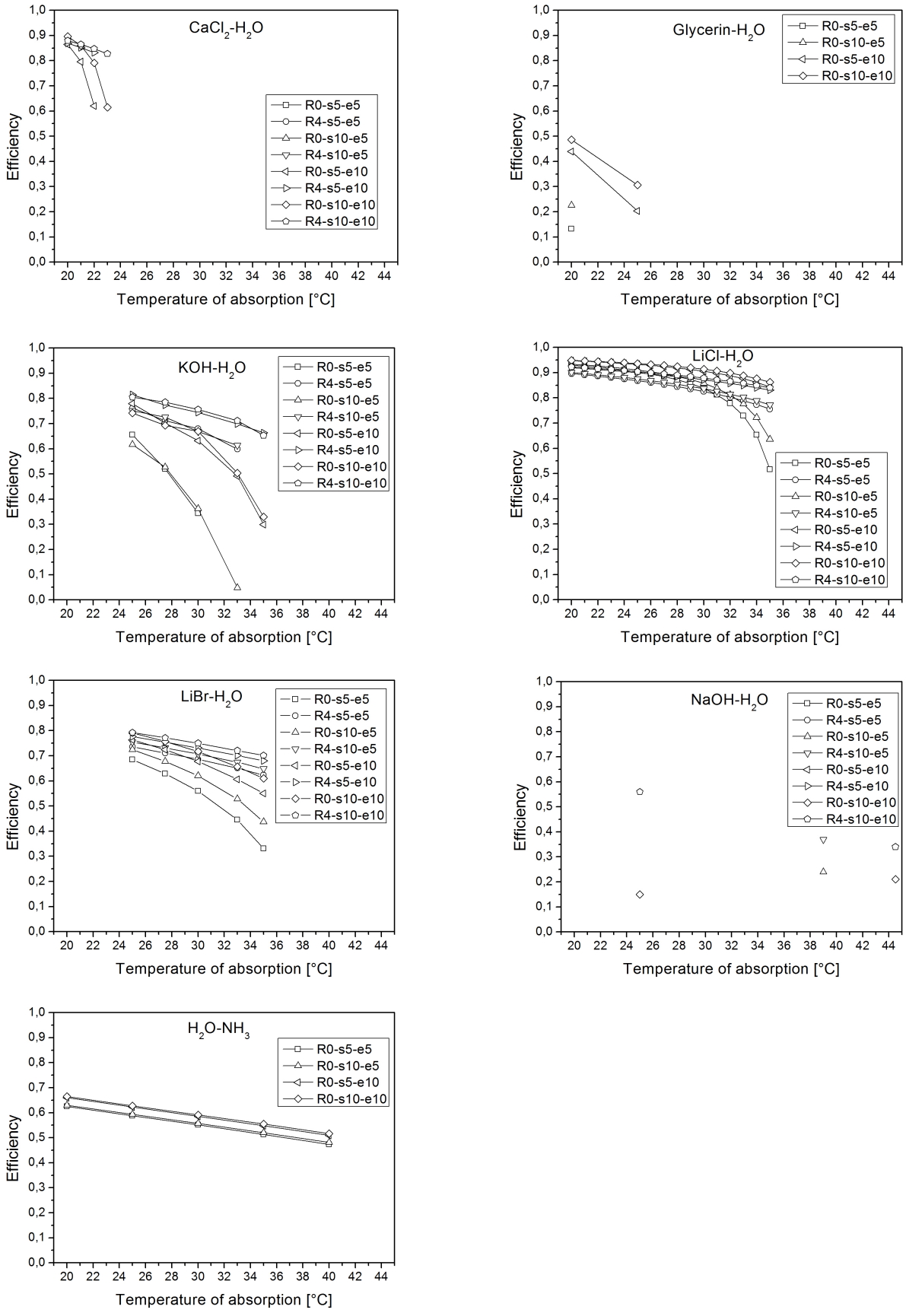

Figure 2-8 Variation of efficiency with operating conditions

The influence of the appearance of crystal on the efficiency is complicated. The appearance of crystal increases the energy need for desorption and the heat loss during the transition phase from summer to winter, as the desorber has to reach a higher temperature than without the appearance of crystals. However, the appearance of crystals also increases the energy production during the winter phase, so depending on the relative value of these three energies, the appearance of crystals generally decreases the efficiency of the process, but can also increase it (especially at high absorption temperature, which means for a lower heat production during the winter than for a low temperature of absorption). Generally speaking, considering the corresponding increase of storage capacity which can decrease evidently the investment cost of absorbent/absorbate and for storage tanks, the decrease in efficiency can still be acceptable.

The efficiency is decreased with the increase of the temperature of absorption. The sensible heat loss from state 3 to state 5 is constant (Figure 2-6), but the energy production of absorption is decreased with the increase of the temperature of absorption. As a result, the ratio of heat loss during the cycle is increased so that the efficiency is decreased. The temperature of absorption depends on the house heating needs. In order to gain the best balance between storage capacity and efficiency, it is better to use this storage system with low temperature house heating systems (for example, heating floor).

The efficiency is increased with the temperature of evaporation. The heat loss from state 3 to state 5 is constant (Figure 2-7), but the energy production of absorption is increased with the temperature of evaporation. As a result, the ratio of heat loss during the cycle is decreased so that the efficiency is increased.

The efficiency is increased with the temperature of the storage tanks before absorption (during the transition period). The sensible heat loss from state 3 to state 5 is decreased with the temperature of the storage before absorption (T_5) and the heat production of absorption is increased with T_5. As a result, the ratio of heat loss during the cycle is decreased so that the efficiency is increased.

2.4 Main evaluation points

In order to compare the characters and performances of the seven couples, the main evaluation points are summed-up in Table 2-4 at the same operating conditions, taken for example:

- Temperature of the condenser, T_c = 30°C;
- Minimum temperature of the absorber, T_1 = 20°C;
- Temperature of the storage tanks before the absorption phase, T_5 = 10°C;
- Temperature of the evaporator, T_e = 10°C.

Table 2-4 Evaluation points for the choice of the absorption couples

Couple		$CaCl_2$ /H_2O	Glycerin /H_2O	KOH /H_2O	LiBr /H_2O	LiCl /H_2O	NaOH /H_2O	H_2O /NH_3
R=0	Mass fraction of absorbent after desorption [%]	39.8	90.0	50.8	58.8	44.3	33.5	90.0
	Storage capacity [kJ/kg material]	914	193	2618	2019	4387	1558	1317
	Required temperature of desorption [°C]	44.8	53.0	63.0	72.0	65.6	50.0	155.5
	Volume of solution [m^3/1000 kWh]	8.4	20.0	3.2	3.2	2.5	6.5	10.2
	Absolute pressure [kPa]	1.2 - 4.2	1.2 - 4.2	1.2 - 4.2	1.2 - 4.2	1.2 - 4.2	1.2 - 4.2	615 - 1167
	Efficiency	0.909	0.545	0.830	0.850	0.950	0.750	0.665
R=4	Mass fraction of absorbent after desorption [%]	48.5	-----	58.8	68.3	52.1	37.8	-----
	Storage capacity [kJ/kg material]	2023	-----	3299	2603	5133	2382	-----
	Required temperature of desorption [°C]	54.2	-----	84.0	93.3	77.6	57.0	-----
	Volume of solution [m^3/1000 kWh]	3.8	-----	2.5	2.5	2.1	4.3	-----
	Absolute pressure [kPa]	1.2 - 4.2	-----	1.2 - 4.2	1.2 - 4.2	1.2 - 4.2	1.2 - 4.2	-----
	Efficiency	0.885	-----	0.856	0.835	0.923	0.767	-----

For the H_2O/NH_3 couple, the system is operating at high pressure (6.15-11.67 Bar). The design of the devices for H_2O/NH_3 has to be careful, considering that the ammonia leaks can be very dangerous. For the six other couples, the system is operating at low pressure. The sealing of these machines is critical because the presence of air in the system can decrease the kinetics of absorption and desorption. In the seasonal solar energy storage system, the energy of desorption is provided by the solar collector. The volume of storage tank is an important part of the investment cost. The volume of the solution for 1000 kWh energy production is shown in Table 2-4.

According to the results in Table 2-4, the $LiCl/H_2O$ has the best storage capacity and the efficiency. But according to its price (about 6000 €/ton), the investment cost of the absorption couple for a seasonal storage system would be really high. The storage capacities of KOH/H_2O, $LiBr/H_2O$ and $NaOH/H_2O$ couples are comparable, but the $LiBr/H_2O$ is also disadvantaged by its high price (about 5000 €/ton). The KOH/H_2O and $NaOH/H_2O$ couples are advantaged by their low price but are disadvantaged by the security problems. The storage capacity and price of the H_2O/NH_3 couple is acceptable. But it is disadvantaged by the temperature requirement of solar energy (>150°C) and the security problems. Compared to other couples, the storage capacity of the $Glycerin/H_2O$ couple is too low to be used in the absorption system. The $CaCl_2/H_2O$ couple is the cheapest material (about 350 €/ton), but its storage capacity is low, so the investment cost for the tanks may be higher than for the other couples. However, with the presence of crystal, the storage capacity of $CaCl_2/H_2O$ is about double. This increase is much higher than the increase of the $LiCl/H_2O$ (about 17%) between the two configurations (with or without crystal). With crystal, the storage capacity of $CaCl_2/H_2O$ is about 40% of the storage capacity of $LiCl/H_2O$. But the price of $CaCl_2$ is only 6% of the LiCl one. Considering these advantages, the $CaCl_2/H_2O$ is chosen for the future experimentation.

2.5 Conclusion on the evolution of the absorption couples performance

This chapter presents the system of seasonal storage of solar energy for house heating systems in buildings. The performance and thermodynamic characteristics of seven absorption couples, $CaCl_2/H_2O$, Glycerin/H_2O, KOH/H_2O, LiBr/H_2O, LiCl/H_2O, NaOH/H_2O and H_2O/NH_3, have been studied.

The storage capacity of the absorption process increases with the evaporator temperature and the storage temperature before the absorption phase, and decreases with the absorber temperature. The appearance of crystal increases the storage capacity. Unavoidably, the complexity of the system will also be increased. But since the storage tank is operating at vacuum conditions and with corrosive solutions, its cost mainly depends on its volume and the material used. With crystal, the volume of the storage tank will be decreased so that should reduce the global cost of the system.

After the comparison of the performance of the seven couples, the $CaCl_2/H_2O$ is an acceptable couple and it is chosen for the future experimentation as the following reasons: the comparable storage capacity with crystal, the low price, the low temperature need for solar energy and the low security risks.

References of Chapter 2

Alibaba. http://www.alibaba.com

Castaing-Lavignottes J.. 2001. Aspects thermodynamiques et technico-économiques des systèmes à absorption liquide, CNAM & IFFI, http://jc.castaing.free.fr/

Conde M.. 2004. Properties of aqueous solutions of lithium and calcium chlorides: formulations for use in air conditioning equipment design. International Journal of Thermal Sciences. 43(4), pp. 367-382

Craig BD., Anderson DS.. 1995. Handbook of corrosion data. ASM International, Materials Park, OH

Feuerecker G., Scharfe J., Greiter I.. 1993. Measurement of thermodynamic properties of aqueous at high temperatures and concentrations. AES, 31, International Absorption Heat Pump Conference. ASME

IEA task 32. 2008. Advanced Storage Concepts for Solar and Low Energy Buildings. http://www.iea-shc.org/task32/index.html

Monnin C., Dubois M., Papaiconomou N., Simonin J. P.. 2002. Thermodynamics of the LiCl + H_2O System. J. Chem. Eng. Data.. 47, pp. 1331-1336.

Multibéton. 2009. sols secs CS, sols secs A: minces, legers, performants…, http://www.multibeton-france.fr/chauffage-sol/proc_solsec.htm (in French).

NFPA704. 2007. Standard System for the Identification of the Hazards of Materials for Emergency Response. http://www.nfpa.org

Oxychem[1] . 2000. Caustic Potash Handbook. www.oxychem.com

Oxychem[2.] 2000. Caustic Soda Handbook. www.oxychem.com

Ripoche P., Rolin M.. 1980. Détermination des Caractéristiques Physicochimiques des Solutions Aqueuses Concentrées D'hydroxyde de Potassium Jusqu'à 180 °C. II. Les Capacités Calorifiques et la Conductivité Thermique. Bull. Soci. Chim. Fr. 9-10, pp. 380-385

Tyner M.. 2004. Enthalpy-Concentration diagrams of binary aqueous mixtures of hydrazine, sodium carbonate, and glycerine. AIChE Journal. 1(1), pp. 87 – 92

Zaytsev I. D., Aseyev G.G.. 1992. Properties of Aqueous Solutions of Electrolytes. CRC Press

Ziegler B., Trepp Ch.. 1984. Equation of state for ammonia-water mixtures. International Journal of Refrigeration. 7(2), pp. 101-106

A paper on this part of the work has been submitted to the Energy Conversation and Management:

Liu H., N'Tsoukpoe K. E., Le Pierrès N., Luo L., 2010, Evaluation of a seasonal storage system of solar energy for house heating using different absorption couples, submitted to Energy Conversion and Management, october 2010

Chapter 3 – Experimentation of the seasonal storage system with the $CaCl_2/H_2O$ couple

Following the analysis of Chapter 2, the seasonal storage system by absorption is theoretically possible. In order to check the feasibility of the process, a prototype is constructed. The conception of the prototype is presented in this chapter. The experimentations are carried out at different operating conditions with the absorption couple $CaCl_2/H_2O$. The thermodynamic performances and the problems of the prototype are analyzed.

3.1 Conception of the prototype

The scheme of the prototype is shown in Figure 3-1. It includes the solution tank, the water tank, the reactor (which includes the evaporator/condenser and the generator/absorber), the inlet tank of solution, the thermostats, the vacuum pump, the circulators (C), the dosing pumps (DP) and the valves (V). The temperature (T), pressure (P), level of liquid (m) and flow rate (D) are measured in the prototype.

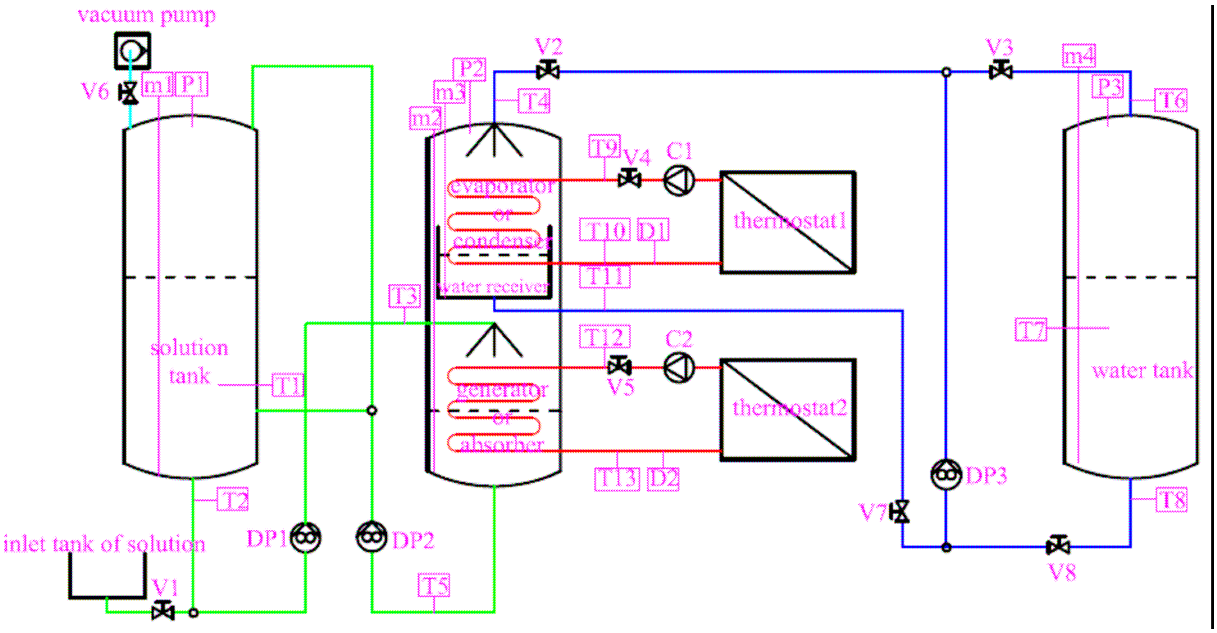

Figure 3-1 Concept of the prototype

The two thermostats are used to provide the heating and cooling energy for the prototype. During desorption, the cooling energy in the condenser which is provided by the environment in Figure 2-1 for the real system is provided by the thermostat 1 in the experimentation. The heating energy in the generator which is provided by the solar collector in Figure 2-1 for the real system is provided by thermostat 2 in the experimentation. Correspondingly, during the absorption, the heating energy used in the evaporator which is provided by the geothermal energy in Figure 2-1 is provided by the thermostat 1 and the heat of absorption which is used for house heating in Figure 2-1 is used to the thermostat 2 in the experimentation.

For the process described in Chapter 2 (Figure 2-1), the seasonal storage system by absorption needs four separated components: the generator, the condenser, the absorber and the evaporator. In order to simplify the process and decrease the volume of the system, these four exchangers are combined into one reactor, and represented by only two heat exchangers that can be used for different functions depending on the process phase. Hence the investment cost of the system is decreased. The seasonal storage process is a batch process which means that the absorption and desorption phases are separated. The generator and the condenser are used only during the desorption phase and the absorber and the evaporator are used only during the absorption phase. Furthermore, the condenser and the evaporator are both used for the phase change of the water which is provided or stored by the same water tank. As a result, in this optimized design, the condenser and the evaporator are one single component used as a condenser during the desorption phase and an evaporator during the absorption phase. Both the generator and the absorber use the solution which comes from the same solution tank. Following the same principle, the generator and the absorber are combined together to be a

generator during the desorption phase and an absorber during the absorption phase. In order to decrease the heat losses and the pressure drop during the water vapor transfer between the evaporator/condenser and the generator/absorber, these components are combined in one reactor shell. The water vapor transfer between the evaporator/condenser and the generator/absorber is direct through the annular space between the water receiver and the reactor wall. After the simplification, the four reactors are simplified to one reactor which is divided into two parts: the evaporator/condenser and the generator/absorber. Below the evaporator/condenser, there is a water receiver which receives the liquid water falling from the evaporator/condenser. Two reactors including two heat exchangers and two distributors are economized by this simplified design.

The functioning of the prototype can be found as follows:

During the desorption phase:

The poor solution in the solution tank is transferred by the pump DP1 to the generator where it is heated by the heat exchanger. The heat for desorption is provided by the thermostat 2. The absorbate which is desorbed from the solution is transferred to the condenser where it is condensed on the heat exchanger. The cold for condensation is provided by the thermostat 1. The valves V2 and V8 are closed. The condensed liquid absorbate is then transferred to the water tank by the pump DP3 through the valves V3 and V7. The rich solution is removed from the generator to the solution tank by the pump DP2. The level meter m3 is used to measure the water level in the water receiver of the condenser. When the water level in the water receiver is higher than a given level (about 70% of the total volume of the water receiver), the water is transferred to the water tank where it mixes with the water already there. The solution is circulated between the solution tank and the generator during the desorption phase. The level meter m2 is used to measure the solution level in the generator. When the solution level in the generator is higher than a given level, the solution is transferred to the solution tank and mix with the solution already there. At the end of the desorption phase, the rich solution is stored in the solution tank and the liquid absorbate is stored in the water tank.

During the transition phase:

After the desorption phase, the temperature of the rich solution in the solution tank (T1) is high because of the circulation of the solution between the solution tank and the generator. In order to prevent this heat of the solution to be used in the absorption phase, the solution must be cooled to a temperature which is lower than the water temperature in the heat exchanger at the inlet of the absorber (T12). The solution in the solution tank is circulated between the solution tank and the generator and cooled by the heat exchanger in the generator. The cold energy is provided by thermostat 2. After the transition phase, the temperature of the solution T1 should be lower than T12 during the following absorption phase.

During the absorption phase:

The valves V3 and V7 are closed. The water in the water tank is transferred by the pump DP3 through the valves V2 and V8 to the evaporator where it is evaporated by the heat coming from thermostat 1 at low temperature. The level meter m3 is used to measure the water level in the receiver of the evaporator. When the level is above a given level (about 70% of the total volume of the water receiver), Valve V8 is closed and Valve V7 is open, the water that has

not been evaporated is recirculated by pumping till the level is below a given level (about 20% of the total volume of the water receiver). Then, the valve V8 is open and the valve V7 is closed. The liquid water in the water tank is transferred to the evaporator. The vapor is transferred to the absorber. The rich solution in the solution tank is transferred by pump DP1 to the absorber where it absorbs the vapor. The heat of absorption is transferred to the thermostat 2 by the heat exchanger. The poor solution is then removed from the absorber by pump DP2 to the solution tank. After the absorption phase, the poor solution is stored in the solution tank. If the liquid water in the water tank has not been totally absorbed due to the limitation of time, the rest of the water will be stored in the water tank. The poor solution and liquid water can then be used for the next experiment cycle with different operating conditions.

Setting of the prototype before the experimentations:

As have been discussed in section 2.1.1, the system must be operated under vacuum. Before the beginning of the experimentations, the vacuum pump is used for the vacuum of the solution tank, the water tank and the reactor. During the vacuum phase, all valves except valve V1 are open in order to make sure that all components of the prototype can be vacuumed. The pressure is measured by the pressure sensors (P1, P2 and P3). This operation is complete when the pressure is lower than the equilibrium pressure of the water in the condenser during the desorption phase and in the evaporator during the absorption phase.

The solution used in the prototype is produced from the absorbate and the absorbent, which are mixed in the inlet tank of solution. The inlet tank of solution is open to the atmosphere. The valve between the inlet tank of solution and the solution tank (V1) is closed during the mixing of the solution and the vacuum of the prototype. After that, the valve V1 is open. The solution is transferred from the inlet tank of solution to the solution tank automatically by the pressure difference. At the end of this step, the solution is stored in the solution tank. Vacuum is checked and completed if necessary.

The different levels, temperatures, flow rates and pressures are measured for future analysis. The experimentation data are collected every 1 minute by Napac and Agilent systems and stored in a computer.

3.2 Design of the components of the prototype

3.2.1 The absorption couple of the experimentation

In chapter 2, the characteristics and performances of seven absorption couples have been analyzed. The couple chosen for the experimentation is $CaCl_2/H_2O$. Indeed, according to the chapter 2, the $CaCl_2/H_2O$ couple has an acceptable storage capacity corresponding to its price. The safety of $CaCl_2$ is higher than other couples such as KOH/H_2O, $NaOH/H_2O$ and H_2O/NH_3.

The anhydrous $CaCl_2$ comes from the Solvay Group. The purity of this $CaCl_2$ is about 95%. Its compositions can be found in Table 3-1.

Table 3-1 The composition of the $CaCl_2$ product [Solvay Group]

Characteristics	Expressed as	Unit	Typical values
Calcium chloride	$CaCl_2$	g/kg	950
Acid insoluble matter		g/kg	<0,1
Magnesium	$MgCl_2$	g/kg	2
Total other chlorides	NaCl	g/kg	10
Sulphates	SO_4	g/kg	<1
Iron	Fe	g/kg	<10
Water insoluble		g/kg	2

3.2.2 The materials used for the prototype

The corrosion data of the absorption couple is an important characteristic for the design of the prototype. The corrosion data of the $CaCl_2/H_2O$ solution for different materials can be found in table 3-2. The material chosen for the system is the stainless steel 316 L (SS-316L), which presents an acceptable corrosion rate and is not too expensive. The 904L, gold/platinum and Mo superalloy have excellent resistance to the corrosion of $CaCl_2$ solution, but their prices are unaffordable (more than two times the price of 316L steel).

Table 3-2 Corrosion data of the $CaCl_2/H_2O$ solution [NACE International]

Material or substance name	mass fraction (%)	Temperature (°C)	corrosion rate (mm/year)
Alloy 20-25-4Mo (904L)	<40	-18 à 100	<0.05
Aluminum Alloy (3003/ 5154)	5 – 55	23 à 107	<0.5
Austenitic Cr-Ni-Mo Stainless Steel (17-12-3; 316L/ 317L)	5 – 75	-4 à 51	<0.5
Brass (>15Zn)	5 – 65	-4 à 79	<0.5
Cast Iron, Gray/ Ductile	5 – 75	-4 à 79	<0.5
Copper/ Bronze/ Low Brass	5 – 75	23 à 79	<0.5
Cr Stainless Steel (17Cr)	5 – 75	-4 à 79	>1.27
Gold/ Platinum	5 – 75	-4 à 107	<0.05
Lead	5 – 75	79 à 107	>1.33
Lead	55 – 75	51 à 79	0.51-1.31
Mo Superalloy (Ni-Cr-Fe-9Mo; 625/ 725)	5 – 75	-4 à 107	<0.05
Nickel (200)	45 – 55	23 à 162	<0.5
Nickel-Copper (400)	25 – 35	-4 à 135	<0.5

3.2.3 Design and description of the devices

3.2.3.1 Tanks

The storage capacity of the $CaCl_2/H_2O$ couple is calculated by the static simulation in the Chapter 2. In table 2-4, the operating conditions are a temperature of the condenser at 30°C; a temperature of the absorber at 20°C; a temperature of the storage tanks before the absorption phase at 10°C and a temperature of the evaporator at 10°C. The solution volume for an energy product by absorption of 1000 kWh is about 8.4 m^3 without crystal. In order to get a storage capacity of 15 kWh in the experimentation, the volume need of the solution tank is about 126 L and the need for the water is about 21 L.

The characteristics of the tanks can be found in Table 3-3. The solution tank is about 150 L. The water tank is about 50 L which is bigger than the calculated volume need for the water. The volume of the water tank is designed to be sufficient in the situation when there is crystal in the solution tank (more water is desorbed from the solution and stored in the water tank). The volume of the reactor is about 130 L which is designed to be sufficient for the distributors and exchangers inside. The water receiver in the reactor is used to store temporarily the water which is circulated in the evaporator or the water condensed in the condenser. The volume of the water receiver is about 5 L. During desorption, water vapor is condensed in the condenser and the liquid water is stored temporally in the water receiver. When the water in the water receiver is more than 70% of the total volume of the water receiver, the water will be transferred to the water tank by pump. During the absorption, the liquid water is transferred from the water tank to the water receiver by a pump when the water in the water receiver is less than 20% of the total volume of the water receiver. The transmission of water stops when the water in the water receiver is more than 70% of the total volume of the water receiver. All components are made of stainless steel 316L, except the water tank. As the water tank is not in contact with the $CaCl_2$ solution, the stainless steel 304L is sufficient.

The system is operated under vacuum. The safety thickness need of the tanks (E) can be calculated following Eq.3-1 to Eq.3-3 [He K. 2002].

$$H > l_{cr}:\ E \geq d_o \sqrt[3]{\frac{3\Delta P}{2.2E^t}} + C \qquad \text{Eq.3-1}$$

$$H < l_{cr}:\ E \geq d_o \left(\frac{3\Delta P}{2.59E^t} \cdot \frac{H_o}{d_0}\right)^{0.4} + C \qquad \text{Eq.3-2}$$

$$l_{cr} = 1.17 d_i \sqrt{d_i / E} \qquad \text{Eq.3-3}$$

in which, H is the height of the tank; d_o is the outside diameter of the tank; d_i is the inside diameter of the tank; ΔP is the pressure difference of inside and outside of the tank [in MPa]; E^t is the modulus of elasticity, for stainless steel $E^t = 2.06\times10^5\ MPa$; l_{cr} is the critical height.

Table 3-3 Characteristics of the tanks

Tanks	Diameter mm	Height mm	Thickness mm	Volume L	Material	Mass kg	Design pressure kPa (absolute)
Solution tank	600	1000	4	150	SS-316L	131	1
Water tank	400	600	3	50	SS-304L	30	1
reactor	400	1200	3	130	SS-316L	124	1
Water receiver	260	100	3	5	SS-316L	4	1

Note: the water tank is made of stainless steel 304L (SS-304L) because there is no solution there.

The thicknesses of the different tanks have been recalculated by the Maquettes et Bureau d'Etudes company which is specialized in the design of mechanical systems. The software used for the calculation is SICAPNet.

3.2.3.2 Heat exchangers and distributors

The heat exchangers which are used in the reactor for the condenser/evaporator and generator/absorber have the same configuration composed 16 tubes with helical fin outside as shown in Figure 3-2.

The water coming from the thermostat flows on the inside of the tubes. It is distributed by the distributor which is connected to the inlet of the heat exchanger and collected by the distributor which is connected to the outlet of the heat exchanger (Figure 3-2). As the distances from the inlet to the outlet through every tube are uniform, the flow rate difference between the 16 tubes will be low. In the generator/absorber, the solution from the solution tank, which needs to be heated (desorption) or cooled (absorption) by the heat exchanger, is distributed by a distributor above to every helical fin on the heat exchanger (the distributor is shown in Figure 3-3). The solution flows along the helical fins outside of the tubes for desorption or absorption. The solution after desorption or absorption is collected at the bottom of the reactor and transferred back to the solution tank. In the condenser/evaporator, during condensation, the vapor is condensed on the heat exchanger and the liquid water flows along the helical fins and is collected in the water receiver. During the evaporation, the water is distributed by a distributor above to every helical fin on the heat exchanger (this distributor is the same as the distributor used in the generator/absorber). The water flows along the helical fins outside of the tubes and is heated by the water inside of the heat exchanger for evaporation. Due to the limitation of the surface and the temperature difference of the heat exchanger and the present of air in the reactor, the water could not be totally evaporated. The water which is not evaporated on the heat exchanger is collected by the water receiver and circulated by the pump to the distributor above the heat exchanger for the succeeding evaporation. The helical fins increase the outside surface for both the heat and mass transfer. The residence time of the water or the solution on the heat exchanger is also increased.

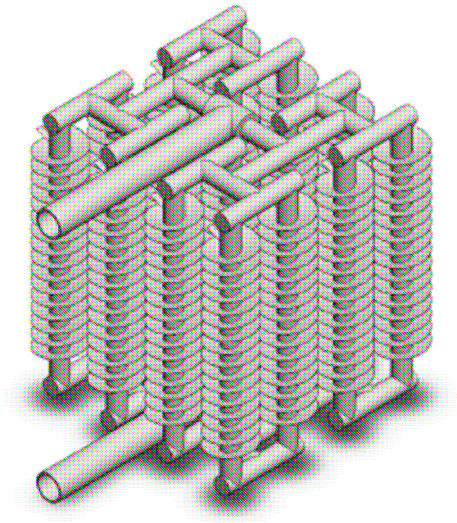

Figure 3-2 The heat exchanger with helical fins

The expected power of the heat exchangers can be calculated as Eq.3-4.

$$\dot{Q} = K_i \cdot S_i \cdot \Delta T_{\ln} \qquad \text{Eq.3-4}$$

The heat transfer coefficients K_i for the heat exchangers can be calculated following Eq.3-5.

$$\frac{1}{K_i} = \frac{1}{\alpha_i} + \frac{Ed_i}{\lambda d_m} + \frac{d_i}{\alpha_o d_o} \qquad \text{Eq.3-5}$$

As the heat transfer at the outside of the tubes is a phase change heat transfer, the corresponding heat transfer resistance $\frac{d_i}{\alpha_o d_o}$ is small compared the others and is neglected. Hence only $\frac{1}{\alpha_i} + \frac{Ed_i}{\lambda d_m}$ is considered for the design of the heat exchangers.

The heat transfer efficiency on the inside of the heat exchangers can be calculated as follows [Yang S. & Tao W. 1987]:

$$\alpha_i = 0.012 \frac{\lambda}{d_i} (\mathrm{Re}^{0.87} - 280)\,\mathrm{Pr}^{0.4} \qquad (\mathrm{Re} \geq 2300) \qquad \text{Eq.3-6}$$

$$\alpha_i = 1.86 \frac{\lambda}{d_i} \left(\frac{\mathrm{Re}\,\mathrm{Pr}}{l/d}\right)^{1/3} \qquad (\mathrm{Re} \leq 2300) \qquad \text{Eq.3-7}$$

The characteristics of the heat exchangers can be found in Table 3-4. The surface area of the helical fin is calculated just as the upper part, which is in contact with the water or the solution during the flowing. The total surface area is the sum of the area of the helical fins and the surface area of the tube. The material of the heat exchangers is stainless steel 316 L.

Table 3-4 Parameters of the heat exchangers

Number of tube	16
Height of tube	200 mm
Height of helical fin	180 mm
Diameter of tube	13.5/10.2 mm
Diameter of helical fin	30/13.5 mm
Thickness of helical fin	1 mm
Number of rotations	19
Surface area of helical fin	0.016×16 m^2
Surface area of tube	0.008×16 m^2
Internal surface area of tube	0.006×16 m^2
Total surface area	0.38 m^2
Total inside area	0.1 m^2
Length of runs on helical fin	1.5 m
Mass	4 kg

The expected power of the heat exchangers at certain operating conditions can be found in Table 3-5. It is only an estimate as the mean temperature difference of the heat exchanger (ΔT_{ln}) is not exactly known.

Table 3-5 Expected power of the heat exchangers

Heat exchanger	Flow rate inside the tubes (kg/h)	K_i (kW/(m^2.K))	ΔT_{ln} (°C)	Expected power (W)
Generator	500	0.73	60	4400
Condenser	200	0.56	40	2200
Absorber	150	0.51	5	250
Evaporator	200	0.56	5	280

The distributor which is used for distributing the solution or the water on the helical fins of the heat exchangers is shown in Figure 3-3. Every outlet of the distributor corresponds to a helical fin of the heat exchanger. The tube used for the distributor has the same characteristics as the heat exchanger. The diameter of the outlets on the tubes is 5 mm. The diameter of the tubes has not been optimized (the flow rate is supposed to be halved at each branch point. Correspondingly, the diameter of the tubes should be decreased). In this prototype, all tubes have the same diameter in order not to increase further the welding work difficulty. The material of the distributor is stainless steel 316 L. Its mass is about 0.5 kg.

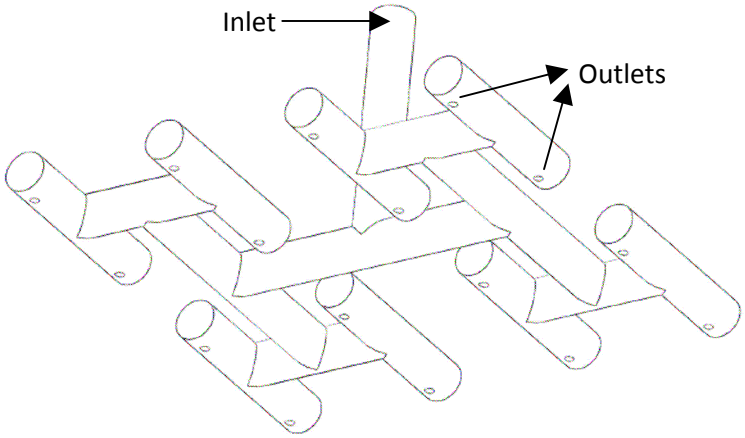

Figure 3-3 Distributor in the reactor

3.2.3.3 Other devices

Other devices used in the prototype can be found as follows:

- Temperature sensor Pt100 class B of TC Direct: 14 piece, precision: $\pm(0.3+0.005\times T(°C))$;
- Pressure sensor PR 23 of KELLER of Sysmatec: 4 pieces, precision: ±0.5%;
- Turbine flow meter PEL-M020 S10 K of Kobold, 2 à 130 L/min: 2 pieces, precision: ±1.25%;
- Thermostat: They are equipped with a heating and a cooling system. The power is 25kW both for heating and cooling;
- Level meter M FMP40 of Endress + Hauser : 4 pieces, 930 mm long for the solution tank, 680 mm long for the water tank, 595 long mm for the water receiver in the condenser/evaporator, 1630 mm long for the generator/absorber, precision: $\pm 5\ mm$.
- Agilent 34970A with two carts 34971A for collecting and transferring the signal of the temperature sensors;
- The Napac system for collecting and transferring of the 4-20 mA signals;
- Dosing pump of Aquacontrol: D050N50F13DV, 230 L/h, 2 pieces, D100N90B13, 24 L/h, 1 piece, precision: ±1%;
- Valves and fittings (stainless steel 316L) of Swagelok.

The overall scheme of the prototype is presented in Figure 3-4. The global dimension of the prototype is about 3.3 m×1.5 m×2.4 m.

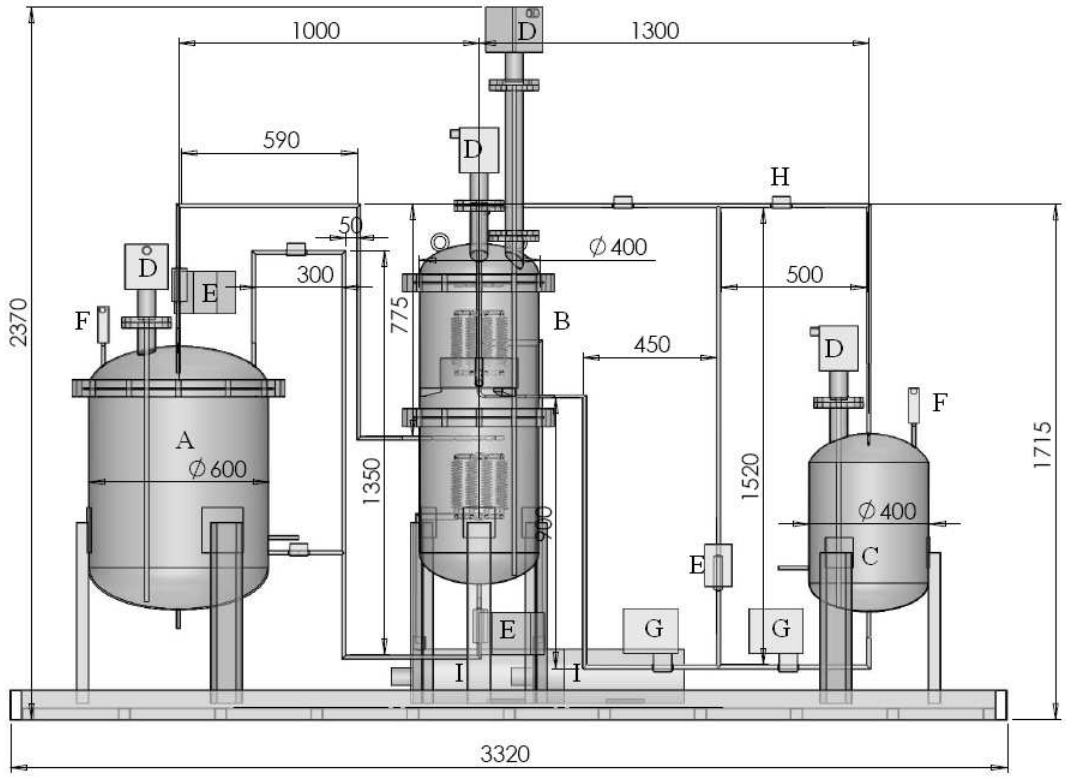

Figure 3-4 Scheme of the prototype

A: solution tank; B reactor; C: water tank; D: level meter;
E: dosing pump; F: pressure sensor; G: electric valve; H: valve; I: circulator

The experimental setup of the absorption storage system can be found in Figure 3-5.

Figure 3-5 Experimental setup of the absorption storage system

3.3 Planning of the experimentations

The operating conditions of the experiments of the prototype are presented in Table 3-6:

Table 3-6 Operating conditions of the experiments

Case			Case 1	Case 2
Constant parameters	Water flow rate in the heat exchanger of the absorber	kg/h	150	150
	Water flow rate in the heat exchanger of the generator	kg/h	500	500
	Water flow rate in the heat exchanger of the condenser	kg/h	200	200
	Solution flow rate in the generator	kg/h	115	115
	Water flow rate in the evaporator	kg/h	24	24
	Mass fraction of solution after desorption	kg salt/kg solution	0,418	0,418
	Duration of absorption	h	10	10
	Water flow rate in the heat exchanger of the evaporator	kg/h	200	200
	Solution flow rate in the absorber	kg/h	115	115
	Water temperature at the inlet of heat exchanger of condenser	°C	30	30
	Water temperature at the inlet of heat exchanger of absorber	°C	20	20
Variable parameters	Water temperature at the inlet of heat exchanger of evaporator	°C	***15***	***10***
	Water temperature at the inlet of heat exchanger of generator	°C	***80***	***70***

At the beginning of the experiment, 207 kg of poor solution with a mass fraction of 0.369 kg salt/kg solution is stored in the solution tank. The water tank is empty.

Case 1:

- Desorption is completed when the mass fraction of the solution in the solution tank is about 0.418 kg salt/kg solution. It is the maximum mass fraction to ensure that there is no crystallization.

- As the temperature difference of the heat exchanger in the evaporator is low and the surface of the heat exchanger is not optimized, the power of the absorption and evaporation is lower than the desorption and condensation. So the duration of absorption to absorb all the water in the water tank is scheduled to be too long. So the absorption is stopped when the absorption length is about 10 hours (one day).

Case 2:

- The solution available after the absorption of Case 1 is used for the second desorption. The water temperature at the inlet of the heat exchanger of the generator is changed from 80°C to

70°C. Desorption is complete when the mass fraction of the solution in the solution tank is 0.418 kg salt/kg solution.

- For the absorption phase, the water temperature at the inlet of the heat exchanger of the evaporator is changed from 15°C to 10°C. Absorption is also stopped when the absorption length is 10 hours.

The water temperature at the inlet of the heat exchanger of the generator is reduced from 80°C to 70°C and the water temperature at the inlet of the evaporator exchanger decreases from 15°C to 10°C (Case 1 → Case 2) to investigate their influence on the performances of the system.

The purpose of the experimentation is to verify the feasibility of the storage system by absorption. In order to reduce the risks of the experimentation, all experiments are carried out in a situation in which no crystal forms in the solution tank.

3.4 Results of the experimentation

Before the solution is introduced into the prototype, its mass fraction is calculated by measuring the density of the solution (Table 3-7). The relationship between the density, temperature and mass fraction can be found in Appendix 7. The average mass fraction of the solution x_t is 0.345 kg $CaCl_2$/kg solution. The solution is also chemically analyzed by Solvay Group. The analyzed mass fraction of $CaCl_2$ in the solution is 34.4% calculated by the percentage of Cl^- and is 33.6% calculated by the percentage of Ca^{2+}. The difference of the two mass fractions is due to the other elements such as Na^+ and Mg^{2+}. The maximum difference compared with the mass fraction calculated by density is about 2.6%. The total mass of the solution introduced into the prototype M_t is 207 kg.

Table 3-7 The calculation of the mass fraction of the solution

Volume	Mass	Temperature	Density	Mass fraction
100 ml	133.36g	22.6°C	1333.6 kg/m^3	34.67%
100 ml	133.03g	22.6°C	1330.3 kg/m^3	34.41%

At the end of each experimentation, the mass balance applied to the system can be found as Eq.3-8 and Eq.3-9, considering that the mass of solution and water in the reactor is negligible (the reactor is emptied by the pumps at the end of each test).

$$M_w + M_s = M_t \quad \text{Eq.3-8}$$

$$M_s x_s = M_t x_t \quad \text{Eq.3-9}$$

In which, M_w is the mass of the water in the water tank, M_s is the mass of the solution in the solution tank, x_s is the mass fraction of the solution in the solution tank, M_t is the total mass of the solution and the water in the system which is the mass of the poor solution before the experimentation, x_t is the mass fraction of the poor solution before the experimentation.

3.4.1 The desorption phases

During the desorption phase, the power $\dot{Q}_d$ and energy Q_d of desorption are calculated by the energy balance on the water side of the heat exchanger in the generator (Eq.3-10 and Eq.3-11):

$$\dot{Q}_d = \dot{m}_{ex,g} \cdot \left[h_{i,ex,g}(T_{i,ex,g}) - h_{o,ex,g}(T_{o,ex,g}) \right] \quad \text{Eq.3-10}$$

$$Q_d = \int \dot{Q}_d \, dt \quad \text{Eq.3-11}$$

In which, $\dot{m}_{ex,g}$ is the flow rate of the water in the heat exchanger of generator, $h_{i,ex,g}$ is the enthalpy of the water at the inlet of the exchanger at its temperature $T_{i,ex,g}$, $h_{o,ex,g}$ is the enthalpy of the water at the outlet of the exchanger at its temperature $T_{o,ex,g}$.

The power $\dot{Q}_c$ and energy Q_c of condensation are calculated by the energy balance of the water side of the heat exchanger in the condenser with similar equations as Eq.3-10 and Eq.3-11:

The sensible heat for the water in the water tank during the desorption phase $Q_{w,d}$ is defined as Eq.3-12.

$$Q_{w,d} = m_{w,d,2} \cdot h_{w,d,2}(T_{w,d,2}) - m_{w,d,1} \cdot h_{w,d,1}(T_{w,d,1}) \quad \text{Eq.3-12}$$

In which, $m_{w,d,2}$ is the mass of the water in the water tank after the desorption phase, $h_{w,d,2}$ is the enthalpy of the water in the water tank after the desorption phase at its temperature $T_{w,d,2}$, $m_{w,d,1}$ is the mass of the water in the water tank before the desorption phase, $h_{w,d,1}$ is the enthalpy of the water in the water tank before the desorption phase at its temperature $T_{w,d,1}$.

The heat transferred to the solution in the solution tank during the desorption phase $Q_{s,d}$ is defined similarly as Eq.3-12.

The experimentation results of the desorption phase can be found in Table 3-8. The Case 1-1 and Case 1-2 are the desorption phases according to the operating conditions of Case 1 in Table 3-6. The Case 1-1 and Case 1-2 have the same operating conditions but different initial conditions of the solution in the solution tank and the water in the water tank. The solution and water after the Case 1-1 is used for the Case 1-2 at another day. The Case 2-1 and Case 2-2 are the desorption phases according to the operating conditions of Case 2 in Table 3-6. The Case 2-1 and Case 2-2 have the same relation as Case 1-1 and Case 1-2.

Table 3-8 Experimentation results of the desorption phase

Parameters	Unit	Case 1-1	Case 1-2	Case 2-1	Case 2-2
Start		11/05 09:50	12/05 08:33	18/05 14:01	20/05 09:00
End		11/05 17:31	12/05 17:01	18/05 18:23	20/05 16:31
$m_{w,d,1}$	kg	0	19.5	27.1	28.7
$m_{w,d,2}$	kg	19.5	35.5	28.4	40.5
$m_{s,d,1}$	kg	207.5	188	180.4	179.1
$m_{s,d,2}$	kg	188	172	179.1	167
$x_{s,d,1}$	kg $CaCl_2$/kg solution	0.345	0.381	0.397	0.4
$x_{s,d,2}$	kg $CaCl_2$/kg solution	0.381	0.417	0.4	0.428
$T_{w,d,1}$	°C	21.2	25.1	19.6	26
$T_{w,d,2}$	°C	30.3	29.1	20.3	25.9
$T_{s,d,1}$	°C	41.7	48.3	20.4	38.5
$T_{s,d,2}$	°C	65.8	64.6	55.7	57
$Q_{w,d}$	kWh	0.7	0.6	0.05	0.35
$Q_{s,d}$	kWh	2.7	0.9	5.9	1.7
Minimum pressure of the reactor	mbar	92	60	68	60
Maximum pressure of the reactor	mbar	168	157	125	85
$T_{o,ex,g}$ minimum	°C	72.3	72.9	64.9	66
$T_{o,ex,g}$ maximum	°C	77.6	80.6	69.3	68.8
$T_{i,ex,g}$ minimum	°C	78.4	80.2	66.7	71.4
$T_{i,ex,g}$ maximum	°C	82	82.7	72.2	72.3
$T_{o,ex,c}$ minimum	°C	33.1	33	28.7	32.7
$T_{o,ex,c}$ maximum	°C	44.4	39.7	33.7	36.4
$T_{i,ex,c}$ minimum	°C	31.4	31.5	28.6	31.3
$T_{i,ex,c}$ maximum	°C	32.1	33.4	31.9	32.2
$\dot{Q}_d$ minimum	kW	1.81	0.65	0.96	1.16
$\dot{Q}_d$ maximum	kW	4	4.4	2.7	3.34
$\dot{Q}_c$ minimum	kW	0.25	0	0.04	0.04
$\dot{Q}_c$ maximum	kW	3	1.85	0.56	1.14
Q_d	kWh	23.5	26.4	10.3	18.2
Q_c	kWh	9.9	12	1.2	6.7

3.4.1.1 Case 1-1

During Case 1-1, the water temperature at the inlet of the heat exchanger in the generator is about 80°C. 19.5 kg of water is desorbed from the solution. The mass of the solution is decreased from 207.5 kg to 188 kg. The mass fraction is increased correspondingly from 0.345 kg $CaCl_2$/kg solution to 0.381 kg $CaCl_2$/kg solution. The masses and the mass fractions are calculated by using the water level in the water tank which is shown in Figure 3-6. The water level increases during the desorption phase because the water which is condensed in the condenser is transferred to the water tank. The increase is discontinuous because the pump works discontinuously corresponding to the water level in the condenser.

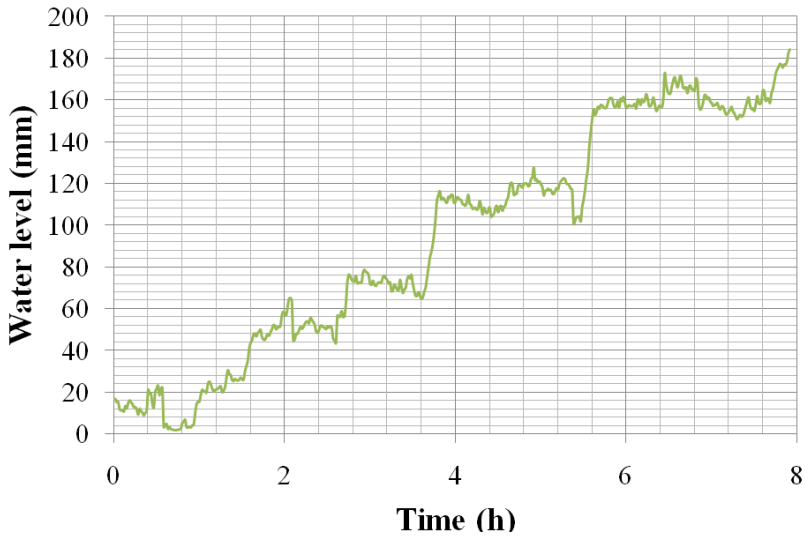

Figure 3-6 Evolution of the water level in the water tank

The evolutions of the temperature of the solution tank (T_{sd}) and the temperature of the water tank (T_{wd}) are presented in Figure 3-7:

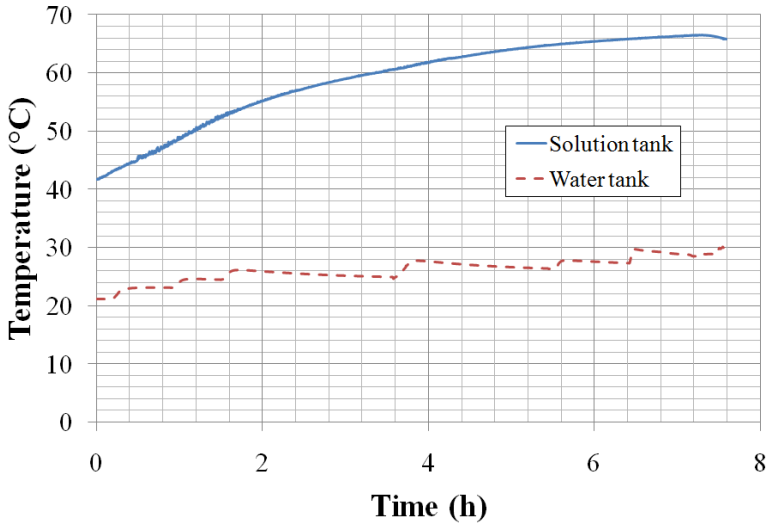

Figure 3-7 Evolutions of the temperature of storage tanks

During the desorption phase, $T_{s,d}$ increases (from 41.7 to 66.4°C) because the solution is heated by the heat exchanger in the generator during the circulation between the solution tank and the generator. But this increase is discontinuous because the pump which transfers the water in the condenser to the water tank is discontinuous. The temperature of the water in the water tank increases rapidly when the water in the condenser is transferred to the water tank and decreases slowly at other times because of the heat loss. The energy accumulated by the water in the water tank is about 0.7 kWh and for the solution in the solution tank, it is about 2.7 kWh. During the desorption phase, the solution in the solution tank is heated to 65.8°C which is much higher than the environment temperature. The energy need for desorption is thus increased due to the heat loss from the solution tank to the environment and the sensible heat for the solution during the desorption phase.

The evolutions of the pressures of the water tank, the solution tank and the reactor are shown in Figure 3-8. The pressure of the water tank is influenced by two factors: temperature and leaks of the tank. The pressure of the water tank increases discontinuously when the water is transferred from the condenser to the water tank because of the increase of the water temperature in the tank. At the beginning of the desorption phase (from 0 h to 1 h), the water temperature of the water tank is low (about 20°C in Figure 3-7). The temperature decrease of the water due to the heat loss is weak. The pressure of the water tank also increases slowly after every transfer of water because of the leak of air in the water tank. Between 1 h and 6.8 h, the pressure of the water tank decreases after every transfer of water, correspondingly to the temperature which is shown in Figure 3-7. Between 6.8 h and 7.2 h, the vacuum pump is used to decrease the pressure of the water tank. Between 7.2 h and 8 h, the pressure of the water tank increases because the air is transferred from the reactor to the water tank by the pressure difference. After that, the pressure is changed with the temperature of the solution in the solution tank (Figure 3-7). Between 0 h and 6.8 h, the pressure of the reactor increases during the desorption phase because of the temperature increase of the solution. Between 6.8 h and 8 h, the pressure of the reactor decreases because the air is transferred from the reactor to the water tank by the pressure difference.

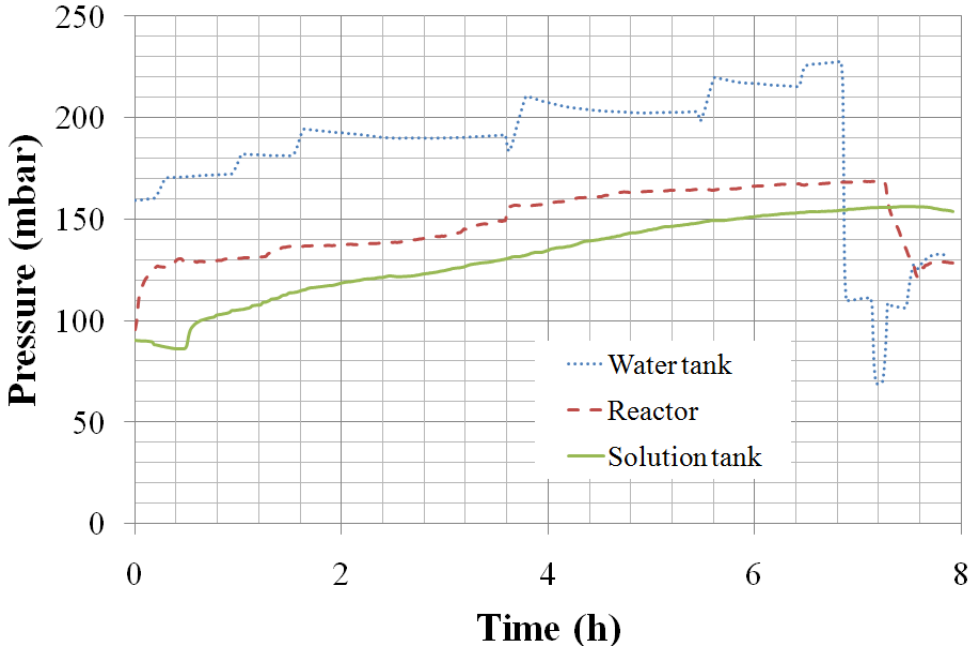

Figure 3-8 Evolution of the pressures of the storage tanks and the reactor

There is a special point at about 3.6 h when the pressure of the reactor increases rapidly. At the same point, the pressure of the water tank decreases rapidly. This is mainly because the air in the water tank is transferred automatically to the reactor by the pressure difference when the valve is opened in order to transfer the water from the condenser to the water tank.

The leaks of the prototype are a serious problem for the experiments. The presence of air decreases the absorption/desorption and the performances of the heat exchangers. The equilibrium water pressure is 42 mbar at 30°C for desorption and is 12 mbar at 10°C for absorption. When the reactor pressure is higher than the equilibrium pressure, because of the incondensable gas (air), desorption and absorption are slow. The minimum pressure which can be achieved in the prototype is about 30 mbar because of the leaks of the prototype (about 1 $Pa{\cdot}m^3/s$) and the ability of the vacuum pump (when a pressure sensor is connected directly to the pump, the pressure can only decrease to 20 mbar). The effect of the air, which is transferred from the water tank to the reactor, on the heat exchangers can be found in the following analysis of the temperature and powers of heat exchangers.

The water temperature at the inlet of the heat exchanger of the generator ($T_{i,ex,g}$) is not constant at 80°C. It changes from 78.4 to 82°C in Case 1-1 and from 80.2 to 82.7°C in case 1-2 because of the self limitation of the thermostat. The average temperature of $T_{i,ex,g}$ is 81.6°C for Case 1-1 with a variance of 0.2 and is 81.7°C for Case 1-2 with a variance of 0.03. The same problem occurs for the water temperature at the inlet of the heat exchanger of the condenser ($T_{i,ex,c}$). $T_{i,ex,c}$ is supposed at 30°C but is achieved at the average temperature of 31.5°C for Case 1-1 with the a variance of 0.003 and 31.8°C for Case 1-2 with a variance of 0.007.

The evolution of the water temperature at the inlet ($T_{i,ex,g}$) and outlet ($T_{o,ex,g}$) of the heat exchanger of the generator and the water temperature at the inlet ($T_{i,ex,c}$) and outlet ($T_{o,ex,c}$) of

the heat exchanger of the condenser of Case 1-1 can be found in Figure 3-9. Those temperatures are used for the calculation of the power and energy which is used for desorption and condensation (Figure 3-10). The difference of the temperatures at the inlet and outlet of the heat exchangers is about 5°C. Considering the precision of the temperature sensors (about 0.3°C) and the flow meters (1.25%), the precision of the calculation for the power and the energy is about 12%.

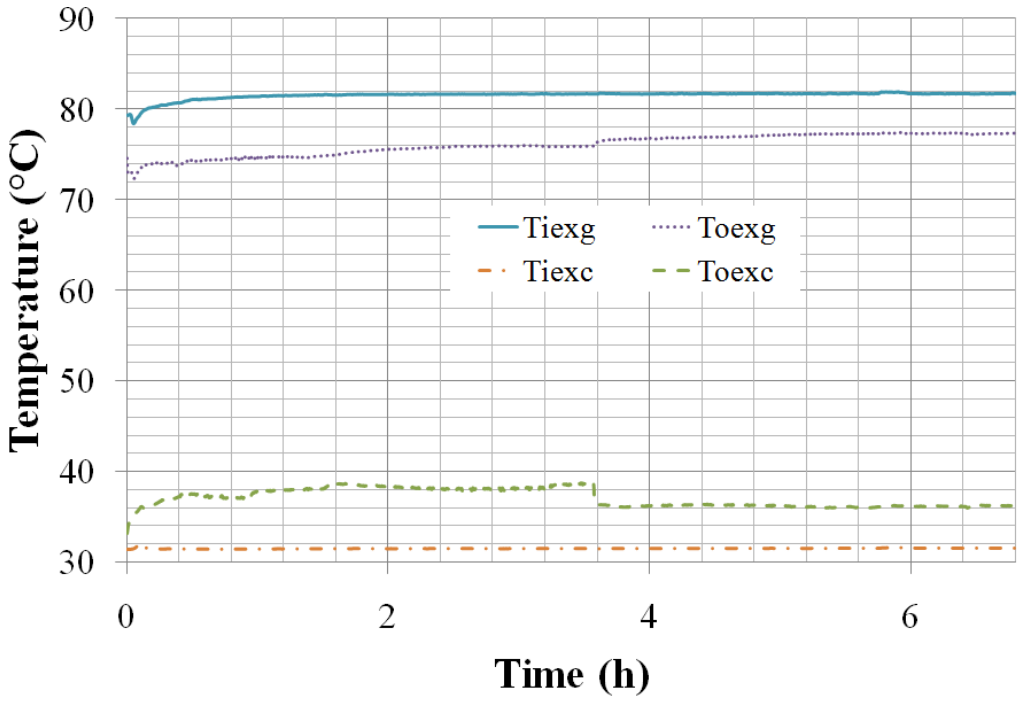

Figure 3-9 Evolution of the temperatures of the heat exchangers

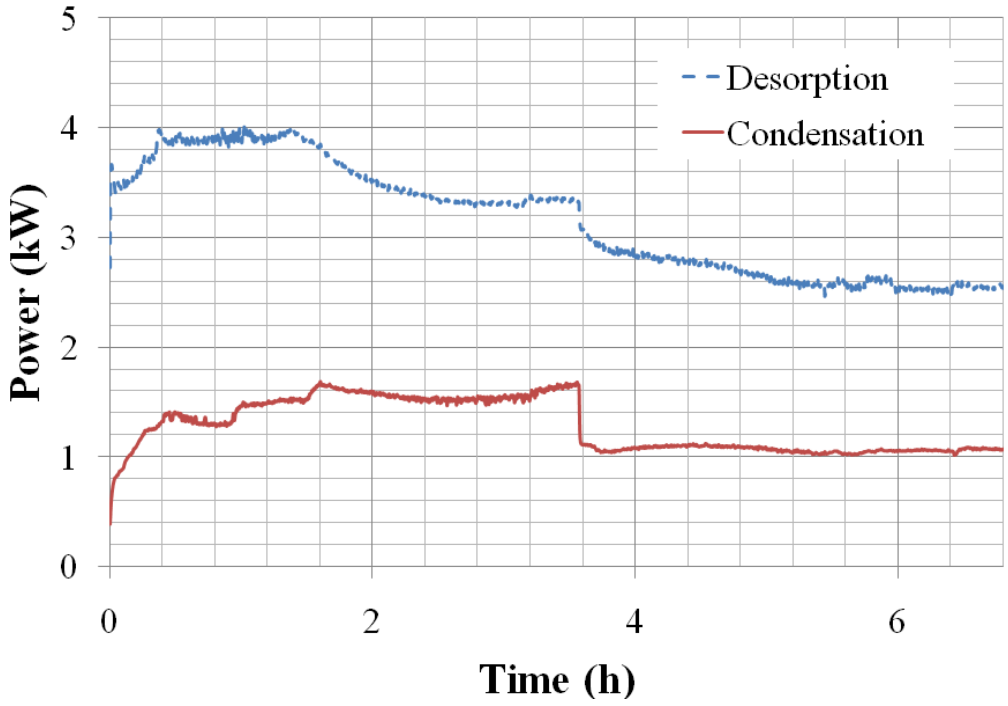

Figure 3-10 Evolution of the powers of the heat exchangers

Generally speaking, the power exchanged by the heat exchanger in the generator decreases during the process. This is mainly because the temperature of the solution coming from the solution tank increases during the process, thus its temperature change in the heat exchanger is decreased. The increase of the power at the beginning (from 0 h to 0.4 h) is due to the temperature increase of the $T_{i,ex,g}$. The thermostat needs that time to adjust the outlet water temperature as the required temperature. At the beginning of the process, with the increase of the solution temperature, the temperature of the water vapor which is desorbed from the solution in the generator increases. Correspondingly, the power exchanged in the condenser increases. But at the special point at 3.6 h (Figure 3-8), the valve between the reactor and the water tank is open in order to transfer the water in the water receiver to the water tank. The air in the water tank is transferred to the reactor due to the pressure difference of the water tank and the reactor. The powers of the heat exchangers in the generator and the condenser decrease rapidly. $\dot{Q}_d$ decreases from 3.35 kW to 3.05 kW (about 9%) and $\dot{Q}_c$ decreases from 1.65 kW to 1.1 kW (about 33%). The effect of the air on the desorption rate is remarkable.

The global energy provided by the heat exchanger in the generator Q_d is 23.5 kWh. The energy rejected by the heat exchanger in the condenser Q_c is 9.9 kWh. The sensible heat for the water in the water tank is 0.7 kWh. The heat for the solution in the solution tank is 2.7 kWh. According to the energy balance, the heat loss is about 10.2 kWh (43.4% of Q_d). The heat losses happen in the pipes, the solution tank, the water tank and the reactor. The water vapor in the reactor which is condensed at the inside surface of the reactor walls by the heat loss will flow back to the generator where it is remixed with the solution. Thus the energy for desorption is also increased because this part of water needs to be desorbed once more. The design and the heat isolation of the reactor play an important part for the efficiency of the seasonal storage system.

3.4.1.2 Case 1-2

During Case 1-2, the operating conditions are the same as Case 1-1. 16 kg of water is desorbed from the solution. The mass of the solution is decreased from 188 kg to 172 kg. The mass fraction is increased correspondingly from 0.381 kg $CaCl_2$/kg solution to 0.417 kg $CaCl_2$/kg solution. The energy provided by the heat exchanger in the generator Q_d is 26.4 kWh. The energy rejected by the heat exchanger in the condenser Q_c is 12 kWh. The sensible heat for the water is 0.6 kWh. The heat for the solution in the solution tank is 0.9 kWh. According to the energy balance, the heat loss is about 12.9 kWh (48.8% of Q_d). The heat for the solution in the solution tank is lower than in Case 1-1 because the initial solution temperature in the solution tank is higher than in Case 1-1. But correspondingly, the heat loss of the solution tank is increased. Thus, the amount of heat loss of Case 1-2 is higher than for Case 1-1.

3.4.1.3 Case 2-1 and Case 2-2

Compared to Case 1-1 and 1-2, the temperature at the inlet of the heat exchanger of the generator ($T_{i,ex,g}$) is decreased from 80 to 70°C in Case 2-1 and 2-2. $T_{i,ex,g}$ is not exactly constant at 70°C. It changes from 66.7 to 77.2°C in Case 2-1 and from 71.4 to 72.3°C in Case 2-2 because of the self limitation of the thermostat. The average temperature of $T_{i,ex,g}$ is 71.6°C for Case 2-1 with a variance of 0.77 and is 72°C for Case 2-2 with a variance of 0.01. The power of the heat exchanger is decreased compared to Case 1 due to the decrease of the $T_{i,ex,g}$. One example of the comparison between Case 1-1 and 2-2 can be found in Figure 3-11.

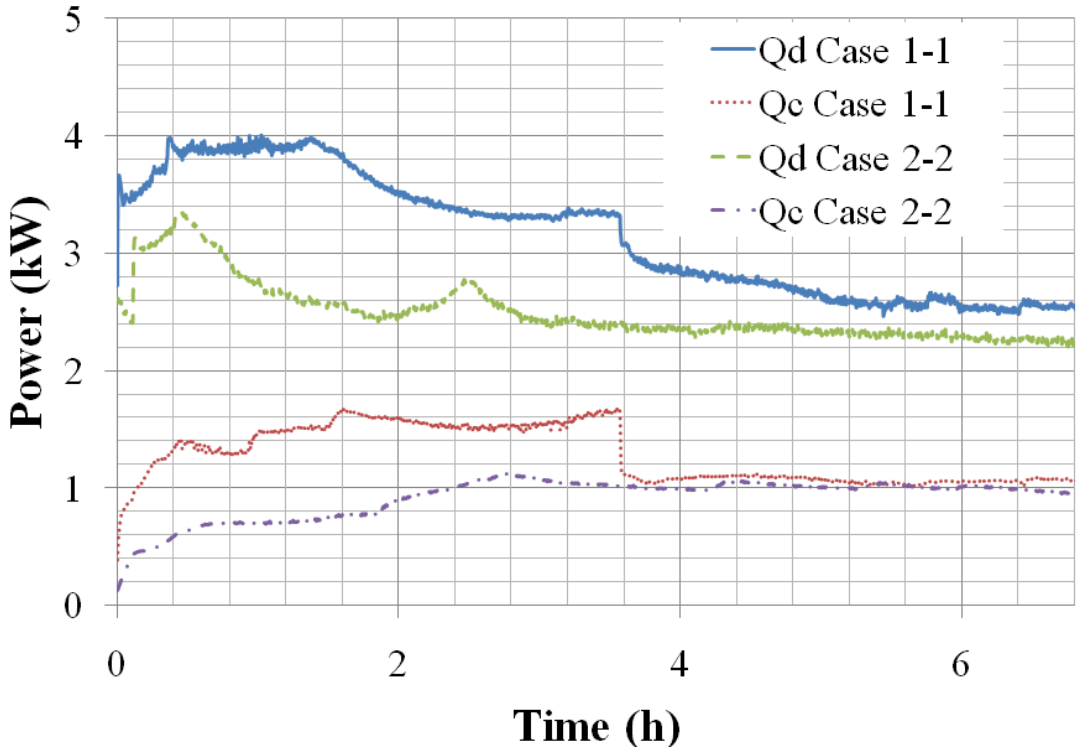

Figure 3-11 The influence of $T_{i,ex,g}$ on the power of heat exchangers

During Case 2-1, 1.3 kg of water is desorbed from the solution. The mass fraction of the solution is increased correspondingly from 0.397 kg $CaCl_2$/kg solution to 0.4 kg $CaCl_2$/kg solution. The energy provided by the heat exchanger in the generator Q_d is 10.3 kWh. The energy rejected by the heat exchanger in the condenser Q_c is 1.2 kWh. The sensible heat for the water in the water tank is 0.05 kWh. The heat for the solution in the solution tank is 5.9 kWh. The sensible heat stored in the solution takes most part of Q_d (57.3%), this is because the initial temperature of the solution is low (20.4°C). Using the rich solution from the generator to the solution tank to preheat the poor solution from the solution tank to the generator is an interesting option to be studied in the future. According to the energy balance, the heat loss is about 3.1 kWh (30.0% of Q_d).

During Case 2-2, 12.1 kg of water are desorbed from the solution. The mass fraction is increased correspondingly from 0.4 kg $CaCl_2$/kg solution to 0.428 kg $CaCl_2$/kg solution. The energy provided by the heat exchanger in the generator Q_d is 18.2 kWh. The energy rejected by the heat exchanger in the condenser Q_c is 6.7 kWh. The sensible heat for the water in the water tank is 0.4 kWh. The heat for the solution in the solution tank is 1.7 kWh. According to the energy balance, the heat loss is about 9.4 kWh (51.9% of Q_d). The energy need for the phase change of 12.1 kg of water in the condenser is about 7.7 kWh, which should be provided by Q_c. As the measured Q_c is lower than this energy need, it is possible that the water vapor is also condensed due to the energy loss of the reactor. In the generator, Q_d is used in the form of heat for the solution, heat loss of the generator and energy for the desorption of water. In fact, the measured Q_d (18.2 kWh) is a lot bigger than the sum of the eat for solution and the energy for the desorption of the water that is condensed (9.4 kWh). This means that there is heat loss in the generator to the surrounding, and that some

desorption heat is used to desorbe water that is not collected afterwards in the condenser: some desorbed water is certainly condensed on the reactor walls and flows directly back to the solution at the bottom of the reactor, and must be desorbed again, increasing Q_d. The difference is also partly due to the precision of the different sensors. The design of the reactor should be optimized in order to minimize these problems.

3.4.2 The absorption phase

During the absorption phase, the power $\dot{Q}_a$ and energy Q_a of absorption are calculated by the energy balance of the heat exchanger in the absorber similarly to Eq.3-10 and Eq.3-11. The power $\dot{Q}_e$ and energy Q_e of evaporation are also calculated. The sensible heat for the water in the water tank $Q_{w,a}$ and the heat for the solution in the solution tank $Q_{s,a}$ during the absorption phase is also calculated similarly to Eq.3-12.

The experimentation results of the absorption phase can be found in Table 3-9. The Case 1-3 and Case 1-4 are the absorption phases according to the operating conditions of Case 1 in Table 3-6. The Case 1-3 and Case 1-4 have the same relation as the Case 1-1 and Case 1-2, which has been explained before. The Case 2-3 is the absorption phases according to the operating conditions of Case 2 in Table 3-6. The Case S-1 is a special case. The operating conditions and results of this test will be discussed at the end.

Table 3-9 Experimentation results of the absorption phase

Parameters	Unit	Case 1-3	Case 1-4	Case 2-3	Case S-1
Start		17/05 11:11	18/05 09:48	21/05 10:30	28/05 10:27
End		17/05 17:55	18/05 13:49	21/05 18:05	28/05 16:40
$m_{w,a,1}$	kg	35.7	32.3	40.5	35.6
$m_{w,a,2}$	kg	32.3	27.1	39.9	31.5
$m_{s,a,1}$	kg	171.8	175.2	167	171.9
$m_{s,a,2}$	kg	175.2	180.4	167.6	176
$x_{s,a,1}$	kg $CaCl_2$/kg solution	0.417	0.409	0.429	0.417
$x_{s,a,2}$	kg $CaCl_2$/kg solution	0.41	0.397	0.427	0.407
$T_{w,a,1}$	°C	19.82	19.7	23.5	21.8
$T_{w,a,2}$	°C	19.79	19.6	21.9	21.6
$T_{s,a,1}$	°C	19.87	19.87	20.3	29.2
$T_{s,a,2}$	°C	21.25	20.4	20.9	33
$Q_{w,a}$	kWh	-0.07	-0.12	-0.09	0.96
$Q_{s,a}$	kWh	0.42	0.42	0.13	-0.11
Minimum pressure of the reactor	mbar	34	48	26	40.5
Maximum pressure of the reactor	mbar	58	57	34	87.5
$T_{o,ex,a}$ minimum	°C	19.72	19.62	19.9	29.3
$T_{o,ex,a}$ maximum	°C	20.29	19.89	20.72	32.3
$T_{i,ex,a}$ minimum	°C	19.47	19.45	19.74	28.5
$T_{i,ex,a}$ maximum	°C	19.73	19.67	20.69	29.2
$T_{o,ex,e}$ minimum	°C	15	15	10.42	39.6
$T_{o,ex,e}$ maximum	°C	15.44	15.34	11.67	41.7
$T_{i,ex,e}$ minimum	°C	15.1	15.22	10.68	40.4
$T_{i,ex,e}$ maximum	°C	15.29	15.31	10.82	42
$\dot{Q}_a$ minimum	kW	0.02	0.02	0	0.08
$\dot{Q}_a$ maximum	kW	0.11	0.04	0.09	0.56
$\dot{Q}_e$ minimum	kW	-0.04	-0.02	-0.21	0
$\dot{Q}_e$ maximum	kW	0.06	0.06	0.09	1.08
Q_a	kWh	0.31	0.17	0.21	2.5
Q_e	kWh	0.2	0.14	0.36	3.4

3.4.2.1 Case 1-3

During Case 1-3, 3.4 kg of water is absorbed by the solution. The mass of the solution is increased from 171.8 kg to 175.2 kg. The mass fraction is decreased correspondingly from 0.417 kg $CaCl_2$/kg solution to 0.41 kg $CaCl_2$/kg solution. The mass and the mass fraction are calculated using the water level in the water tank which is shown in Figure 3-12. The water level is decreased during the absorption phase because the water is transferred to the evaporator where it is evaporated by the heat exchanger. The decrease is discontinuous because the pump works discontinuously corresponding to the water level in the evaporator. At the end of the absorption phase (after 6.5 h), the water which is not evaporated is transferred back to the water tank.

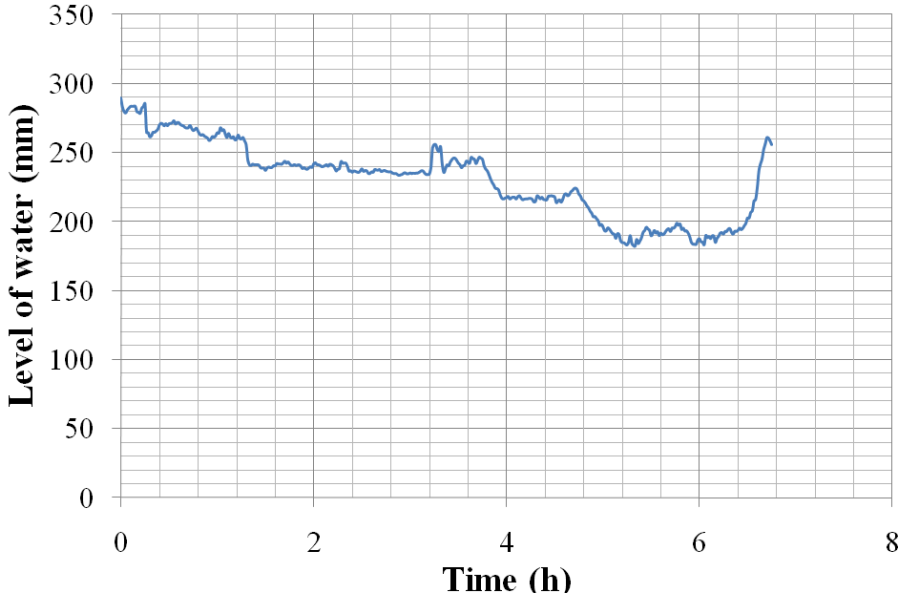

Figure 3-12 Evolution of the water level in the water tank

The evolution of the temperature of the solution tank (T_{sa}) and the temperature of the water tank (T_{wa}) are shown in Figure 3-13:

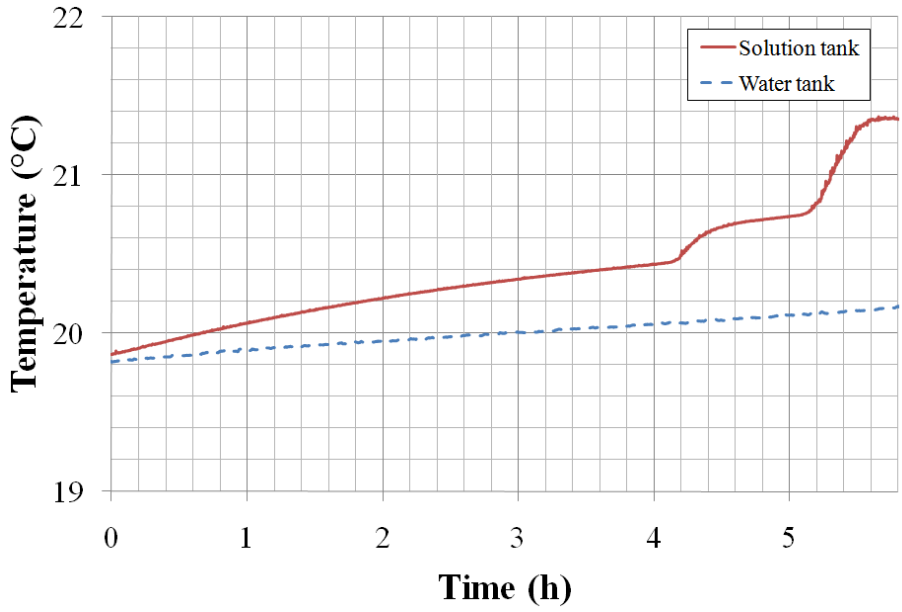

Figure 3-13 Evolution of the temperatures of the storage tanks

During the absorption, $T_{s,a}$ increases (from 19.9 to 21.4°C) because the solution is heated by the absorption heat in the absorber during the circulation between the solution tank and the absorber. $T_{w,a}$ increases from 19.8 to 20.2°C due to the increase of the environment temperature (from morning to afternoon). The sensible energy for the water in the water tank $Q_{w,a}$ is about -0.07 kWh and the heat for the solution in the solution tank $Q_{s,a}$ is about 0.42 kWh. $Q_{w,a}$ is negative mainly because of the decrease of the water mass in the water tank. $Q_{s,a}$ comes mainly from the absorption heat.

The evolutions of the pressures in the water tank, the solution tank and the reactor are shown in Figure 3-14. The pressure of the water tank increases because of the leaks of the tank. But from 0.1 h to 0.3 h, 3.7 h to 3.9 h and 4.8 h to 5.1 h, the pressure of the water tank decreases because the volume of the water in the water tank is decreased when the water is transferred from the water tank to the evaporator. The pressure of the solution tank increases from 32 mbar to 42 mbar between 0 and 6.5 h because of the increase of the solution temperature. The pressure of the reactor changes with the temperature of the water in the evaporator. It increases when the water is transferred from the water tank to the evaporator because the water temperature in the water tank (about 20°C) is higher than the water temperature in the evaporator (about 15°C).

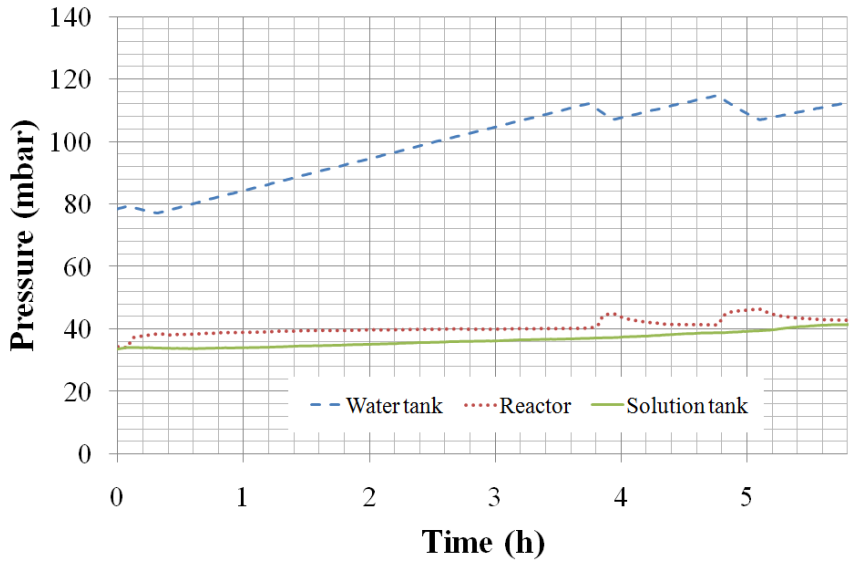

Figure 3-14 Evolution of the pressures of the storage tanks and the reactor

The evolution of the water temperature at the inlet of the heat exchanger of the absorber ($T_{i,ex,a}$) and outlet of the heat exchanger of the absorber ($T_{o,ex,a}$) and the water temperature at the inlet of the heat exchanger of the evaporator ($T_{i,ex,e}$) and outlet of the heat exchanger of the evaporator ($T_{o,ex,e}$) of case 1-3 can be found in Figure 3-15. Those temperatures are used for the calculation of the power and energy which are used for absorption and evaporation (Figure 3-16). But the average temperature difference between the inlet and the outlet of the heat exchanger is low (about 0.2°C). This temperature difference is not relevant because it is even lower than the precision of the temperature sensors (0.3°C). The data for the calculation of powers are not reliable. What we can conclude from this experimentation is the power for absorption and evaporation is low.

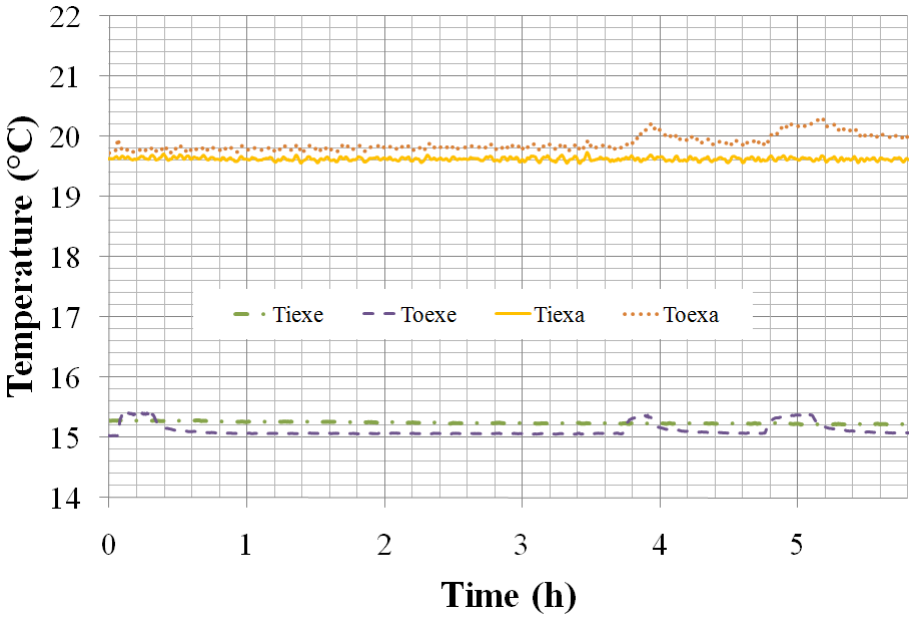

Figure 3-15 Evolution of the temperatures of the heat exchangers

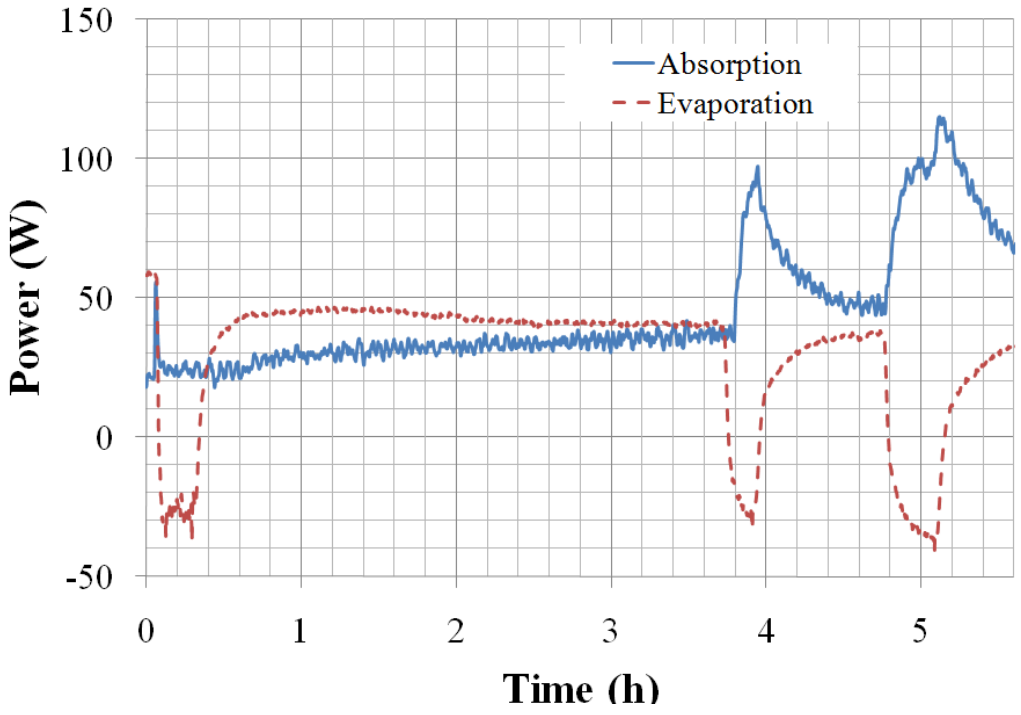

Figure 3-16 Evolution of the powers of the heat exchangers

At 0 h, 3.7 h and 4.8 h, the water in the water tank is transferred to the evaporator. The water temperature in the water tank is about 20°C, which is higher than the water temperature at the inlet of the heat exchanger in the evaporator ($T_{i,ex,a}$). The water in the heat exchanger is heated by the water which comes from the water tank. Hence the power of the evaporator ($\dot{Q}_e$) is negative after every transfer of water. After that, when the water temperature in the evaporator is lower than the $T_{i,ex,a}$, the power is positive. At the same time (0 h, 3.7 h and 4.8 h), the power of the absorption ($\dot{Q}_a$) is increased because the increase of the water temperature in the evaporator increases the water equilibrium pressure. After that, due to the heat which is released to the heat exchanger and also the heat needed by the evaporation, the water temperature in the evaporator is decreased. The water equilibrium pressure decreases with the water temperature in the evaporator. As a result, $\dot{Q}_a$ is decreased. From 0.8 h to 3.6 h, the absorption is not influenced by the water coming from the water tank. The power is about 30 W for absorption and about 40 W for evaporation. This power is low. The reason for this low power can be found as follows:

- The air in the reactor: The air present in the reactor because of the leaks decreases the the heat and mass transfers. The influence of the air for the heat and mass transfer is present in the desorption phase, but this influence is even more serious for the absorption phase because the water equilibrium pressure in the evaporator and the absorber is lower than it is in the generator and the condenser (Chapter 2, Figure 2-2).

- The heat exchanger dimensioning: The small surface area of the heat exchangers and the low flow rate in the heat exchangers cannot provide enough power for evaporation. It also can not take off the energy produced by absorption from the absorber efficiently enough, which is proved by the increase of the temperature of the solution in the solution tank.

- The thermodynamic characteristics of the $CaCl_2/H_2O$ linked to the dimensioning of the heat exchanger: The maximum temperature of absorption can be found in Figure 3-17. The maximum temperature of absorption is about 29°C when the temperature of evaporation is 15°C and the mass fraction of the solution is about 0.4 kg $CaCl_2$/kg solution. As the water temperature at the inlet of the heat exchanger in the absorber is about 20°C, the maximum temperature difference for the heat exchanger is 9°C. The low temperature difference for the heat exchanger decreases the power of heat transfer.

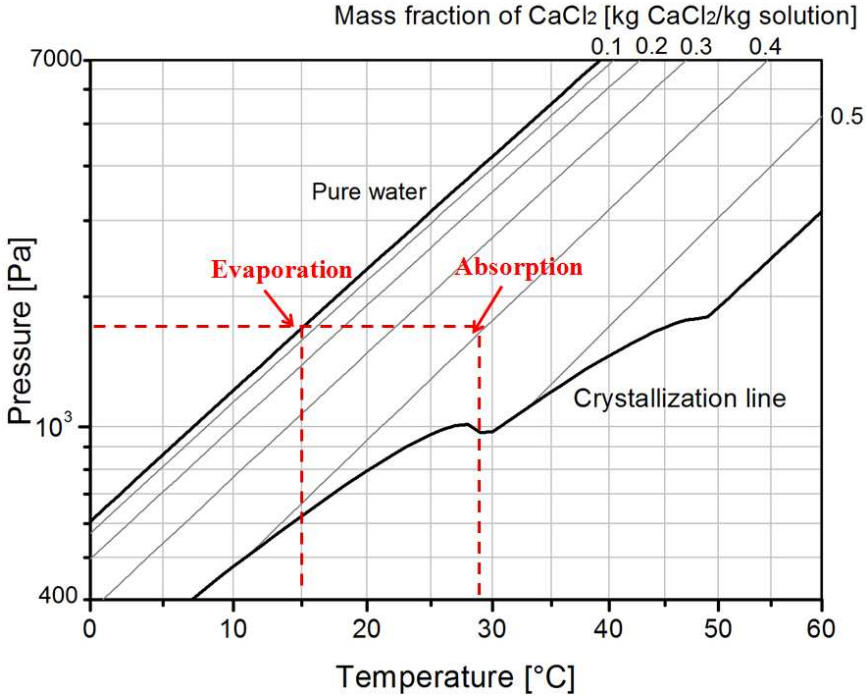

Figure 3-17 Maximum temperature of absorption for an evaporation at 15°C

The energy of absorption released by the heat exchanger in the absorber Q_a is 0.31 kWh. The energy provided by the heat exchanger in the evaporator Q_c is 0.2 kWh. The sensible heat for the water is –0.07 kWh. The heat for the solution is 0.42 kWh. According to the energy balance, at least 0.46 kWh of energy are provided by the environment for evaporation, for the water in the water tank and the solution in the solution tank through the walls of the components.

3.4.2.2 Case 1-4

During Case 1-4, the operating conditions is the same as Case 1-3. 5.2 kg of water is absorbed by the solution. The mass fraction is decreased correspondingly from 0.409 kg $CaCl_2$/kg solution to 0.397 kg $CaCl_2$/kg solution. The energy released by the heat exchanger in the absorber Q_a is 0.17 kWh. The energy provided by the heat exchanger in the evaporator Q_e is 0.14 kWh.

3.4.2.3 Case 2-3

Compared with Case 1-3 and 1-4, the water temperature at the inlet of the heat exchanger in the evaporator ($T_{i,ex,e}$) is decreased from 15°C to 10°C in Case 2-3 to study its influence on the power of absorption and evaporation. Generally speaking, the power is decreased because the decrease of $T_{i,ex,e}$ decreases the water equilibrium pressure in the evaporator. The pressure difference between the water equilibrium pressure in the evaporator and the solution

equilibrium pressure in the generator is the force for absorption. The evolution of power of absorption and evaporation can be found in Figure 3-18.

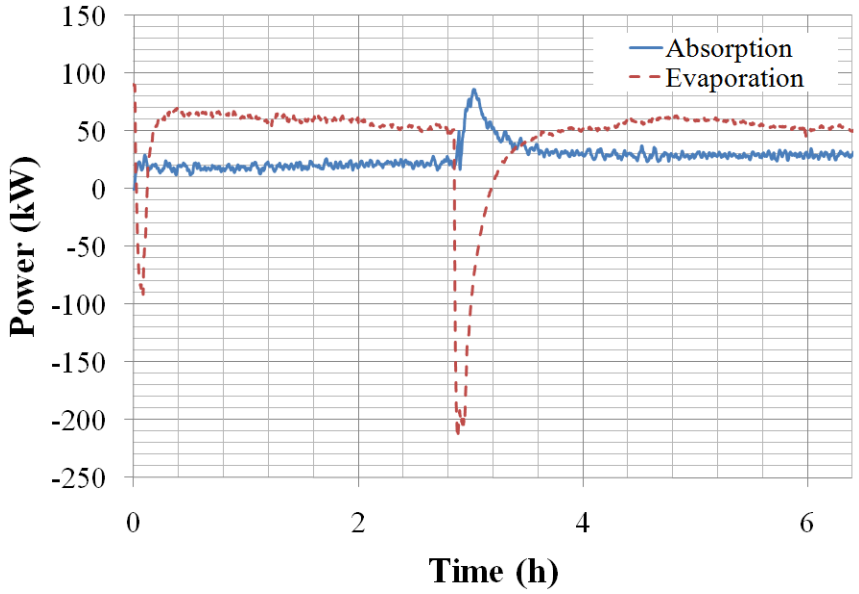

Figure 3-18 Evolution of power of absorption and evaporation (Case 2-3)

According to the Figure 3-18, the power does not decrease but increases compared to Case 1-3. The reason is that the air partial pressure in the reactor in Case 2-3 is lower than in Case 1-3. The comparison of the pressures in the reactor of Case 1-3 and Case 2-1 can be found in Figure 3-19. The difference of the pressures in the reactor is about 12 mbar. But the equilibrium pressure difference for water between 15°C (17.7 mbar) and 10°C (12.2 mbar) is theoretically about 5.5 mbar. That means the air partial pressure in Case 1-3 is about 6.5 mbar higher than it is in Case 2-3. The influence of the air is higher than the influence of the temperature for evaporation in this experiment. Hence the air in the system is, again, one of the most important problems for the seasonal storage systems by absorption.

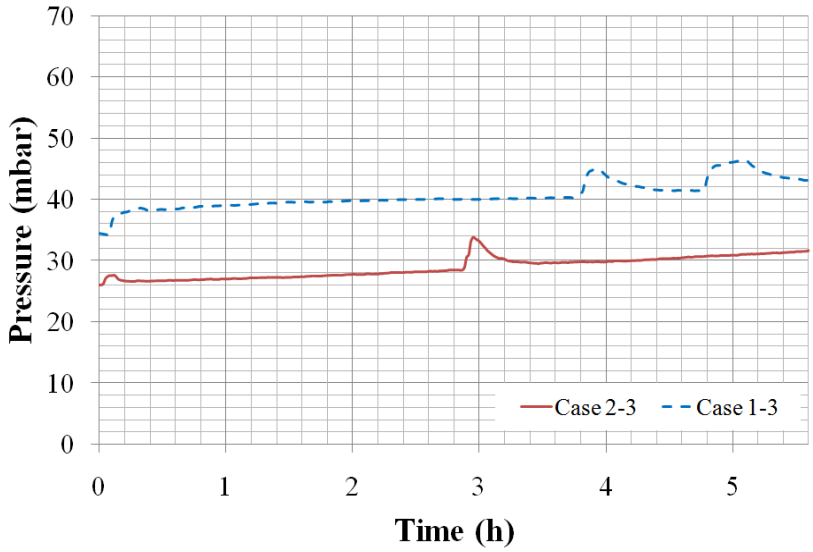

Figure 3-19 Comparison of the pressures in the reactor during Case 1-3 and Case 2-1

3.4.2.4 Case S-1

As the vacuum problem in the prototype cannot be solved easily, in order to decrease the influence of the air in the reactor, a Case S-1 is carried out. In Case S-1, $T_{i,ex,e}$ is increased to about 40°C. The flow rate of the water in the heat exchanger of the evaporator is also increased from 200 kg/h to 1000 kg/h to make sure that the power for evaporation is not decreased by the water flow on this side of the heat exchanger. The $T_{i,ex,a}$ is 30°C. The water pressure equilibrium at 40°C is 73.6 mbar. The range of the pressure in the reactor in Case S-1 is from 40.5 to 87.5 mbar (Figure 3-20). The pressure of the reactor is lower than the water equilibrium pressure at 40°C. This is mainly because the water in the evaporator cannot be heated as the same temperature as the water in the heat exchanger. But it is sure that for this case, the air partial pressure is decreased compared to the previous experiments.

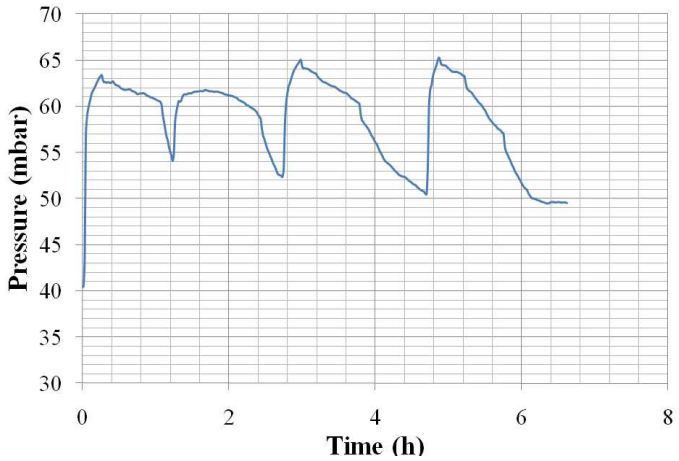

Figure 3-20 The pressure in the reactor of Case S-1

The power of the heat exchanger in the absorber ($\dot{Q}_a$) and in the evaporator ($\dot{Q}_e$) is shown in Figure 3-21. The power is between 80 W and 560 W for absorption and is between 0 W and 1080 W for evaporation. The power is much higher than for Case 1-3, Case 1-4 and Case 2-3.

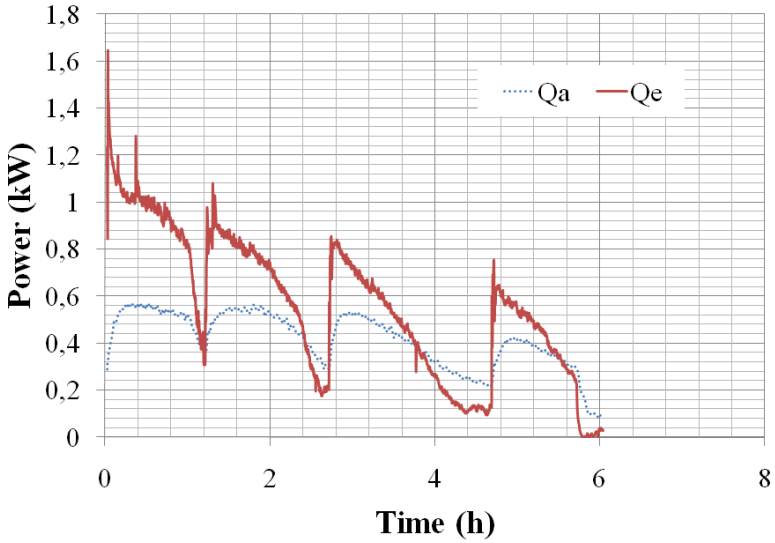

Figure 3-21 The evolutions of the powers of Case S-1

During Case S-1, 4.1 kg of water is absorbed by the solution. The mass fraction is decreased correspondingly from 0.417 kg $CaCl_2$/kg solution to 0.407 kg $CaCl_2$/kg solution. The energy released by the heat exchanger in the absorber Q_a is 2.5 kWh. The energy provided by the heat exchanger in the evaporator Q_e is 3.4 kWh. This case proves that the absorption process is possible. But for the real application of the seasonal storage systems, the energy source for evaporation cannot be as high as 40°C. Normally, the energy source is geothermal energy at about 10°C or even lower. The only solution to solve the air problem is to make sure that the system is really hermetically sealed.

3.5 Conclusion of the experimentation

A prototype has been built for verifying the feasibility of the seasonal storage system by absorption using the $CaCl_2/H_2O$ couple. According to the experimentation and the analysis of the results, several conclusions can be found here:

- The desorption phase is possible. During the desorption phase, water has been desorbed from the solution and stored in the water tank. The power obtained for the desorption (about 0.6-4 kW) and the condensation (about 0-3 kW) is sufficient for measuring and corresponds to the expected values.

- It has been verified that air in the system can decrease significantly the heat and mass transfer.

- When the water temperature at the inlet of the heat exchanger in the evaporator is between 10 and 15°C, the performance of the absorption phase is poor. Although the water is absorbed by the solution, the power of absorption and the temperature increase for the water in the heat exchanger in the absorber are low because of leakage problems of the prototype.

- During the desorption phase, the temperature of the solution at the outlet of the generator is about 60°C, which is much higher than the environment temperature. Hence the energy loss of the tube and the solution tank is remarkable. As a result, the consumption of energy for desorption is increased. In order to decrease this disadvantage, the rich solution flowing from the generator to the solution tank can be used to preheat the poor solution from the solution tank to the generator. But the corresponding risk is that crystal will be formed, because of the decrease of temperature of the rich solution.

- The air in the reactor is the main problem for the low power obtained during absorption. The influence is more serious than in the desorption phase because the water equilibrium pressure in the reactor is much lower than in the desorption phase.

- In order to verify the feasibility of the absorption phase, the water temperature at the inlet of the heat exchanger in the evaporator has been tested at about 40°C. This case is carried out to decrease the influence of the air in the reactor, and present interesting results. However, these temperature conditions in the evaporator are not realistic for a real storage system. The power of absorption and the temperature increase of the water in the heat exchanger in the absorber are thus increased and sufficient for measuring.

References of Chapter 3

He Kuangguo. 2002. Simple chemical containers and equipment design manual: Version 2. Chemical industry press, Beijing, (in Chinese)

NACE International. 2002. Corrosion Survey Database (COR•SUR). http://www.knovel.com

Solvay Group. 2008. Product Data Sheet: Granular anhydrous calcium chloride >94% for technical uses. SPE - CC 05.02.16. http://www.solvaycaso.com/

Yang Shiming, Tao Wenquan. 1987. Heat transfer. Beijing: Higher Education Publishing Company, (In Chinese)

Chapter 4 – Dynamic simulation of the prototype with the $CaCl_2/H_2O$ couple

The experimentation has been carried out in order to verify the feasibility of the seasonal storage system by absorption in Chapter 3. The desorption and absorption phases are possible. But the power for the absorption phase is lower than expected. The experimental results are influenced by several factors such as the presence of air in the system (especially for the absorption phase), the precision of the sensors and some human factors during the operation. For a better understanding of the process, a dynamic simulation which does not present these problems is developed. The model and its simulation results are presented in this chapter.

4.1 Dynamic simulation model

The model for the simulation is developed according to the parameters used for the operation and control of the prototype and based on the $CaCl_2/H_2O$ couple.

The labels for the components in the model are defined in Table 4-1:

Table 4-1 Definition of the labels of the components in the model

Label	Component
1	Thermostat 2 during desorption
2	Generator
3	Condenser
4	Thermostat 1 during desorption
5	Solution tank
6	Water tank
7	Absorber
8	Thermostat 2 during absorption
9	Evaporator
10	Thermostat 1 during absorption

The characteristics of a component are defined as the follow principle:

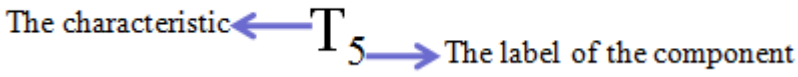

In which, 'T' is the characteristic. '5' is the label of the component. Following this principle, T_5 means the temperature of the solution in the solution tank. And correspongly, x_2 means the mass fraction of the solution in the generator for example.

The characteristics of the flows are defined following this principle:

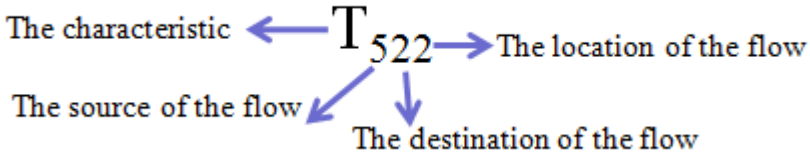

In which, 'T' is the characteristic. The first subscript '5' is the label of the component which is the source of the flow. The second subscript '2' is the label of the component which is the destination of the flow. The third subscript '2' is the label of the component which is the location of the flow (at the outlet of the source 5 or at the inlet of the destination 2). Following this principle, T_{522} means the temperature of the flow from the solution tank (source) to the generator (destination) at the inlet of the generator (location). And correspondingly, x_{525} means the mass fraction of the flow from the solution tank (source) to the generator

(destination) at the outlet of the solution tank (location). If the third subscript is neglected, it means that the characteristic is supposed to be uniform at any position.

If a characteristic is variable with time, there is a '(t)' at the end of the characteristic. For example, $\dot{m}_{522}(t)$ means that the flow rate of the flow from the solution tank to the generator at the inlet of the generator is variable with time.

The hypothesis of the simulation can be found as follows:

- The water in the water tank and the reactor and the solution in the solution tank and the reactor are always at the thermodynamic equilibrium state.
- The mass transfer kinetics is not the phenomenon limitation.
- The water in the water tank and the solution in the solution tank are homogeneous at any position. There is no temperature, pressure and mass fraction gradient in the same storage tank.
- Water is only evaporated or condensed on a heat exchanger. The water which is condensed or evaporated at other places, such as the walls of the reactor, is neglected.
- The influence of the presence of air for the heat and mass transfer is not considered in the simulation.
- The mass of the solution in the generator/absorber is supposed constant. This means that the solution which comes from the solution tank to the generator/absorber is immediately and totally transferred to the solution tank after the desorption/absorption.

4.1.1 Model for the desorption phase

The scheme during the desorption phase is shown in Figure 4-1. The model includes the solution tank, the water tank, the condenser, the generator and two thermostats.

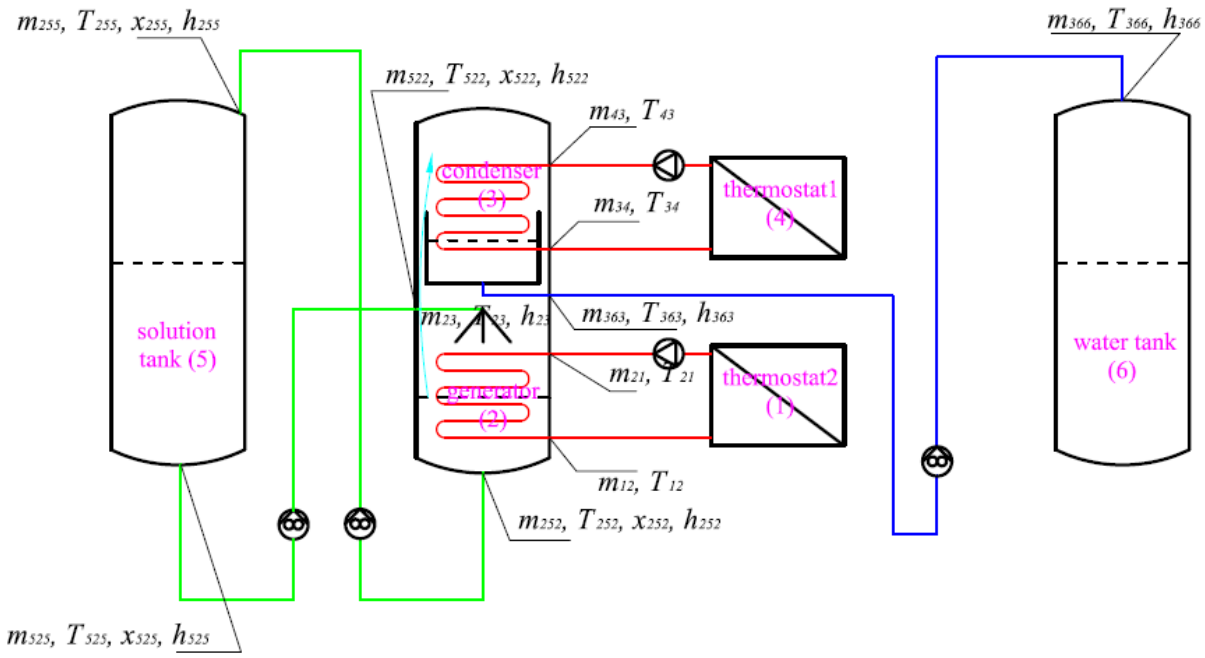

Figure 4-1 Simulation scheme of the desorption phase

- In the generator, the solution which comes from the solution tank ($\dot{m}_{522}(t)$) is heated by the energy which comes from the thermostat 2. The water vapor ($\dot{m}_{23}(t)$) which is evaporated from the solution is transferred to the condenser. The solution after desorption $\dot{m}_{252}(t)$ flows back to the solution tank. The mass of solution in the generator is $m_2(t)$. The mass balance in the generator can be found as Eq.4-1.

$$\frac{dm_2(t)}{dt} = \dot{m}_{522}(t) - \dot{m}_{252}(t) - \dot{m}_{23}(t) \qquad \text{Eq.4-1}$$

As the hypothesis that the mass of the solution in the generator/absorber is supposed constant, the $dm_2(t)/dt$ is zero.

The balance for $CaCl_2$ in the generator can be found as Eq.4-2.

$$\frac{dm_2(t)x_2(t)}{dt} = \dot{m}_{522}(t)x_{522}(t) - \dot{m}_{252}(t)x_{252}(t) \qquad \text{Eq.4-2}$$

The energy balance in the generator is as follows:

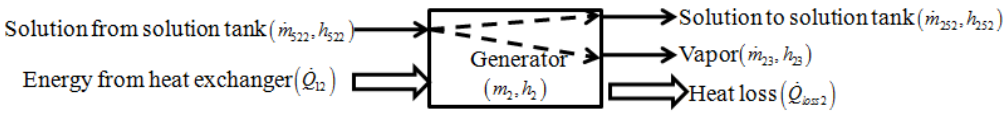

$$\frac{dm_2(t)h_2(t)}{dt} = \dot{Q}_{12}(t) + \dot{m}_{522}(t)h_{522}(t) - \dot{m}_{23}(t)h_{23}(t) - \dot{m}_{252}(t)h_{252}(t) - \dot{Q}_{loss2}(t) \quad \text{Eq.4-3}$$

As the hypothesis that the mass of the solution in the generator/absorber is supposed constant, the $dm_2(t)h_2(t)/dt$ is zero.

The power for desorption which is provided by the heat exchanger in the generator $\dot{Q}_{12}(t)$ can be calculated by the energy balance of the water in the heat exchanger:

$$\dot{Q}_{12}(t) = \dot{m}_{12}\left(h_{12}(t) - h_{21}(t)\right) \quad \text{Eq.4-4}$$

$\dot{Q}_{12}(t)$ can also be calculated by the heat transfer performance of the heat exchanger:

$$\dot{Q}_{12}(t) = K_{ex2}s_{ex2}\left(\left(T_{21}\text{-}T_{252}\right)\text{-}\left(T_{12}\text{-}T_{252}\right)\right)/\mathrm{Ln}\left(\left(T_{21}\text{-}T_{252}\right)/\left(T_{12}\text{-}T_{252}\right)\right) \quad \text{Eq.4-5}$$

In which, K_{ex2} is the heat transfer coefficient of the heat exchanger in the generator, s_{ex2} is the surface of the heat exchanger in the generator.

The enthalpy of the solution can be calculated as follows (see Appendix 4):

$$h(t) = f\left(T(t), x(t)\right) \quad \text{Eq.4-6}$$

The enthalpy of the water vapor can be calculated as follows (see Appendix 5):

$$h(t) = f\left(T(t)\right) \quad \text{Eq.4-7}$$

The power of the heat loss of the generator $\dot{Q}_{loss2}$ can be calculated as follows:

$$\dot{Q}_{loss2} = K_2 \cdot s_2 \cdot (T_{252}(t) - T_{atm}(t)) \quad \text{Eq.4-8}$$

In which, K_2 is the heat transfer coefficient of the wall of the generator, s_2 is the surface area of the wall of the generator.

The equilibrium in the generator can be calculated as: (see Appendix 2).

$$P_{23}(t) = f\left(T_{23}(t)\right) = P_2(t) = f\left(T_{252}(t), x_{252}(t)\right) \quad \text{Eq.4-9}$$

- In the condenser, the water vapor which comes from the generator ($\dot{m}_{23}(t)$) is condensed, the liquid water $\dot{m}_{363}(t)$ is transferred to the water tank. The mass of the water in the condenser is $m_3(t)$. The mass balance in the condenser can be found as Eq.4-10.

$$\frac{dm_3(t)}{dt} = \dot{m}_{23}(t) - \dot{m}_{363}(t) \quad \text{Eq.4-10}$$

The energy balance in the condenser can be found as follows:

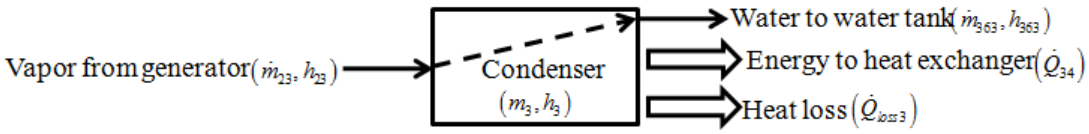

$$\frac{dm_3(t)h_3(t)}{dt} = \dot{m}_{23}(t)h_{23}(t) - \dot{m}_{363}(t)h_{363} - \dot{Q}_{34}(t) - \dot{Q}_{loss3}(t) \qquad \text{Eq.4-11}$$

The power for condensation which is provided by the heat exchanger in the condenser $\dot{Q}_{34}(t)$ can be calculated by the energy balance of the water in the heat exchanger:

$$\dot{Q}_{34}(t) = \dot{m}_{43}\left(h_{34}(t) - h_{43}(t)\right) \qquad \text{Eq.4-12}$$

$\dot{Q}_{34}(t)$ can also be calculated by the heat transfer performance of the heat exchanger:

$$\dot{Q}_{34}(t) = K_{ex3}s_{ex3}\left(\left(T_{363}\text{-}T_{43}\right)\text{-}\left(T_{363}\text{-}T_{34}\right)\right)/\mathrm{Ln}\left(\left(T_{363}\text{-}T_{43}\right)/\left(T_{363}\text{-}T_{34}\right)\right) \qquad \text{Eq.4-13}$$

In which, K_{ex3} is the heat transfer coefficient of the heat exchanger in the condenser, s_{ex3} is the surface of the heat exchanger in the condenser.

The power of the heat loss of the condenser $\dot{Q}_{loss3}$ can be calculated as follows:

$$\dot{Q}_{loss3} = K_3 \cdot s_3 \cdot (T_{363}(t) - T_{atm}(t)) \qquad \text{Eq.4-14}$$

In which, K_3 is the heat transfer coefficient of the wall of the condenser, s_3 is the surface area of the wall of the condenser.

The liquid-vapor equilibrium in the condenser can be calculated as (see Appendix 3):

$$P_{23}(t) = f\left(T_{23}(t)\right) = P_3(t) = f\left(T_3(t)\right) = P_2(t) = f\left(T_2(t), x_2(t)\right) \qquad \text{Eq.4-15}$$

- In the solution tank, the solution $\dot{m}_{525}(t)$ is transferred to the generator and the solution from the generator $\dot{m}_{255}(t)$ flows back into the solution tank. The mass balance is calculated by Eq.4-16.

$$\frac{dm_{5sol}(t)}{dt} + \frac{dm_{5cry}(t)}{dt} = \dot{m}_{255}(t) - \dot{m}_{525}(t) \qquad \text{Eq.4-16}$$

In which, $m_{5sol}(t)$ is the solution and $m_{5cry}(t)$ is the crystal. The appearance of the crystal is decided depending on the solubility of the solution at its temperature. The solubility of the solution can be found in Appendix 1.

The balance for $CaCl_2$ in the solution tank can be found as Eq.4-17.

$$\frac{dm_{5sol}(t)x_{5sol}(t)}{dt}+\frac{dm_{5cry}(t)x_{5cry}(t)}{dt}=\dot{m}_{255}(t)x_{255}(t)-\dot{m}_{525}(t)x_{525}(t) \quad \text{Eq.4-17}$$

In which, $x_{5cry}(t)$ is the mass fraction of $CaCl_2$ in the crystal. This mass fraction is linked to the form of the crystal (the water of hydration in the crystal). The crystal of $CaCl_2$ is at the form of $CaCl_2 \cdot 6H_20$ when the temperature of the crystal in the solution tank is lower than 29°C (Appendix 1). The corresponding mass fraction of $CaCl_2$ in the crystal is 50.7%.

The energy balance in the solution tank can be calculates as:

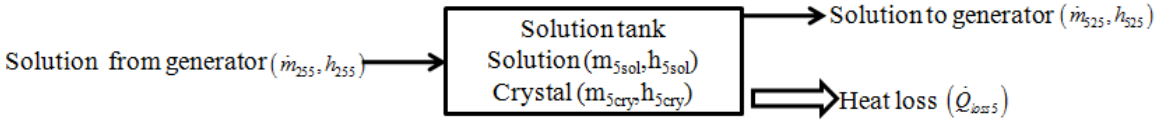

$$\frac{dm_{5sol}(t)h_{5sol}(t)}{dt}+\frac{dm_{5cry}(t)h_{5cry}(t)}{dt}=\dot{m}_{255}(t)h_{255}(t)-\dot{m}_{525}(t)h_{525}-\dot{Q}_{loss5}(t) \quad \text{Eq.4-18}$$

In which, the enthalpy of the solution $h(t)$ can be calculated by Eq.4-18, the enthalpy of the crystal $h_{cry}(t)$ can be calculated by Appendix 6.

The power of the heat loss of the solution tank $\dot{Q}_{loss5}(t)$ can be calculated as:

$$\dot{Q}_{loss5}(t)=K_5 \cdot s_5 \cdot (T_5(t)-T_{atm}(t)) \quad \text{Eq.4-19}$$

- In the water tank, the change of the water mass ($dm_6(t)/dt$) is decided by the flow rate of the water which comes from the condenser ($\dot{m}_{366}(t)$).

$$\frac{dm_6(t)}{dt}=\dot{m}_{366}(t) \quad \text{Eq.4-20}$$

The energy balance in the water tank is:

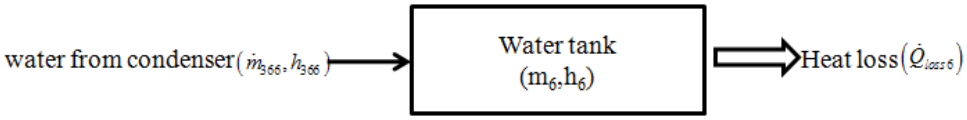

$$\frac{dm_6(t)h_6(t)}{dt}=\dot{m}_{366}(t)h_{366}(t)-\dot{Q}_{loss6}(t) \quad \text{Eq.4-21}$$

In which, $h(t)$ can be calculated byEq.4-19.

The power of the heat loss of the water tank $\dot{Q}_{loss6}(t)$ $dQ_{loss6}(t)/dt$ is calculated as:

$$\dot{Q}_{loss6}(t)=K_6 \cdot s_6 \cdot (T_6(t)-T_{atm}(t)) \quad \text{Eq.4-22}$$

- During the transfer in the tubes, the masses and mass fractions are constant:

$$\dot{m}_{522}(t) = \dot{m}_{525}(t) \quad \text{Eq.4-23}$$

$$\dot{m}_{252}(t) = \dot{m}_{255}(t) \quad \text{Eq.4-24}$$

$$x_{522}(t) = x_{525}(t) \quad \text{Eq.4-25}$$

$$x_{252}(t) = x_{255}(t) \quad \text{Eq.4-26}$$

$$\dot{m}_{363}(t) = \dot{m}_{366}(t) \quad \text{Eq.4-27}$$

The energy balance for the tube which is used for the transfer of solution from the solution tank to the generator (tube 52 for short) is:

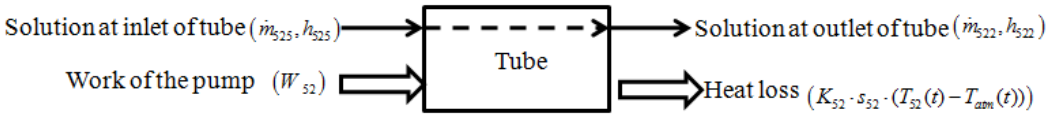

$$\dot{m}_{525}(t)h_{525}(t) + \frac{dW_{52}(t)}{dt} = \dot{m}_{522}(t)h_{522}(t) + K_{52} \cdot s_{52} \cdot (T_{52}(t) - T_{atm}(t)) \quad \text{Eq.4-28}$$

The power of pump at the tube 52 $W_{52}(t)$ is calculated as [Yao Y. 2003]:

$$\frac{dW_{52}(t)}{dt} = \left(\frac{64}{\mathrm{Re}} \cdot \frac{l_{52}}{2d_{52}} \cdot \left(\dot{m}_{525} / \left(\frac{1}{4}\pi \cdot d_{525}^2 \cdot \rho_{525}(t) \right) \right)^2 + (P_2 - P_5)/\rho_{525} + g\Delta H_{52} \right) \times \dot{m}_{525} \quad \text{Eq.4-29}$$

The energy balance for the tube which is used for the transfer of solution from the generator to the solution tank (tube 25 for short) is:

$$\dot{m}_{252}(t)h_{252}(t) + \dot{W}_{25}(t) = \dot{m}_{255}(t)h_{255}(t) + K_{25} \cdot s_{25} \cdot (T_{25}(t) - T_{atm}(t)) \quad \text{Eq.4-30}$$

The power of pump at tube 25 $\dot{W}_{25}(t)$ is calculated as:

$$\dot{W}_{25}(t) = \left(\frac{64}{\mathrm{Re}} \cdot \frac{l_{25}}{2d_{25}} \cdot \left(\dot{m}_{252} / \left(\frac{1}{4}\pi \cdot d_{252}^2 \cdot \rho_{252}(t) \right) \right)^2 + (P_5 - P_2)/\rho_{252} + g\Delta H_{25} \right) \times \dot{m}_{252} \quad \text{Eq.4-31}$$

The density of the solution is (Appendix 7):

$$\rho_{525}(t) = f\left(x_{525}(t), T_{525}(t)\right) \quad \text{Eq.4-32}$$

$$\rho_{252}(t) = f\left(x_{252}(t), T_{252}(t)\right) \quad \text{Eq.4-33}$$

For the tube which is used for the transfer of water from the condenser to the water tank (tube 36 for short):

$$\dot{m}_{366}(t)h_{366}(t)+K_{36}\cdot s_{36}\cdot(T_{36}(t)-T_{atm}(t))=\dot{m}_{363}(t)h_{363}(t)+\dot{W}_{36}(t) \qquad \text{Eq.4-34}$$

The power of the pump in the tube 36 $\dot{W}_{36}(t)$ is calculated as:

$$\dot{W}_{36}(t)=\left(\frac{64}{\mathrm{Re}}\cdot\frac{l_{36}}{2d_{36}}\cdot\left(\dot{m}_{363}/\left(\frac{1}{4}\pi\cdot d_{363}^2\cdot\rho_{363}(t)\right)\right)^2+(P_6-P_3)/\rho_{363}+g\Delta H_{36}\right)\times\dot{m}_{363} \qquad \text{Eq.4-35}$$

All heat transfer coefficients for the heat exchangers, tubes and tanks can be calculated as Eq.4-36.

$$\frac{1}{K_i}=\frac{1}{\alpha_i}+\frac{Ed_i}{\lambda d_m}+\frac{d_i}{\alpha_o d_o} \qquad \text{Eq.4-36}$$

For the heat exchangers, as the heat transfer at the outside of the tubes is a phase change heat transfer, the corresponding heat transfer resistance $\frac{d_i}{\alpha_o d_o}$ is small compared the others and is supposed to be negligible in the simulation. Hence only $\frac{1}{\alpha_i}+\frac{Ed_i}{\lambda d_m}$ is considered in the simulation. The heat transfer of the tubes is increased. For all the tanks, thermal insulation material is used to decrease the heat loss. The material is glass wool which has a small heat conductivity of $\lambda=0.033+0.00023\cdot \mathrm{T}_{(°C)}$. The thickness of the glass wool for all the tanks is 20 mm.

The heat transfer efficiency on the inside of the heat exchangers can be calculated as follows [Yang S. & Tao W. 1987]:

$$\alpha_i=0.012\frac{\lambda}{d_i}(\mathrm{Re}^{0.87}-280)\,\mathrm{Pr}^{0.4} \qquad (\mathrm{Re}\geq 2300) \qquad \text{Eq.4-37}$$

$$\alpha_i=1.86\frac{\lambda}{d_i}\left(\frac{\mathrm{Re}\,\mathrm{Pr}}{l/d}\right)^{1/3} \qquad (\mathrm{Re}\leq 2300) \qquad \text{Eq.4-38}$$

4.1.2 Model for absorption phase

The model at the absorption phase is shown in Figure 4-2.

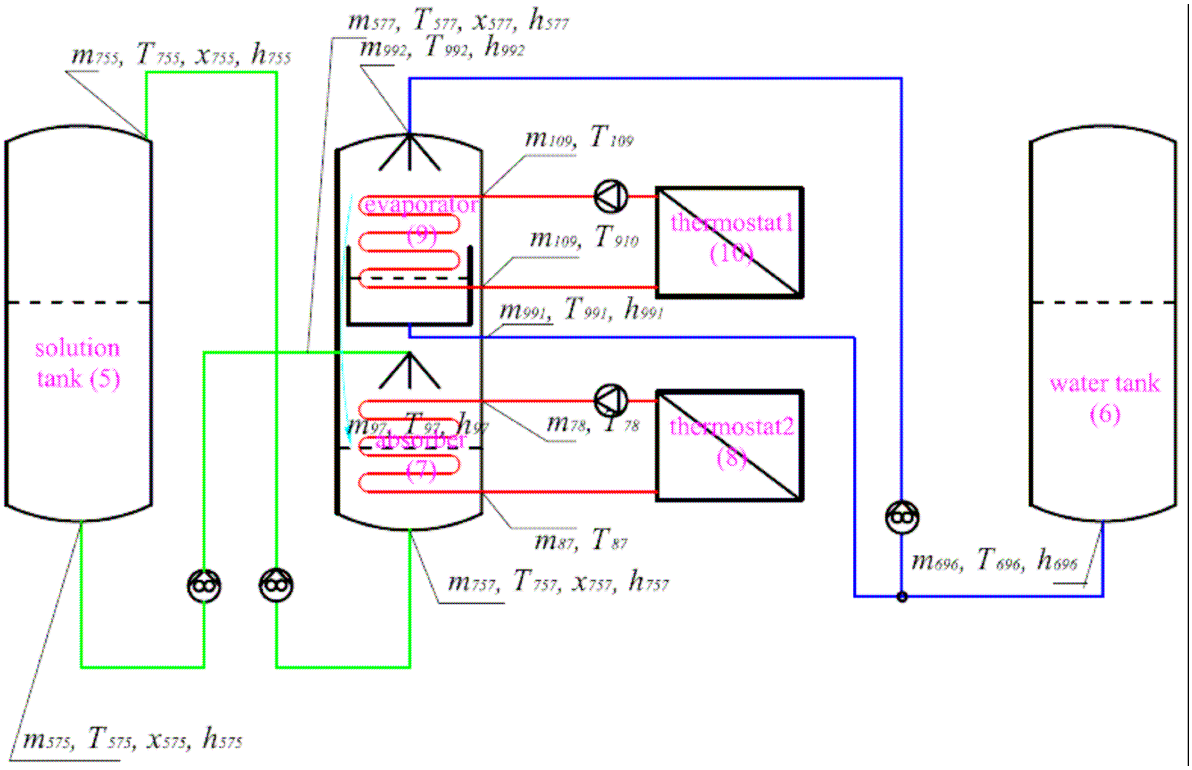

Figure 4-2 Simulation model of the absorption phase

- In the absorber, the water vapor which comes from the evaporator ($\dot{m}_{97}(t)$) is absorbed by the solution which comes from the solution tank ($\dot{m}_{577}(t)$). The solution after absorption ($\dot{m}_{757}(t)$) flows back to the solution tank. The mass of solution in the generator is $m_7(t)$. The mass balance in the absorber is:

$$\frac{dm_7(t)}{dt} = \dot{m}_{577}(t) + \dot{m}_{97}(t) - \dot{m}_{757}(t) = 0 \qquad \text{Eq.4-39}$$

In order to simplify the model, $m_7(t)$ is also supposed constant as in the desorption phase.

The balance for $CaCl_2$ in the absorber can be found as Eq.4-40.

$$\frac{dm_7(t)x_7(t)}{dt} = \dot{m}_{577}(t)x_{577}(t) - \dot{m}_{757}(t)x_{757}(t) \qquad \text{Eq.4-40}$$

The energy balance in the absorber is:

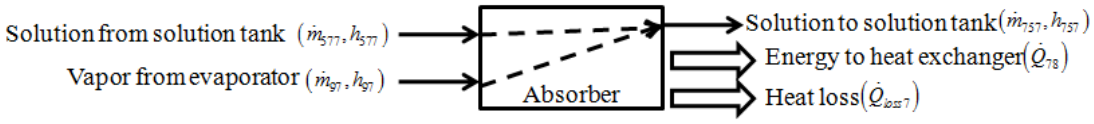

$$\frac{dm_7(t)h_7(t)}{dt} = \dot{m}_{577}(t)h_{577}(t) + \dot{m}_{97}(t)h_{97}(t) - \dot{m}_{757}(t)h_{757}(t) - \dot{Q}_{78}(t) - \dot{Q}_{loss7}(t) \quad \text{Eq.4-41}$$

The heat loss of the absorber $\dot{Q}_{loss7}(t)$ is calculated similarly to Eq.4-8.

The power of the heat of absorption which is released by the heat exchanger in the absorber $\dot{Q}_{78}(t)$ is calculated by the heat balance of the water in the heat exchanger similarly to Eq.4-4 and Eq.4-5.

- In the evaporator, the water $\dot{m}_{992}(t)$ is evaporated and the water vapor $\dot{m}_{97}(t)$ is transferred to the absorber. The water which is not evaporated is $\dot{m}_{991}(t)$. It will be circulated by the pump for the evaporation succeeding. The mass balance in the evaporator is:

$$\frac{dm_9(t)}{dt} = \dot{m}_{992}(t) - \dot{m}_{97}(t) - \dot{m}_{991}(t) \quad \text{Eq.4-42}$$

The energy balance in the evaporator is as follows:

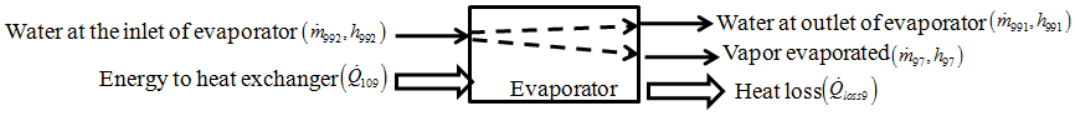

$$\frac{dm_9(t)h_9(t)}{dt} = \dot{Q}_{109}(t) + \dot{m}_{992}(t)h_{992}(t) - \dot{m}_{991}(t)h_{991} - \dot{m}_{97}(t)h_{97} - \dot{Q}_{loss9}(t) \quad \text{Eq.4-43}$$

The power of the heat loss of the evaporator $\dot{Q}_{loss9}(t)$ $Q_{loss9}(t)$ is calculated similarly as Eq.4-8.

The power used for evaporation which is provided by the heat exchanger in the evaporator $\dot{Q}_{109}(t)$ is calculated similarly to Eq4-12 and Eq.4-13.

The liquid-vapor equilibrium in the evaporator and absorber can be calculated following Appendix 3.

$$P_{97}(t) = f\left(T_{97}(t)\right) = f\left(T_{991}(t)\right) = P_7(t) = f\left(T_7(t), x_7(t)\right) \quad \text{Eq.4-44}$$

- In the solution tank, the solution flow $\dot{m}_{575}(t)$ is transferred to the absorber and the solution from the absorber $\dot{m}_{755}(t)$ flows into the solution tank. The mass balance and the energy balance are calculated similarly as in the desorption phase.

- In the water tank, the water is transferred from the water tank to the evaporator ($\dot{m}_{696}(t)$), the mass balance of the water tank is as:

$$\frac{dm_6(t)}{dt} = -\dot{m}_{696}(t) \quad \text{Eq.4-45}$$

$\dot{m}_{696}(t)$ is discontinuous. It is decided by the water level in the evaporator as discussed in chapter 3.

- During the transfer in the tubes:

$$\dot{m}_{577}(t) = \dot{m}_{575}(t) \quad \text{Eq.4-46}$$

$$x_{577}(t) = x_{575}(t) \quad \text{Eq.4-47}$$

$$\dot{m}_{757}(t) = \dot{m}_{755}(t) \quad \text{Eq.4-48}$$

$$x_{757}(t) = x_{755}(t) \quad \text{Eq.4-49}$$

$$\dot{m}_{992}(t) = \dot{m}_{696}(t) + \dot{m}_{991}(t) \quad \text{Eq.4-50}$$

The energy balance of the tubes is calculated similarly to the desorption phase.

4.2 Simulation results and comparison with the experimentation

The dynamic simulation is carried out corresponding to the operating conditions of case 1 (water temperature at the inlet of the heat exchanger in the generator at 80°C, water temperature at the inlet of the heat exchanger in the evaporator at 15°C) and case 2 (water temperature at the inlet of the heat exchanger in the generator at 70°C, water temperature at the inlet of the heat exchanger in the evaporator at 10°C) in Table 3-6 (Chapter 3). The initial mass, mass fraction and temperature of solution and water correspond to the experimental conditions in Table 3-8. The simulations are stopped when the masses of the solution in the solution tank and the water in the water tank after the desorption or absorption phases are the same as it is in the experimentation. As the influence of air in the system and the mass transfer kinetics are not take in account in the simulation, and also the exchangers is not exactly simulated, the powers of the desorption and absorption phases are different between the simulation and the experiment. Hence their duration is different.

4.2.1 Desorption cases

The simulations for desorption case 1-1, case 1-2 (water temperature at the inlet of the heat exchanger in the generator at 80°C, water temperature at the inlet of the heat exchanger in the evaporator at 15°C), case 2-1 and case 2-2 (water temperature at the inlet of the heat exchanger in the generator at 70°C, water temperature at the inlet of the heat exchanger in the evaporator at 10°C) are carried out and compared with the experimental results.

4.2.1.1 Case 1-1 (water temperature at the inlet of the heat exchanger in the generator at 80°C, water temperature at the inlet of the heat exchanger in the evaporator at 15°C)

For Case 1-1, the simulation results are as follows.

The evolution of the temperatures is shown in Figure 4-3:

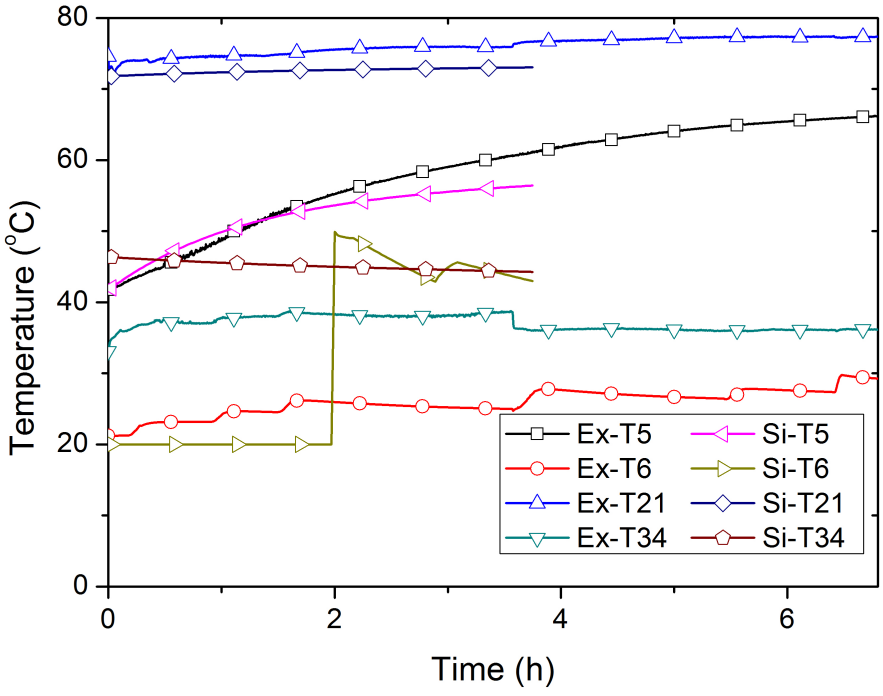

Figure 4-3 Evolution of temperatures of desorption Case 1-1, experiment (Ex) and simulation (Si)

According to the simulation, the solution temperature in the solution tank (Si-T_5) increases continuously during desorption because the rich solution after desorption at high temperature flows back to the solution tank. At the beginning, there is no water in the water tank. The water temperature in the water tank (Si-T_6) actually represents the air temperature in the water tank. It is the same as the ambient temperature (20°C). At about 2 h when the water is transferred from the condenser to the water tank, the water temperature in the water tank (Si-T_6) increases rapidly to about 50°C, which is about the same temperature as the water in the condenser. . After that, Si-T_6 decreases because of the heat loss from the water tank to the environment. The decrease is much rapidly than in the experimentation because the water temperature in the simulation (40-50°C) is much higher than it is in the experimentation (20-25°C). The evolution of the temperatures of the solution tank is the same between the experiment and the simulation. The water temperature at the outlet of the heat exchanger in condenser in the simulation (Si-T_{34}) is about 8°C higher than in the experiment (Ex-T_{34}), increases of and the water temperature at the outlet of the heat exchanger in generator in the simulation (Si-T_{21}) is about 2°C lower than it is in the experimentation (Ex-T_{21}) . The difference is mainly because the heat and mass transfer performance in the simulation is better than in the experiment (due to the presence of air during the experiment, as analyzed in Chapter 3).

Due to the increase of the Si-T_5, the temperature difference for the heat exchanger in the generator decreases. The power of the heat exchanger in the generator thus decreases (Si-$\dot{Q}_{12}$ in Figure 4-4). Hence the water temperature at the outlet of the heat exchanger in the generator (Si-T_{21}) increases continuously. As the power of the heat exchanger in the generator decreases, the quantity of water vapor which is desorbed from the solution is decreased. The power of the heat exchanger in the condenser decreases (Si-$\dot{Q}_{43}$ in Figure 4-4). Hence the water temperature at the outlet of the heat exchanger in the condenser (Si-T_{34}) decreases with time.

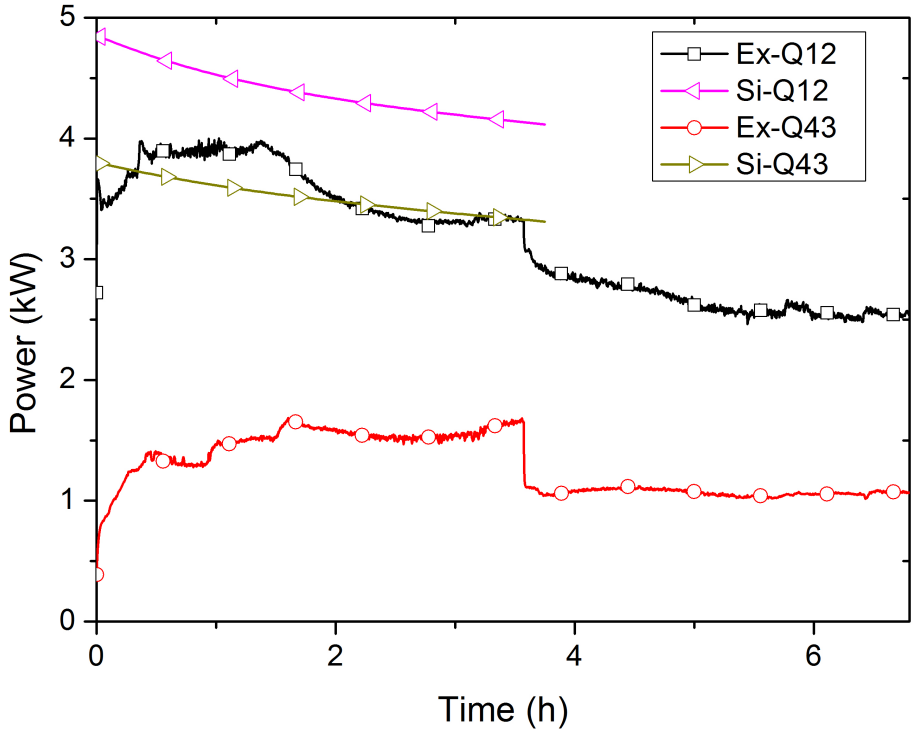

Figure 4-4 Evolution of powers of desorption Case 1-1, experiment (Ex) and simulation (Si)

Compared with the powers of the heat exchangers in the experimentation, the powers in simulation are higher. This is mainly because the performance of the heat exchanger is decreased by the presence of air in the reactor during the experiments. As the powers in the simulations are higher than they are in the experiments, the time consumption is decreased from 7.6 h in the experiment to 3.8 h in the simulation. The water vapor which is condensed at the inner surface of the reactor during the experiments is also not considered in the simulation. All the water vapor is condensed in the condenser in the model. As a result, the difference between the $\dot{Q}_{12}$ and $\dot{Q}_{43}$ is decreased in the simulation.

The evolutions of the pressures of the solution tank, the reactor and the water tank are shown in Figure 4-5:

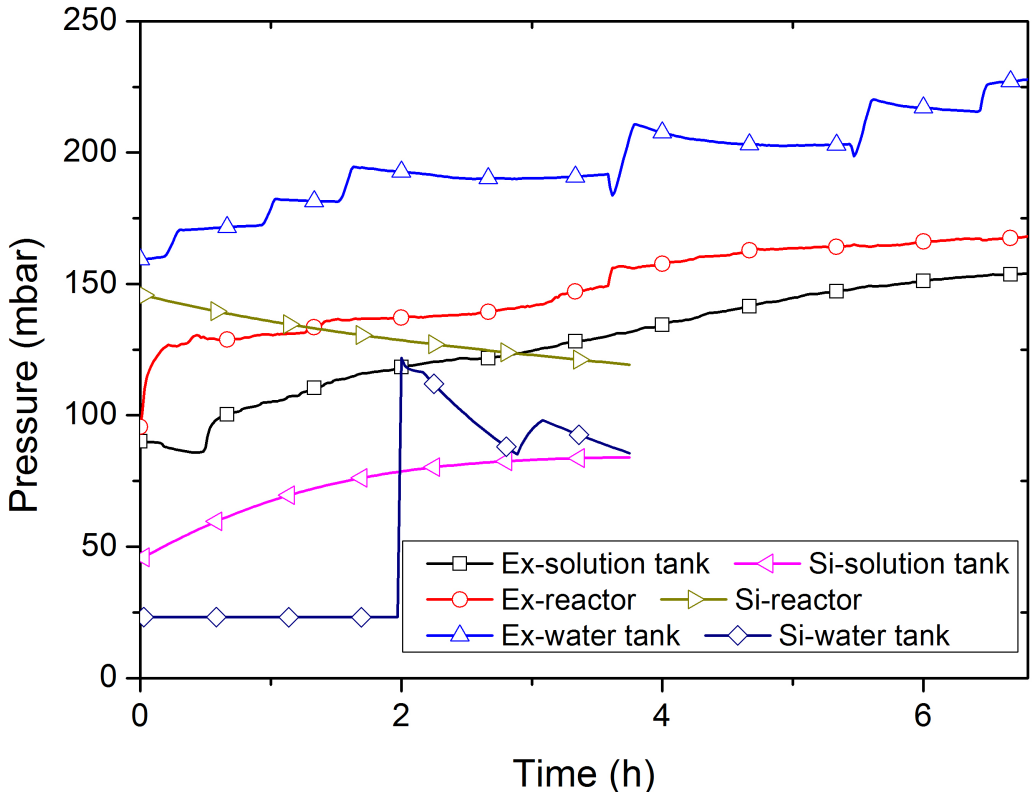

Figure 4-5 Evolution of pressures of desorption Case 1-1, experiment (Ex) and simulation (Si)

Compared with the experimental results, the pressure in the simulation is the equilibrium pressure without the influence of the air. During the desorption, the temperature of the solution tank increases, which should increase the pressure of the solution tank. But the mass fraction of the solution increases during the desorption, which should decrease the pressure of the solution tank. According to the simulation results in Figure 4-5, the pressures increase during the desorption phase, which means that the temperature is the main influence factor for the pressure of the solution tank. The pressure of the water tank of the simulation (Si-Water tank) changes with the water temperature in the water tank (Si-T_6 in Figure 4-3). The pressure of the reactor (Si-Reactor) depends on the temperature of the water in the condenser. As the quantity of water vapor which is desorbed in the generator decreases with time, the temperature of water in the condenser decreases. Thus the pressure in the reactor in the simulation decreases with time.

The overall performance comparison between the experimentation and simulation of Case 1-1 is shown in Table 4-2:

Table 4-2 Performance comparison of the experimentation and simulation (desorption Case 1-1)

Parameters	Unit	Case 1-1 Ex	Case 1-1 Si
m_6 Start	kg	0	0
m_6 End	kg	19.5	19.5
m_5 Start	kg	207.5	207.5
m_5 End	kg	188	188
x_5 Start	kg $CaCl_2$/kg solution	0.345	0.345
x_5 End	kg $CaCl_2$/kg solution	0.381	0.381
T_6 Start	°C	21.2	21.2
T_6 End	°C	30.3	43
T_5 Start	°C	41.7	41.7
T_5 End	°C	65.8	56.4
P_3 minimum	mbar	92	119
P_3 maximum	mbar	168	145
T_{21} minimum	°C	72.3	71.8
T_{21} maximum	°C	77.6	73
T_{12} minimum	°C	78.4	80
T_{12} maximum	°C	82	80
T_{34} minimum	°C	33.1	44.3
T_{34} maximum	°C	44.4	46.4
T_{43} minimum	°C	31.4	30
T_{43} maximum	°C	32.1	30
$\dot{Q}_{12}$ minimum	kW	1.81	4.1
$\dot{Q}_{12}$ maximum	kW	4	4.8
$\dot{Q}_{43}$ minimum	kW	0.25	3.3
$\dot{Q}_{43}$ maximum	kW	3	3.8
Q_{12}	kWh	23.5	16.5
Q_{43}	kWh	9.9	13.2
Time	h	6.8	3.8

According to the simulation of Case 1-1, 19.5 kg of water is desorbed from the solution. The mass of the solution is decreased from 207.5 kg to 188 kg. The mass fraction is increased correspondingly from 0.345 kg $CaCl_2$/kg solution to 0.381 kg $CaCl_2$/kg solution. The energy provided by the heat exchanger in the generator for desorption Q_{12} is 16.5 kWh. The difference of energy consumption for desorption (Q_{12}) between the experiment and the simulation is due to the water vapor which is condensed at the inner surface of the reactor and flows back to the generator in the experiment. The water which flows back to the generator dilutes the solution in the generator. In order to redesorb this part of water in the solution, the consummation of energy for desorption is increased. The energy rejected by the heat exchanger in the condenser for condensation Q_{43} is 13.2 kWh, which is higher than it is in the experiment. This is mainly because the difference of the quantity of heat loss of the condenser to the environment. The heat loss of the condenser can condense the vapor to water in the condenser. As the time consummation of the experimentation (6.8) is about two times longer

than it is in the simulation (3.6h), the heat loss in the experimentation could be higher than in the simulation. As a result, the energy which is rejected to the heat exchanger in the condenser in the simulation is decreased. The powers of the heat exchangers ($\dot{Q}_{12}$ and $\dot{Q}_{43}$) in simulation are larger than they are in experiment. The decrease of the power in the experiment is mainly due to the presence of air in the reactor which is not taken into account in the simulation. Due to the difference power, the time for desorption in the simulation is decreased compared to the experimental time (7.6 h to 3.8 h). The vacuum in the reactor is extremely important for the functioning of the process.

4.2.1.2 Other cases

The overall performance comparison between the experimentation and simulation of Case 1-2, 2-1 and 2-2 is shown in Table 4-3:

Table 4-3 Performance comparison of the experimentation and simulation during desorption

Parameters	Unit	Case 1-2 Ex	Case 1-2 Si	Case 2-1 Ex	Case 2-1 Si	Case 2-2 Ex	Case 2-2 Si
m_6 Start	kg	19.5	19.5	27.1	27.1	28.7	28.7
m_6 End	kg	35.5	35.5	28.4	28.4	40.5	40.5
m_5 Start	kg	188	188	180.4	180.4	179.1	179.1
m_5 End	kg	172	172	179.1	179.1	167	167
x_5 Start	kg $CaCl_2$/kg solution	0.381	0.381	0.397	0.397	0.4	0.4
x_5 End	kg $CaCl_2$/kg solution	0.417	0.417	0.4	0.4	0.428	0.428
T_6 Start	°C	25.1	25.1	19.6	19.6	26	26
T_6 End	°C	29.1	31.2	20.3	21.3	25.9	27.2
T_5 Start	°C	48.3	48.3	20.4	20.4	38.5	38.5
T_5 End	°C	64.6	58.5	55.7	29	57	53.9
P_3 minimum	mbar	60	55.7	68	10.2	60	29.7
P_3 maximum	mbar	157	78.4	125	16.6	85	58.2
T_{21} minimum	°C	72.9	72.4	64.9	63.1	66	64
T_{21} maximum	°C	80.6	73.6	69.3	63.5	68.8	65.4
T_{12} minimum	°C	80.2	80	66.7	70	71.4	70
T_{12} maximum	°C	82.7	80	72.2	70	72.3	70
T_{34} minimum	°C	33	43.1	28.7	41.1	32.7	39.2
T_{34} maximum	°C	39.7	44.8	33.7	41.3	36.4	40.8
T_{43} minimum	°C	31.5	30	28.6	30	31.3	30
T_{43} maximum	°C	33.4	30	31.9	30	32.2	30
$\dot{Q}_{12}$ minimum	kW	0.65	3.8	0.96	4.1	1.16	2.7
$\dot{Q}_{12}$ maximum	kW	4.4	4.5	2.7	4.8	3.34	3.5
$\dot{Q}_{43}$ minimum	kW	0	3	0.04	2.6	0.04	2.1
$\dot{Q}_{43}$ maximum	kW	1.85	3.4	0.56	3.5	1.14	2.5
Q_{12}	kWh	26.4	13.9	10.3	1.4	18.2	10.4
Q_{43}	kWh	12	11	1.2	0.9	6.7	8
Time	h	8.5	3.42	4.3	0.36	7.3	3.47

According to the simulation results and comparison with the experimental results, several conclusions can be found as follows:

- The results of the experimentation can not completely prove the model of the simulation as the leak of air in the experimentation and the limitation of the model (the hypotheses in the simulation).

- The powers of the heat exchanger in the generator and the condenser in the simulation are bigger than in the experimentations. The main reason is the presence of air in the reactor during the experiments which decreases the heat and mass transfer.
- As the power of the heat exchangers in the simulation is higher than it is in the experiment, the time consumption for the desorption phase decreases of more than 50%.
- As the time consumption for the desorption phase is decreased in the simulation compared with the experimentation, the accumulated heat for the solution in the solution tank by the circulation of the solution between the solution tank and the generator is decreased. The temperature of solution in the solution tank at the end of the desorption in the simulation is lower than it is in the experiment.
- The heat need for desorption in the simulation is lower than it is in the experimentation because the heat for solution is decreased and the water vapor which is condensed at the inner surface of the reactor and flows back to the solution in the generator is neglected in the simulation.
- According to simulation results, if the leak of air can be avoided in the experimentation, the performance of the experimentation could be improved.

4.2.2 Absorption cases

The simulations for absorption cases of Case 1-3, 1-4 and 2-3 are carried out at the same operating conditions as in the experiment and compared with the experimental results.

4.2.2.1 Case 1-3

For the Case 1-3, the simulation results are as follows.

The evolution of the temperatures is shown in Figure 4-6:

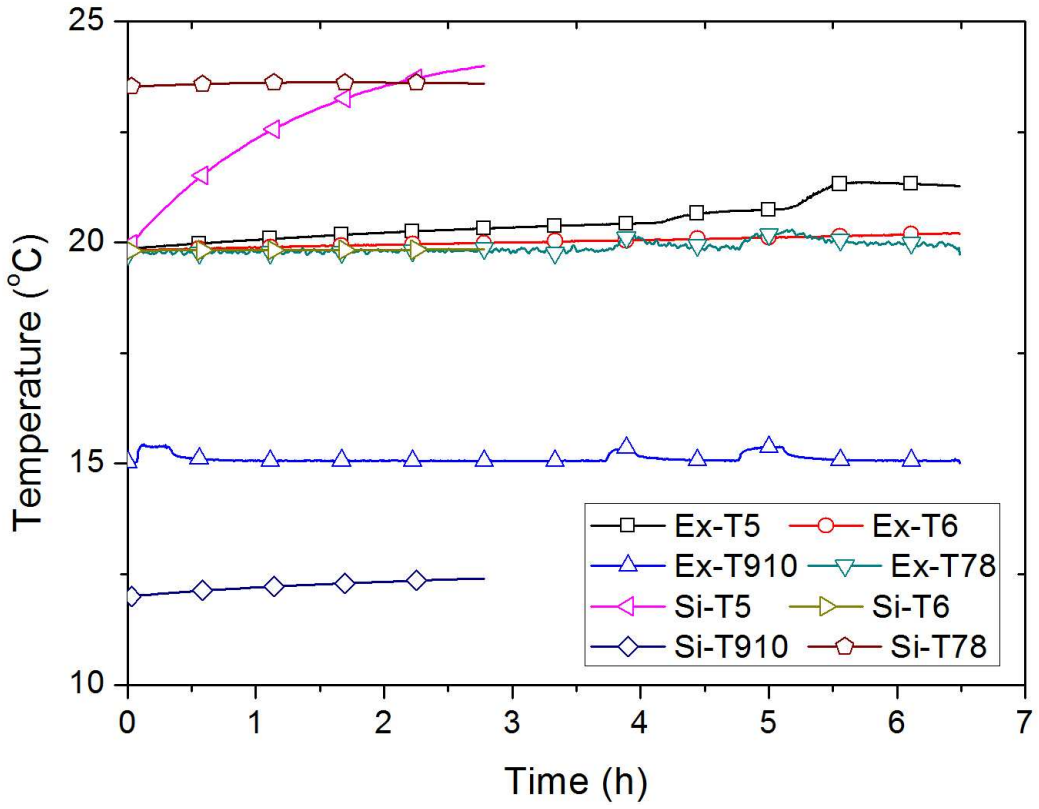

Figure 4-6 Evolution of temperatures of absorption Case 1-3, experiment (Ex) and simulation (Si)

According to the simulation, the temperature of solution in the solution tank (Si-T_5) increases continuously with absorption because the solution which is circulated between the solution tank and the absorber is heated by the absorption heat. The temperature of water in the water tank (Si-T_6) only depends on the heat transfer between the environment and the water tank. As the simulation temperature of environment is supposed constant at 20°C, and the initial temperature of water in the water tank is about 19.8°C, the temperature Si-T_6 is almost constant.

In the simulation, due to the increase of the solution temperature in the solution tank (Si-T_5) and the decrease of the mass fraction of the solution in the solution tank during the absorption, the equilibrium pressure of the rich solution which is transferred from the solution tank to the absorber is increased. The equilibrium pressure of water in the evaporator should be increased in order to meet the pressure balance for the absorption. Hence, the water temperature at the outlet of the heat exchanger in the evaporator (Si-T_{910}) increases continuously. As the temperature difference of the heat exchanger in the absorber is decreased, the power of the heat exchanger in the evaporator decreases (Si-$\dot{Q}_{109}$ in Figure 4-7). With the increase of the Si-T_5, the temperature difference of the heat exchanger in the absorber is increased. But the absorption ability of the solution is decreased as its increase of the temperature and decrease of the mass fraction during absorption. Hence the power of the heat exchanger in the absorber is about constant (Si-$\dot{Q}_{78}$ in Figure 4-7). Correspondingly, the water temperature at the outlet of the heat exchanger in the absorber (Si-T_{78}) is about constant.

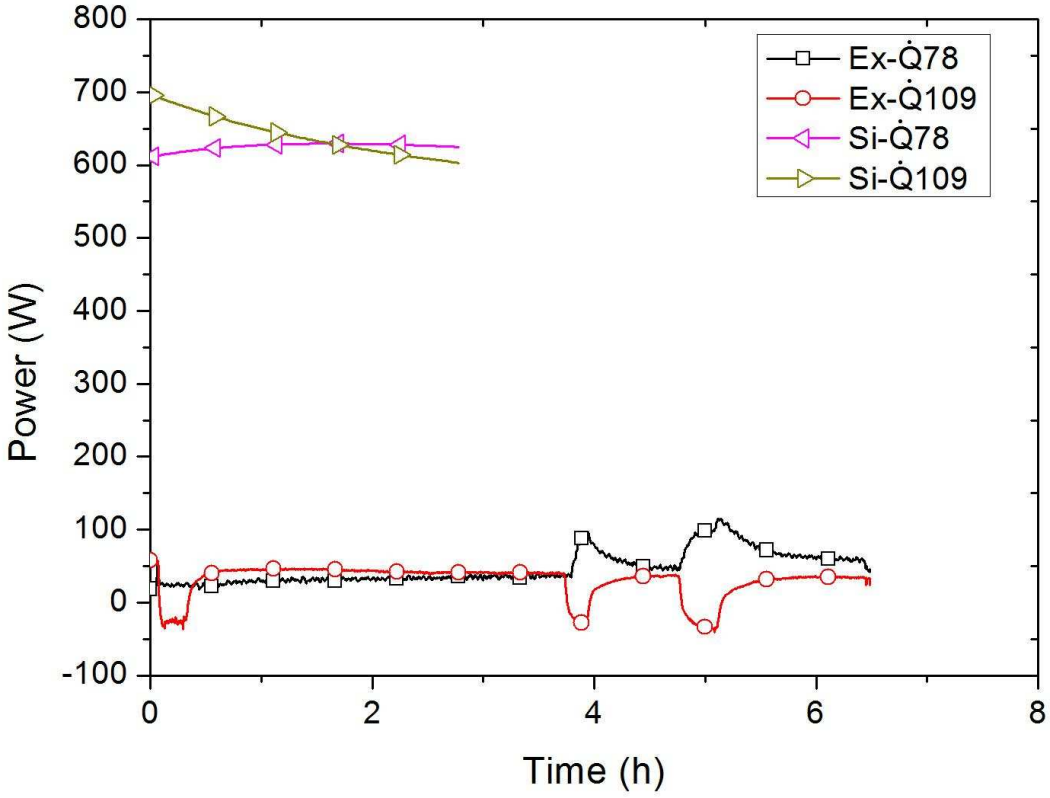

Figure 4-7 Evolution of powers of absorption Case 1-3, experiment (Ex) and simulation (Si)

Compared with the power of the heat exchangers in the experimentation, the power of the heat exchanger in simulation is much higher. This is mainly because the performance of the heat exchanger is decreased by the presence of air in the reactor during the experiments. In the experiment, when the water is transferred to the evaporator, the power of the heat exchanger in the evaporator is decreased because the temperature of water is higher than the water temperature at the inlet of the heat exchanger in the evaporator. But in the simulation, without the influence of air, the power of evaporation and absorption is enhanced. Compared with the energy provided by the heat exchanger in the absorber, the sensible heat of the water which comes from the water tank is much smaller. Hence the influence of the water coming from the water tank on the power of absorption and evaporation is low in the simulation results.

The evolutions of the pressures of the solution tank, the water tank and the reactor are shown in Figure 4-8:

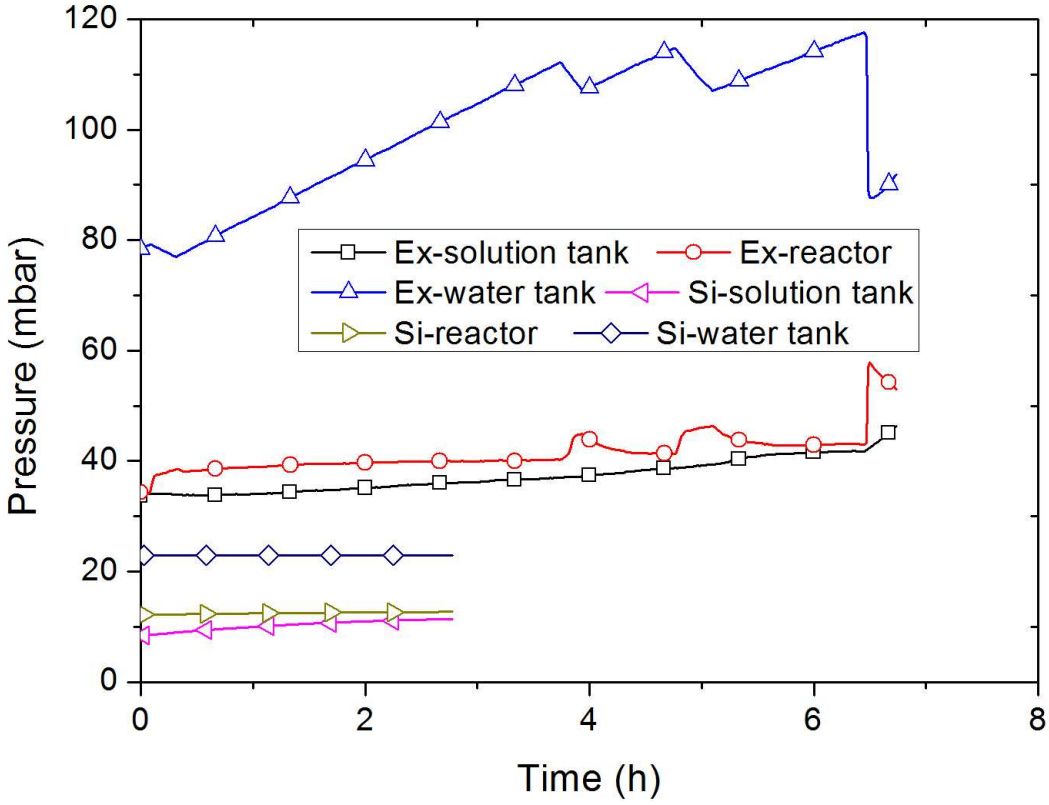

Figure 4-8 Evolution of pressures of absorption Case 1-3, experiment (Ex) and simulation (Si)

Compared with the experimental results, the pressures in the simulation are the equilibrium pressures without the influence of the air. According to the thermodynamic equilibrium law of the solution, the pressure of the solution increases with the solution temperature at a given mass fraction and increases with the decrease of the mass fraction of the solution at a given temperature. As a result, as the temperature of the solution tank increases during absorption (Si-T_5 in figure 4-6) and the mass fraction of the solution tank obviously decreases during the absorption period, the pressure of the solution tank in simulation increases with time (Si solution tank in Figure 4-8). The pressure of the water tank of the simulation (Si-Water tank) is changed with the water temperature in the water tank (Si-T_6 in Figure 4-6). The pressure of the reactor (Si-Reactor) depends on the temperature of water in the evaporator. As the power of the heat exchanger in the evaporator decreases with time, the temperature of water in the evaporator decreases. Thus the pressure of the reactor in the simulation decreases with time.

The overall performance comparison of the experimentation and simulation of Case 1-3 is shown in Table 4-4:

Table 4-4 Performance comparison of the experimentation and simulation (absorption Case 1-3)

Parameters	Unit	Case 1-3 Ex	Case 1-3 Si
m_6 Start	kg	35.7	35.7
m_6 End	kg	32.3	32.3
m_5 Start	kg	171.8	171.8
m_5 End	kg	175.2	175.2
x_5 Start	kg $CaCl_2$/kg solution	0.417	0.417
x_5 End	kg $CaCl_2$/kg solution	0.41	0.41
T_6 Start	°C	19.82	19.82
T_6 End	°C	19.79	19.84
T_5 Start	°C	19.87	19.87
T_5 End	°C	21.25	24
P_9 minimum	mbar	34	12.2
P_9 maximum	mbar	58	12.7
T_{78} minimum	°C	19.72	23.5
T_{78} maximum	°C	20.29	23.6
T_{87} minimum	°C	19.47	20
T_{87} maximum	°C	19.73	20
T_{910} minimum	°C	15	12
T_{910} maximum	°C	15.44	12.4
T_{109} minimum	°C	15.1	15
T_{109} maximum	°C	15.29	15
$\dot{Q}_{78}$ minimum	kW	0.02	0.61
$\dot{Q}_{78}$ maximum	kW	0.11	0.63
$\dot{Q}_{109}$ minimum	kW	-0.04	0.6
$\dot{Q}_{109}$ maximum	kW	0.06	0.7
Q_{78}	kWh	0.31	1.74
Q_{109}	kWh	0.2	1.78
Time	h	6.7	2.8

During Case 1-3, 3.4 kg of water is absorbed by the solution. The mass fraction is decreased correspondingly from 0.417 kg $CaCl_2$/kg solution to 0.41 kg $CaCl_2$/kg solution. The energy provided by the heat exchanger in the evaporator Q_{109} is 1.78 kWh in the simulation. The energy production which is rejected by the heat exchanger in the absorber Q_{78} is 1.74 kWh, which is larger than it is in the experiment. The power of the heat exchangers ($\dot{Q}_{78}$ and $\dot{Q}_{109}$) in the simulation is much larger than they are in the experiment. The decrease of the power in the experiment is again due to the presence of air in the reactor which is neglected in the simulation. Due to the difference of power, the time for desorption in simulation is shorter than in experiment (6.7 h compared to 2.8 h).

4.2.2.1 Other absorption cases

The overall performance comparison of the experimentation and simulation of Case 1-4 and Case 2-3 is shown in Table 4-5:

Table 4-5 Performance comparison of the experimentation and simulation during absorption

Parameters	Unit	Case 1-4 Ex	Case 1-4 Si	Case 2-3 Ex	Case 2-3 Si
m_6 Start	kg	32.3	32.3	40.5	40.5
m_6 End	kg	27.1	27.1	39.9	39.9
m_5 Start	kg	175.2	175.2	167	167
m_5 End	kg	180.4	180.4	167.6	167.6
x_5 Start	kg $CaCl_2$/kg solution	0.409	0.409	0.429	0.429
x_5 End	kg $CaCl_2$/kg solution	0.397	0.397	0.427	0.427
T_6 Start	°C	19.7	19.7	23.5	23.5
T_6 End	°C	19.6	19.8	21.9	23.3
T_5 Start	°C	19.87	19.87	20.3	20.3
T_5 End	°C	20.4	24	20.9	21.8
P_9 minimum	mbar	48	12.4	26	9.9
P_9 maximum	mbar	57	13.2	34	10.2
T_{78} minimum	°C	19.62	23.2	19.9	22.2
T_{78} maximum	°C	19.89	23.4	20.72	22.5
T_{87} minimum	°C	19.45	20	19.74	20
T_{87} maximum	°C	19.67	20	20.69	20
T_{910} minimum	°C	15	12.2	10.42	8.2
T_{910} maximum	°C	15.34	12.7	11.67	8.4
T_{109} minimum	°C	15.22	15	10.68	10
T_{109} maximum	°C	15.31	15	10.82	10
$\dot{Q}_{78}$ minimum	kW	0.02	0.56	0	0.43
$\dot{Q}_{78}$ maximum	kW	0.04	0.59	0.086	0.44
$\dot{Q}_{109}$ minimum	kW	-0.02	0.53	-0.21	0.37
$\dot{Q}_{109}$ maximum	kW	0.06	0.65	0.09	0.41
Q_{78}	kWh	0.17	3.26	0.21	0.44
Q_{109}	kWh	0.14	3.22	0.36	0.42
Time	h	4	5.6	5.5	1.08

According to the simulation and the experimental results, several conclusions can be found as follows:

- The power of the heat exchanger in the absorber and the evaporator in the simulation is bigger than it is in the experiment and the difference is a lot bigger than for the desorption cases. The main reason is that the equilibrium pressure should be lower during that phase than during desorption, causing even more air leaks and a bigger proportion of air in the prototype.

- The heat need for evaporation and the heat product by absorption in the simulation are higher than it is in the experimentation. Take Case 1-4 for example, 5.2 kg of water are absorbed by the solution, but the measured energy for evaporation is only 0.14 kWh and the energy production is only 0.17 kWh. However, this amount of energy is too low to evaporate 5.2 kg of water (the phase change enthalpy is about 2500 kJ/kg). The possible explanation is that when the water is circulated on the heat exchanger in the evaporator, the liquid water spills to the absorber and mixes with the solution directly. The design of the reactor still needs to be improved. The precision of the temperature sensors is also a possible reason of that inconsistency, because the temperature difference between the inlet and the outlet of the heat exchangers is very small.

4.3 Conclusion of the dynamic simulation

A model for the dynamic simulation of the prototype has been built. Simulations are carried out at the same conditions as in the experiments. After the analysis of the results and comparison with the experimental results, several conclusions can be found here:

- The feasibility of the system is validated by the simulation. But the results of the experimentation can not completely prove the model of the simulation as the leak of air in the experimentation and the limitation of the model (the hypotheses in the simulation). The phenomenon of desorption, absorption, evaporation and the condensation in the reactor is really complicated. The model should be enriched to get more realistic results.

- The powers of the heat exchanger in the components in the simulation are bigger than they are in the experiment. The main reason is the presence of air in the reactor during the experiment which decreases the heat and mass transfer.

- The time consumption for the desorption phase is decreased more than 50% in the simulation, since the power of the heat exchangers in the simulation is higher than it is in the experiment. As the time consumption for the desorption phase is decreased, the heat transferred to the solution in the solution tank is decreased.

- The heat need for desorption in the simulation is lower than it is in the experimentation because the heat loss is decreased and the water vapor which is condensed at the inter surface of the reactor is neglected in the simulation.

- Contrarily, the heat need for evaporation and the heat product by absorption in the simulation are higher than they are in the experimentation. A possible explanation is that liquid water spills to the absorber when the water is circulated on the heat exchanger in the evaporator. The design of the reactor needs to be improved. Another explanation is the precision of the measurement in the experimentation, as the temperature difference of the water is very feeble at that power.

References of Chapter 4

Yang Shiming, Tao Wenquan. 1987. Heat transfer. Beijing: Higher Education Publishing Company, (In Chinese)

Yao Yuying. 2003. Unit operation of chemical engineering. Tianjin: Tianjin University Publishing Company, (In Chinese)

Chapter 5 – Annual dynamic simulation of a building with a seasonal storage system by absorption

In order to obtain the annual performance of the seasonal storage system in a building, the model which is used for the dynamic simulation of the prototype is adapted in this chapter. Models of a solar collector, a building and the weather conditions are added to the dynamic simulation. The characteristics such as the pressure, the temperature, the mass, the mass fraction, the power and the energy etc. of the storage system in the building are presented and analyzed in this chapter.

In this model, we assume that the leakage problems highlighted in the previous comparison between experimental and simulation results are solved, and thus that the efficiency of the components is an optimal one. It is expected that the future experimental work will present better results than this preliminary study.

The simulation results thus obtained in this global simulation are representative of the potential of this process.

5.1 Annual dynamic simulation model

The model of the desorption phase is shown in Figure 5-1, and the absorption phase in Figure 5-2. The model of the machine for the annual dynamic simulation is the same as the model for the prototype, except that models of a solar collector, a building and external weather conditions are added and connected.

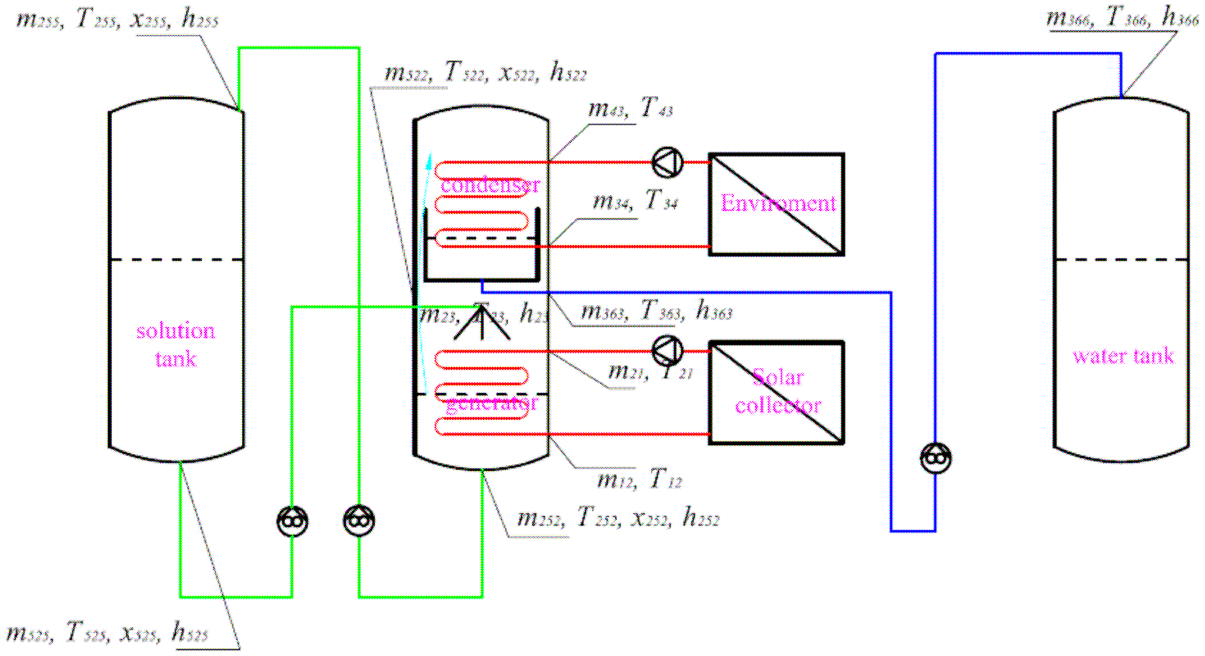

Figure 5-1 Global Simulation scheme of the desorption phase

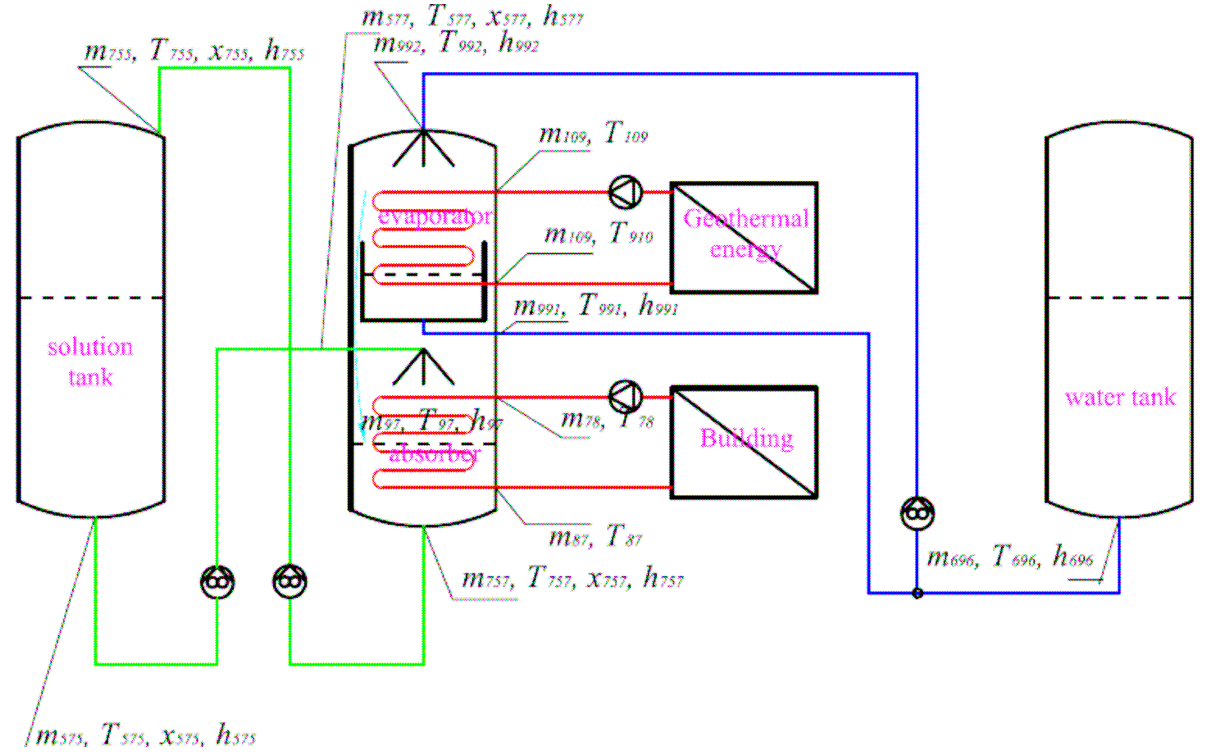

Figure 5-2 Global simulation scheme of the absorption phase

During the desorption phase, the energy for desorption is provided by a solar collector, the model for the solar collector can be found as follows [ISO 1994, Oscar M. et al 2005]:

$$\dot{Q}_s = (0,8G_s / 3600 \times 1000 - 3,5((T_{12} + T_{21}) / 2 - T_{atm}) - 0,015((T_{12} + T_{21}) / 2 - T_{atm})^2) \times S_{cs} / 1000 - \dot{Q}_n \quad \text{Eq.5-1}$$

In which, $\dot{Q}_s$ is the power which can be provided for the heat exchanger in the generator, G_s is the horizontal global solar radiation, $\dot{Q}_n$ is the power need of the building. $\dot{Q}_s$ is calculated by the energy which is provided by the solar collector subtracts the energy need of the building. This means that when there is a hating need for the house, the energy which comes from the solar collector will be firstly used directly for the building heating. If the energy which comes from the solar collector is higher than the energy need of the building, the excess energy will be used for the desorption.

The horizontal global solar radiation G_s comes from the weather conditions at Chambéry (France) and can be found in Figure 5-3.

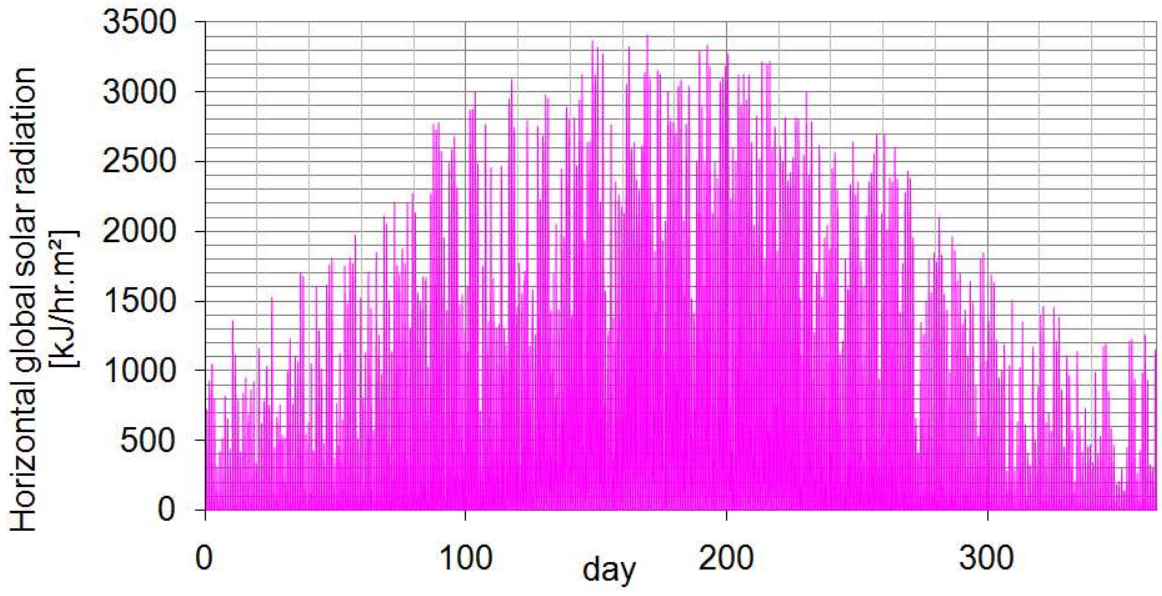

Figure 5-3 Horizontal global solar radiation at Chambéry, France

The ambient temperature T_{atm} also comes from the weather conditions at Chambéry France (Figure 5-4).

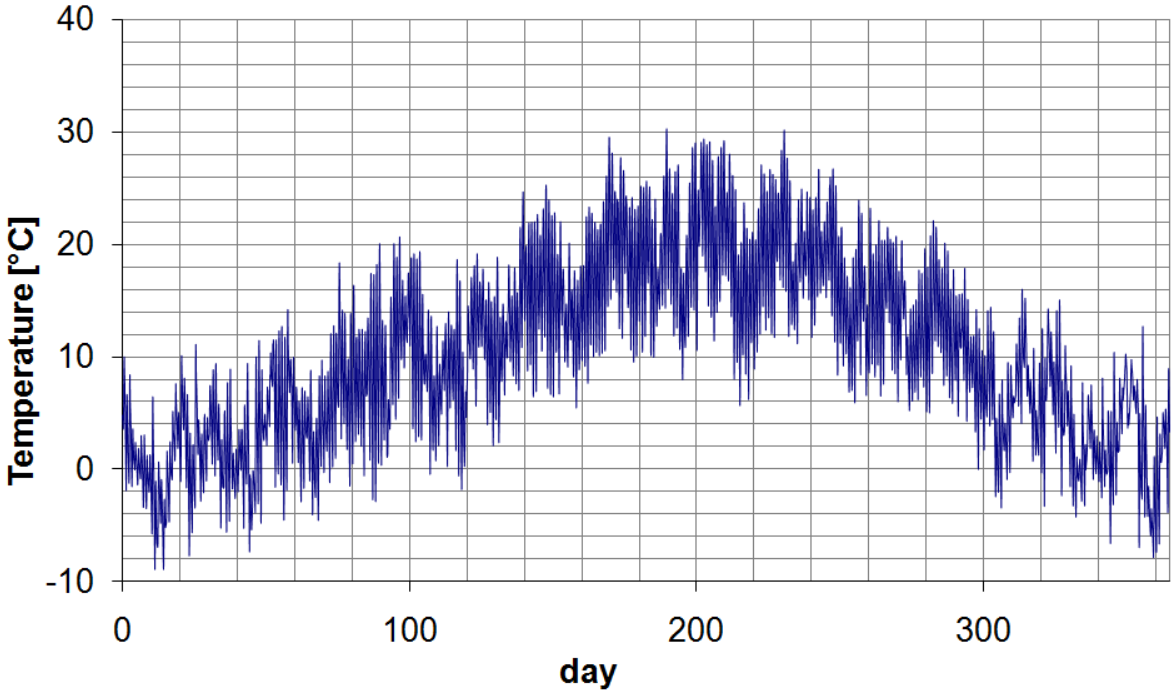

Figure 5-4 Ambient temperature at Chambéry, France

The water in the condenser is cooled by the ambient air. The temperature at the inlet of the heat exchanger T_{43} (Figure 5-1) is supposed the same as the ambient temperature T_{atm}. In a real system, this heat could also be rejected to the ground, thus at a lower temperature than T_{atm}.

During the absorption phase, the energy for evaporation is provided by geothermal pipes. The water temperature at the inlet of the heat exchanger T_{109} (Figure 5-2) is supposed constant at 15°C during the absorption phase, which is the same as in the dynamic simulation on the prototype.

The heat of absorption is used for building heating by the heat exchanger in the absorber. A simple model of the building is developed in Trnsys using type 56a in the software TRNBuild (Appendix 8). The surface of the building is 120 m^2 (15 m x 8 m). The height of the building is 2.5 m.

To keep the building temperature at 20°C during the day (6h-22h) and 18°C during the night (22h-6h), the heating need can be found in Figure 5-5. The total heating need for the building is 4950 kWh/year. The corresponding maximum heating power is 2.8 kW.

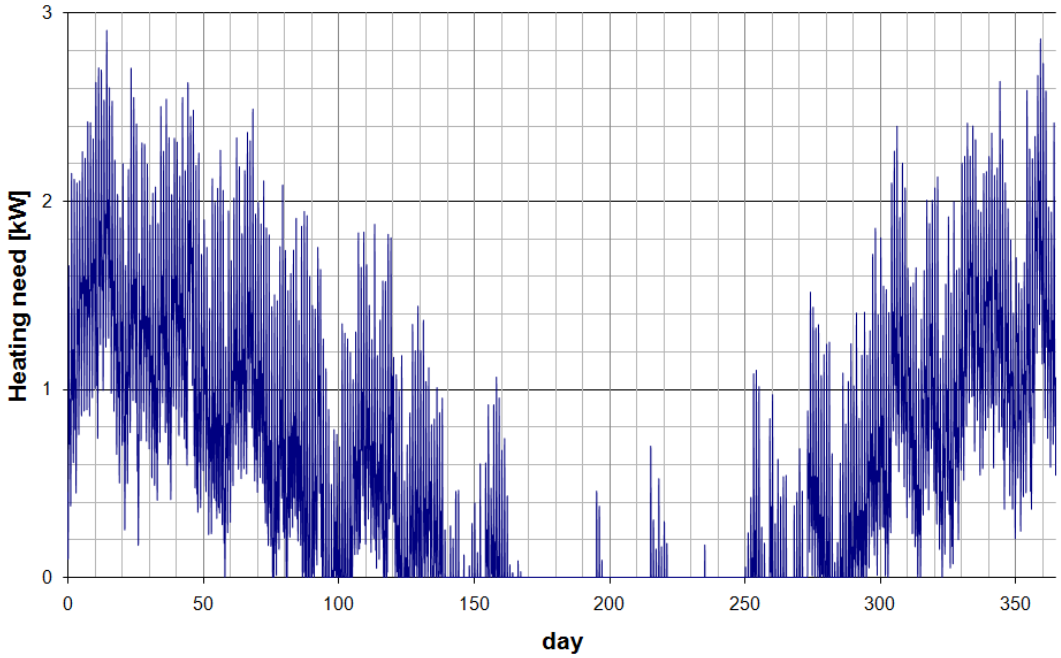

Figure 5-5 Energy need for building heating

The solution and the water tanks are supposed to be stored underground. Their depth is 4 m.

The temperature at this depth T_{ug4} for solution and water tanks is supposed as follows [TRILLAT-BERDAL V. 2006]:

$$T_{ug4} = 283.15 + 8 \cdot \sin\left(2\pi \cdot \left(t - 142.75 \cdot 86400\right) / 86400 / 365\right) \qquad \text{Eq.5-2}$$

in which, t is the time in second.

The scheme of T_{ug4} during one year can be found in Figure 5-6.

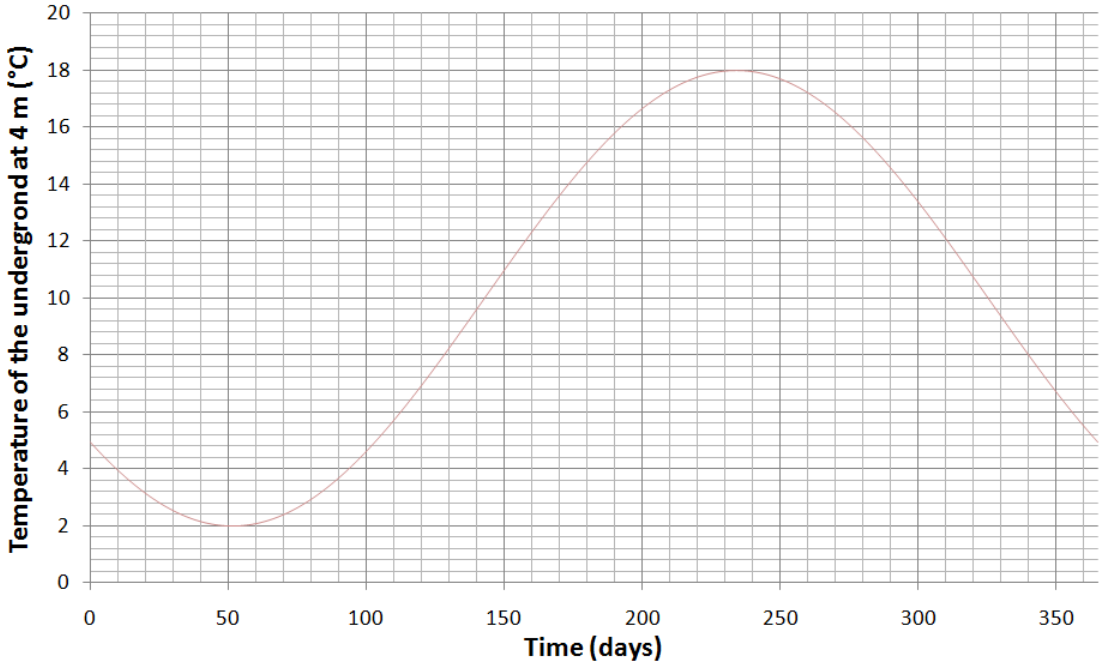

Figure 5-6 The scheme of T_{ug4} during one year [TRILLAT-BERDAL V. 2006]

The tempearture of T_{ug4} is just the enviroment temperature for water and solution tanks: The temperature of the geothermoal energy for evaporation is chosen at 15°C as the geothermal energy souce is supposed much deeper.

Compared to the dynamic simulation of the prototype, the environment temperature for calculation of the heat loss of the water and solution tanks is changed from the ambient temperature T_{atm} to the underground temperature T_{ug4}. Correspondingly, the heat losses are calculated as follows:

$$\frac{dQ_{loss5}(t)}{dt} = K_5 \cdot s_5 \cdot (T_5(t) - T_{ug4}(t)) \qquad \text{Eq.5-3}$$

$$\frac{dQ_{loss6}(t)}{dt} = K_6 \cdot s_6 \cdot (T_6(t) - T_{ug4}(t)) \qquad \text{Eq.5-4}$$

5.2 Dimension and operating conditions of the system

Due to the bigger heating and power need, the components of the storage system in the annual simulation are larger than they are in the prototype. The size of the components of the solar energy storage system can be found as follows: the volume of the solution tank is 21.9 m^3; the volume of the water tank is 9.4 m^3; the area of the solar collector is 12 m^2; the area of the heat exchangers in the reactor is 2 m^2. Those values are sized corresponding to the heating and power need of the building.

The system has three operational phases: the desorption, the absorption and the storage. The choice of the operation phase of the storage system depends on the heat production of the solar collector and the heating need of the building.

- Desorption phase: if the heat production of the solar collector is higher than the heating need of the building, the excess heat will be used for desorption. As discussed in Chapter 3, to avoid entire crystal formation in the storage tank, the maximum mass fraction of absorbent after desorption is limited depending on the crystal form (hydratation of the solid). The crystal of $CaCl_2$ at state 5 (10°C) is in form of $CaCl_2 \cdot 6H_2O$ with the percentage of absorbate at 50.7%. The maximum mass fraction in the solution tank is thus decided at 0.495. When the mass fraction in the solution tank is higher than 0.495, even if the heat production of the solar collector is higher than the heating need of the building, the system can not be operated for a desorption phase.

- Absorption phase: if the heat production of the solar collector is lower than the heating need of the building and the level in the water tank is higher than 0, the needed heat will be provided by absorption. The system is thus in an absorption phase.

- Storage (transition) phase: if the heat production of the solar collector is lower than the heating need of the building and there is no water in the water tank, or the heat production of the solar collector is higher than the heating need of the building and the mass fraction in the solution tank is higher than 0.495, or the heat production of the solar collector is the same as the heating need of the building, the system is in a storage phase.

During desorption phase, the operating conditions are: the water flow rate in the heat exchangers of the condenser and the generator is 2100 kg/h, which is the minimum flow rate to achieve a turbulent regime. The turbulent flow insures a sufficient heat transfer coefficient. The solution flow rate from the solution tank to the generator is 200 kg/h. The flow rate of water from the condenser to the water tank is 20 kg/h when the water level in the condenser is above the maximum level (100 mm) and zero when the level is below the minimum level (50 mm). This flow rate is sufficient to remove the water in the condenser to the water tank.

During absorption phase, the operating conditions are: the water flow rate of the heat exchanger of the evaporator is 5000 kg/h to make sure that the power of the evaporation is sufficient for any heat need of the building. The water flow rate of the heat exchanger in the

absorber is 1000 kg/h. The solution flow rate from the solution tank to the generator is not constant. It is calculated according to the heat need of building at each time step. The flow rate of water that is circulated in the evaporator is 10 kg/h. When the water level in the evaporator is below the minimum level (50 mm), the water in the water tank is transferred to the evaporator at the same flow rate (10 kg/h).

During storage phase, the operating conditions are: the water is stored in the water tank and the solution is stored in the solution tank. The temperature of the water and solution are changing depending on the heat transfer between the tanks and their environment.

5.3 Simulation results

All parameters such as mass, mass fraction, temperature, pressure, power etc. are calculated by the dynamic simulation.

The evolutions of the mass of the water in the water tank, the solution in the solution tank, the crystal in the solution tank, the mixture in the solution tank (the solution and the crystal) with time are presented in Figure 5-7. In the figure, the day 0 means January, the 1st, 2005; the day 1 means January, the 2nd, 2005; and, at last, the day 365 means January, the 1st, 2006. The mass of the mixture is the sum of the mass of solution and crystal. The mass of mixture in the solution tank decreases during the desorption phase (mostly in summer) and increases during the absorption phase (mostly in winter). When the solubility is less than the mass fraction of the mixture (days 0 to 60 and 180 to 365), there is crystal in the solution tank. The maximum mass of crystal is 13 700 kg. The corresponding solution mass (which corresponds to the minimum mass of solution) is 1 900 kg. This amount of minimum solution is chosen to avoid flowing problems within the system, even in the presence of solid crystal. The crystal disappears when the solubility is bigger than the mass fraction of the mixture in the solution tank (days 60 to 180). The mass of water in the water tank increases during the desorption and decreases during absorption. The maximum mass of water is 5300 kg. The sum of the amount of mixture (in the solution tank) and water (in the water tank) is logically constent in the system (closed system). At the day 90, there is a large gradient. That is because during the simulation, the day 90 (April, the 1st, 2005) is in fact the starting point of the simulation. At this point, the mass of water is 0. But one year later, when the simulation comes back to this date, the mass of solution and of water is different. There are still about 277 kg of water in the water tank. It is really difficult to make sure that all the water desorbed can be absorbed during one year. Compared to the mass of water circulated during one cycle (5 300 kg), the difference of mass of water in the water tank between the beginning and the end of the simulation is considered acceptable.

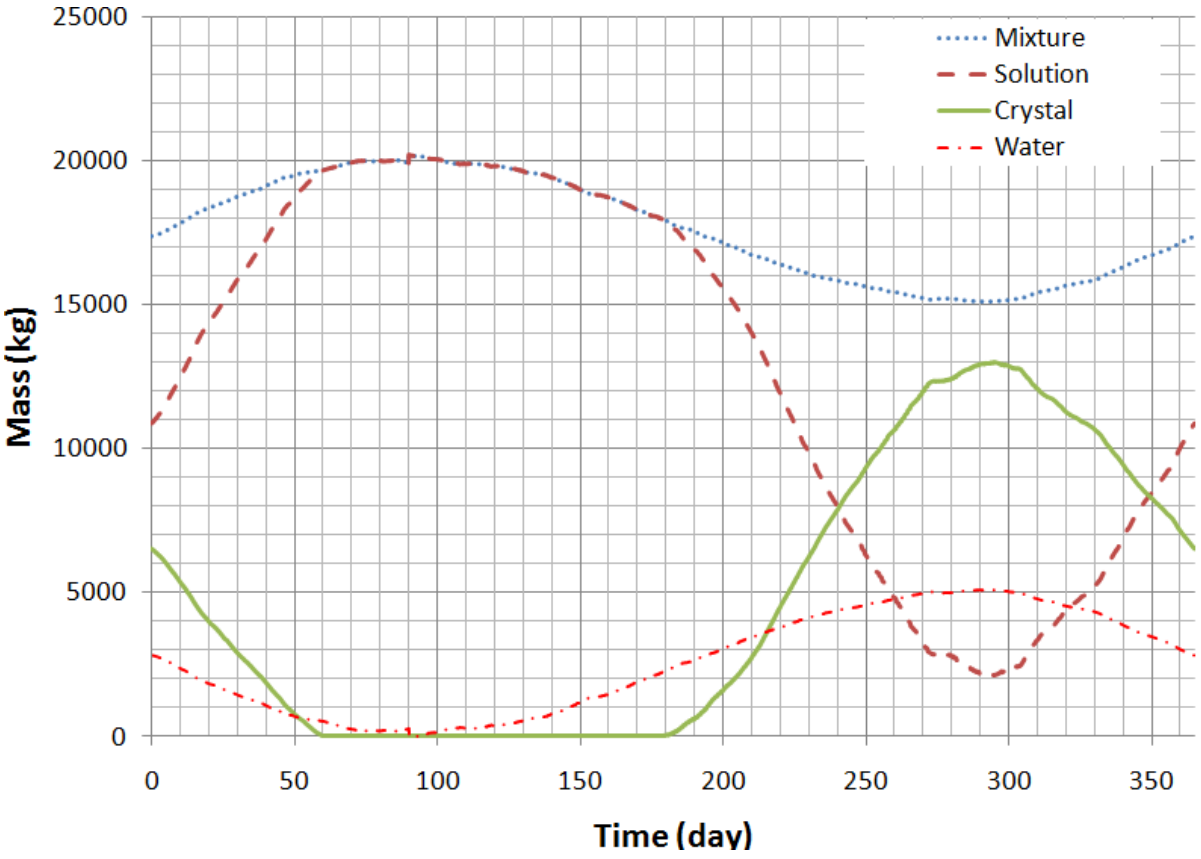

Figure 5-7 Annual evolution of the mass in the water tank and the solution tank

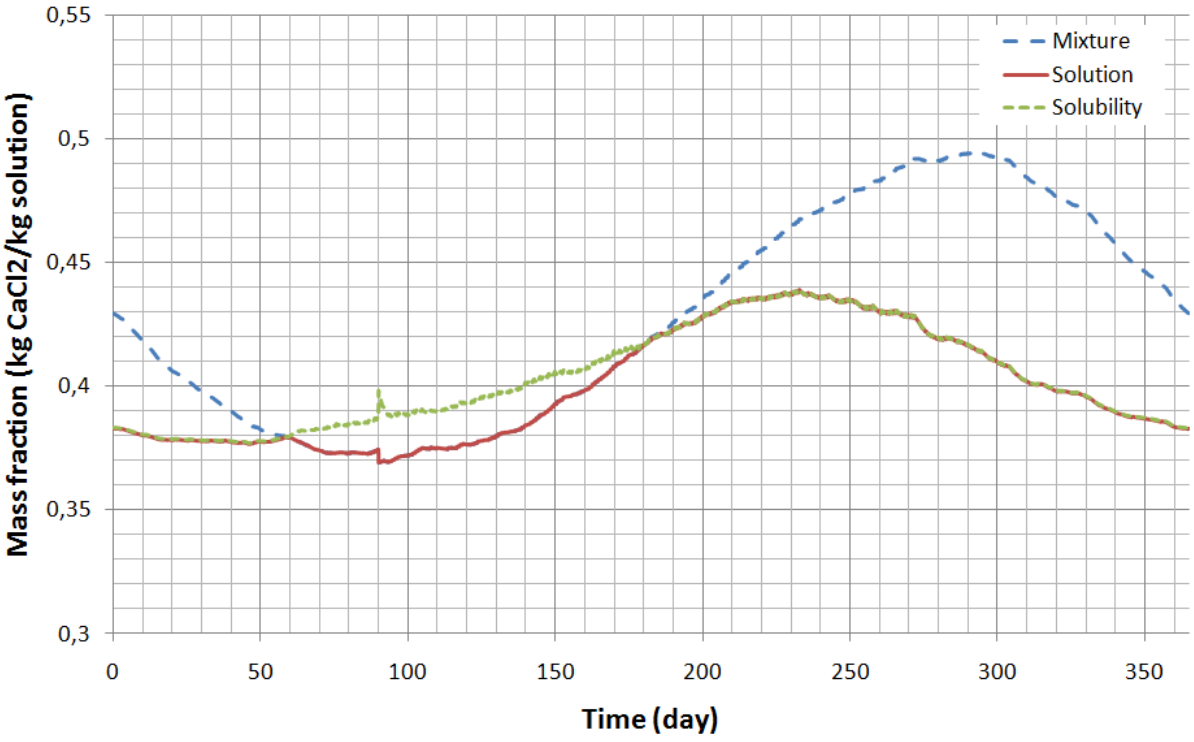

Figure 5-8 Annual evolution of mass fraction in the solution tank

The evolution of mass fraction in the solution tank is presented in Figure 5-8. The mass fraction of the mixture decreases during the desorption and increases during the absorption.

When there is crystal (days 0 to 60 and 180 to 365), the solubility is less than the mass fraction of the mixture, the mass fraction of solution is equal to the solubility. When there is no crystal (days 60 to 180), the solubility is greater than the mass fraction of the mixture. The mass fraction of the solution is the same as of the mixture. There is also a large gradient at day of 90. The reason is the same as for Figure 5-7.

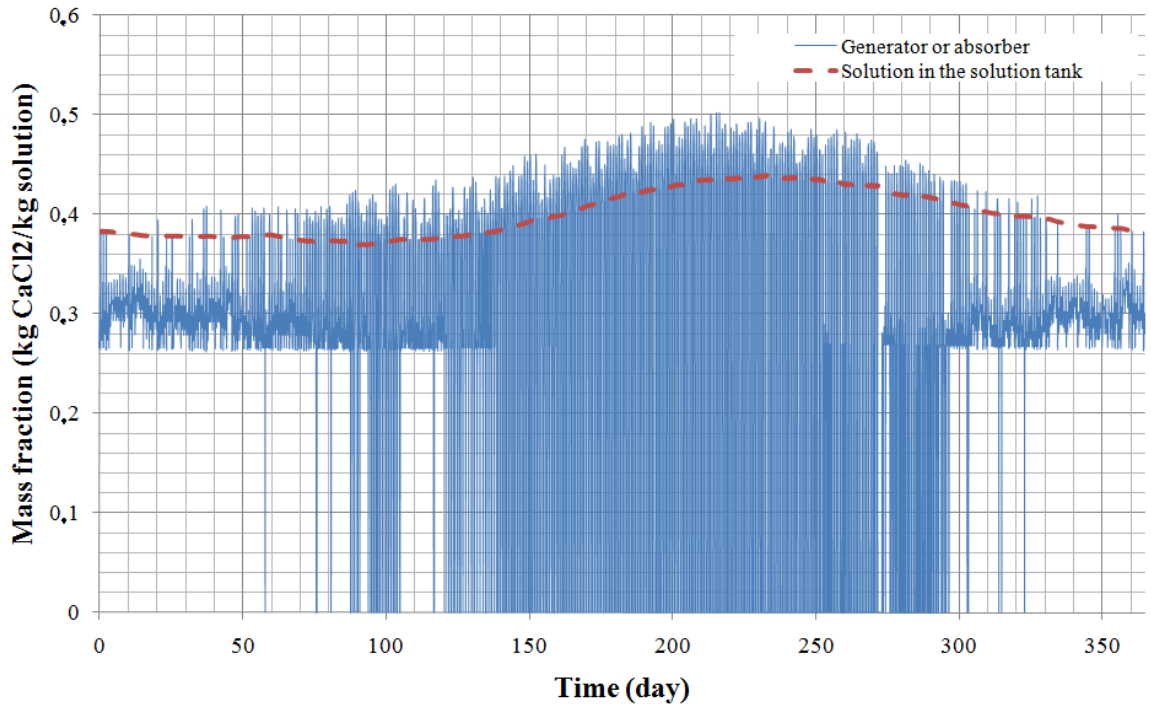

Figure 5-9 Annual evolution of mass fraction at the outlet of the generator or absorber

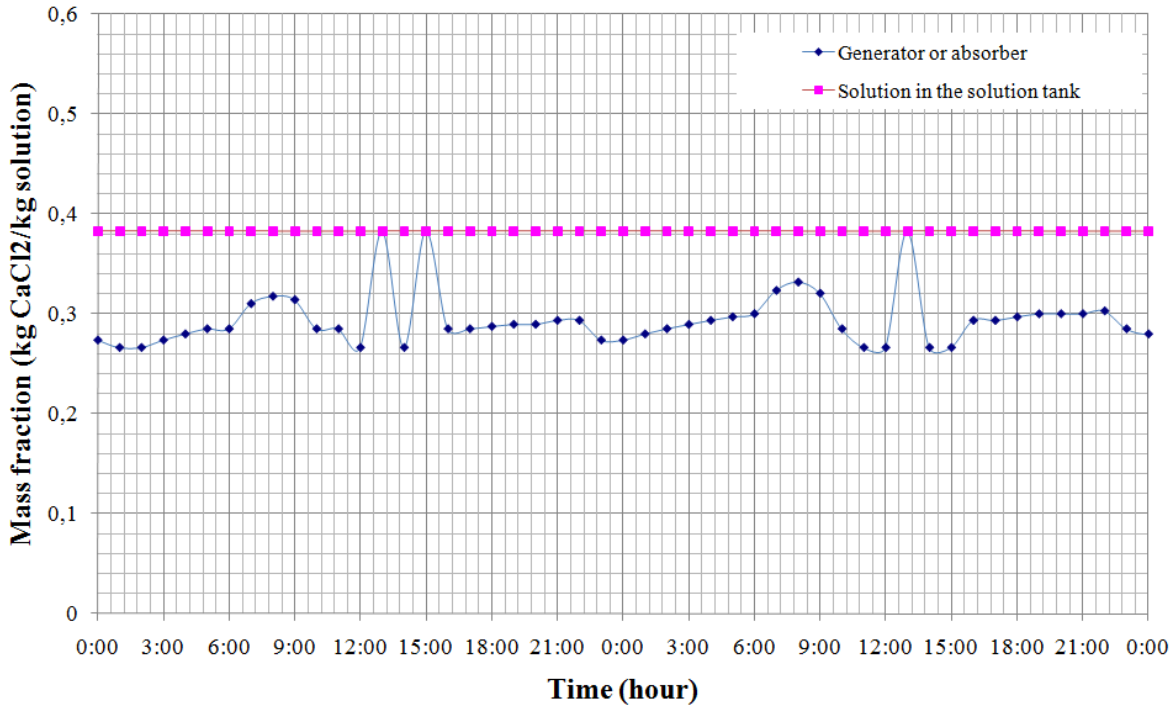

Figure 5-10 Zoom of the evolution of the mass fraction (January, 1st, 2005 and January, 2nd, 2005)

The evolution of mass fraction of solution at the outlet of the generator or absorber is presented in the Figure 5-9. During the storage phase, as there is no solution circulated in the reactor, the mass fraction at the outlet of the generator or absorber is decided at 0. For better understanding, a few days are detailed in the following figures. In the absorption phase (0h to 12h on January, 1st, 2005, Figure 5-10), the mass fraction in the solution leaving the absorber is less than the mass fraction in the solution tank as the water vapor is absorbed by the solution. In the desorption phase (8h to 18h on July, 20th, 2005, Figure 5-11), the mass fraction of solution leaving the generator is greater than the mass fraction of solution tank as the water vapor is desorbed from the solution. The storage phase mostly occurs at night in summer (0h to 6h on July, 20th, 2005, Figure 5-11 for example) because there is neither heating need nor solar energy.

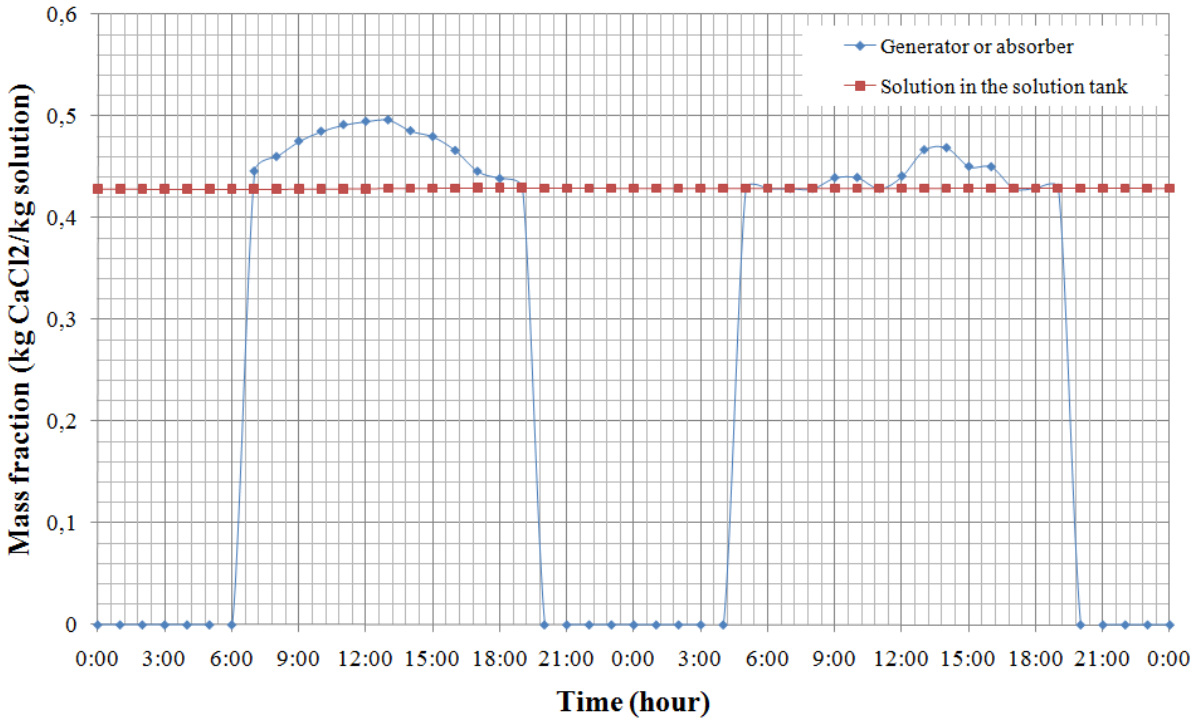

Figure 5-11 Zoom of the evolution of the mass fraction (July, 20th, 2005 and July, 21st, 2005)

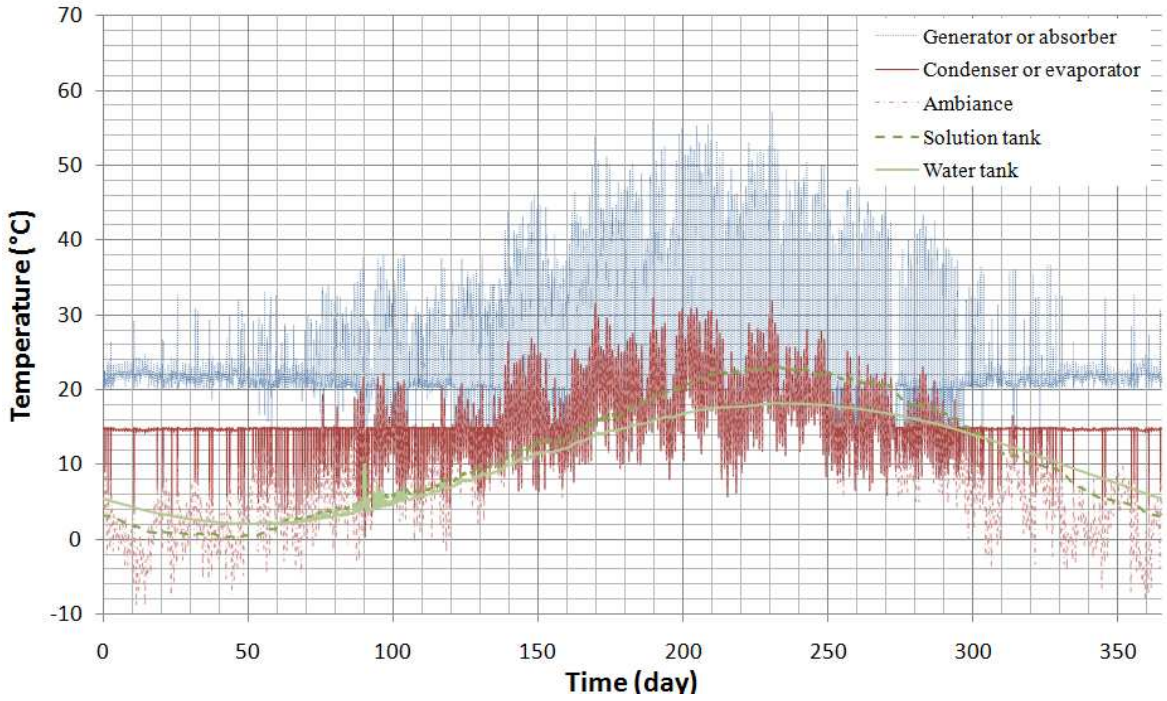

Figure 5-12 Annual evolution of the temperatures

Figure 5-12 shows the evolution of the temperature of the generator or the absorber, the condenser or the evaporator, the solution tank, the water tank and the atmosphere. Figure 5-13 shows the detail of those evolutions over 2 days. The temperatures of the generator and condenser change with the power of heat product of the solar collector. The temperature of the solution tank is higher than the temperature of the water tank because the temperature of the solution which comes from the generator is always higher than the temperature of the water which comes from the condenser. The temperature of the water tank is close to the temperature of the atmosphere. In absorption (Figure 5-14), the temperature of the absorber is higher than 20°C for building heating. The evaporator temperature is about 15°C. During storage, as there is neither desorption nor absorption, the temperature of the generator and the condenser are the same as the ambient temperature.

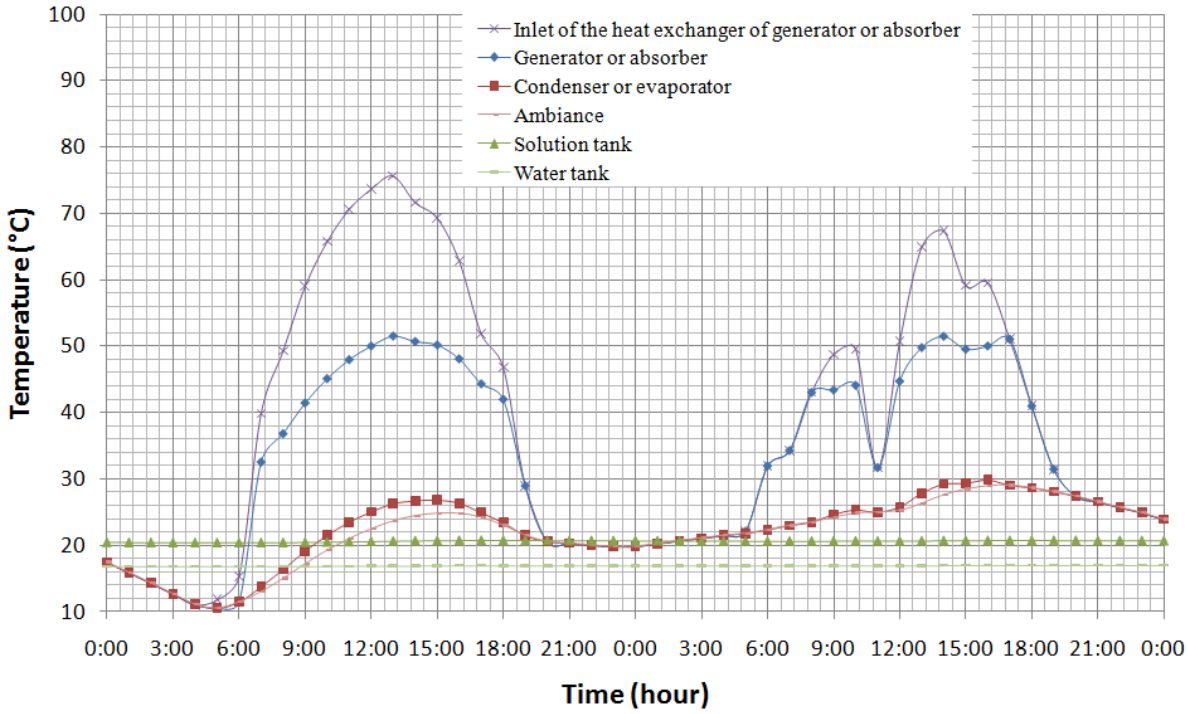

Figure 5-13 Zoom of the evolution of the temperatures (July, 20th, 2005 and July, 21st, 2005)

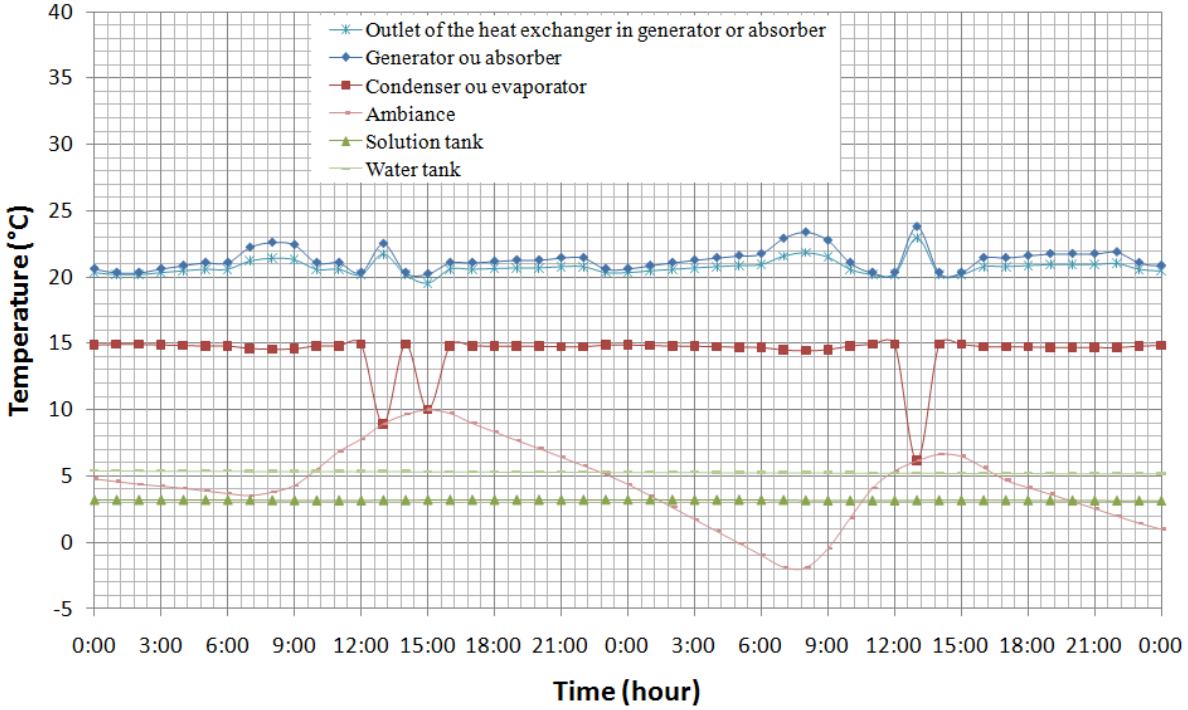

Figure 5-14 Zoom of the evolution of the temperatures (January, 1st, 2005 and January, 2nd, 2005)

Figure 5-15 presents the evolution of the pressure of the generator or absorber (depending on the phase), the solution tank and the water tank. During the desorption or absorption phases, the pressure of the generator or the absorber changes with its temperature and mass fraction (thermodynamic equilibrium pressure). During the storage phase, the pressure of the generator or absorber is assumed at the same pressure as the pressure of the water tank because the

generator and the absorber do not function. The pressure of the solution tank at thermodynamic equilibrium changes with its temperature and mass fraction. The pressure of the water tank changes with its temperature (saturated pressure of water). The system pressures vary from 200 Pa to 5000 Pa.

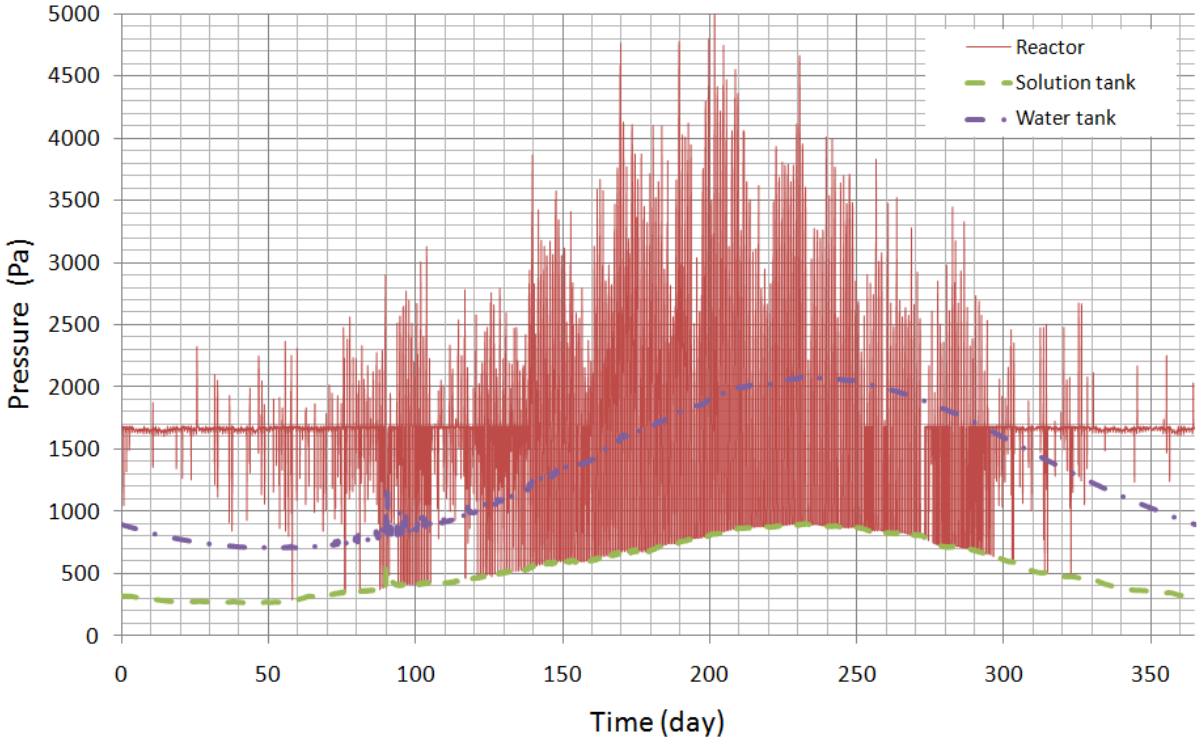

Figure 5-15 Annual evolution of the pressures

Figure 5-16 shows the evolution of the power of heat exchangers in the solar collector, the generator, the absorber, the condenser, the evaporator and the heating need of the building. During the storage phase, the powers are zero because the process is inert. The solution flow from the solution tank to the absorber is calculated to achieve a sufficient power.

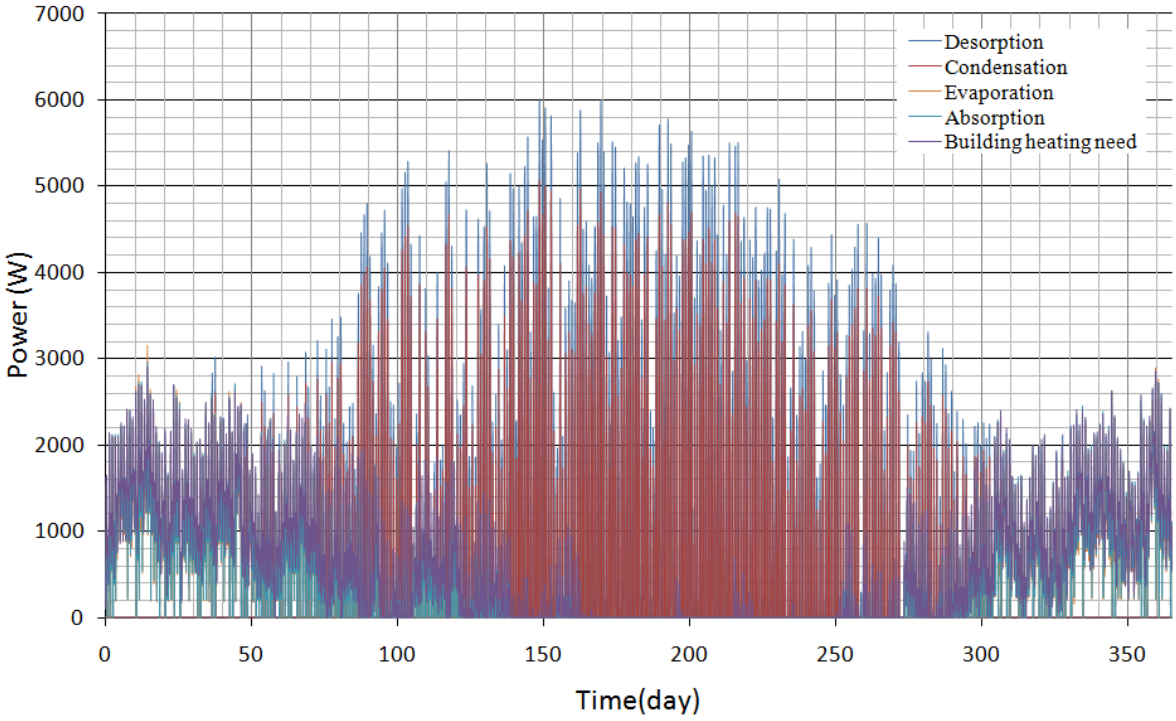

Figure 5-16 Annual evolution of the powers of heat exchangers

Figure 5-17 shows two days in summer. From 8h to 18h on July, the 20th, 2005, the desorption happens. The power of desorption is decided by the power of the solar energy which is received by the solar collector. The power in condensation is lower than it is in desorption because one part of the energy in desorption is used to heat up the solution which is circulated between the solution tank and the generator. The other parts of energy in desorption is used for the desorption of vapor from the solution, which is almost the same energy for the condensation in the condenser. From 0h to 8h on July, the 20th, 2005, as the solar energy and the building need are 0, the system is inert and the storage happens.

Figure 5-18 presents two days in winter. The absorption power is approximately the same as the heating need when there is no solar energy (from 0h to 9h on January, the 1st, 2005). When there is solar energy, the absorption power is lower than the building need (from 9h to 12h on January, the 1st, 2005) because the solar energy is also used for building heating directly by hot water. The lacking energy is produced by absorption. During some periods (from 12h to 15h on January, the 1st, 2005), solar energy is sufficient for the heating need of the building, there is no need for absorption. The excess energy is used for desorption.

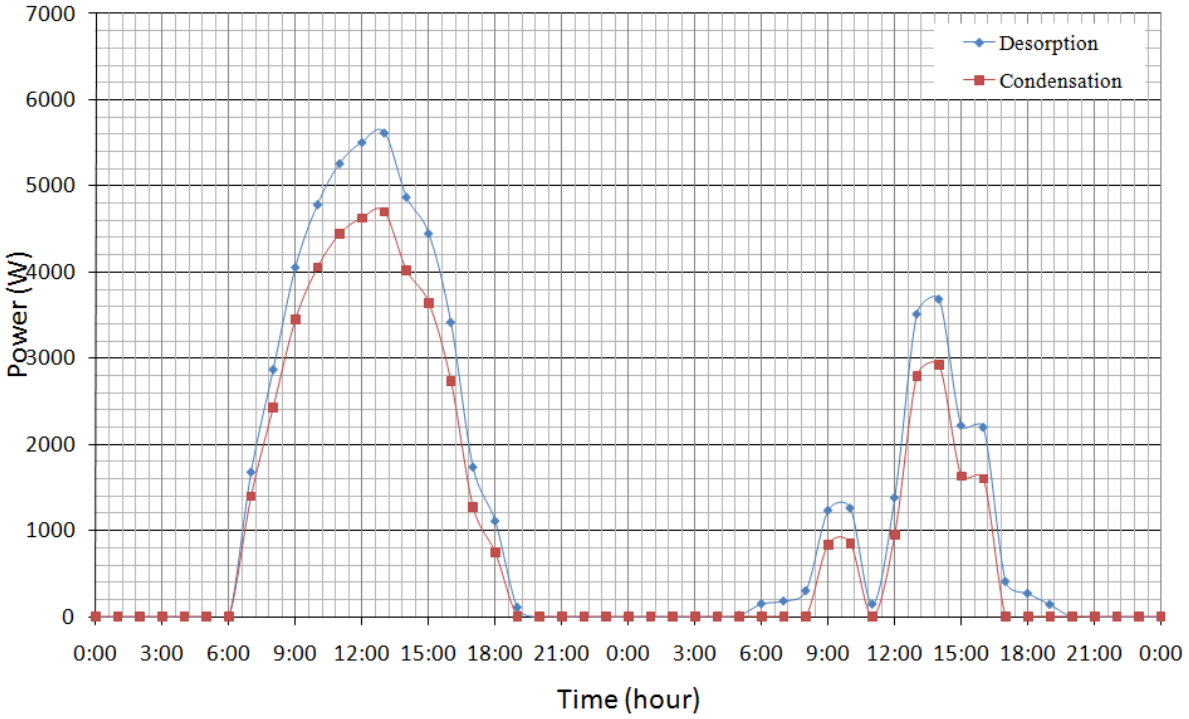

Figure 5-17 Zoom of the evolution of powers (July, 20th, 2005 and July, 21st, 2005)

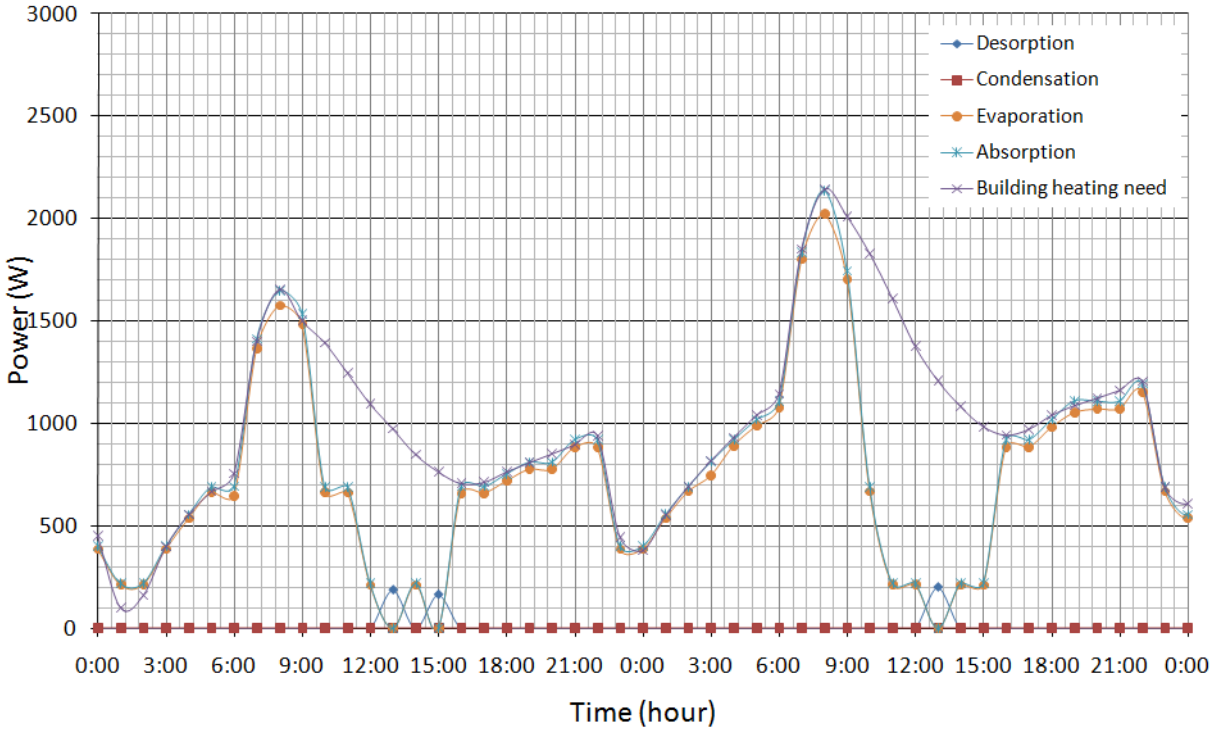

Figure 5-18 Zoom of the evolution of powers (January, the 1st, 2005and January, the 1st, 2005)

During absorption, the flow rate of the solution from the solution tank to the absorber is varied to meet the power need for building heating (Figure 5-19). The power increases with the flow because there is more solution used by the absorption process during a given period. But the relation is not linear because the water flow in the evaporator exchanger is constant.

Thus, there is a maximum power available for evaporation. Although the flow of solution is increased, the water vapor flow rate which comes from the evaporator reaches a maximum value. Consequently, the absorption power changes slowly with the flow rate when the flow rate is higher than 30 kg/h.

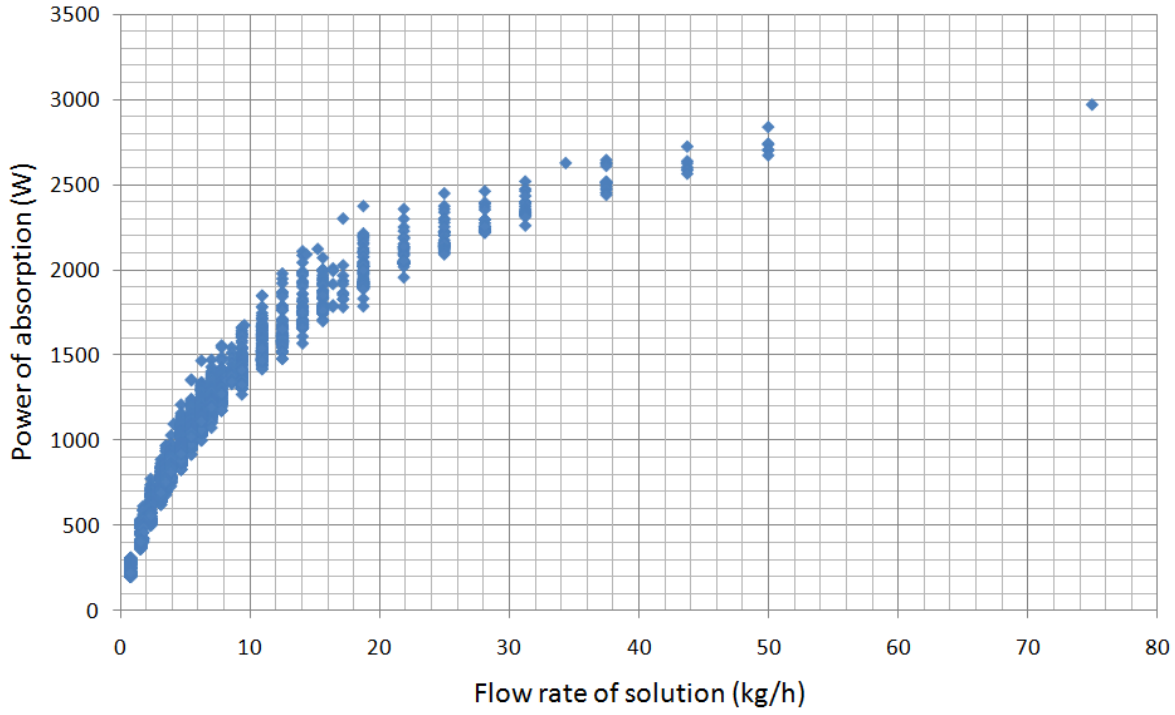

Figure 5-19 The absorption power in function of the solution flow rate

A calculation is used to prevent crystallization in the generator. The result is shown in Figure 5-20. For each temperature of condenser, there is a maximum mass fraction of solution in the generator and thus a maximum temperature of the generator to prevent crystallization. Figure 5-21 is easier to be used for experiments. During the operation of the system, the temperatures in the generator and condenser are measured and positioned in Figure 5-21. If the point is in the 'crystallization' region, the temperature of condensation should be raised by decreasing the flow rate or increasing the temperature of the water in the heat exchanger of the condenser or the temperature of desorption should be decreased by decreasing the flow rate or the temperature of the water in the heat exchanger of the generator.

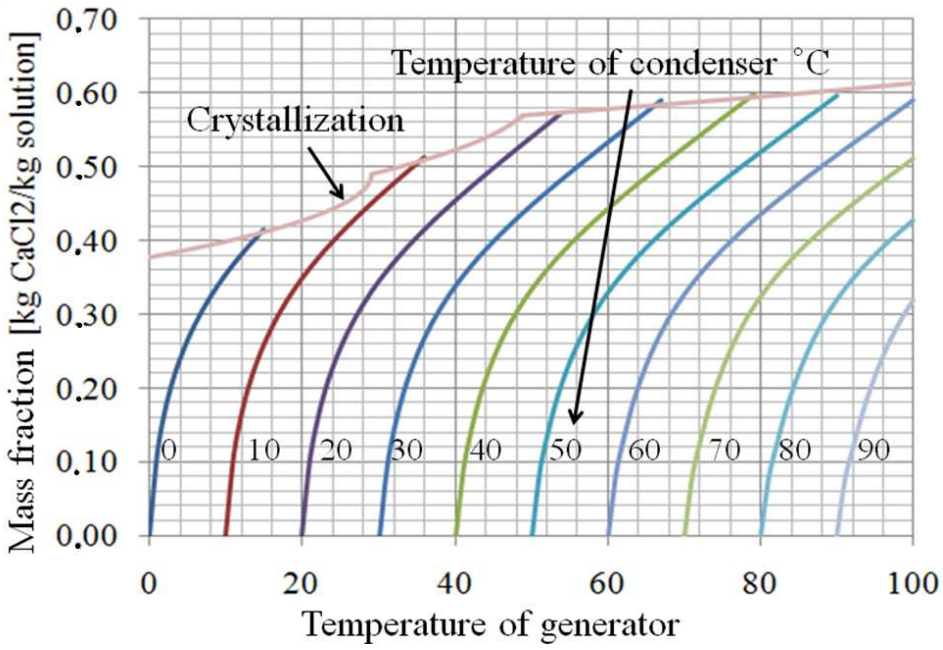

Figure 5-20 Crystallization in the generator (T-x-T)

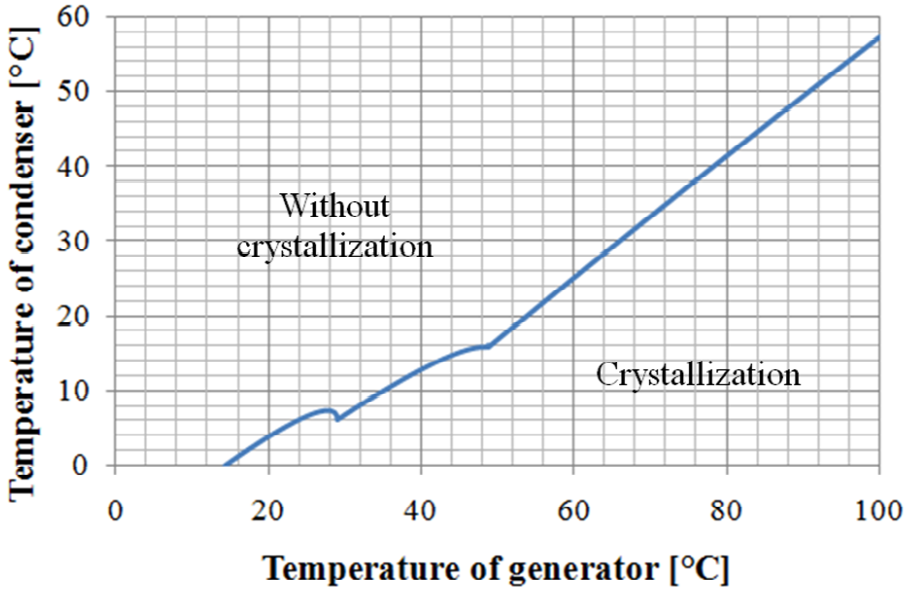

Figure 5-21 Crystallization in the generator (T-T)

During the simulation, all the conditions presented in the tube from the generator or absorber to the solution tank are in the region without crystallization (Figure 5-22). That is to say when the system is in an active phase, there is no crystallization. But the problem is when the system is in the storage phase. The solution can remain in the tubes and its temperature decreases to the room temperature. In the figure, there are many points near the line of solubility. The problem of crystal and blocking cannot be neglected. The possible solution to avoid this risk is to put all the tubes above the level of the solution tank. During the storage phase, the solution in the tubes can then flow back to the solution tank due to gravity. Thus as there is no solution in the tubes during the storage, there is no risk of blockage.

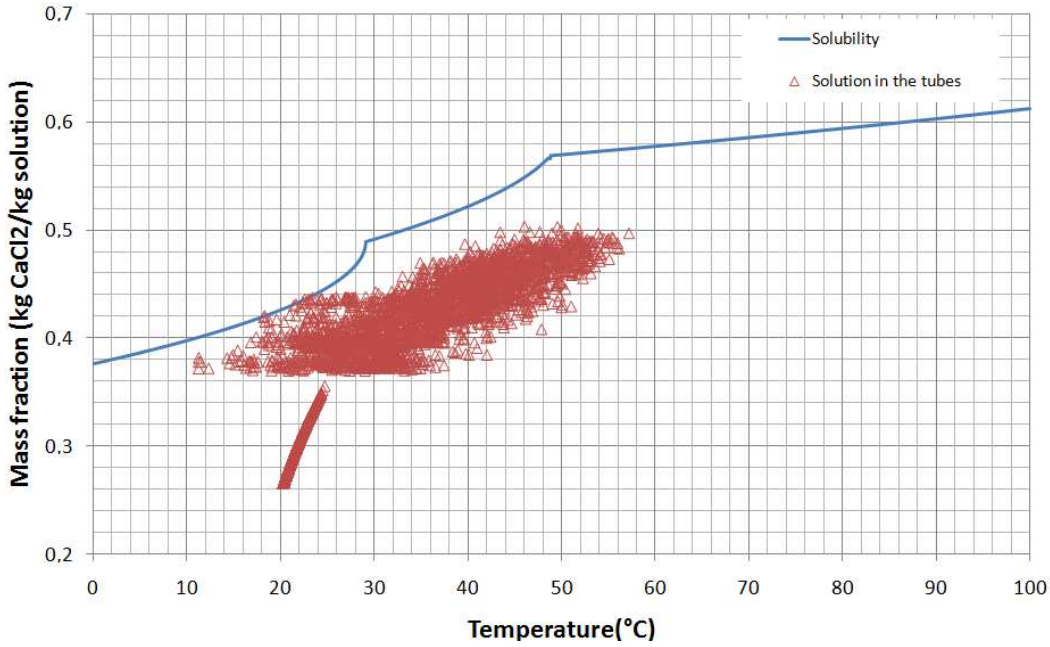

Figure 5-22 Risk of crystallization in the system tubes

According to the simulation, the main annual results are presented in Table 5-1:

Table 5-1 Annual results of the simulation

Solar energy received by the collector	14 619 kWh
Energy used in the generator	5 492 kWh
Energy released in the condenser	4 467 kWh
Building heating need	4 950 kWh
Solar energy used directly for the building in winter	1 374 kWh
Energy produced in the absorber	3 645 kWh
Energy used in the evaporator	3 534 kWh
Heat loss (all components)	1 099 kWh
Storage Capacity	116 kWh/m^3
Efficiency of solar collector	37.6%
Efficiency of storage system	66.4%
Efficiency of storage system with solar collector	24.9%

The solar energy which is received by the solar collectors is 14 619 kWh with 12 m^2 of solar collectors. The average efficiency of the solar collector is 37.6%. Hence the energy that is used in the generator is 5 492 kWh. It is mainly used for the desorption of the water vapor

from the solution. This part is about the same as the energy released in the condenser (4 467 kWh). The other part is transferred to the solution tank because the solution at the generator output is warmer than at the entrance. The energy produced in the absorber is 3 645 kWh. The solar energy used directly for the building in winter is 1 374 kWh. The energy required for evaporation is 3 534 kWh. The storage capacity of the system is 116 kWh/m^3 (volume of the solution and water tanks). It is about 1.6 times higher than the sensible storage system by water (70 kWh/m^3).

The efficiency of the storage system which is defined as the energy produced in the absorber divided by the energy used in the generator is 66.4%. The solar efficiency of the storage system is defined as the energy produced in the absorber divided by the solar energy received by the solar collector. It is about 24.9%, taking into account the solar collectors efficiency. The water temperature for heating the building is 21°C on average. It is not excellent for the building heating. The reason for the low temperature output of the system is explained in chapter 2 and 3. The $CaCl_2$ has a low temperature need for the desorption but also has a low temperature output of the absorption. In order to increase the temperature output of the system, one possible method is to increase the evaporation temperature. The energy of absorption could be used for evaporation in order to increases the temperature of evaporation. But that needs a two stage system, which needs another reactor and thus is more complicated. And as one part of the absorption energy is used for the evaporation, the storage capacity and the efficiency of the global system would be decreased if using a cascade process.

5.4 Conclusion of the annual simulation

The annual simulation on the building with the seasonal solar energy storage system has been carried out in this chapter. The evolutions of mass, mass fraction, temperature, pressure, power etc. with time are analyzed.

The model for the annual simulation considers almost all the components which are used in the building with the seasonal storage system. It can be used for other simulations with different heating needs and weather conditions, and even for other absorption couples by the change of the thermodynamic characteristics.

According to the simulation results, the building heating needs can be completely covered by the heat produced by the seasonal storage system and the solar energy used directly for building heating. As this feasibility has been shown by the simulation, the storage capacity and the efficiency are key factors of the seasonal storage system by absorption. The storage capacity of the example given using $CaCl_2/H_2O$ is about 116 kWh / m^3 and the efficiency of the storage system is about 66.4%. For a building of 120 m^2, however, it is difficult to have 30 m^3 of storage tanks. The quality of the heat production (about 21°C) is not sufficient, too. The next step of the research should concentrate in the improvement of the storage capacity, the efficiency of storage and the quality of the heating production. The possible methods are the optimizations of the flow rates during the process, the design of the components and the development of a cascade process.

References of Chapter 5

ISO (1994). 1994. ISO 9806-1, Thermal performance of glazed liquid heating collectors.

Oscar Menger, Zsebik Albin, BME Energetikai Gépek és Rendszerek Tanszék. 2005. Analysis of thermal solar system parameters through dynamic simulation. Climate Change – Energy Awareness – Energy Efficiency, Visegrad

TRILLAT-BERDAL Valentin. 2006. Thèse : Intégration énergétique dans les bâtiments par l'utilisation combinée de l'énergie solaire et de la géothermie basse température. Université de Savoie – Chambéry

General conclusion

During this thesis, the innovative concept of a system of seasonal storage of solar energy for house heating by absorption is introduced and described. This thesis is the first study on a storage system using the absorption phenomena with the $CaCl_2/H_2O$ couple. Little literature was to be found on this subject, and no experimental test rig had been described before on absorption storage. The performance and thermodynamic characteristics of seven possible absorption couples of the storage system, $CaCl_2/H_2O$, Glycerin/H_2O, KOH/H_2O, LiBr/H_2O, LiCl/H_2O, NaOH/H_2O and H_2O/NH_3, have been studied and compared to choose the best option for this innovative concept. A prototype has been built for verifying the feasibility of the seasonal storage system by absorption, using the $CaCl_2/H_2O$ couple. A precise model for the dynamic simulation which corresponds to the prototype has been built. An annual simulation on a building with the seasonal solar energy storage system has also been carried out to obtain the performance of the seasonal storage system.

After the analysis of the performance and characteristics of the seasonal storage system by absorption, several general conclusions are presented here:

1. Following the static simulation, dynamic simulation and annual simulation, the seasonal storage by absorption is theoretically possible. The solar energy is stored during the summer phase and is released for house heating during the winter phase.

2. The performance of the storage system changes with the different couples. For the $CaCl_2/H_2O$ couple, the investment cost for the tanks may be higher than for the other couples due to its low storage capacity. However, considering that its price and the temperature requirement for the solar collector are low, it is a interesting candidate.

3. The storage capacity increases with the evaporator temperature and the storage temperature before the absorption phase, and decreases with the absorber temperature. The appearance of crystal increases the storage capacity.

4. The feasibility of the storage system by absorption is proved by the experimentation. During the experiment, the desorption phase is possible. The water has been desorbed from the solution and stored in the water tank. The temperature needed for desorption is compatible with the use of flat plate solar collectors. But the performance of the absorption phase is not satisfying due to its low power.

5. The results of the experimentations are not significative. The air in the reactor is the main problem for the low power of absorption. In the dynamic simulation, the air influence is not considered. The power of the heat exchangers in the components is much bigger than in the experiment. The conception of the heat exchangers is not optimized in the experimentation. If those problems can be solved, the performance of the experimentation will be better.

6. According to the annual simulation results, the building heating needs can be completely covered by the heat produced by the seasonal storage system and the solar

energy used directly for building heating. The storage capacity of the example given using $CaCl_2/H_2O$ is about 116 kWh/m^3 and the efficiency of the storage system is about 66.4%. A building of about 120 m^2 needs about 30 m^3 of storage tanks.

As the potential and interest of this storage concept has been proved by the simulation, the storage capacity and the efficiency are key factors of the seasonal storage system by absorption. The quality of the heat production (about 21°C) is not sufficient, however. The next step of the research should concentrate in the improvement of the storage capacity, the efficiency of storage and the quality of the heating production and the phenomenon of the absorption, desorption, evaporation and condensation. . The prospectives are as follows:

1. The design of the components.

   Concerning the experimentation, the surface of the heat exchangers should be increased in order to increase their heat and mass transfer rates. As the water vapor can be condensed on the inner surface of the reactor and the water on the heat exchanger of the evaporator can spill to the absorber and mix with the solution directly, the storage capacity and the efficiency of the process are decreased. The design of the reactor has also to be improved. For the simulations as well as the experiments, the flow rates of the process were not optimal. The optimization of these flow rates could improve the power and the temperature output of the absorber.

2. The development of a cascade process.

   In order to increase the temperature output of the system, one possible method is to increase the evaporation temperature. The energy of absorption could be used to heat up an evaporator in order to increases the temperature of evaporation by a two stage system. However, this new process would need another reactor. Thus, it would bring other problems such as the complexity of the system, the possible decrease of the storage capacity and efficiency, the difficult coordination of the power of the two reactors, etc. The feasibility and the performance of the cascade process could be researched in the future work.

3. The influence of the kinetic characteristics for the desorption, absorption, condensation and evaporation phases, which are not considered in the simulation, should be added to the simulation model. Thus the simulation would approach more the real situation.

4. The influence of the purity of the absorption couple for the absorption and desorption phases, which has not been analyzed, can be carried out in the future work. Just as we know, the price of a material increases quickly with the increase of its purity. If this influence is not serious, the investment cost of the storage system will be evidently decreased.

5. The prototype has not been used in situations in which crystals appear in the storage tank. The simulation have, however, shown the interest of these crystals in the process to decrease the tank size, and the quantity of materials used. The experimental study of

the crystals control and the crystallization/melting rates inside the tank still has to be performed.

6. Concerning the problems presented in the experimentation (especially the air leak in the system), it is a long way to realize this system for house using. The scale-up of the system can be studied in the future work.

Appendix

Appendix 1 Solubility

For $CaCl_2$–H_2O solution, the crystallization line is complex, particularly due to the formation of various hydrates. Boundaries are shown in Figure A1-1.

The equation is described by the Eq.A1-1 [Manuel R. Conde 2004, Solvay Group[1] 2008].

$$\theta = \sum_{i=0}^{2} A_i x^i + A_3 x^{7.5} \qquad \text{Eq.A1-1}$$

The parameters of Eq.A1-1 for the various ranges of the crystallization line are given in Table A1-1.

Table A1-1 Parameters of equations describing the solubility boundary of $CaCl_2$–H_2O solutions [Manuel R. Conde 2004]

Boundary	A0	A1	A2	A3
Ice Line	0.422088	−0.066933	−0.282395	−355.514247
$CaCl_2$–$6H_2O$	−0.378950	3.456900	−3.531310	0.0
$CaCl_2$–$4H_2O$ α	−0.519970	3.400970	−2.851290	0.0
$CaCl_2$–$4H_2O$ β	−1.149044	5.509111	−4.642544	0.0
$CaCl_2$–$2H_2O$	−2.385836	8.084829	−5.303476	0.0
$CaCl_2$–H_2O	−2.807560	4.678250	0.0	0.0

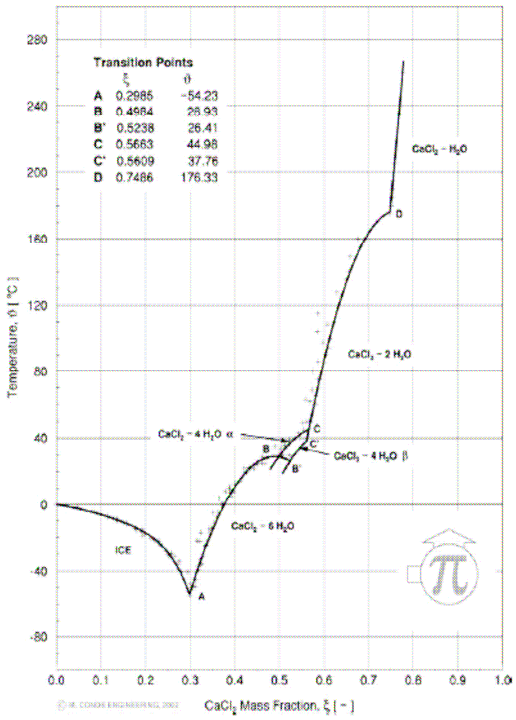

Figure A1-1 The transition points between the boundaries of $CaCl_2$ [Manuel R. Conde 2004].

Appendix 2 Equilibrium of solution

For $CaCl_2$, the relation of equilibrium pressure, temperature and concentration can be described as Eq.A2-1 [Manuel R. Conde 2004, Solvay Group[1] 2008]:

$$\frac{P_{sol}(x,T)}{P_{H_2O}(T)} = \pi_{25} f(x,\theta) \qquad \text{Eq.A2-1}$$

$$f(x,\theta) = A + B\theta \qquad \text{Eq.A2-2}$$

Where θ is defined as Eq.A1-1

$$A = 2 - \left[1 + \left(\frac{x}{\pi_0}\right)^{\pi_1}\right]^{\pi_2}, \quad B = \left[1 + \left(\frac{x}{\pi_3}\right)^{\pi_4}\right]^{\pi_5} - 1 \qquad \text{Eq.A2-3}$$

$$\pi_{25} = 1 - \left[1 + \left(\frac{x}{\pi_6}\right)^{\pi_7}\right]^{\pi_8} - \pi_9 e^{\frac{(x-0.1)^2}{0.005}} \qquad \text{Eq.A2-4}$$

Parameters in Eq.A2-2 to Eq.A2-4 can be found in Table A2-1.

Table A2-1 Parameters for the vapor pressure equation [Manuel R. Conde 2004]

π_0	0.31
π_1	3.698
π_2	0.60
π_3	0.231
π_4	4.584
π_5	0.49
π_6	0.478
π_7	−5.20
π_8	−0.40
π_9	0.018

Appendix 3 Equilibrium of water

The relation between equilibrium liquid/vapor pressure of water and temperature can be described as Eq.A3-1 [Bridgeman, O.C. & Aldrich, E.W 1964]:

$$\log P_{H_2O}(T) = A - \frac{B}{T + C} \qquad \text{Eq.A3-1}$$

Where, $P_{H_2O}(T)$ is the liquid/vapor pressure of water (bar), T is its temperature (K). The A, B and C can be found in Table A3-1.

Table A3-1 Parameters in Eq.A3-1[Bridgeman, O.C. & Aldrich, E.W 1964]

Temperature range (K)	A	B	C
273-373	5.40221	1838.675	-31.737
304-333	5.20389	1733.926	-39.485
334-363	5.07680	1659.793	-45.854

Appendix 4 Enthalpy of solution

For the salt solutions considered here, the absorption (dilution) is an exothermic process, while the desorption (regeneration) requires the supply of thermal energy to the solution. This thermal energy required (or liberated) is larger than that corresponding to the vaporization (or condensation) of pure water. This difference constitutes the energy of dilution, and when referred to the unit mass of water is named differential enthalpy of dilution.

For $CaCl_2$, the differential enthalpy of dilution can be calculated as Eq.A4-1 [Manuel R. Conde 2004, Solvay Group[1] 2008].

$$h_d = h_{d,0}\left[1+\left(\frac{\varsigma}{H_1}\right)^{H_2}\right]^{H_3} \qquad \text{Eq.A4-1}$$

Where ς is defined from the salt mass fraction as Eq.A4-2.

$$\varsigma = \frac{x}{H_4 - x} \qquad \text{Eq.A4-2}$$

The reference $h_{sol,0}$ is related to the temperature as Eq.A4-3.

$$h_{d,0} = H_5 + H_6 \times \theta \qquad \text{Eq.A4-3}$$

H_1 to H_6 can be found in Table A4-1.

Table A4-1 Parameters of the differential enthalpy of dilution equations for solutions of lithium and calcium chlorides [Manuel R. Conde 2004]

H_1	0.855
H_2	−1.965
H_3	−2.265
H_4	0.8
H_5	−955.690
H_6	3011.974

With the differential enthalpy of dilution, the enthalpy of solution can be calculated as follows:

Supposing the water vapor (m_v, h_v) is absorbed by large amount of solution (m_s, h_s), the energy balance can be found as Eq.A4-4:

$$m_s h_s + m_v h_v = \left(m_s + m_v\right) h_s + Q_1 \qquad \text{Eq.A4-4}$$

In which, because the water vapor mass is very small compared with the mass of solution, the mass fraction of the solution and the temperature of solution is considered constant during the absorption. Hence the enthalpy of the solution after the absorption is the same as the solution before absorption.

Supposing the water vapor (m_v, h_v) is absorbed by large amount of water (m_w, h_w) at the same operating conditions, the energy balance can be found as Eq.A4-5:

$$m_w h_w + m_v h_v = (m_w + m_v) h_w + Q_2 \qquad \text{Eq.A4-5}$$

In which, as the same reason in the absorption by solution, the enthalpy of water is constant during the absorption.

With Eq.A4-4 and A4-5, the enthalpy of solution h_s can be calculated by Eq.A4-6:

$$h_s = h_w - \frac{Q_1 - Q_2}{m_v} \qquad \text{Eq.A4-6}$$

In which, $(Q_1 - Q_2) / m_v$ is the differential enthalpy of dilution h_d .

Appendix 5 Enthalpy of water vapor

The relation between enthalpy of water vapor and temperature at liquid/vapor equilibrium state can be described as Eq.A5-1 [Wagner W. & Pruss A. 2002].

$$h_v(T) = 1.7549(T - 273.15) + 2223.5 \qquad \text{Eq.A5-1}$$

Appendix 6 Enthalpy of crystal

The standard enthalpy of crystal can be calculated as follows,

It is supposed that the crystal dissolves in the poor solution at a constant temperature. The operational temperature of this process is T . The crystal m_c dissolves in the poor solution m_p, x_p and forms the rich solution m_r, x_r . The heat exchange between the solution and the surroundings is calculated both by heat of solution and enthalpy (h_{hs}).

$$m_r \cdot h_r - m_p \cdot h_p - m_{cry} \cdot h_{cry} = m_{cry} \cdot h_{hs} \qquad \text{Eq.A6-1}$$

$$m_r = m_p + m_{cry} \qquad \text{Eq.A6-2}$$

The enthalpy of solution can be calculated by Appendix 4. The heat of solution h_{hs} can be found in Figure A6-1. The mass and concentration of poor solution and crystal are given. The enthalpy of crystal can be calculated at this temperature [Group Solvay[2] 2008].

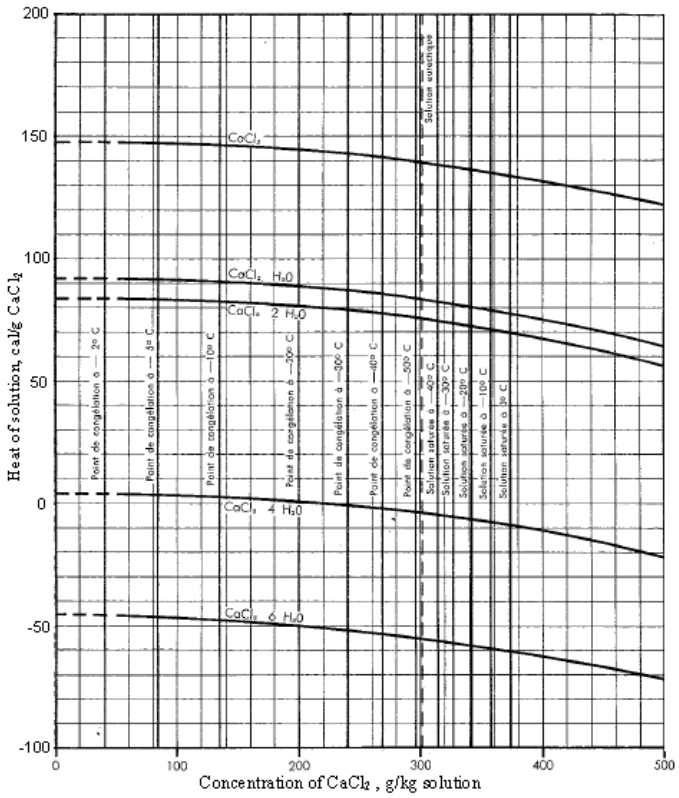

Figure A6-1 heat of solution of $CaCl_2$ and its crystals [Group Solvay[2] 2008]

Appendix 7 Density

For $CaCl_2$–H_2O, the relative (to saturated liquid water at the same temperature) densitiy may be represented by a single cubic function of the mass fraction ratio solute solvent $x/1-x$. This function has the form as Eq.A7-1[Manuel R. Conde 2004].

$$\rho_{sol}(x,T)=\rho_{H_2O}(T)\sum_{i=0}^{3}\rho_i\left(\frac{x}{1-x}\right)^i \qquad \text{Eq.A7-1}$$

Where ρ_i are given in Table A7-1 for the solutions $CaCl_2$–H_2O.

Table A7-1 Parameters of the density equation [Manuel R. Conde 2004]

ρ_0	1.0
ρ_1	0.836014
ρ_2	−0.436300
ρ_3	0.105642

$\rho_{H_2O}(T)$ is the density of saturated liquid water at the temperature T. It is calculated from

$$\rho_{H_2O}(T)=\rho_{c,H_2O}\left(1+B_0\tau^{1/3}+B_1\tau^{2/3}+B_2\tau^{5/3}+B_3\tau^{16/3}+B_4\tau^{43/3}+B_5\tau^{110/3}\right) \qquad \text{Eq.A7-2}$$

Where $\tau=1-\theta$ and B_i are given in Table A7-2. ρ_{c,H_2O} is the density of water at the critical point (322 kg/m^3).

Table A7-2 Parameters for the liquid water density equation [Manuel R. Conde 2004]

i	B_i
0	1.9937718430
1	1.0985211604
2	−0.5094492996
3	−1.7619124270
4	−44.9005480267
5	−723692.2618632

The range of application of the equation for solutions $CaCl_2$–H_2O is $0\le x\le 0.60$.

Appendix 8 Building model in Trnsys

The model of the building can be found in Figure A8-1. The surface of the building is 120 m^2 (15m x 6m). The height of the building is 2.5 m.

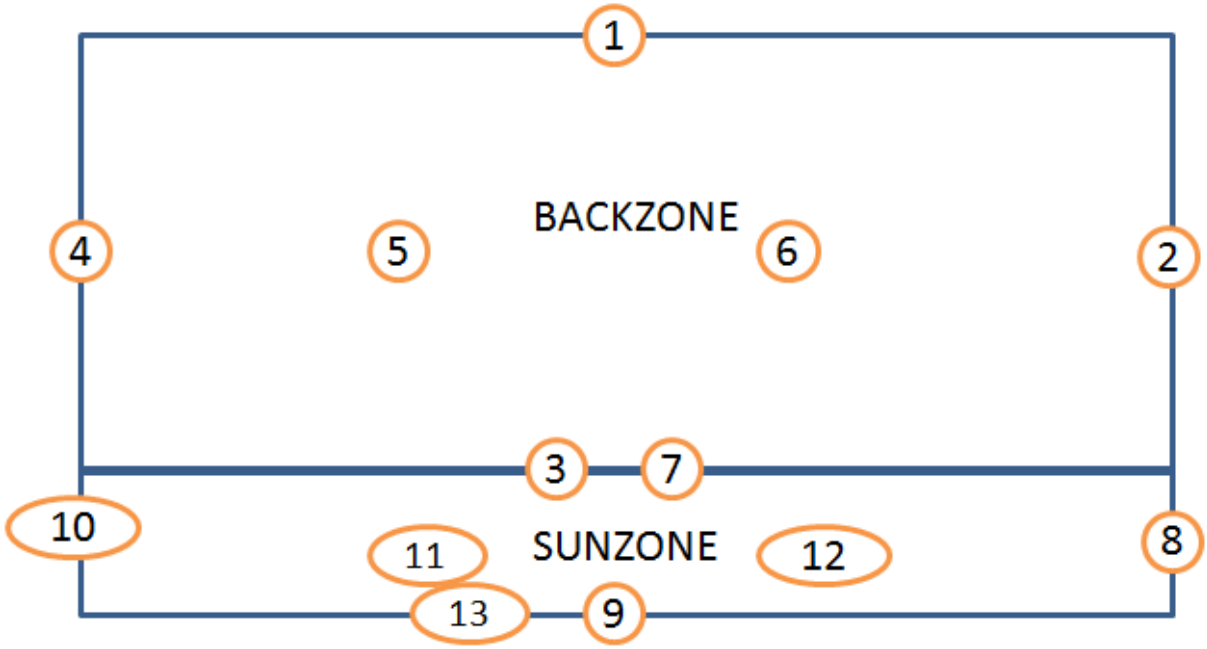

Figure A8-1 Zones of the building

There are two zones (Backzone and du Sunzone) in the building.

Backzone

The type, the surface and the direction of the walls in the BackZone are presented in the Table A8-1.

Table A8-1Walls of the BackZone

Number	Type	Surface (m^2)	Direction
1	Wall bst_l_ext	30	north
2	Wall bst_l_ext	10	east
3	Wall bst_com	30	south
4	Wall bst_l_ext	15	west
5	Wall bst_l_roo	96	ceiling
6	Wall bst_l_flo	96	floor

Zone Sunzone

The type, the surface and the direction of the walls and windows of the BackZone are presented in the Table A8-2.

Table A8-2 Walls and windows in the BackZone

Number	Type	Surface (m^2)	Direction
7	Wall bst_com	30	north
8	Wall bst_h_ext	5	east
9	Wall bst_h_ext	30	south
10	Wall bst_h_ext	5	west
11	Wall bst_h_roo	24	ceiling
12	Wall bst_h_flo	24	floor
13	Window ins2_kr_3	16	south

The parameters of the types of wall and windows are presented below:

Wall bst_l_ext

Layer = plasterbrd and fibreglass and woodsiding

Thickness = 0.012 m and 0.066 m and 0.009 m

The heat transfer coefficient is 0.51039 W/m^2k

Wall bst_com

Layer = concretebl

Thickness = 0.2 m

The heat transfer coefficient is 1.77886 W/m^2k

Wall bst_l_roo

Layer = plasterbrd and fibreglass and roofdeck

Thickness = 0.01 m and 0.1118 m and 0.019 m

The heat transfer coefficient is 0.31613 W/m^2k

Wall bst_l_flo

Layer = timberfl and insulation

Thickness = 0.025m and 0 m

The heat transfer coefficient is 0.03933 W/m^2k

Wall bst_h_ext

Layer = concretebl and foaminsul and woodsiding

Thickness = 0.1 m and 0.0615 m and 0.009 m

The heat transfer coefficient is 0.50817 W/m^2k

Wall bst_h_roo

Layer = plasterbrd and fibreglass and roofdeck

Thickness = 0.01 m and 0.1118 m and 0.019 m

The heat transfer coefficient is 0.31613 W/m^2k

Wall bst_h_flo

Layer = concslab and insulation

Thickness = 0.08 m and 0 m

The heat transfer coefficient is 0.03950 W/m^2k

Window ins2_kr_3

Winid = 2003; hinside = vertical; houtside = 58.93; slope = 90; spacid = 0; wwid = 0; wheig = 0; fframe = 0.15; uframe = 8.17; absframe = 0.6; rishade = 0; reshade = 0; reflishade = 0.5; refloshade = 0.1; ccishade = 0.5

The configurations of those layers are presented follows:

Layer plasterbrd

Conductivity = 0.576 kJ/hmK; heat capacity = 0.84 kJ/kgK; density = 950 kg/m^3

Layer fibreglass

Conductivity = 0.144 kJ/hmK; heat capacity = 0.84 kJ/kgK; density = 12 kg/m^3

Layer woodsiding

Conductivity = 0.504 kJ/hmK; heat capacity = 0.9 kJ/kgK; density = 530 kg/m^3

Layer concretebl

Conductivity = 1.836 kJ/hmK; heat capacity = 1 kJ/kgK; density = 1400 kg/m^3

Layer roofdeck

Conductivity = 0.504 kJ/hmK; heat capacity = 0.9 kJ/kgK; density = 530 kg/m^3

Layer timberfl

Conductivity = 0.504 kJ/hmK; heat capacity = 1.2 kJ/kgK; density = 650 kg/m^3

Layer insulation

Resistance = 6.9653 hm^2K/kJ

Layer foaminsul

Conductivity = 0.144 kJ/hmK; heat capacity = 1.4 kJ/kgK; density = 10 kg/m^3

Layer concslab

Conductivity = 4.068 kJ/hmK; heat capacity = 1 kJ/kgK; density = 1400 kg/m^3

References for the appendix

Bridgeman O.C., Aldrich E.W.. 1964. Vapor pressure tables for water. J. Heat transfer. 86, pp 279-286

Manuel R. Conde. 2004. Properties of aqueous solutions of lithium and calcium chlorides: formulations for use in air conditioning equipment design. International Journal of Thermal Sciences. 43(4), pp 367-382

Solvay Group[1]. 2008. Solubility and water vapor tension of the $CaCl_2/H_2O$ system. Document of Solvay Group. D'apres international critical tables, volume iii, pp 295-368, 1926

Group Solvay[2]. 2008. Heat of solution with different hydrates of $CaCl_2$. Document of Group Solvay, On the Chemical Industry Beleg t xvi 3, 1951

Wagner W., Pruss A.. 2002. The iapws formulation 1995 for the thermodynamic properties of ordinary water substance for general and scientific use. J. Phys. Chem. Ref. Data. 31(2), pp 387-535